Last Glacial to Holocene changes in carbonate ion content of deep waters of the Eastern Arabian Sea

A THESIS SUBMITTED IN PARTIAL FULFILMENT FOR THE DEGREE OF

DOCTOR OF PHILOSOPHY

in

Marine Sciences

School of Earth, Atmosphere and Ocean Sciences

GOA UNIVERSITY

by

Smita Namdeo Naik

University Reg. no. 200707161

Under the Supervision of

Dr. Sushant S. Naik

Principal Scientist

Geological Oceanography Division

CSIR-National Institute of Oceanography

June - 2021

DECLARATION

I, **Smita Namdeo Naik** hereby declare that this thesis entitled **"Last Glacial to Holocene changes in carbonate ion content of deep waters of the Eastern Arabian Sea"** represents work which has been carried out by me and that it has not been submitted, either in part or full, to any other University or Institution for the award of any research degree.

Place: Goa University, Taleigao, Goa

Date: Smita Namdeo Naik

CERTIFICATE

I hereby certify that the above Declaration of the candidate, **Ms. Smita Namdeo Naik** is true and the work was carried out under my supervision.

Goa University, Talegao, Goa.

Dr. Sushant Suresh Naik

Research Supervisor

Principal Scientist

CSIR-National Institute of Oceanography

Dona Paula – 403 004

Goa, India

ACKNOWLEDGEMENT

CONTENTS

PREFACE

Rising carbon dioxide (CO_2) in the atmosphere is one of the major concerns of humanity today. Carbon dioxide being a greenhouse gas, traps heat radiations within earth's atmosphere, which results in a gradual rise in annual temperatures. The concentration of CO_2 gas in the atmosphere has fluctuated between 180-280 ppmv between glacial to interglacial cycles from last 800 kyr (Lüthi *et al.,* 2008) but it never exceeded 300 ppmv. It is only after the human impact, due to the burning of fossil fuels, the concentration of CO_2 began to cross 300 ppmv in the 1950's and is still increasing with a present concentration of 411.29 ppmv (NOAA data). Carbon dioxide from the atmosphere is in equilibrium with the surface ocean and is taken up by the oceans through two major processes; biological process and chemical process. Biological process includes biological pump wherein the CO_2 from surface layer is taken up by the phytoplankton during photosynthesis, thus capturing the carbon in the organic matter. Chemical process involves dissolution of CO_2 in seawater forming carbonic acid (H_2CO_3) which further dissociates into bicarbonate (HCO_3^-) and carbonate ion (CO_3^{2-}). Many marine calcifying organisms like corals, foraminifera and coccolithophores build their exoskeletons by precipitating carbonate ion and calcium to form calcium carbonate ($CaCO_3$). These shells/exoskeletons sink in the water column and remain preserved in the sediment for a long period of time after the death of the organism.

Carbonate saturation determines the dissolution/preservation of these shells in sediment, which is indeed controlled by carbonate ion concentration [CO_3^{2-}] of deep waters. Under low [CO_3^{2-}], the carbonate saturation decreases and dissolution of $CaCO_3$ on the seafloor is observed, which liberates CO_3^{2-} to the seawater, increasing its alkalinity, whereas under high [CO_3^{2-}], carbonate saturation increases, preservation of $CaCO_3$ occurs and CO_3^{2-} and alkalinity are consumed. Hence through the knowledge of deep-water [CO_3^{2-}] one can explain the role played by oceans in regulating global carbon cycling including the process and mechanisms involved in past atmospheric CO_2 changes.

Previous studies on variation in deep water [CO_3^{2-}] in the Atlantic, Pacific and Indian Ocean during the last deglaciation have indicated a hike in [CO_3^{2-}] (Yu *et al.,* 2007, Yu *et al.,* 2010a, 2010b, 2013, 2014; Allen *et al.,* 2015; Ma *et al.,* 2020), which is thought to be due to the degassing of CO_2 from deeper waters. Depletion in ^{14}C activity and incursion of aged water was observed in intermediate water of the western Arabian Sea by Bryan *et al.,* (2010) and outgassing of pCO_2 (Naik *et al.,* 2015) and a decrease in [CO_3^{2-}] from surface

waters of the eastern Arabian Sea (EAS) during the deglaciation by Naik and Naik, (2018). If so there should be a rise in $[CO_3^{2-}]$ observed in deep waters at the same time, as CO_2 and carbonate ion share an inverse relationship. Hence the present study is aimed at understanding the Last Glacial to Holocene carbonate ion changes in deeper waters of the EAS.

Chapter 1: -

This chapter provides general introduction to the study conducted and rationale of the problem addressed. Various factors affecting $[CO_3^{2-}]$ in seawater are listed and briefly explained. Further the vertical distribution of modern day $[CO_3^{2-}]$ in the world oceans is also provided in this chapter. It further includes the literature review on glacial to interglacial changes in $[CO_3^{2-}]$ of deep waters over the world oceans using different proxies. A detailed description and the principles of various proxies used in the study are also given. In the view of above the hypothesis on which this study is based is given along with the research objectives.

Chapter 2: -

This chapter describes the study area in detail with the hydrography of study area, which includes the physical and biogeochemical processes taking place at the study site. The Arabian Sea surface and deep water circulation is discussed in detail with different water masses of the Arabian Sea and their flow paths. Furthermore, a description of material and methods used to accomplish the objectives are put forth in this study, which covers collection of sediments, processing, identification and picking of foraminifera, and method adopted for analyses using various instruments.

Chapter 3: -

This chapter consists of results obtained from various proxies. Here I have graphically represented all the data obtained from various analyses and explained the observed variations, which includes the radiocarbon dates for age determination and sedimentation accumulation rates at the core sites. The results from carbon and oxygen isotope analysis in cores AAS-9/21 and SK-129/CR-05 core for last 30 kyr predicting the changes in nutrient/ventilation conditions and temperature respectively have been described in this chapter. It further includes results of shell weight analysis carried out from core SK-129/CR-05 and SK-129/CR-02. Furthermore, description of results from B/Ca analysis of

cores AAS-9/21, SK-129/CR-05 and SK-129/CR-02 for understanding variations in $[CO_3^2]$ are provided. Variations in V/Ti from core AAS-9/21 are described in light of understanding the bottom water oxygenation conditions for last 30 kyr.

Chapter 4: -

The modern day distribution of carbonate ion content and dissolved oxygen in the Indian Ocean, and the vertical distribution and relation between $[CO_3^{2-}]$ and dissolved oxygen in the EAS is discussed here. Variation in sedimentation accumulation rates in three studied cores (AAS-9/21, SK-129/CR-02 and SK-129/CR-05) are discussed in detail in this section. Further I have discussed about the changes in deep-water circulation and temperature, which are deduced from carbon and oxygen isotopic ratios from these cores. The carbonate ion concentration from the Last Glacial Maximum (LGM) to the Holocene in deep-waters of the EAS is quantified using the B/Ca proxy, supported by the shell weight data. Oxygenation conditions at core sites were assessed using V/Ti ratios. Finally, a story of change in $[CO_3^2]$ since the LGM is presented in this thesis with necessary supportive data taken from the other studies. Possible mechanism responsible for this change is also discussed.

Chapter 5: -

This chapter provides a summary on the important observations made in the entire thesis. It further concludes the observation on carbonate ion variations at three different water depths from the LGM to the Holocene, and a significant carbonate ion increase during the last deglaciation observed at all depths.

List of Figures

and Younger Dryas (YD). White band indicates the Bølling-Ållerød (BA). The Last Glacial Maximum (LGM), deglaciation and Holocene are marked with arrows on the top axis.

List of Tables

1. INTRODUCTION

Climate change is one of the biggest challenges faced bymankind today which will gradually affect our future. Climate change basically includes the gradual increase in average temperatures of the atmosphere and ocean and this condition is termed as global warming. Global warming is caused due to the presence of greenhouse gases like water vapour, methane, nitrous oxide, carbon dioxide and other halogenated gases. These gases trap heat and warm the atmosphere. Out of all the gases, carbon dioxide is of major concern, as due to human impact of burning of fossil fuels the concentration of carbon dioxide is increasing sharplywith present monthly mean atmospheric concentrations of 411.2 ppmv recorded at the Mauna Loa Observatory (MLO). In the past, the concentration of carbon dioxide gas in the atmosphere has fluctuated between 180 to280 ppm between glacial to interglacial cycles for the last 800 kyr (Figure 1.1; Lüthi *et al.,* 2008).
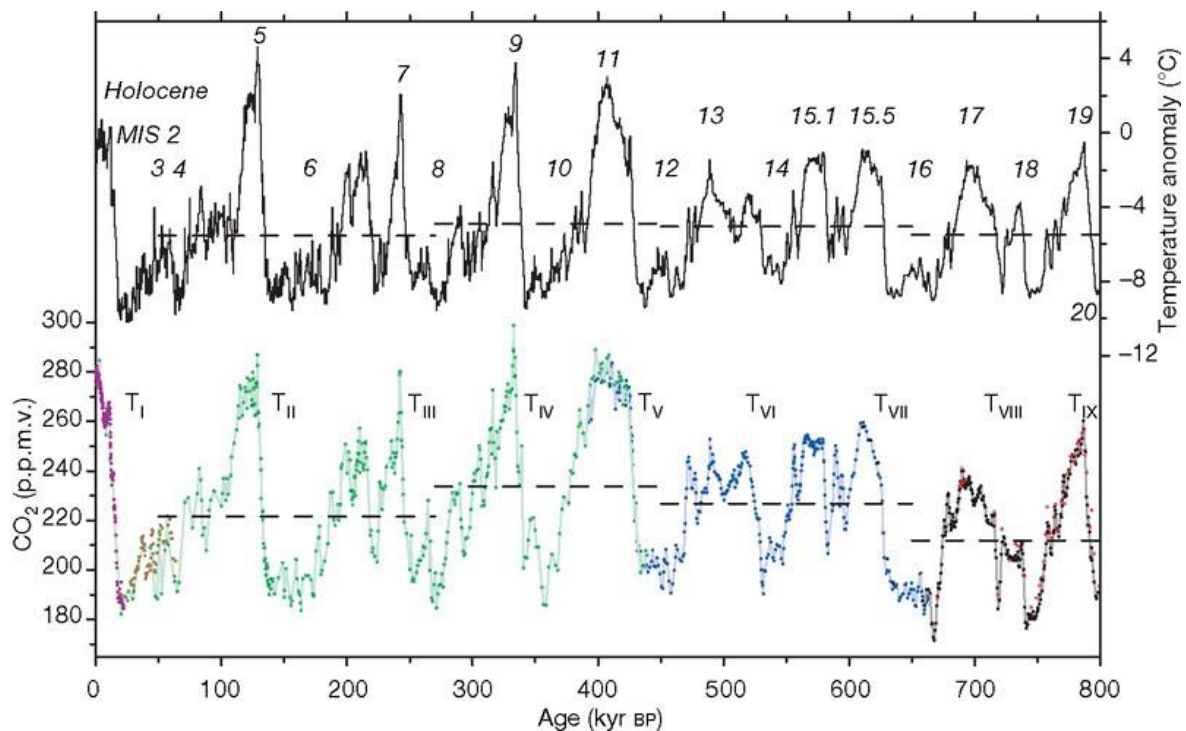
Figure1.1: The history of atmospheric CO_2 and air temperature recorded from air trapped in Antarctic ice cores for the last 800 kyr (Lüthi *et al.,* 2008).

Atmospheric CO_2 is in equilibrium with surface ocean and is taken up by the oceans through two major processes, biological and chemical (Figure 1.2). Biological process includes the biological pump wherein the CO_2 from surface layer is taken up by

phytoplankton during photosynthesis, thus capturing carbon in the organic matter. Chemical process involves dissolution of CO_2 in seawater forming carbonic acid (H_2CO_3) which dissociates into bicarbonate (HCO_3^-) and further into carbonate ion (CO_3^{2-}).

$$CO_2 \text{ (atm)} \leftrightarrows CO_2 \text{ (aq)} + H_2O \text{ (Sea water)} \leftrightarrows H_2CO_3$$

$$H_2CO_3 \leftrightarrows HCO_3^- + H^+$$

$$HCO_3^- + H^+ \leftrightarrows CO_3^{2-} + H^+$$
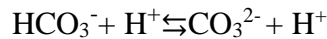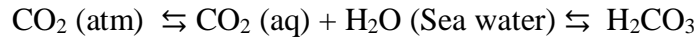
Dissolved inorganic carbon (DIC) species includes the free aqueous carbon dioxide (CO_2) (aq), HCO_3^- and CO_3^{2-}.

$$DIC = CO_2 \text{ (aq)} + [H_2CO_3] + [HCO_3^-] + [CO_3^{2-}]$$

$$\text{Total Alkalinity (TA)} = [HCO_3^-] + 2[CO_3^{2-}] + [B(OH)_4^-] + [OH^-] - [H^+] + \text{minor component}$$
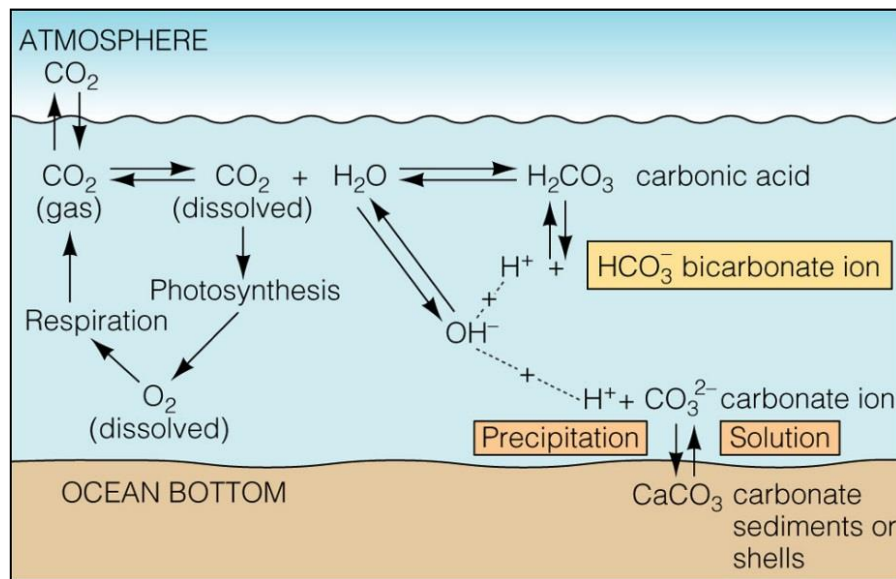
Figure 1.2: Schematic representation ofcarbon dioxide exchange between atmosphere -ocean and carbonate chemistry in sea water.

Alkalinity represents the excess base that affects deprotonation of aqueous CO_2 into HCO_3^- and CO_3^{2-}. Increase in alkalinity results in conversion of DIC to $[CO_3^{2-}]$, thus it leads to decrease in DIC. Lowering of DIC causes conversion of aqueous CO_2 to DIC. Thus the partial pressure of CO_2 decreases in surface waters which than effectively increases the CO_2 solubility in seawater thus decreasing atmospheric CO_2. Hence, any changes in the

concentration of alkalinity in seawater can lead to significant changes in taking up or giving out CO_2 from sea surface to atmosphere and thus influencing the climate at longer timescales.

$$[CO_3^{2-}] \approx \text{Alkalinity - DIC (Zeebe and Wolf-Gladrow, 2001)}$$

Many marine calcifying organisms like corals, foraminifera and coccolithophores precipitate CO_3^{2-} by combining with calcium to form calcium carbonate ($CaCO_3$) and build their exoskeletons, shells or other structures.

$$Ca^{2+} + CO_3^{2-} \rightarrow CaCO_3$$
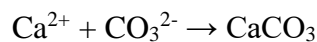
These shells/exoskeleton sink throughthe water column and remain preserved in the sediments for a long period of time after the death of the organism. These shells of calcareous organisms are fairly distributed in the world ocean, but their occurrence in any ocean depends on the $CaCO_3$ solubility in the deep ocean. The solubility of $CaCO_3$ in deep waters is mainly dependent on temperature, pressure and $[CO_3^{2-}]$ which determines the calcium carbonate saturation state (Ω) at particular depth. Hence the solubility of $CaCO_3$ in the deep waters is mainly controlled by the calcium carbonate saturation state (Ω). On contrary, because the surface waters are supersaturated with CO_3^{2-}, $CaCO_3$ precipitation is seen in surface waters. The calcium carbonate saturation state is defined by the product of carbonate ion concentration and concentration of calcium ions divided by the stoichiometric solubility product and expressed as:

$$\text{Calcium carbonate saturation state } (\Omega) = ([CO_3^{2-}] * [Ca^{2+}]) / K_{sp}^*$$

Where

$[CO_3^{2-}]$ = in situ carbonate ion concentration

$[Ca^{2+}]$ = in situ calcium ion concentration

K_{sp}^* = stoichiometric solubility, $K_{sp}^* = [CO_3^{2-}]$ saturation$* [Ca^{2+}]$ saturation

Wherein K_{sp}^* is the function of salinity, temperature and pressure.

The calcium carbonate has two polymorphs aragonite and calcite wherein aragonite crystal is orthorhombic and calcite crystal is trigonal. Further the calcite is more stable than the aragonite, hence aragonite dissolves faster than calcite and has higher K_{sp}^* than calcite. Calcium carbonate saturation state of aragonite is expressed as (Ω_{arg}) and calcium carbonate

saturation of calcite is expressed as (Ω_{cal}). Since the calcium carbonate formation and dissolution in seawater causes calcium ions to change by <1% in ocean the calcium carbonate saturation state (Ω) can be simplified and expressed in terms of concentration of carbonate ions only [CO_3^{2-}]:

Calcium carbonate saturation state (Ω) = [CO_3^{2-}] in situ / [CO_3^{2-}] saturation

The solubility of $CaCO_3$ in seawater is determined by the value of calcium carbonate saturation state (Ω), if Ω >1, then the waters are supersaturated with calcium carbonate and hence preservation of $CaCO_3$ shells is seen in such waters. Whereas, when Ω < 1, then waters areunder saturated with calcium carbonate and hence dissolution of $CaCO_3$ shells is seen in such waters. In waters where Ω = 1, the seawater is exactly in equilibrium/ saturation with respect to calcite and the depth in the water column at which Ω = 1 is called as the saturation horizon.

After the death of the calcifying organism their shell sink to the bottom and undergoes dissolution, liberating Ca^{2+} and CO_3^{2-} ions back into solution. The depth in seawater where the dissolution of $CaCO_3$ begins and increases dramatically is called as the Lysocline. Whereas, the depth at which all the calcium carbonate gets dissolved is called the Carbonate Compensation Depth (CCD) hence this is the depth at which the supply of $CaCO_3$ is balanced by dissolution. Since aragonite is less stable than calcite the lysocline and CCD are shallower for aragonite than calcite and referred to as the Aragonite Compensation Depth (ACD). In the Arabian Sea, ACD ranges from 250 m to 700 m and can remarkably vary in shallower continental margins (Berger, 1978) wherein the deepening and shallowing of ACD can occur due to supply of organic carbon from surface to the sediments. Usually where the productivity and organic carbon export to the sediment is high, the microbial decomposition of organic carbon in such sediments liberates CO_2 which decreases the pH and carbonate ion concentration of the ambient water, resulting in shallower ACD and vice versa.

Peterson and Prell, (1984) suggested the foraminiferal lysocline depth to be at 3800 m by using the percentage of whole planktic foraminifera, percentage of benthic foraminifera, weight percentage of carbonate and the percentage of coarse fraction in the sediments. Cullen and Prell, (1984) determined the foraminiferal lysocline depth in the equatorial Indian Ocean to lie at 3800 m, 3300 m in the Arabian Sea and 2600 m in the Bay of Bengal by studying the changes in relative abundance of species with depth. Initially CCD

in the Arabian Sea was concluded to be at 4800 m (Kolla *et al.,* 1976). But later, Cullen and Prell, (1984) observed the absence of whole foraminiferal test below the depth of 4600 m in the eastern equatorial region, below 5000 m water depth in the western equatorial regionand below 3000 m in the Bay of Bengal which is considered to be very similar to the foraminiferal compensation depth in Indian Ocean.

1.1 Factors affecting carbonate ion concentration in seawater

Carbonate ion concentration in the sea water is non-conservative and can be affected by (1) Biological processes

(2) Alkalinity Changes

(3) Mixing of deep water masses, and

(4) Air-Sea exchange

1.1.1 Biological Processes

➢ Photosynthesis

Photosynthesis is a process wherein CO_2 from the seawater, present in the form of DIC, is utilised by marine phytoplankton for production of organic carbon (Figure 1.3A). At rain rate ratio ($C_{organic}$: C_{CaCO_3}) of 4:1 (Broecker and Peng, 1982), photosynthesis consumes DIC and alkalinity of seawater by a ratio of 3.58:1 (Yu *et al.,* 2008) hence increases $[CO_3^{2-}]$ of surface waters. It is because of this reason $[CO_3^{2-}]$ of the surface waters of the world ocean is elevated.

$$106CO_2 + 16NO_3^- + HPO_2^{-4} + 122H_2O + 18H^+ \rightarrow (CH_2O)_{106}(NH_3)_{16}\,H_3PO_4 + 138O_2$$
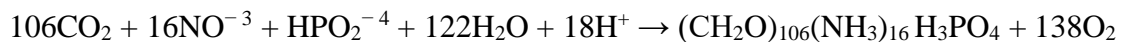
➢ Regeneration of nutrients/decomposition

This is a process wherein the dead organic matter which sinks down the water column is broken down into simpler forms using dissolved oxygen, leading to a release of CO_2 and nutrients in water column. The release of CO_2 increases DIC but decreases the alkalinity and hence the $[CO_3^{2-}]$ (Figure 1.3A).

$$(CH_2O)_{106}(NH_3)_{16}H_3PO_4 + 138O_2 \rightarrow 106CO_2 + 16NO_3^- + HPO_2^{-4} + 122H_2O + 18H^+$$

➢ Formation and dissolution of calcium carbonate

During the formation of calcium carbonate, carbonate ion is utilised and its concentration decreases in the water column.

$$Ca^{2+} + CO_3^{2-} \rightarrow CaCO_3$$
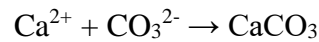
Whereas during dissolution, carbonate ion is released back in water, which increases the alkalinity and DIC of seawater by 2:1 ratio. This is also one of the process by which the decrease in $[CO_3^{2-}]$ and pH at deeper depths is compensated by dissolution of preserved calcium carbonate in sediments.

1.1.2 Alkalinity change

Number of process such as evaporation, precipitation and brine formation affect the surface alkalinity of the seawater. Theses processes are mostly involves changes in salinity and DIC of the sea water. Seawater $[CO_3^{2-}]$ is insensitive to salinity variation and could be calculated as:

$$[CO_3^{2-}] \approx ALK - DIC$$

Thus, seawater $[CO_3^{2-}]$ usually increases with increase in alkalinity by processes such as evaporation and ice formation, these increase the difference between alkalinity and DIC. However, changes occurring in seawater $[CO_3^{2-}]$ are relatively small due to evaporation and ice formation as both of theses processes affect alkalinity and DIC proportionally. Whereas, erosion and dissolution of $CaCO_3$, increases the seawater ALK and DIC in the proportion of 2:1 and drives up the seawater $[CO_3^{2-}]$ as can be seen Figure 1.3A.
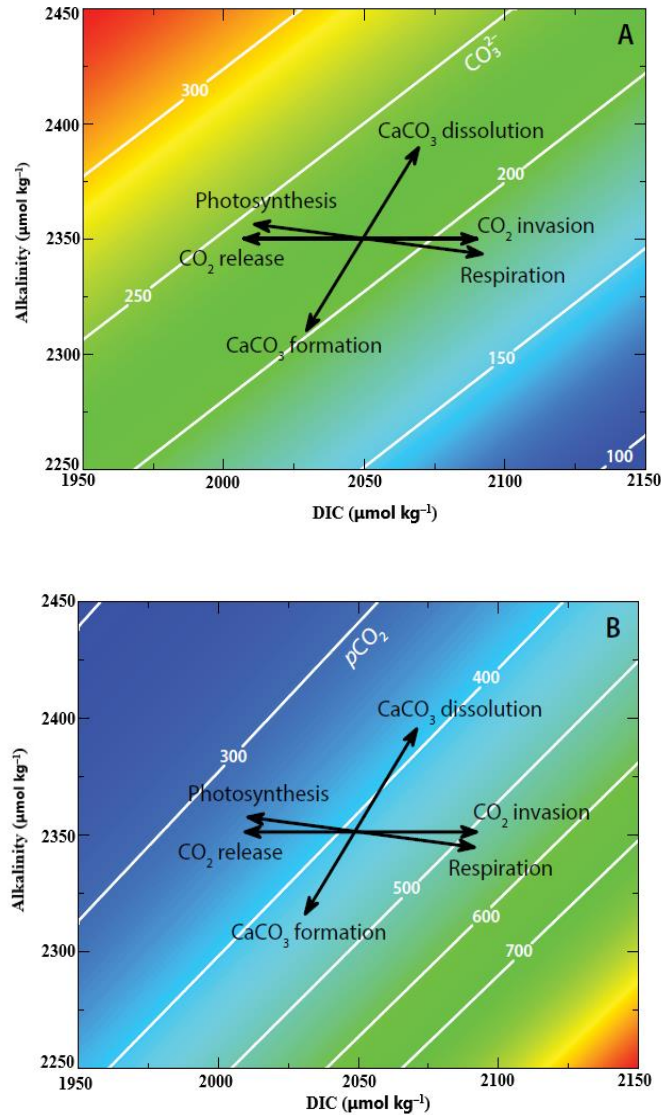
Figure 1.3: Graph showing the effect of various processes on (A) Carbonate ion concentration, $[CO_3^{2-}]$ (μmol/kg), and (B) pCO_2 (μatm) of surface sea water. Wherein $[CO_3^{2-}]$ and pCO_2 of seawater are calculated at temperature = 25°C, salinity = 35 (psu), pressure = 1 atm (water depth = 0 m) (Yu *et al.,* 2014).

1.1.3 Mixing of deep water masses

Every deep water masshas a unique preformed $[CO_3^{2-}]$. Furthermore, biological effects on the deep water masses are less significant and therefore mixing plays an important role in affecting $[CO_3^{2-}]$ of deep waters (Yu *et al*., 2008). North Atlantic Deep Water (NADW) has the highest $[CO_3^{2-}]$ of ~120 μmol/kg, North Pacific Deep Waters (NPDW) has the lowest $[CO_3^{2-}]$ of ~50 μmol/kg and the Southern Ocean has a $[CO_3^{2-}]$ of ~80 μmol/kg. Any mixing between these water masses can subsequently lead to a change in $[CO_3^{2-}]$.

Changes in $[CO_3^{2-}]$ of seawater due to air sea exchange can only be seen in case of surface water masses rather than the deep water masses. At the surface there are factors like temperature, salinity, CO_2 evasion/invasion which affect $[CO_3^{2-}]$. The temperature effect on $[CO_3^{2-}]$ is small, at about 0.5 μmol/kg per °C, whereas the seawater $[CO_3^{2-}]$ is insensitive to salinity variations (Yu *et al.,* 2008). The CO_2 evasion and invasion has opposite effect on $[CO_3^{2-}]$. CO_2 evasion is escape of CO_2 from the sea surface which results in an increase in $[CO_3^{2-}]$ of the surface waters and the opposite is seen in case of CO_2 invasion.

1.2 Distribution of modern day $[CO_3^{2-}]$ in the world Ocean

The carbonate ion concentration in seawater is a derived variable and cannot be directly measured due to the unavailability of suitable analytical methods. It is usually derived from any two primary variables (which can be directly measured from seawater) including Total Alkalinity (TA), pH, Total carbondioxide (TCO_2) and the partial pressure of carbon dioxide (pCO_2) in seawater. Although Byrne and Yao, (2008) and Sharp and Byrne, (2019) have attempted to directly measure the carbonate ion concentration in seawater through spectrophotometric measurements, but these methods are not widely used. The modern day vertical $[CO_3^{2-}]$ as well as sectional view of variation in $[CO_3^{2-}]$ in different oceans and water masses given in various studies (Yu *et al.,*2013; Yu *et al.,*2014) have been calculated and presented by using TA and TCO_2 data taken from the Global Ocean Data Analysis Project (GLODAP) (Key *et al.,* 2004).

Modern carbonate ion concentration of surface waters of all three oceans i.e. Indian, Atlantic and Pacific is greater than that of the deep waters (Figure 1.4) and it is as low as 60 μmol/kg in the deep waters of Northern Pacific and Indian Oceans (Broecker *et al.,* 2000). On contrary the $[CO_3^{2-}]$ of surface waters can beas high as 220 μmol/kg. This is because of the marine phytoplankton which consumes aqueous carbondioxide from seawater, thus consuming DIC and alkalinity in a ratio of 3.58:1, hence leading to an increase in $[CO_3^{2-}]$ of surface water. Organic matter formed at surface sinks to deeper depths and constantly undergoes decomposition while sinking, during which the oxygen from surrounding water masses is used up and CO_2 is released and thus decreases the $[CO_3^{2-}]$ of deep waters.

Deep water $[CO_3^{2-}]$ of the world ocean (Figure 1.5) is controlled by two major water masses, NADW formed in North Atlantic Ocean with a modern $[CO_3^{2-}]$ of~120 μmol/kg and deep waters formed in the Southern Ocean with a $[CO_3^{2-}]$ of~80 μmol/kg (Yu *et al.,* 2014).

At the NADW formation sites in the North Atlantic, there is an extensive utilisation of nutrients by phytoplankton which contributes to an increased $[CO_3^{2-}]$ and productivity in surface waters. These surface waters after gaining desired density, through intensive ice formation, sink to deeper depths forming the NADW. This process makes NADW a water mass having high oxygen concentration and low nutrients as evident from low PO_4 values close to 0.73 µmol/kg (Broecker *et al.*, 1995). Also since this watermass is newly formed, it is well ventilated and there is less accumulation of respired CO_2 making it the watermass with highest $[CO_3^{2-}]$ of~120 µmol/kg. Whereas, deep waters formed in the Southern Ocean have high nutrient contents due to under-utilisation of nutrients by phytoplankton as evident from high PO_4 values of 1.95 µmol/kg (Broecker*et al.*, 1995) which correspond to excess respired CO_2 in deep waters of Southern Ocean which is then released from the surface (Broecker and Peng, 1992) and transported to and absorbed by the North Atlantic Ocean.
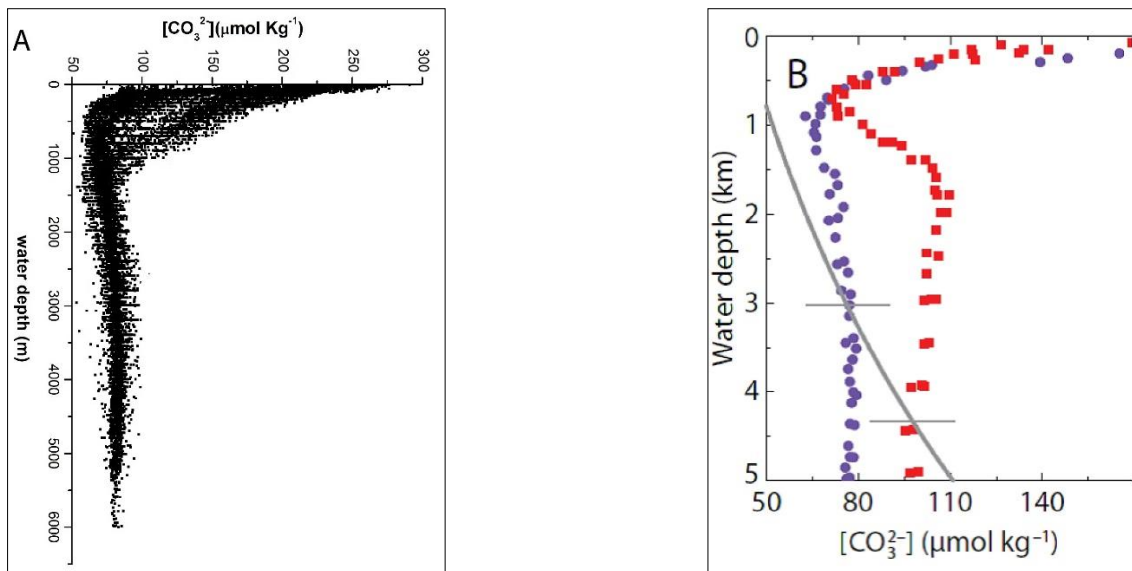
Figure 1.4: Vertical distribution of $[CO_3^{2-}]$ in (A) Indian Ocean, (GLODAP data) (B) Atlantic (red squares) and Pacific Ocean (purple circles), grey line describes the calcium calcite saturation in Atlantic and Pacific Ocean. The calcite saturation is the depth where in-situ $[CO_3^{2-}] = [CO_3^{2-}]$ saturation (is determined by pressure or water depth) (Yu *et al.,* 2014)

In the other two major oceans i.e. Pacific and Indian Ocean there is no formation of deep waters; hence deep waters here are exported from the North Atlantic and the Southern Ocean following the thermohaline circulation. So, as the NADW with a highest $[CO_3^{2-}]$ of~ 120 µmol/kg starts its grand journey from North Atlantic and moves to Indian and Pacific Ocean, there is continuous decomposition of sinking organic matter which give rise to utilisation of oxygen and cumulative accumulation/build-up of CO_2 which consequently

results in decreased $[CO_3^{2-}]$. Pacific Ocean being less ventilated and the last station for NADW (here it upwells and contributes to surface waters) the $[CO_3^{2-}]$ further decreases to ~ 60 µmol/kg (Broecker *et al.*, 2000). This transition of $[CO_3^{2-}]$ in deep waters of the world Ocean with NADW having highest $[CO_3^{2-}]$ to Pacific deep waters having lowest $[CO_3^{2-}]$ and Indian and Southern Ocean waters having moderate values is seen in Figure 1.5 (Yu *et al.*, 2014)
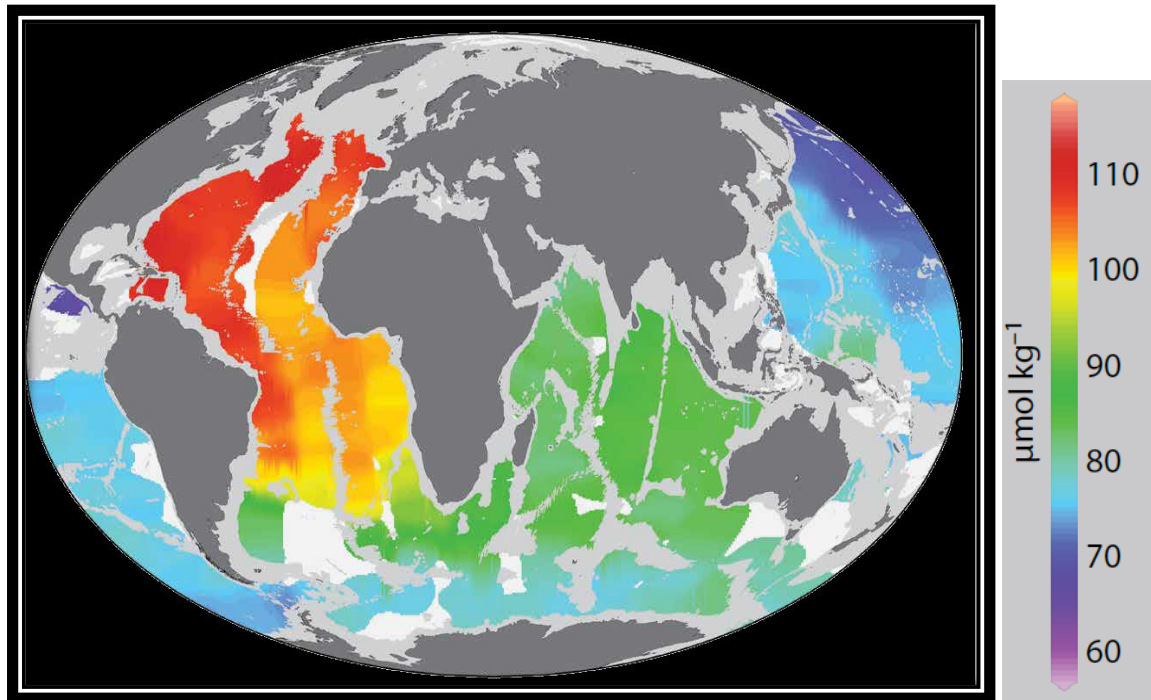
Figure 1.5: Schematic representation of modern day deep water $[CO_3^{2-}]$ at 3500 m water depth (Yu *et al.*, 2014).

1.3 Glacial - interglacial variations in carbonate ion concentration

Calcium carbonate studies in sediments gained more attention after the Swedish Deep-Sea Expedition (1947-1948), which were mainly focused on the amount of calcium carbonate content in the sediments on a glacial to interglacial timescale. The $CaCO_3$ content in sediments is important as it reflects the carbonate ion content in the overlying waters making them saturated or undersaturated with respect to carbonate ion, which in turn leads to preservation or dissolution of $CaCO_3$. Arrhenius, (1952) observed alternating highs and lows in $CaCO_3$ content in the Pacific Ocean during glacial and interglacial periods respectively, whereas, opposite trends of low $CaCO_3$ during glacial and high during interglacial were observed by Schott (1937) in the Atlantic Ocean. Initially these trends of

glacial to interglacial $CaCO_3$ in sediments were argued to be controlled by productivity changes (Arrhenius, 1952; 1988; Emerson and Bender, 1981; Archer, 1991) and by changes in the rate of dissolution (Berger, 1973; Broecker, 1971; Gardner, 1975). The Indian Ocean does not exhibit a specific pattern but a mixed pattern was observed with some sites showing a Pacific trend (Olausson, 1965; Oba, 1969; Naidu, 1991) and some showing an Atlantic trend (Peterson and Prell, 1985; Naidu *et al.,* 1993). However, some records showed prominent dissolution during interglacials (Murray and Prell, 1992; Bassinot *et al.,* 1994). In the Atlantic Ocean, better preservation of $CaCO_3$ in sediments was seen during the interglacials than during the glacials (Emerson and Bender, 1981; Crowley *et. al*., 1982; Archer, 1991; Coxall *et al.*, 2005). The Pacific and Indian Ocean showed preservation and lysocline deepening during the glacial period as compared to modern and interglacial period (Farrell and Prell, 1989; Wu *et. al.*, 1990; Karlin *et. al*., 1992; Howard and Prell, 1994; Stephens and Kadko, 1997). However, the use of the $CaCO_3$ proxy is only qualitative and limited by factors like variations in surface water productivity, dilution and pore water dissolution.

Foraminifera dissolution based proxies like selective species of planktic foraminifera susceptible and resistant to dissolution were used by Ruddiman and Heezen, (1967) and Berger, (1970a) and determined the different depths showing mild to severe calcite dissolution in the Atlantic Ocean. Tappa and Thunnel, (1984) used planktic foraminiferal biofacies to determine dissolution patterns in the Vema Channel. Benthic to planktic foraminifera ratio as a proxy was introduced by Arrhenius, (1952) which was based on the fact that benthic foraminifera are more resistant to dissolution than planktic foraminifera. Coarse fraction and fragmentation of planktic foraminifera were used (Berger, 1970a; Berger, 1973; Berger *et al.*, 1982) for determining the lysocline and the Calcium Carbonate Compensation Depth (CCD) depths in the western equatorial Pacific. Later, Lohmann, 1995 developed the shell weight proxy where he showed that the weight of whole foraminifera shells picked from a narrow size range provides a measure of the extent of dissolution and in doing so has the potential to serve as a paleocarbonate ion proxy. Shell weight proxy was then extensively used for studying deep carbonate ion content of Atlantic, Pacific and Indian Ocean (Broecker and Clark, 2001a; Broecker and Clark, 2001b; Broecker and Clark, 2001c; Broecker and Clark, 2002a; Broecker and Clark, 2002b; Broecker and Clark, 2003). This proxy showed large vertical gradients in CO_3^{2-} in the Atlantic and Pacific Ocean. The first attempt in utilisation of shell weights in the Indian Ocean showed that most intense calcite

dissolution undergoes from 3900 m depth and foraminiferal shell weights for depths above the carbonate ion saturation horizon depends on the surface water carbonate ion concentrations (Naik and Naidu, 2007; Naik and Naidu, 2008). Furthermore, the shell weight proxy was used to determine the changes in surface [CO_3^{2-}] from the Last Glacial Maximum (LGM) to Holocene (Naik *et al.,* 2010; Naik *et al.,* 2011) and on a million year's time-scale (Mungekar *et al.,* 2020). Planktic foraminifera shell weight proxy also revealed a rise in [CO_3^{2-}] of deep waters through better preservation during deglaciation in the northern Indian Ocean (Naik and Naidu, 2016). However, the shell weight proxy suffers due to certain drawbacks such as pore water dissolution (de Villiers, 2005) and optimal growth conditions in upwelling areas (Naik *et al.,* 2011; Naik *et al.,* 2013).

Another proxy, the size index proxy (Broecker and Clark, 1999) is based on the ratio of coarse calcite to total calcite and given by the formula; -

$$[(>63\mu m\ CaCO_3/\ Total\ CaCO_3) * 100]$$

The size index proxy was used to determine the [CO_3^{2-}] at various depths in the Atlantic, Pacific and Indian Ocean (Broecker and Clark, 1999; Naik and Naidu, 2007). Later the size index proxy was evaluated by Naik and Naidu, (2010) and found that apart from organic carbon respiration which lowers the pH of the bottom waters through release of CO_2 and causes dissolution and fragmentation of foraminiferal shells, dilution from terrigenous input also decreases the total $CaCO_3$ in sediments thus altering the size index. The changes in the productivity and the presence of coccolithophores (nannofossils) which compose the <10 µm fraction of $CaCO_3$, can give opposite picture at sites where productivity is dominated by cocolithophores, thus limiting the use of size index proxy.

Some of the other proxies developed to quantify carbonate ion concentration are zinc/ calcium (Zn/Ca) and cadmium/calcium (Cd/Ca) from benthic foraminiferal shells. Using the Zn/Ca ratio, studies yielded a 10-15 µmol/kg lower [CO_3^{2-}] during the LGM in comparison to the Holocene, in the deep North Atlantic and deep tropical Pacific Ocean with a $\sim$25–30 µmol/kg peak in Δ[CO_3^{2-}] (bottom water saturation state with respect to calcite) during the deglaciation. Although these proxies can quantify the [CO_3^{2-}], it is necessary to know the concentration of Zn and Cd of seawater in the past, which is why using these proxies remains a challenge. Other element/calcium ratios of benthic foraminifera such as magnesium/calcium ratio (Mg/Ca), lithium/calcium ratio (Li/Ca) and strontium/calcium ratio (Sr/Ca) are found to be sensitive to the temperature as well as carbonate ion saturation

(Δ [CO_3^{-2}]) of the overlying waters (Hall and Chan, 2004; Rosenthal *et al.,* 2006; Bryan and Marchitto, 2008; Doss *et al.,* 2018; Marchitto *et al.,* 2018, Ma *et al.,* 2020). Using the Mg/Ca in the western equatorial Pacific Ocean, [CO_3^{2-}] at 3.3 km depth was estimated to be ~19 μmol/kg higher during the Holocene than during the LGM. An increase in [CO_3^{2-}] during deglacial was observed by Fehrenbacher *et al*., (2006) and, Fehrenbacher and Martin*,* (2011), whereas, Sadekov, *et al.*, (2014) observed an ~30 μmol/kg increase in [CO_3^{2-}] during the LGM than the Holocene in the eastern Equatorial Pacific Ocean at 2.5 km depth. Furthermore, Rickaby *et al*., (2010) observed ~25 μmol/kg elevated [CO_3^{2-}] during the glacial in the Weddell Sea using Mg/Ca. In the Indian Ocean, Ma *et al.,* (2020) used element/Ca proxy where in the sample was analysed for several elements such as Mg/Ca, Li/Ca, Sr/Ca and uranium/calcium (U/Ca) to determine the [CO_3^{2-}] of deep waters in the Arabian Sea and the Bay of Bengal and observed a prominent increase in [CO_3^{2-}] of deep waters during the deglaciation in the Northern Indian Ocean. Besides the above proxies, X-ray Fluorescence (XRF) derived calcium/titanium ratio (Ca/Ti) together with the $CaCO_3$ content in sediments was also used to study the [CO_3^{2-}] variation on glacial to interglacial timescales in the South Atlantic Ocean (Gottschalk *et al.,* 2018).

Numerous studies have carried out the deep-water reconstructions of [CO_3^{2-}] in the major oceans of the world from LGM to Holocene using B/Ca proxies (Yu *et al.,* 2007; Yu *et al.,* 2010a; 2010b; 2013; 2014; Allen *et al.,* 2015; Kerr *et al.,* 2017) and showed that the [CO_3^{2}] variation from LGM to Holocene occurred in three stages, the LGM, deglacial period and Holocene. During the LGM, the deep water [CO_3^{2-}] in Indian and Pacific Ocean was 5 μmol/kg higher than the Holocene. Furthermore, during the deglaciation period, a 15 μmol/kg rise in [CO_3^{2-}] was seen which then decreased during the Holocene, hence both of these ocean basins showed <6 μmol/kg change in [CO_3^{2-}] from the LGM to Holocene (Yu *et al.,* 2010a). Whereas, the deep Atlantic Ocean showed an18 μmol/kg rise in [CO_3^{2-}] during the Holocene as compared to the LGM and it also showed a slight increase of 3 μmol/kg during the deglaciation (Yu *et al*., 2007; Yu *et al.,* 2010a). Allen *et al.,* 2015 showed a 60 to 90 μmol/kg rise in [CO_3^{2-}] during the Heinrich Stadial and higher [CO_3^{2-}] during the Antarctic Cold Reversal (14.5-12.8 kyr) than the LGM, in the upper deep waters of Southwest Pacific Ocean.

All of these studies showed a rise in [CO_3^{2-}] during the last deglaciation which was attributed to the escape of carbon dioxide from deep waters and further related to a two-step atmospheric rise in CO_2 (Monnin *et al*., 2001). The atmospheric CO_2 rise during deglaciation

is said to be caused due to the extensive upwelling of deep waters in the Southern Ocean (Anderson *et al.,* 2009) which contained stored CO_2. This stored CO_2 from deep waters entered the intermediate waters during the extensive upwelling in Southern Ocean, leading to lowered $[CO_3^{2-}]$ in intermediate waters (Yu *et al.,* 2008; Yu *et al.,* 2010b). The CO_2 from intermediate waters was then transferred to surface waters through upward mixing evident through increased pCO$_2$ and decreased carbonate ion concentration in surface waters of world ocean (Palmer and Pearson, 2003; Foster, 2008; Palmer *et al.,* 2010; Henehan *et al.,*2013; Naik *et al.,* 2015; Naik and Naik, 2018) and finally emitted to atmosphere leading to atmospheric rise in CO_2 (Monin *et al.,* 2001), thus invoking the deep ventilation hypothesis. But the recent intermediate and deep water $[CO_3^{2-}]$ reconstruction using B/Ca and δ^{11}B has revealed that during the LGM North Atlantic carbon pump efficiency was almost doubled as compared to Holocene which resulted in enhanced CO_2 sequestration in oceans through air-sea exchange and contributed to atmospheric CO_2 lowering (Yu *et al.,* 2019) during LGM. Thus the recent studies point towards two main processes involved in the rise of atmospheric CO_2: i) enhanced North Atlantic carbon pump during LGM which lowered the atmospheric CO_2 (Yu *et al.,* 2019) and ii) out gassing of deep water CO_2 through extensive upwelling in Southern Ocean which contributed to atmospheric rise in CO_2 during deglaciation (Yu *et al.,* 2007; Yu *et al.,* 2010a; 2010b; 2013; 2014; Allen *et al.,* 2015; Kerr *et al.,* 2017).

Studies carried out for understanding the variations in $[CO_3^{2-}]$ of intermediate waters using B/Ca in theSouth Atlantic Ocean (Lacerra *et al.,* 2017; Lacerra *et al.,* 2019) provided a different view on deglacial $[CO_3^{2-}]$. These studies reported decreased $[CO_3^{2-}]$ in the intermediate waters of the Atlantic Ocean (cores presently bathed by North Atlantic Deep Water; NADW) during deglaciation, accept for one South Atlantic core (KNR-159-5-990GGC, water depth = 1105 m) currently bathed by Antarctic Intermediate Water (AAIW), which showed deglacial increase in $[CO_3^{2-}]$ (Lacerra *et al.,* 2019). Earlier studies interpreted the decreased $[CO_3^{2-}]$ in intermediate waters of North Atlantic to be due to the outgassing of deep water CO_2 entering the intermediate waters and reducing the $[CO_3^{2-}]$ in intermediate waters (Yu *et al.,* 2008; Yu *et al.,* 2010b; Yu *et al.,* 2014). However, Lacerra *et al.,* (2019) attributed the decreased $[CO_3^{2-}]$ to increased remineralized carbon during Heinrich Stadial (HS1) and Younger Dryas (YD) when the AMOC was weak, and accumulated carbon due to increased residence time of intermediate waters which enhanced carbon respiration, increasing the ΣCO_2. The increased $[CO_3^{2-}]$ in core KNR-159-5-990GGC from the South

Atlantic is supported by elevated $[CO_3^{2-}]$ in core RR0503-83 at 1627m depth from the southwest Pacific Ocean (Allen *et al.,* 2015). The elevated $[CO_3^{2-}]$ in this core was mainly attributed to decreased remineralized carbon in AAIW during the deglaciation (Lacerra *et al.,* 2019) which again highlights the effect of carbon remineralization on $[CO_3^{2-}]$.

Additionally, the B/Ca proxy was also used for reconstructing millennial scale variability in $[CO_3^{2-}]$ of deep waters of Atlantic (Sosdian *et al.,* 2018; Chalk *et al.*, 2019), Pacific (Kerr *et al.*, 2017; Chalk *et al.*, 2019; Wan *et al.*, 2021) and Indian Ocean (Kerr *et al.*, 2017). Chalk *et al.,* (2019) used B/Ca along with the $\delta^{13}C$ from benthic foraminifera to study the changes in water mass structure and divided the changes in Atlantic Ocean circulation operating in 3 different modes: overturning mode, weak glacial mode and full glacial mode. Their data showed low $[CO_3^{2-}]$ and low pH during the glacial times in deep North Atlantic which closely resembles the ventilation changes in the North Atlantic. Overall the study showed the significant role played by the Southern Ocean in controlling atmospheric CO_2. The atmospheric CO_2 was drawn down by the Southern Ocean during the cold phases and it was stored in the expanded deep Southern Ocean cell, lowering carbonate ion and the pH of the deep waters. The study also highlighted the western basin accumulated more respired carbon and showed good correlation with the atmospheric CO_2 than the eastern basin. The study also confirmed the B/Ca proxy as a semi-conservative proxy and when used in combination with fully conservative tracers such as $\delta^{13}C$ and ε_{Nd} places a strong curb on the results. Wan *et al.,* (2020) linked carbonate ion variations in the South China Sea and Pacific Ocean to the sluggish deep water circulation, and increased carbon storage in the Pacific Ocean during glacials correlated with the increase oceanic alkalinity and hence would have contributed to drawdown of atmospheric carbon dioxide during glacials. On contrary, Rickaby *et al.* (2010), by taking Southern Ocean and Weddle Sea cores reconstructed the $[CO_3^{2-}]$ in deep waters for last 800 kyr and proposed that the atmospheric CO_2 is mostly controlled by the changes in alkalinity brought about by the shelf carbonate burial, which than controls the $[CO_3^{2-}]$ in deep waters. Similar to this, Kerr *et al.,* (2017) using Indian and Pacific Ocean cores showed high $[CO_3^{2-}]$ and preservation of $CaCO_3$ during glacials. These reconstructions were focussed on the carbonate preservation on long time scales and revealed that preservation during glacials was due to the drop in sea level, which resulted in decreased burial of neritic carbonate (including corals), which increased ocean alkalinity and in order to balance this alkalinity rise in the Indian and Pacific Ocean there was preservation of carbonate in deep ocean (Kerr *et al.,* 2017).

Through the observation of $[CO_3^{2-}]$ and the carbonate preservation in the Atlantic and Pacific Ocean on 1.5 Myr timescale, Sosdian *et al.,* (2018) came up with the idea of shifting of the calcium carbonate burial locus from the Atlantic to the Pacific Ocean. This mainly occurs through the changes in ventilation wherein the increase in stratification and corrosivity of Antarctic Bottom Water during the cold phases causes the dissolution of calcium carbonate in Atlantic sediments and this dissolution is balanced by the enhancing burial in Pacific Ocean which causes preservation of calcium carbonate during the glacials. The whole mechanism of shifting the locus of calcium carbonate preservation occurs through the changes in the $\Delta[CO_3^{2-}]$ of the deeper waters and not through the delivery of alkalinity during low sea levels (Sosdian *et al.,* 2018).

1.4 Proxies used in this study

1.4.1 Foraminifera

Foraminifera are protozoans with single cell and having a amoeboid internal structure. The cell mostly consist of a nucleus, vacuoles and cytoplasm which are usually protected by a shell or 'test' which is made out of calcium carbonate or agglutinated sand particles. The size of these foraminiferal shells usually ranges from 0.1 to 1.5mm. Many of the foraminifera species have multiple chambers which keeps increasing in size as the foraminifera grows. Forams are pervasive in marine environments; and widely found in tropics, polar seas, surface ocean, deepest seafloor, salt marshes and estuaries. Foraminiferal tests along with the remains of coccolithophorids, diatoms, radiolarians, pteropods, and other calcareous nanofosils make up the sediment which is present at the bottom of the sea and distributed to a larger extent beyond the continental margins and above the CCD.

Planktic foraminifera are free floating near-surface dwelling organisms and are found from the surface mixed layer to the thermocline. The greatest concentration of foraminiferal species and individuals are seen in the upper 100-150 m water column where the solar light penetration is maximum. Benthic foraminifera are bottom-dwelling organisms, those dwelling at the sediment-water interface are called as epifaunal species and those dwelling in upper 10 cm of sediments are called as infaunal species. Foraminifera precipitate their shell by using calcium and carbonate ion from seawater thus capturing seawater conditions during shell formation, and after the death of these organisms their shells sink to the bottom and remain preserved in the sediment for several thousands of years

thus making them very powerful tools for surface as well as bottom water paleoceanographic reconstructions.

Paleoceanographic reconstructions using foraminifera can be done by two main techniques; non-destructive technique and the destructive technique. Non-destructive technique involves the study of abundance and morphology of foraminifera by observing the physical properties of shell under the microscope. Relative abundance of planktic and benthic foraminifera can be used to determine physico-chemical conditions prevailing at that time. For example, the relative abundance of planktic foraminifera *Globigerina bulloides* has been extensively used to reconstruct monsoon upwelling history in the Arabian Sea (Prell, 1984; Naidu and Malmgren, 1996; Naidu, 2007; Godad *et al*., 2011). The morphology of benthic shells are used to reconstruct bottom water oxygenation condition in the Arabian Sea as well as in the world oceans (Severin, 1983; Kaiho, 1990; Nigam *et al.,* 1992; Naik *et al.,* 2017; Khare *et al.,* 2017; Suokhrie *et al.,* 2017). The Benthic Foraminiferal Number (BFN) is also extensively used to reconstruct the organic carbon content in the sediments, as the foraminiferal number and their distribution is closely linked to the transport of organic carbon to the sea floor and organic carbon in the sediment (Smart, 1994; Wahyudi and Minagawa, 1997; Van der Zwaan *et al.,* 1999; Dulk *et al*., 2000; Cappelli *et al.,* 2019). Several studies have used benthic foraminifera as a proxy for indicating the organic carbon content in sediments (Smart, 1994; Wahyudi and Minagawa, 1997; Van der Zwaan *et al.,* 1999; Dulk *et al*., 2000). It is well understood that the organic carbon content in the sediments is closely related to the oxygen content. In sediments having higher organic carbon content, oxygen from the water column is utilised for the decomposition of organic matter which is very commonly observed in the oxygen minimum zone of the Arabian Sea at the depth of 200-1500 m.

Destructive technique involves the dissolution and analysis of shells to determine their isotopic and elemental compositions in order to decipher the paleoclimatic conditions. It includes the use of proxies like carbon and oxygen isotopes, boron isotopes, Mg/Ca, Zn/Ca and B/Ca in foraminifera. The stable isotopic analyses of foraminifera were initiated in the early fifties (Urey *et al*., 1951; Emiliani and Epstein, 1953; Emiliani, 1955), while the first successful attempts to analyse trace element ratio of foraminiferal tests were made in early eighties (Boyle, 1981; Boyle and Keigwin, 1985). Later, carbon and oxygen isotope proxies and trace element ratios in planktic and benthic foraminifera were successfully utilised for paleoclimate investigations.

1.4.2 Shell weight of foraminifera

The shell weight proxy was initially developed by Lohmann, (1995). Shells of foraminifera are made of primary and secondary calcite. Foraminifera synthesize their chamber from primary calcite and the secondary calcite is responsible in thickening the shells and forms the crust. The deposition of secondary calcite is dependent on the $[CO_3^{2-}]$ concentration of the ambient waters, if the $[CO_3^{2-}]$ of ambient waters is higher it leads to increase in thickness of the chambers and results in heavier shell weights. This was supported by culture experiments carried out in laboratory under controlled conditions (Spero *et al.,* 1997; Bijma *et. al.,* 1999; Russell *et. al.,* 2004). Thus by measuring the foraminifera shell weight one can determine the $[CO_3^{2-}]$ of the ambient waters. This proxy was extensively used to determine the surface and deep water carbonate ion content in Atlantic, Pacific and the Indian Ocean (Broecker and Clark,2001a; Broecker and Clark, 2001b; Broecker and Clark, 2001c; Broecker and Clark, 2002a; Broecker and Clark, 2002b; Broecker and Clark, 2003). When CO_2 dissolves in seawater, it forms DIC which comprises of H_2CO_3, HCO_3^- and CO_3^{2-} (see section 1). Planktic foraminifera utilise CO_3^{2-} in seawater to form their shells and thus record $[CO_3^{2-}]$ of surface waters during their formation. After the death of foraminifera, their shells sink to the bottom and remain preserved in the sediment for thousands of years thus recording the history of $[CO_3^{2-}]$ in surface waters which then can be used to determine the changes in atmospheric CO_2. The preservation of foraminiferal shells in sediment is again controlled by the bottom water $[CO_3^{2-}]$. Better preservation of shells is seen in waters having high carbonate ion content and dissolution is observed in low carbonate ion waters. Thus the well/ poorly preserved shells reflect $[CO_3^{2-}]$ of ambient waters. The shell weight proxy in Indian Ocean was successfully utilised for estimating the surface carbonate ion content as well as the variation in atmospheric CO_2 from LGM to Holocene (Broecker and Clark, 1999; Broecker and Clark, 2001a; Naik and Naidu, 2007; Naik and Naidu, 2008; Beer *et al.,* 2010; Naik *et. al.,* 2010; Naik *et. al.,* 2011; Naik *et. al.,* 2013; Naik and Naidu, 2014; Naik and Naidu, 2016).

Although the shell weight proxy was extensively used to determine the surface carbonate ion concentration, there are studies which show that the shell weights are not only controlled by ambient $[CO_3^{2-}]$ but also controlled by diverse factors like presence of symbionts, genotypic variability and optimum shell growth conditions of the species. Planktic foraminifera host various kinds of algae as intracellular symbionts, which provide foraminifera with the supply of limiting nutrients like nitrogen, in oligotrophic environments

(LeKiffre *et al.,* 2020), which help in supplying energy through photosynthesis, calcification and growth. Symbionts, through photosynthesis elevate the oxygen, pH and $[CO_3^{2-}]$ in waters very close to the test wall, thus helping the foraminifera in calcification and growth. Hence the shell weight of foraminifera bearing the symbionts may not reflect the actual $[CO_3^{2-}]$ of ambient waters. Various genotypes of planktic foraminifera can exist within a single morphotype which can have different responses to changes in environment. For example, the different genotypes of *G. bulloides* morphospecies can have different response of shell weight to $[CO_3^{2-}]$ in ambient waters (Beer *et al.,* 2010).

The optimum shell growth conditions of the species is generally defined by the ecological niche which in simpler terms refers to the suitable environment in which the species exist, and that suitable environment will provide optimum growth conditions to the foraminiferal species which results in an increase in shell weight as well as abundance of that species (de Villiers, 2004). For example, *Neogloboquadrina pachyderma* thrives in cooler, low saline and high nutrient waters and hence shows high abundance as well as higher shell weights in the South Atlantic surface waters which are cooler, low saline and nutrient rich (de Villiers, 2004). In the Western Arabian Sea (WAS) which is an intense upwelling site, shell weights of *G. bulloides* were controlled by surface water $[CO_3^{2-}]$ from 22 –16 kyr time period, whereas from 16 kyr to present the shell weights were seen to be controlled by the optimum growth conditions (Naik *et al.,* 2011). On contrary, Beer *et al.,* (2010) observed that shell weights were neither controlled by $[CO_3^{2-}]$ nor by optimal growth conditions. Additionally, pore dissolution is also one factor which affects the use of this proxy. The dissolution of foraminiferal shells above the lysocline is mostly caused due to oxidation of the organic matter sourced from increased surface productivity and occurs at the sediment water interface. Intense oxidation of organic carbon at the sediment water interface leads to a carbonate ion gradient between the sediment water interface and the overlying saturated bottom waters, which induces dissolution (de Villiers, 2005). The presence of benthic fluff layer is also noted in several studies (Smith *et al.,* 1996; Beaulieu and Smith, 1998; Martin and Sayles, 1999; Beaulieu, 2002) which varies from a thin layer in the open ocean to several centimetres in shallow waters (Beaulieu, 2002). This fluff layer consists of phytodetritus which undergoes decomposition, releases CO_2 and decreases $[CO_3^{2-}]$, resulting in calcium carbonate remineralisation of foraminiferal shells transiting this layer thus decreasing the shell weight and hence this supralysoclinal dissolution hinders the use of shell weight proxy in the marine environment (de Villiers, 2005).

1.4.3 Geochemistry of sediments

The concentrations of elements in marine sediments are regulated by discrete processes which comprise of terrestrial influx, biological processes, *in-situ* precipitation and hydrothermal activities occurring within the water column. The elements enter into the sea through rivers, atmosphere and hydrothermal activities. As soon as they arrive in the marine environment they are acted upon by series of reactions which can be chemical or biological, depending upon the sedimentation site. After undergoing various reactions, they either dissolve or precipitate and get deposited in sediments and remain preserved for several years. The geochemical analysis of such sediments can then predict their depositional environment. Thus elemental concentration and ratios are largely used in paleoceanography for studying provenance changes, paleo-productivity and oxygenation conditions of the bottom waters. Elements such as aluminium and titanium have been used to trace terrigenous inputs in the Arabian Sea (Nath *et al*., 1989; Pattan *et al.,* 2003; Pattan *et al*., 2017; Pattan *et al.,* 2019), barium for biogenic productivity (Schmitz, 1987) and chromium, manganese, molybdenum, rhenium, uranium, vanadium, cerium, cadmium and zinc as they undergo changes in response to varying oxygen concentrations in bottom waters and hence can be used to scrutinize the bottom water oxygenation conditions on a longer time scale (Pattan and Pearce, 2009; Chandana *et al.,* 2017).

1.4.4 Oxygen isotope ratios

An oxygen atom has two isotopes O^{16} and O^{18} which are reffered to as "light" oxygen and "heavy" oxygen respectively. The "light" oxygen is composed of 8 protons, and 8 neutrons, hence resulting in atomic weight of 16 (O^{16}) and is most common type of oxygen atom found in environment. On the other hand, O^{18} has two extra neutrons which result in atomic weight of 18 thus making it heavier than O^{16} and is rarely found in environment only about 1 in 500 atoms of oxygen. The oxygen isotope fractionation and the environmental factors affecting their concentration are shown in Figure 1.6. The difference in atomic weights of these atoms impart distinct physical properties i.e. O^{16} being lighter, easily evaporates from seawater than O^{18}, and O^{18} being heavier falls out first during precipitation. This process makes the rainfall depleted in O^{18} and seawater from where evaporation takes place becomes enriched in O^{18}. Foraminifera calcify from seawater, locking up the seawater isotopic signatures into their shells and in turn when these shells are analysed they reflect the oxygen isotopic composition of seawater. These analyses are done on an Isotope Ratio Mass Spectrometer (IRMS) which compares the sample with a reference and isotopic ratios are expressed using the following equation.

$$\delta^{18}O_{sample} = \{[(^{18}O/^{16}O)_{sample}/(^{18}O/^{16}O)_{standard}]-1\} * 1000$$

The stable oxygen isotope analyses of foraminifera were initiated by Urey in 1947 wherein he investigated the isotope exchange reactions between water and CO_3^{2-}. Later in 1948 he pointed out that these small differences can be measured. The isotopic values observed were also found to be consistent with the isotopic ratios of biogenic carbonates. Later Emiliani in 1954 used oxygen isotope ratios of foraminiferal shells from deep-sea sediments and reconstructed the glacial–interglacial climate swings in Late Pleistocene (Emiliani, 1955). He was also responsible for the initial use of Marine Isotope Stages (MIS) (Emiliani, 1955). Shackleton in 1967 revised Emiliani's work and found that the foraminiferal oxygen isotope records are not only controlled by changes in seawater temperature but are indeed controlled by changes occurring in the oxygen isotopic composition of seawater. In subsequent years, MIS finally emerged as a basic stratigraphic tool (Shackleton and Opdyke, 1973). Thus, paleoceanography field was launched by developing fundamental concepts through the intense work carried out by Urey, Shackleton and their students. Since than analysing foraminiferal shells and estimating the oxygen

isotopic composition became one of the most effective techniques for reconstructing paleoceanography and paleoclimate.
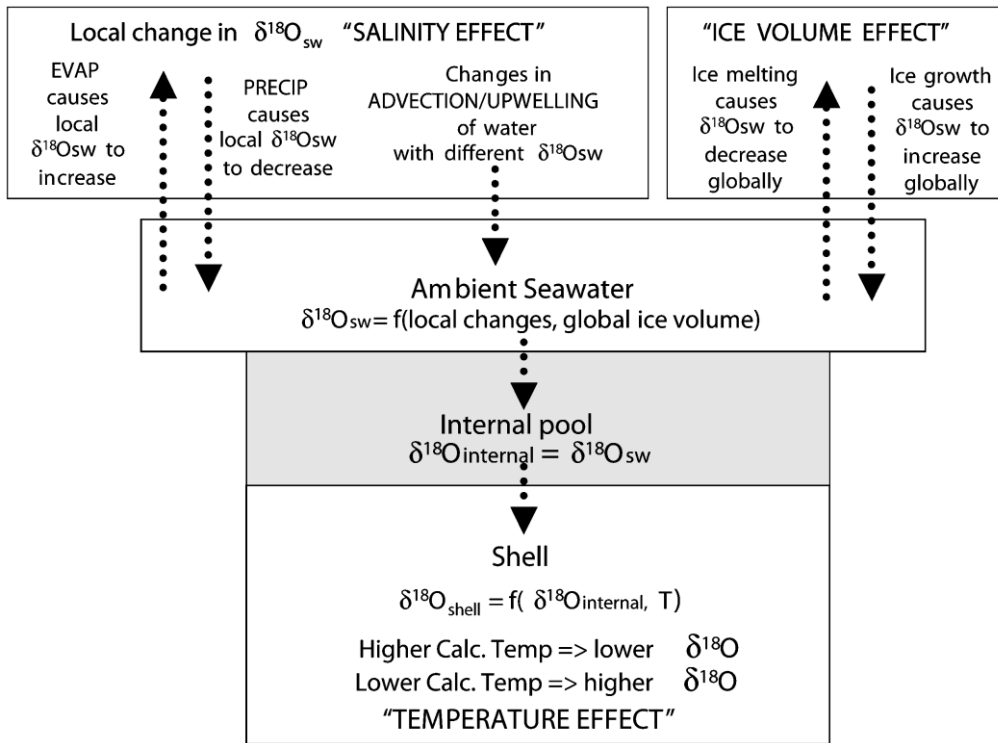
Figure 1.6: Schematic representation of oxygen isotopic fractionation and environmental factors affecting oxygen isotope ratios in foraminiferal shells (Ravelo and Hillaire-Marcel, 2007).

1.4.5   Carbon isotope ratios

Carbon has two stable isotopes ^{12}C, ^{13}C and one radioactive isotope [14]C. Amongst the three isotopes, ^{12}C is abundant than ^{13}C, and [14]C. Atmospheric CO_2 dissolves in seawater and forms aqueous CO_2. Part of this aqueous CO_2 is converted to DIC and part of it is taken up by phytoplankton during photosynthesis. There is preferential uptake of ^{12}C during photosynthesis i.e. during photosynthesis ^{12}C which is lighter is taken up first than [13]C (Figure 1.7). In this process ^{12}C gets trapped in organic matter and ^{12}C concentration in seawater DIC decreases, whereas concentration of ^{13}C increases. Oxidation of this organic matter at deeper depths than releases nutrients and CO_2 which is rich in [12]C. Lighter ^{12}C coming from oxidation of organic matter dilutes ^{13}C present in seawater DIC. Foraminifera calcify their shells from seawater DIC and thus $\delta^{13}C$ of foraminiferal shells reflects the carbon isotopic composition of DIC in seawater and thus can be used as a proxy for determining nutrient contents of water masses and tracing the water mass itself as every

22

water mass has an unique concentration of nutrients and DIC. These foraminiferal shells are analysed by using an IRMS and isotopic ratios are expressed using the following equation.

$$\delta^{13}C_{Sample} = \left\{ \frac{\left(\frac{^{13}C}{^{12}C}\right)_{Sample}}{\left(\frac{^{13}C}{^{12}C}\right)_{Reference}} - 1 \right\} * 1000$$

Carbon isotopic ratios of foraminiferal shells have been successfully utilised for reconstructing the nutrient contents of water masses and paleo circulation in the Atlantic and Pacific Ocean (Duplessy *et al.,* 1983; Zahn *et al.,* 1986; Duplessy *et al.,* 1988; Curry *et al.,* 1988; Bickert and Mackensen, 2003), Indian Ocean (Kallel *et al.,* 1988; Naqvi, 1993; Ahmad and Labeyrie, 1994; Murgese and Deckker, 2007; Ahmad *et al.,* 2008; Piotrowski *et al.*, 2009; Raza and Ahmad, 2013; Raza and Ahmad, 2014; Banerjee *et al.,* 2017), Southern Ocean (Siani *et al.,* 2013). The $\delta^{13}C$ along with $[CO_3^{2-}]$ derived using certain proxies, are also used for tracing water masses (eg. Yu *et al.,* 2008). The difference in $\delta^{13}C$ ratios of epifaunal and deep infaunal species of benthic foraminifera can also be used for determining the bottom water oxygenation conditions in sediments (Schmiedl and Mackensen, 2006; Hoogakker *et al.,* 2014; Hoogakker *et al.,* 2015).
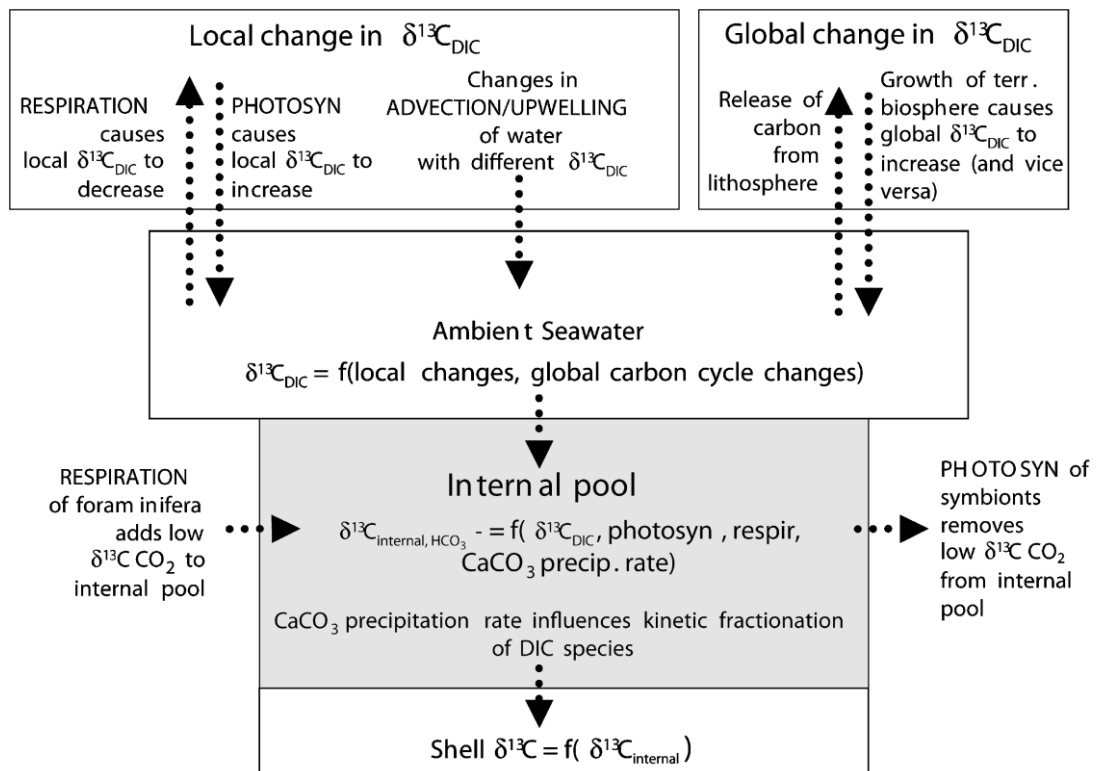
Figure 1.7: Schematic representation of carbon isotopic fractionation and environmental factors affecting carbon isotope ratios in foraminiferal shells (Ravelo and Hillaire-Marcel, 2007).

1.4.6 Boron/calcium proxy

Boron is the 10th most abundant and a conservative element in seawater, having a residence time of ~10-20 Ma (Foster *et al.,* 2012). Boron in seawater is generally sourced from weathering of igneous rocks (Lemarchand *et al.,* 2002), hydrothermal vents (Smith *et al.,* 1995), and fluids from accretionary prisms (You *et al.*, 1993). The dissolved boron in seawater exist as boric acid ($B(OH)_3$) and borate ion (BOH_4^-), the boric acid is trigonally coordinated and borate ion is tetrahedrally coordinated. The concentration of both the species is dependent on the pH of seawater, at lower pH virtually all boron is in the form of $B(OH)_3$ species, whose concentration goes on decreasing as the pH of seawater increases and at high pH all boron is present as $B(OH)_4^-$ species whose concentration increases with increasing pH (Figure 1.8a).

$$B(OH)_3 + H_2O \longrightarrow B(OH)_4^- + H^+$$
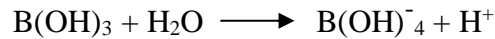
Two stable isotopes of boron exist in nature they are, the heavier ^{11}B (~80%) and lighter ^{10}B (~20%). As the abundance of boron species vary their isotopic composition must also vary accordingly (Figure 1.8b). Isotope exchange reaction between these two species is given by

$$^{11}B(OH)_3 + {}^{10}B(OH)_4^- \leftrightarrow {}^{10}B(OH)_3 + {}^{11}B(OH)_4^-$$
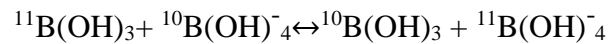
The equilibrium constant ($^{10}_{11}K$) for the above reaction is greater than unity hence products are stable (Kakihana, 1977; Oi, 2000a). During precipitation of calcium carbonate in sea water, boron gets incorporated in foraminifera shells as $B(OH)_4^-$ (Hemming and Hanson 1992; Hemming *et al.*, 1995; Sanyal *et al.*, 2000). Since only the charged species enters the calcite, boron isotopic composition of calcite also increases with pH.

$$CaCO_3 + B(OH)_4^- \rightarrow Ca(HBO_3) + HCO_3^- + H_2O$$
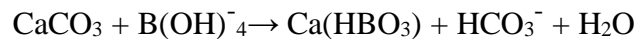
Isotopic composition of marine carbonates ($\delta^{11}B_{marine\ carbonates}$) is ~15-20 ‰ which is lower than that of seawater ($\delta^{11}B_{SW}$= 39.61 ‰). As the isotopic concentration of borate increases with pH its isotopic concentration should also increase in marine carbonates. Hence $\delta^{11}B$ and boron /calcium (B/Ca) are proxies which can be used to estimate the paleo-pH of seawater. Ocean pH is a component of the ocean carbonate system and is controlled by the ratio of ALK to DIC. pH also closely parallels [CO_2] and [CO_3^{2-}] hence boron isotope

ratios of fossil marine carbonate, typically foraminifera, may thus be used to investigate past atmospheric pCO$_2$, [CO$_3^{2-}$] and changes in the deep ocean carbon cycle.

Boron isotopic studies were initiated by Spivack *et al.*, (1987) on clay minerals who showed that boron in clays is not in isotopic equilibrium with seawater and thus cannot be used for indicating depositional environments and is not suitable for paleoenvironmental reconstructions; instead marine carbonates can be used for paleoenvironmental reconstructions as seawater is the main source of boron for marine carbonates. Later, studies carried out on biogenic carbonates by experimental biological precipitation of calcite and foraminiferal culture experiments showed that preferentially the borate ion is incorporated in carbonates and boron isotopic compositions of these carbonates is strongly dependent on pH of seawater in which they calcify (Hemming and Hanson 1992; Hemming *et al.*, 1995; Sanyal *et al.*, 1996; Sanyal *et al.*, 2000; Sanyal *et al.*, 2001). This proxy was used for different foraminiferal species and species specific calibrations were made (Henehan *et al.*, 2013; Yu *et al.*, 2013). Boron isotopic composition of planktonic foraminifera was successfully utilised for reconstructing pH and pCO$_2$ of surface waters in the North Atlantic, equatorial Atlantic, Sub-Antarctic Atlantic (Foster, 2008; Seki, 2010; Henehan *et al.*, 2013; Yu *et al.*, 2013), Pacific Ocean (Pearson and Palmer, 1999; Palmer and Pearson, 2003; Honisch and Hemming, 2005; Foster, 2008; Martinez-Boti, 2015) and in the Arabian sea (Palmer *et al.*, 2010; Naik *et al.*, 2015).

Boron/calcium is a proxy which is based on the above explained principle of boron isotopic composition i.e. as the pH of seawater increases the borate ion will get incorporated in foraminiferal shell thus increasing boron concentration in shell. Initially this proxy was used to reconstruct the paleo-pH and carbonate ion concentration in surface waters. Paleo-pH of surface waters have been reconstructed using the B/Ca ratios of planktic foraminifera in the Atlantic Ocean (Yu *et al.*, 2007; Foster, 2008; Yu *et al.*, 2013) and Pacific Ocean (Tripati *et al.*, 2009; Tripati *et al.*, 2011). But the use of this proxy is limited by factors like surface water DIC, wherein B/Ca ratios in planktonic foraminifera were initially found to be controlled by pH and later it was observed to be also controlled by the DIC wherein carbonate species competes with borate ion for incorporation in calcite and thus reflect the abundance of DIC in seawater rather than the pH (Allen *et al.*, 2012). Boron partition coefficient K_D is also one of the controlling parameter of B/Ca based pCO$_2$ reconstruction (Tripati *et al.*, 2009; Tripati *et al.*, 2011; Naik and Naidu, 2014). Naik and Naidu, (2015)

carried out pCO_2 reconstructions in the Western Arabian Sea (WAS) and the Eastern Arabian Sea (EAS) using different K_D given by Tripati *et al.,* (2009).
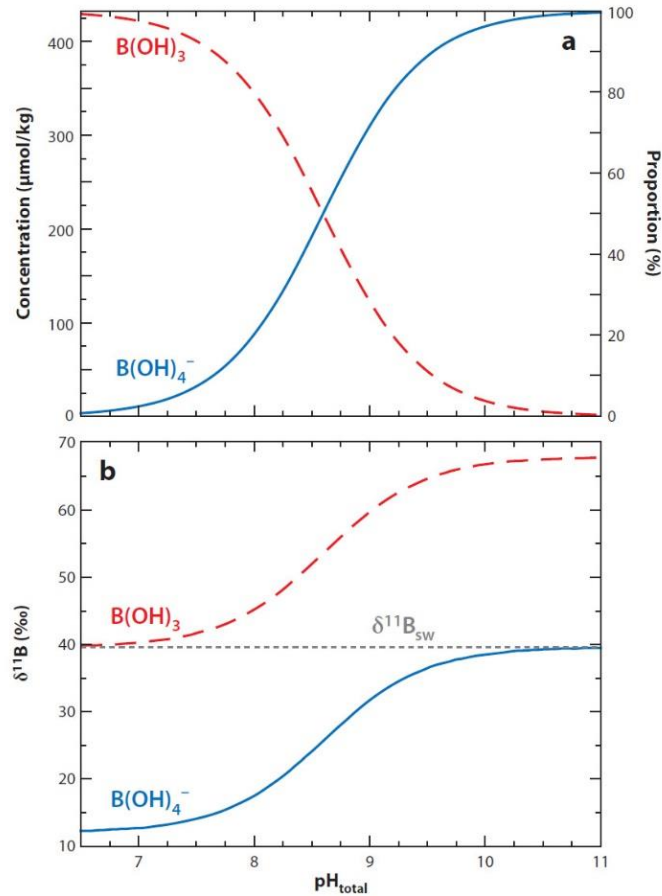
Figure 1.8: The schematic graph depicts the variation in (a) concentration of borate ion [B(OH)$_4^-$] and boric acid [B(OH)$_3$] with seawater pH and (b)isotopic composition of borate ion [B(OH)$_4^-$] and boric acid [B(OH)$_3$] with seawater pH. Under the surface water conditions (T=25°C, S=35 psu) with $\delta^{11}B_{SW}$ = 39.61 ‰ (Foster *et al*., 2010) and total boron of 432.6 µmol/kg (Lee *et al.,* 2010). Image source Rae *et al.,* 2011.

Results showed that the WAS acted as sink for CO_2 whereas the EAS acted as source as well as sink for CO_2 for last 25 kyr. However currently, the WAS is an extensive upwelling site and acts as strong source of CO_2 and the EAS shows weaker upwelling and CO_2 outgassing. The contrasting results indicate that the use of K_D for pCO_2 reconstructions is not a robust one.

The epifaunal benthic foraminifera species *Cibicidoides wuellerstorffi* resides at the sediment water interface and utilises calcium and carbonate ion from the overlying bottom waters to build their $CaCO_3$ shell and thus smartly incorporates and records the variations in oxygen and carbon isotope composition as well as the boron concentration (as mentioned

above, incorporation of boron in calcite is highly controlled by pH) of deep waters in the shell. Hence B/Ca values of benthic foraminifera reflect the carbonate chemistry of bottom waters and thus this proxy can be used to determine the $[CO_3^{2-}]$ of the bottom waters. Boron isotopic measurements require large sample size for analysis and hence the measurements carried out are located at few locations and have low temporal resolution (Hönisch *et al.*, 2008; Yu *et al.*, 2010b; Rae *et al.*, 2011). Hence B/Ca in benthic foraminifera (*Cibicidoides wuellerstorffi* and *Cibicidoides mundulus*) are employed after extensive core top calibrations and it clearly shows a linear relationship with the deep-water Δ $[CO_3^{2-}]$ (Figure 1.9), from which the $[CO_3^{2-}]$ in deep waters can be calculated. This proxy requires a smaller sample size for analysis and also no significant effects of temperature and dissolution are seen on B/Ca ratios of benthic foraminifera. This proxy has also been utilised by paleoceanographers to quantify the $[CO_3^{2-}]$ of bottom waters on glacial to interglacial timescales in all the three major oceans of the world (Yu *et al.*, 2007; Yu *et al.*, 2010a; 2010b; 2013; 2014; Allen *et al.*, 2015, Kerr *et al.*, 2017).
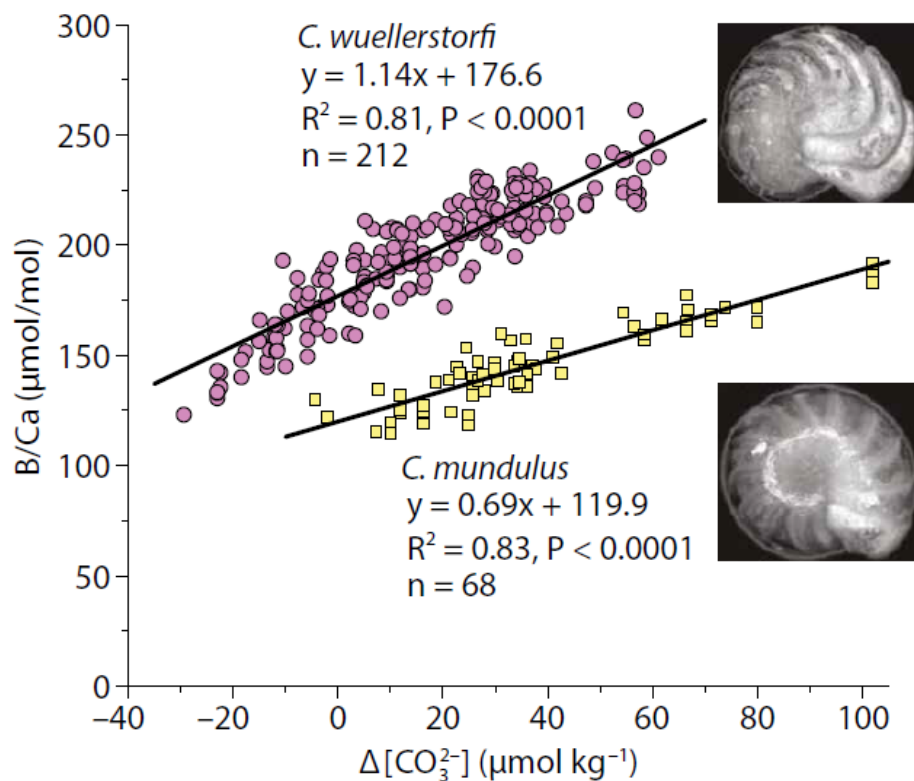
Figure 1.9: Graphical representation depicting the linear relationship between B/Ca and carbonate ion saturation ($\Delta[CO_3^{2-}]$) (Yu and Elderfield, 2007; Brown *et al.*, 2011; Rae *et al.*, 2011; Raitzsch *et al.*, 2011; Yu *et al.*, 2013a). The equations mentioned in this figure are used to calculate Δ $[CO_3^{2-}]$ and $[CO_3^{2-}]$ is further calculated (see section 2.3.6 for details). Plot from Yu *et al.* (2014).

1.5 Study hypothesis

The atmospheric CO_2 concentration has varied between 180 to 280 ppm on glacial to interglacial timescale for the last 800 kyr (Lüthi *et al.,* 2008). The specific process underlying these variations is partially known and is still debated. However, the oceans are being proposed as the major controllers of this glacial-interglacial CO_2 concentration (Archer *et al.,*2000*;* Sigman and Boyle*,* 2000). Oceans control CO_2 in the atmosphere by drawing it in and out, through its surface. Carbon dioxide in oceans is taken up by two main processes, biological and chemical process (refer to section 1). Chemical processes include dissolution of CO_2 in surface water which forms the DIC in seawater. This process mostly occurs between 20-60° N latitude and intensively in the southern hemisphere (Takahashi *et al.,* 2009). Thus this part of the global oceans acts as a sink for atmospheric CO_2. Whereas CO_2 is given out of the oceans through processes like intense upwelling, wherein the subsurface waters rich in nutrients and CO_2 upwells at the sea surface and leads to the increase in partial pressure of CO_2 in surface water thus exhaling CO_2 from surface, thus acting as source of CO_2 to the atmosphere. This exhaling of CO_2 mostly occurs in the tropical belt between 14° N to 14° S. Wherein, the tropical Pacific 14° N-14° S is the largest source of CO_2 to atmosphere whereas the Nordiac Seas and parts of Arctic Seas in the North Atlantic are the largest sinks for CO_2 (Takahashi *et al.,* 2009).

Southern temperate (14°-50° S) Indian Ocean is seen to act as a sink for atmospheric CO_2 while north of 14° N i.e. the north western Arabian Sea act as source of CO_2 during peak upwelling time in summer monsoon (June, July and August) due to high monsoon wind speed and higher *p*CO_2 in sub-surface waters (Takahashi *et al.,* 2009), thus making the Arabian Sea a strong source of CO_2 to atmosphere after the equatorial Pacific (Takahashi *et al.,* 2002; Sarma *et al.,* 2003).The *p*CO_2 in the Arabian Sea is found to be above 355 µatm for most part of the year (Sarma *et al.,* 1998) and thus a perennial source of CO_2 to the atmosphere (Somasundar *et al.,*1990; Kumar *et al.,* 1992; George *et al.,* 1994; Goyet *et al.,* 1998; Sarma *et al.,* 1998; Sarma *et al.,* 2000, Sarma *et al.,* 2003). Although the Arabian Sea acts as the source of CO_2, it is the western and the North Arabian Sea which majorly contribute to the emitted *p*CO_2 rather than the EAS wherein, the excessive influx of fresh water from precipitation and river runoff from the Western Ghats of India decreases the *p*CO_2 in surface waters of the EAS. Hence the Arabian Sea shows a considerable spatial contrast in *p*CO_2.

The spatial pCO_2 contrast in the Arabian Sea has also been maintained on the glacial to interglacial timescale. The western Arabian Sea was seen to act as a constant source of the CO_2 to atmosphere for last 29-5 kyr (Palmer *et al.,* 2010) whereas the EAS has acted as the constant sink for atmospheric CO_2 for last 25 kyr (Naik *et al*., 2015; Naik and Naik, 2018), accept during the deglaciation wherein the surface waters of the EAS showed a spike in pCO_2 and emitted CO_2 to the atmosphere during the time period of 15-13 kyr (Naik *et al*., 2015; Naik and Naik, 2018). Although the WAS constantly emitted CO_2 to atmosphere for 29 kyr its intensity was maximum from 14 – 11 kyr, during the deglaciation (Palmer *et al.,* 2010), indicating similar processes control pCO_2 variations in the EAS and WAS during the deglaciation. A similar pCO_2 spike in surface waters of western and East Equatorial Pacific (Palmer and Pearson, 2003; Martinez-Boti *et al.,*2015), south-west Pacific (Shao *et al.,* 2018), Caribbean Sea (Foster, 2008), Equatorial and South Atlantic (Henehan *et al.,*2013; Martinez-Boti *et al.,* 2015), North Atlantic (Ezat *et al.,* 2017) and Southern Ocean (Moy *et al.,*2019, Shuttleworth *et al.,* 2021) was also observed, indicating a global event which is considered to be the cause of deglacial atmospheric CO_2 rise. Simultaneously, the intermediate water studies indicate deglacial incursions of depleted radiocarbon activity ($\Delta^{14}C$) into the intermediate waters of the Arabian Sea (Bryan *et al.,* 2010) and Pacific Ocean (Marchitto *et al.,* 2007; Stott *et al.,* 2008; Lindsay *et al.,* 2015) which were attributed to the incursions of lighter isotopic carbon from deeper waters through extensive upwelling in Southern Ocean. Similar studies carried out in intermediate waters of the Atlantic Ocean showed lowered $[CO_3^{2-}]$ due to the penetration of deep water CO_2 in intermediate waters (Yu *et al.,* 2008; Yu *et al.,* 2010b; Yu *et al.,* 2014) (as these two parameters are inversely proportional to each other). Studies in deeper waters showed increased $[CO_3^{2-}]$ in all the three major oceans of the world (Yu *et al.,* 2010a, 2010b, 2013, 2014; Allen *et al.,* 2015; Kerr *et al.,* 2017; Ma *et al.,* 2020). The Indian Ocean exhibited a rise of~10 µmol/kg, Atlantic Ocean showed a rise of~21µmol/kg and Pacific Ocean observed rise of~11 µmol/kg during the deglacial (Yu *et al.,* 2010a). This was attributed to the escape of CO_2 from deep waters leading to increased $[CO_3^{2-}]$ during deglacial time. All these studies point to previously isolated glacial carbon stored in the deep ocean which was re-exposed to the atmosphere through extensive wind driven upwelling of deep waters in the Southern Ocean during the last deglaciation (Anderson *et al*., 2009; Yu *et al*., 2010). This glacial carbon was released in the form of CO_2 which raised the $[CO_3^{2-}]$ of deep-waters. This signal was then transferred to intermediate waters of the global oceans, thus depleting its radiocarbon signal and decreasing $[CO_3^{2-}]$ during the deglaciation. This lighter CO_2 then entered the surface waters

producing a pCO$_2$ spike in global waters and was finally emitted from surface waters giving rise to a two-step rise of atmospheric CO$_2$ during deglaciation.

My study is based on hypothesis that, as Naik *et al.,* (2015) observed a clear peak of pCO$_2$ in surface waters of the EAS and Bryan *et al.,* (2010) observed the Δ^{14}C depletion of the intermediate waters due to the incursion of isotopically light carbon during the deglaciation, then there should also be rise in [CO$_3^{2-}$] of deep waters of the Arabian Sea during the deglaciation. Therefore, I intend to understand the variations in [CO$_3^{2-}$] in deep and intermediate waters from theLGM to Holocene with special emphasis on the deglaciation. Although the variation in [CO$_3^{2-}$] has been studied in all the three major oceans of the world, there has been very small amountof work carried out in the Indian Ocean, one in the southwest Indian Ocean (Yu *et al.,* 2010a; Kerr *et al.,* 2017) and other in the Arabian Sea off southern tip of Indian peninsula (Ma *et al.,* 2020), whereas, the other parts of Indian Ocean like the Arabian Sea remain unexplored. The Indian Ocean being unique and different from the Atlantic and Pacific Ocean, there is a need to explore it more and understand the variation in [CO$_3^{2-}$] of deep-waters.

The deglaciation time also coincides with the changes in the deep-water circulation of the Arabian Sea, wherein increased flow of Antarctic Intermediate Water (AAIW) was observed during the Heinrich Stadials (Jung *et al.,* 2009; Yu *et al.,* 2018) and decreased the intensity of the Oxygen Minimum Zone (OMZ). The OMZ in the Arabian Sea are depths where oxygen concentration falls between 0-0.5 ml/l (Schulte *et al.,* 1999) and result in the Carbon Maximum Zones (CMZ) (Paulimer *et al.*, 2011). The Carbon Maximum Zones are associated with high DIC, low pH and low carbonate ion content, inducing CaCO$_3$ dissolution. Several studies in the Arabian Sea have shown poor preservation or dissolution of CaCO$_3$ shells in the OMZ regions (Calvert *et al.,* 1995; Singh, 1998; Singh *et al,* 2006; Sing *et al.,* 2007; Naik *et al.,* 2014). On the other hand, better preservation of CaCO$_3$ shells is also observed in the OMZ of Arabian Sea due incursions of oxygenated waters during the stadials (Klöcker and Henrich, 2006; Boning and Bard, 2009; Naidu *et al.*, 2014). These studies figure out a close relationship between oxygen, CO$_2$ in seawater and CaCO$_3$ in sediment, wherein higher oxygen concentrations are associated with lower CO$_2$ and better preservation of CaCO$_3$.
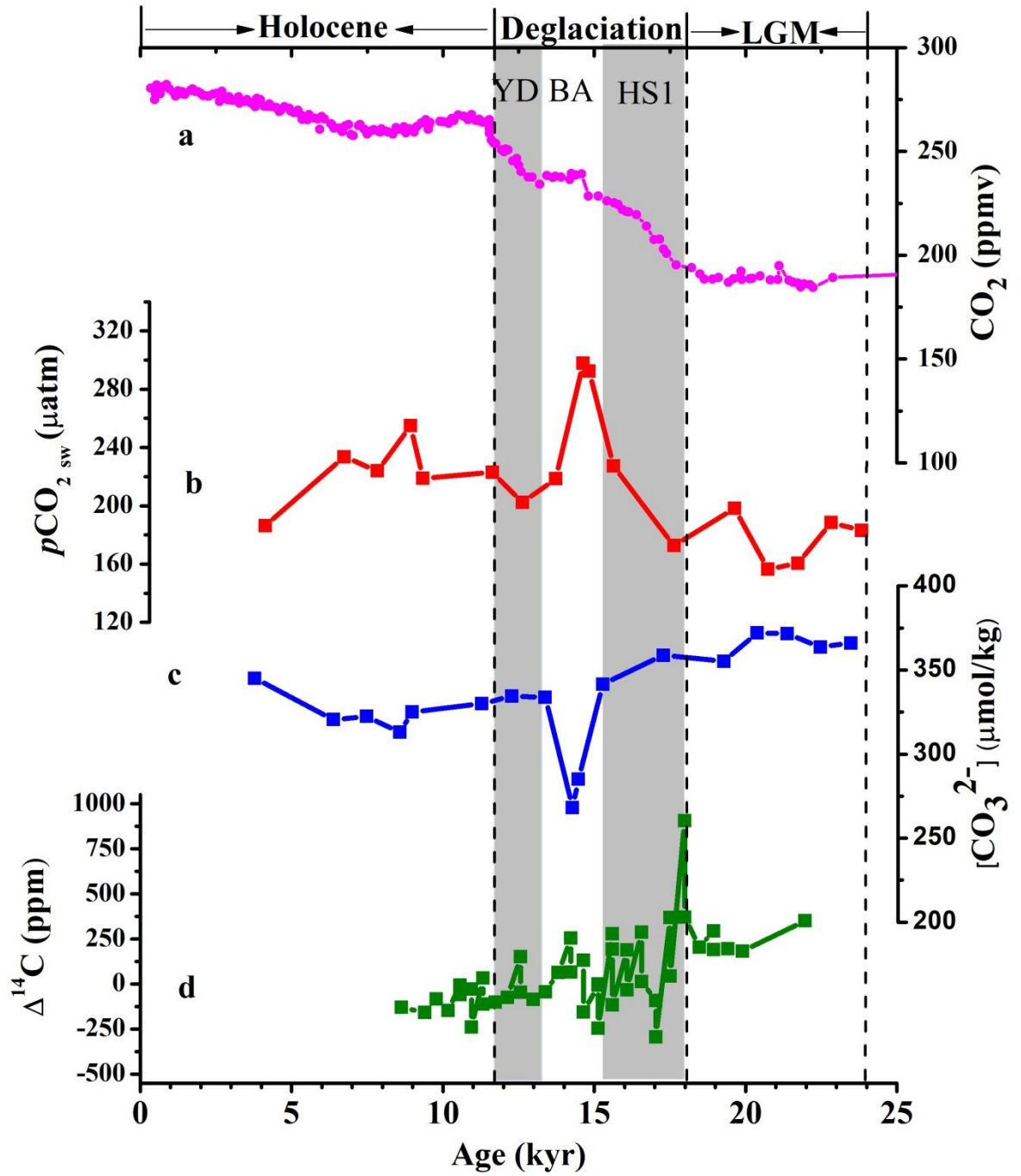
Figure 1.10: Graph showing variation in (a) atmospheric CO_2 (Bazin *et al.,* 2013), (b) surface water pCO_2 (Naik *et al.,* 2015), (c) surface water $[CO_3^{2-}]$ (Naik and Naik, 2018), and (d) radiocarbon activity (^{14}C) of intermediate waters (Bryan *et al.,* 2010).

My thesis objectives were framed in light of this hypothesis.

1.6 Objectives

My thesis is aimed at fulfilling the following objectives:

I. To understand the Last Glacial Maximum to Holocene changes in carbonate ion concentration in deep waters of the Eastern Arabian Sea.

II. To understand variations in bottom water oxygenation from the Last Glacial Maximum to Holocene in accordance with carbonate ion concentration in deep waters of the Eastern Arabian Sea.

2. STUDY AREA, MATERIALS AND METHODS

2.1 Study Area: -Eastern Arabian Sea

The eastern Arabian Sea (EAS) is geographically located between the eastern side of Laxmi-Laccadive Ridge and the western coast of India. The surface circulation of Arabian Sea is controlled by summer and winter monsoon winds which develops surface currents that run in exactly opposite direction to each other in both seasons, and contribute to upwelling and productivity in this region. This region also receives huge fresh water runoff during the summer monsoon from the Western Ghat rivers, which brings considerable changes in surface salinity of the EAS (Banse, 1959, 1968; Darbyshire, 1967; Johannessen *et al.,* 1987; Shetye *et al.,* 1990). The south eastern Arabian Sea (SEAS) also receives low salinity waters from the Bay of Bengal (BoB) brought in by the West Indian Coastal Current (WICC) during the northeast monsoon. Hence the SEAS shows the influence of summer monsoon as well as winter monsoon which brings about considerable changes in hydrography. Narmada and Tapi are the two major rivers that bring sediments into this region. The sediments here are mostly a mixture of terrigenous and biogenous material. The terrigenous sediments are comprised of silt and clay and the biogenous sediments consist of benthic and planktic foraminiferal shells along with traces of pteropods and diatoms (Govil and Naidu, 2010). Another important feature of the Arabian Sea is the world's thickest Oxygen Minimum Zone (OMZ) at 200-1250 m depth, with oxygen concentrations falling to ≤ 5 µmol/kg.

2.1.1 Surface water circulation

Surface circulation in the Arabian Sea is governed by the monsoon. It experiences a unique climate throughout the year with semi-annual reversal of surface currents during the northeast (Figure 2.1) and southwest (Figure 2.2) monsoons. Currents developed during these seasons run in exactly opposite directions to each other. On account of these currents, upwelling is mostly seen during the southwest monsoon along Somalia, Oman and the West Coast of India (Wyrtki, 1973) due to Ekman transport of waters, which leads to high inputs of nutrients to surface waters and gives rise to higher productivity.

During the northeast monsoon, the wind direction reverses and results in development of northeast monsoon current, which flows in opposite direction to the Somalia

current. This wind reversal causes an onshore Ekman transport of surface waters, which suppresses upwelling and lowers productivity in the western and southern Arabian Sea. Whereas extensive convective mixing is observed at the head of the Arabian Sea (Madhupratap *et al.,* 1996; Reichart *et al*., 1998) and results in high biological productivity (Yentsch and Phinney, 1992; Banse and English, 1993) which causes the formation of an extensive OMZ at a depth of 150 to1200 m (Wyrtki, 1973; Naqvi, 1991).
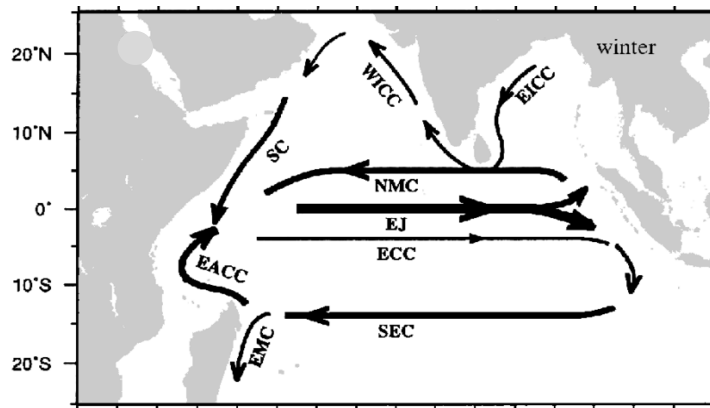
Figure 2.1: Schematic of major surface currents in the northern Indian Ocean during the Northeast monsoon (Winter). The major currents depicted are: South Equatorial Current (SEC), Northeast Monsoon Current (NMC), Equatorial Jet (EJ), Equatorial Counter Current (ECC), East African Coastal Current (EACC), Somali Current (SC), West India Coastal Current (WICC), East India Coastal Current (EICC) and East Madagascar Current (EMC) (From Shenoi *et al.,* 1999).
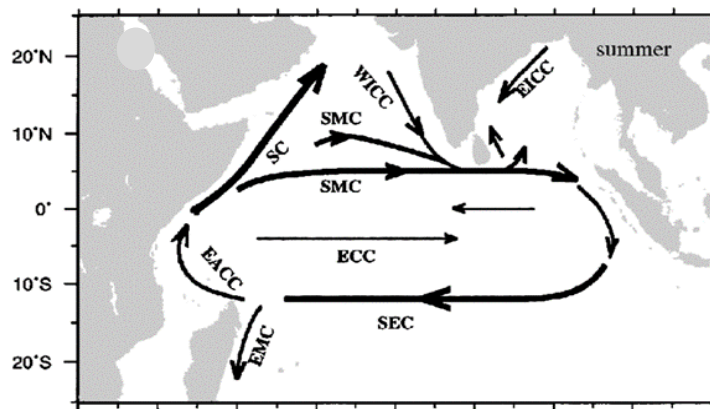
Figure 2.2: Schematic of major surface currents in the northern Indian Ocean during the southwest monsoon (Summer). The major currents depicted are: South Equatorial Current (SEC), Equatorial Counter Current (ECC), East African Coastal Current (EACC), Somali Current (SC), Southwest Monsoon Current (SMC), West India Coastal Current (WICC), East India Coastal Current (EICC) and East Madagascar Current (EMC) (From Shenoi *et al.,* 1999).

The EAS receives annual rainfall of 1600 km^3 and is comparable to annual Ganga-Brahmaputra run off of about 1,176 km^3 (Dai and Trenberth, 2002). Additionally, 80 % of the precipitation on the Western Ghats finds its way into the EAS through numerous streams and rivers (Shankar and Shetye, 1999). This leads to the lowering of near surface salinity off the southwest coast of India during July-August (Banse, 1959, 1968; Darbyshire, 1967; Johannessen *et al.,* 1987; Shetye *et al.,* 1990). However, the surface salinity in the EAS during summer monsoon is seen to be below 36 psu and drops as much as 33.5 psu off southwest coast of India for the duration of winter monsoon (Behara *et al.,* 2019). Freshening of EAS waters are also observed during the northeast monsoon due to inflow of low salinity water from the BoB along with the WICC flowing from south towards north (Thadathil and Gosh, 1992; Rao and Sivakumar, 1999; Shenoi *et al.,* 1999; Jensen, 2001; 2003; Durand *et al.*, 2004; Prasanna kumar *et al.,* 2004; Shankar *et al.,* 2005; Masson *et al.,* 2005; Gopalakrishna *et al.*, 2005; Durand *et al.*,2007; Thadathil *et al.,* 2008; Nyadjro *et al.,* 2012).

2.1.2 Terrigenous inputs into the Eastern Arabian Sea

The Arabian Sea receives input of lithogenous sediments by fluvial as well as aeolian sources. Aeolian sediments are mostly sourced from the Arabian and Thar Desert (Manjunatha and Shankar, 1992) whereas the fluvial sources mostly include the sediment discharge from Indus River which brings about 300 to 675 million tons of sediment per year (Milliman *et al.,* 1984). Narmada and Tapti River bring in~60 million tons of Suspended Particulate Matter (SPM) per year (Borole *et al.,* 1982). Sediment brought down by these rivers are larger in volume in comparison to the sediments discharged by rivers from the Western Ghats. For this reason, the sedimentation rates in the southeast Arabian Sea are comparatively lesser than the northern Arabian Sea (Manjunatha and Shankar, 1992).

2.1.3 Upwelling and OMZ in the Eastern Arabian Sea

The eastern Arabian Sea experiences semi-annual wind reversals which affects numerous processes like surface circulation, upwelling, productivity, precipitation, salinity, temperature, terrestrial inputs and CO_2 uptake. During the southwest monsoon, winds blow parallel to the Indian Coast which causes Ekman Transport of water away from the coast and results in upwelling of cooler and nutrient rich subsurface waters which later contribute to productivity in the Arabian Sea. The EAS experiences milder upwelling in comparison to the Western Arabian Sea (WAS) (Shetye *et al.,* 1990; Muraleedharan and Prasanna Kumar,

1996) which causes a mild increase in productivity in the EAS. High primary production in the WAS causes export of produced carbon, whereas in the EAS, the carbon is recycled (Sarma, 2004). The exported carbon in the form of organic matter undergoes remineralisation/decomposition throughout the water column, consuming oxygen and liberating CO_2. Hence the excessive liberated CO_2 together with sluggish intermediate water ventilation in the Arabian Sea causes development of a strong and perennial OMZ with oxygen concentration reaching upto < 5 μmol/kg at depths of 200-1200 m. In addition, strong winds blowing over the North Arabian Sea (NAS) during the northeast monsoon cause cooling and convective mixing (Madhupratap *et al.,* 1996; Reichart *et al.*, 1998) which result in cooler and nutrient rich subsurface waters to come to surface and leads to higher productivity (Yentsch and Phinney, 1992; Banse and English, 1993) which later also contributes to the extensive OMZ development.

Although mild upwelling and low productivity is seen in the EAS as compared to the WAS, the OMZ formed is oriented mostly towards the central and the eastern AS rather than the WAS. This shift in OMZ is caused due to strong advection of O_2 rich Persian Gulf Water (PGW) and Red Sea Water (RSW) and the transport of organic detritus from highly productive western Arabian Sea to less productive EAS through eastward moving currents. Oxygen Minimum Zones in the Arabian Sea are also termed as Carbon Maximum Zones (CMZ) (Paulmier *et al.,*2011) and are associated with high Dissolved Inorganic Carbon (DIC), low pH and low carbonate ion content inducing $CaCO_3$ dissolution. On account of strong and perennial OMZ formed at intermediate waters of the Arabian Sea, several studies have reported dissolution of $CaCO_3$ shells (Calvert *et al.,* 1995; Singh, 1998; Singh *et al,* 2006; Singh *et al.,*2007; Naik *et al.,* 2014b).

2.1.4 Carbon dioxide system in surface waters of Eastern Arabian Sea

The CO_2 system in the surface waters of the Arabian Sea is also greatly affected by the seasonal wind reversals. The Arabian Sea generally acts as perennial source of CO_2 to the atmosphere (Somasundar *et al.,* 1990; Kumar *et al.,* 1992; George *et al.,* 1994; Sarma *et al.,* 1998; Goyet *et al.,* 1998; Sarma *et al.,* 2000, Sarma *et al.,* 2003) with surface pCO_2 concentrations above 355 μatm for almost most part of the year (Sarma *et al.,* 1998). The increased pCO_2 in surface waters mostly result from the upwelling and convective mixing of subsurface waters containing 1100 μatm of pCO_2 resulting from nutrient regeneration (Sarma *et al.,* 1998). However, a very small region of the EAS i.e. coastal waters at ~ 15° N

shows low pCO_2 during southwest monsoon on account of high fresh water influx from small rivers in the Western Ghats which are highly active during summer monsoons (Sarma *et al.*, 1998). Thus physical processes control pCO_2 concentrations in surface waters during monsoon season, whereas, biological activities control pCO_2 during the inter-monsoon seasons (Sarma *et al.,* 2000). Similarly, the EAS shows lower DIC as compared to western and northern Arabian Sea, due to influx of fresh waters from the Western Ghats and BoB during the southwest monsoon and northeast monsoon respectively (Sarma *et al.,* 2000).

2.1.5 Deep-water circulation of the Arabian Sea

During the northeast monsoon the continental winds cool the surface of northern Arabian Sea which results in the formation of high salinity water mass having temperature of 24-28° C and salinity of 35.3 – 36.7 psu and termed as the Arabian Sea High Salinity Water (ASHSW) (Shetye *et al.,* 1994; Prasanna Kumar and Prasad, 1999) which is found in the upper 100 m of the water column. This water moves southwards and its extent to the east is limited to 67° E due to presence of WICC progressing northward, which restricts its spreading in the shelf areas. However, during southwest monsoon, the circulation reverses in direction and ASHSW spreads southward along the West Coast of India (Prasanna Kumar and Prasad, 1999). Its movement towards south is again limited by the North Equatorial Current (NEC) and eastward flowing monsoon current during the winter and summer monsoon respectively.

The Arabian Sea is also influenced by the Persian Gulf Water mass (PGW) entering the Gulf of Oman from Strait of Hormuz. The PGW is formed by excess of evaporation over precipitation during the winter season and is characterised by temperatures of ~17° C, salinity of > 36.2 psu (Prasad *et al.,* 2001) and oxygen concentration of 3.5 ml/l (Wyrtki, 1971). This water spreads southward during winter, along the western boundary, with its core found at 200-300 m depth (Prasad *et al.,* 2001). During the reverse circulation in summer monsoon, the PGW moves southward but is pushed towards the central Arabian Sea by currents moving in opposite direction. The core of this water mass progressively deepens as it moves southwards. Shankar *et al.* (2005) reported the presence of PGW in the southeast Arabian Sea. Shenoi *et al.* (2005) observed PGW at a depth of 200-300 m in southeast Arabian Sea wherein the salinity of the water mass was reduced to 35.2 psu.

The Red Sea Water mass (RSW) is formed due to excess of evaporation over precipitation and enters the Gulf of Aden through the Strait of Bab-el-Mandeb and then

spreads in the Arabian Sea forming a salinity maximum at 500-800 m depth which deepens as it moves towards the equator. The Red Sea Water mass can be identified with distinct high salinity of 35.1- 35.6 psu and temperatures of 9-11° C (Prasanna Kumar and Prasad, 1999). This water mass spreads towards the equator along the Somalia Coast and it has been reported to reach the Agulhas Current (Beal *et al.,* 2000). Patches of this water mass were also reported in the central Arabian Sea to Southwest Coast of India (Shankar *et al.,* 2005; Shenoi *et al.,* 2005). Babu *et al.* (1980) and Shankar *et al.* (2005) have observed the equatorward movement of RSW along the southwest coast of India.

Intermediate water masses in the Arabian Sea mostly consist of the above discussed ASHSW, PGW and RSW occupying the upper 1000 m water depth. The PGW and RSW water masses are bound by the Indian Central Water (ICW) (Emery and Meincke, 1986; Tomczak and Godfrey, 2003; Carton *et al.,* 2012) which are derived from the South Indian Ocean and are formed from subducted water in the Subtropical Convergence (Sprintall and Tomczak, 1993; Tomczak and Godfrey, 2003) along with contributions from Antarctic Intermediate Water (AAIW) and Indonesian Intermediate Waters (IIW) (Emery and Meincke, 1986; You and Tomczak, 1993). AAIW is the dominant water mass among the intermediate water masses of the Indian Ocean. It originates from deep convection of Sub Antarctic Front in the southern hemisphere (You, 1998) and enters the Indian Ocean from mid of the Indian sector of the Southern Ocean, whereas, in the North Indian Ocean it propagates as western boundary current off Madagascar (You, 1998). However, AAIW in the North Indian Ocean can only be traced up to 5° N (You, 1998).

Since there is no deep-water production in the Indian Ocean, the deep water masses in the Indian Ocean basin are mostly of global origin and are sourced from the North Atlantic and the Antarctic Ocean. The deep water mass originating from the North Atlantic basin is termed as the North Atlantic Deep Water (NADW) and that arising from the Antarctic basin is termed as the Antarctic Bottom Waters (AABW). Both of these water masses are together referred to as Circumpolar Deep Waters (CDW) and represent one arm of the global conveyor belt circulation that enters the Indian Ocean. The North Atlantic Deep Water originates from the North Atlantic and is formed from the excessive cooling and brine rejections during ice formation from the upwelled surface waters brought by the Gulf Stream. Whereas, the AABW is formed from Antarctic surface waters which is cooled to freezing and also subjected to brine rejection during sea ice formation in Weddle and Ross Sea. The Antarctic surface waters are mixture of waters sourced from upwelled NADW in

the Southern Ocean, cooled surface waters of Antarctica which is freshened by precipitation and near surface water obtained from melting of ice (Talley, 2013). The Antarctic Bottom Water is northward moving water mass with greater density than southward moving NADW and therefore it is overlain by the NADW. Both these water masses meet at the 50-60° S at the southern tip of South Africa in the Agulhas basin wherein they mix and give rise to CDW which occupies deeper depths and thus comprise deep-water circulation in the Indian Ocean and Pacific Ocean. The Circumpolar Deep Water is further divided into the Upper Circumpolar Deep water (UCDW; 2.0-3.8 km), and Lower Circumpolar Deep Water (LCDW; below 3.8 km). The UCDW has a greater component of NADW with little homogenization by the Southern Ocean (Schott and McCreary, 2001; Mc Cave *et. al.,* 2005), whereas, the LCDW is mostly sourced from the densest water arising from Antarctica.

Deep-water circulation in the Indian Ocean (Figure 2.3) is primarily controlled by the bottom topography and the complex ridge system on the Indian Ocean floor. The two main ridges, namely; the Central Indian Ocean Ridge and the Ninety-East Ridge divides the Indian Ocean deep circulation into three different circulation systems (Warren, 1981). The Central Indian Ocean Ridge separates the western from the central Indian Ocean circulation and the Ninety-East ridge splits the West Australian Basin circulation from the Central Indian Ocean Circulation system (Warren, 1981). Circumpolar Deep Water enters the Indian Ocean through two flow pathways in the south western and south eastern Indian Ocean (Figure 2.3) (Mantyla and Reid 1995). The deep waters entering through the south western Indian Ocean flow as the Deep Western Boundary Current (DWBC) (Pichon, 1960; Warren, 1974; 1978; Fieux, 1986; Johnson *et al.,* 1991a, b; Warren and Johnson, 1992). The Deep Western Boundary Current which is sourced from CDW entering from the south western pathway first enters the Crozet Basin. Its movement further is controlled by the southwest Indian Ocean Ridge which is heavily fractured and the height of the ridge decreases along the north, near the central Indian Ocean Ridge (Fisher *et al.,* 1971). Hence, the deep waters flow from the Crozet Basin to the Madagascar Basin through the fracture zones in the southwest Indian Ocean Ridge (Warren, 1973; Warren, 1978).

In the Madagascar Basin the water masses flow northward along the western part of the basin, at the same time some amount of NADW which leaves the Atlantic Basin moves northward into the southwest Indian Ocean near the Agulhas and joins the CDW entering the Madagascar Basin (Talley *et al.,* 2013). From the Madagascar Basin, the CDW enters the Mascarene Basin from where it is expected to flow into the Somalia Basin since no return

flow was observed from the Mascarene Basin (Wyrtki *et al.,* 1971). The Circumpolar Deep Water from Mascarene Basin then progresses to the Somalia Basin through the Amirante Passage which is the deepest connection between the Mascarene and Somalia Basin (Johnson *et al.,* 1998). In Somalia Basin, the CDW moves northward along the Somalia Coast and further crosses the equator and moves eastwards and enters the Arabian Basin through the Owen Fracture Zone on Carlsberg Ridge (Jhonson *et al.,* 1991a). The Arabian Sea also receives CDW emerging from the Central Indian Ocean Basin, which forms the second source of CDW to the Arabian Sea (Jhonson *et al.,* 1991b).

The south western Indian Ocean circulation is better studied than the south eastern Indian Ocean. The CDW entering the Indian Ocean from the south eastern pathway bifurcates at the north of southeast Indian Ridge in South Australian Basin, one branch enters the central Indian Ocean Basin and other enters the Perth Basin (Hufford *et al.,* 1997; Donohue *et al.,* 1999). The water masses entering the central Indian Ocean Basin further move northward and splits into two branches, one entering the Arabian Sea through the passage in the Chagos-Laccadive Ridge and other turns north till the southern tip of Chagos-Laccadive Ridge and then feeds the deep-waters of the BoB. The branch of the CDW which has branched at the north of southeast Indian Ocean Ridge moves northward, surrounds the Broken Ridge and feeds the western boundary flow in the Perth Basin (Hufford *et al.,* 1997; Donohue *et al.,* 1999). The CDW then moves northward along the Ninety-East Ridge circulating deep-water in the West Australian Basin.

North Indian Deep Water (NIDW) is a southward moving high salinity water mass formed from upwelling of CDW entering the Arabian Basin and the BoB Basin and is also referred to as aged CDW (You, 2000). Shetye *et al.,* (1994) refers to this water mass as the Modified North Atlantic Deep Water (MNADW) found below 1500 m depth in the Arabian Sea. NIDW has major components of CDW and minor contributions from intermediate water masses such as PGW, RSW (Kumar and Li, 1996) and even the AAIW as it moves south. Kumar and Li, (1996) also refer to this water mass as the High Salinity Deep Water (HSDW) observed in the Arabian Sea as well as in the BoB. This water mass in the Arabian Sea is found between depth of 1100 m and 2200 m (Beal *et al.,* 2000).
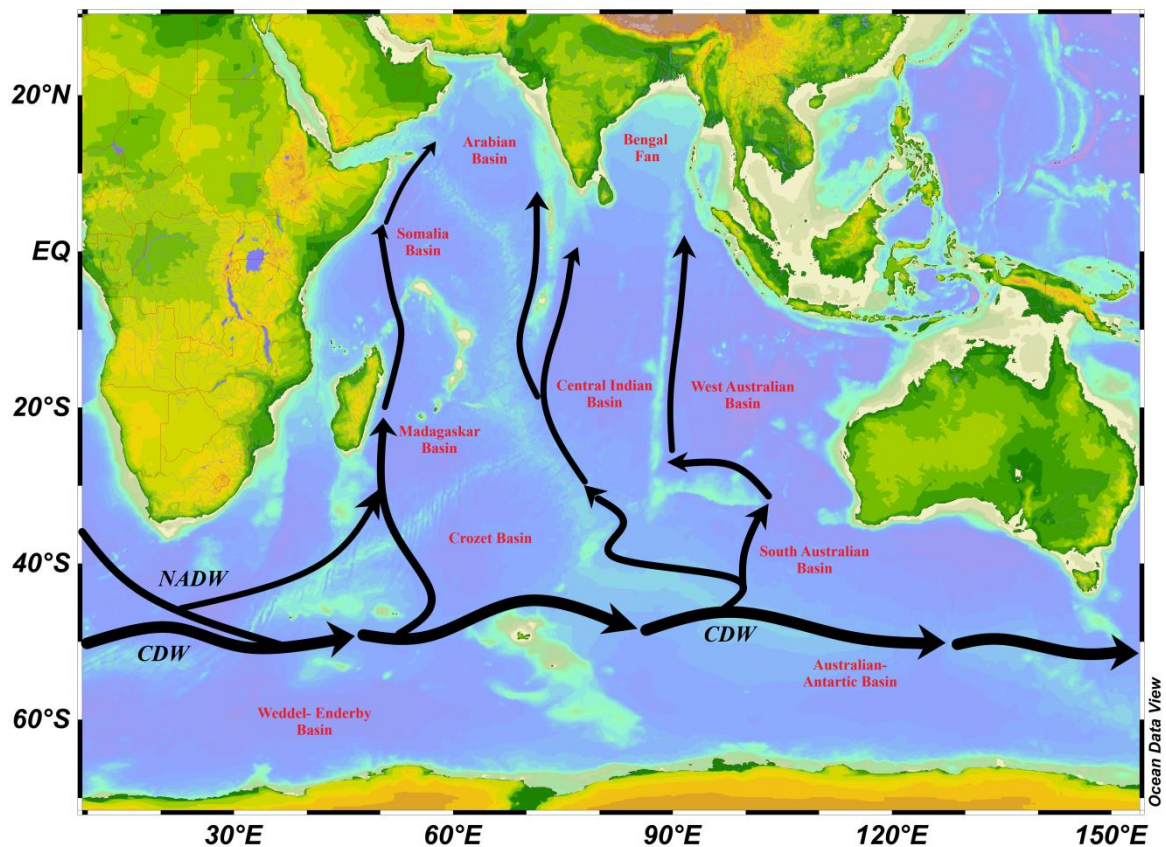
Figure 2.3: Schematic representation shows deep water circulation in the Indian Ocean wherein black arrows indicate the direction of flow of CDW and NADW. The thicknesses of arrows indicate the intensity of flow, CDW: Circumpolar Deep Water and NADW: North Atlantic Deep Water (You, 2000; Talley *et al.,* 2013).

2.2 Materials

2.2.1 Sediment cores

Sediment cores for this study were selected based on depths of various water masses in the Arabian Sea. The map of study area along with the core locations and their details are shown in Figure 2.4 and Table 2.1 respectively. In order to study the carbonate ion content of deep waters of the EAS, three sediment cores were selected which are: core AAS-9/21, retrieved from a depth of 1800 m from the eastern Arabian Sea during A. A. Sidorenko cruise 9 in the year 1995 and cores SK-129/CR-05 and SK-129/CR-02 were raised from the southeastern Arabian Sea from a depth of 2300 m and 3800 m respectively during ORV Sagar Kanya cruise 129. The selected cores are well below the present day OMZ and above the Foraminiferal Lysocline (FL) depth of the Arabian Sea (FL= 3300 m; Cullen and Prell, 1984), except for core SK-129/CR-02, hence precluding the possibility of $CaCO_3$ dissolution at these depths. Cores SK-129/CR-05 and SK-129/CR-02 are presently bathed by CDW entering the Indian Ocean and core AAS-9/21 is bathed by the High Salinity Deep Waters

41

(HSDW) derived from the CDW. These cores lie in the flow path of southern sourced waters entering the Arabian Sea and have minimum effect of surface processes (explained in above section 2.1) making them appropriate core sites for investigating LGM to Holocene variation in deep water [$CO_3^=$].
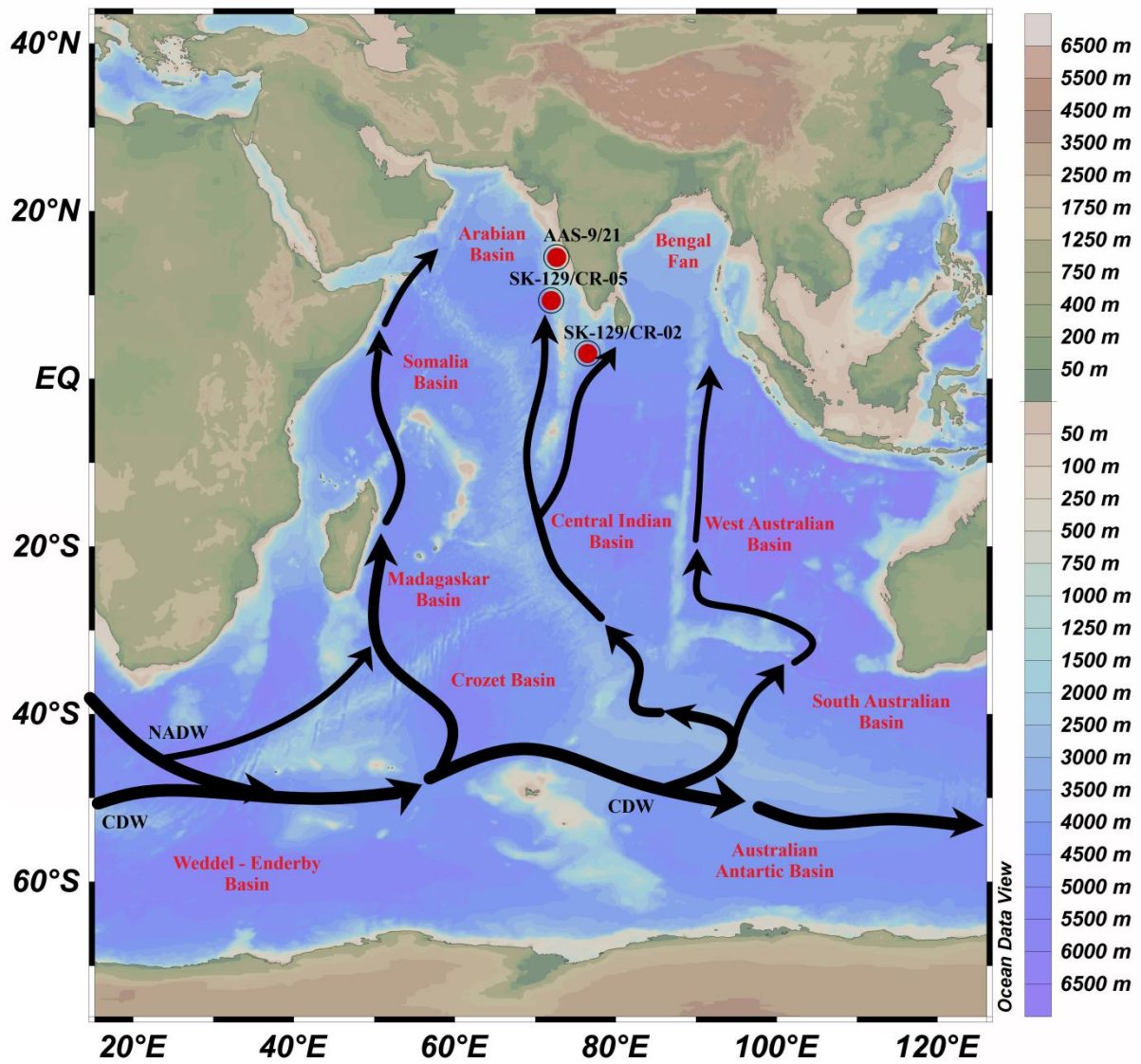
Figure 2.4: Map showing deep-water circulation in the Indian Ocean wherein red circles indicate location of the cores used in the study. Black arrows indicate the flow paths of Circumpolar Deep Waters (CDW) entering the Indian Ocean by two pathways from southwest and southeast Indian Ocean. Thickness of the arrows refers to the intensity of the flow (You, 2000; Talley *et al.*, 2013).

Table 2.1: Sediment cores used in this study with core IDs, location, water depth and year and month of retrieval.

Sr. No.	Core ID	Water Depth (m)	Latitude	Longitude	Year and Month of retrieval
1	AAS-9/21	1800	14.50° N	72.65° E	Jan 1995
2	SK-129/CR-05	2300	9.35° N	71.98° E	Dec 1997
3	SK-129/CR-02	3800	3.02° N	76.50° E	Dec 1997

2.3 Methods

2.3.1 Processing of Sediment Sample

The sediment cores were sub-sampled at 2 cm interval and were processed in a laboratory. Approximately 10 g of sediment sample was taken and oven dried at 60° C. The dried sample was then transferred to a 100 ml beaker and soaked in water and 10 ml of 10% sodium hexa-meta-phosphate was added (for disintegration of sample if required) and kept overnight. Properly disintegrated sample was wet sieved through > 63 μm sieve using distilled water. Washing of sample through sieve was done carefully to avoid breakage of foraminifera. The sample was washed to remove the clay and, the > 63 μm fraction (coarse fraction) were transferred to 25 ml beaker with great care and kept in the oven at 60° C for drying. Dried coarse fraction was then dry sieved to appropriate size fraction and used for picking of benthic and planktic foraminifera for radiocarbon analysis, oxygen and carbon isotope analysis and B/Ca analysis. Same procedure was followed for the rest of the samples.

2.3.2 Age Model

The chronology of all the cores used in the study (SK-129/CR-05, SK-129/CR-02 and AAS-9/21) are based on radiocarbon (^{14} C) dates obtained by Accelerated Mass Spectrometer (AMS). Accelerated Mass Spectrometer ^{14}C dates were obtained on minimum of 13 mg of mixed species of *Globigerinoides sacculifer* and *Globigerinoides ruber* and wherever sample quantity was not adequate (minimum 13 mg), *Neogloboquadrina dutertrei* was picked and added to obtain the desired quantity of sample. The chronology of core SK-129/CR-05 is based on seven AMS ^{14}C dates analysed at University of Cologne, Germany. Radiocarbon analysis were performed on 13 mg of sample consisting of *G. sacculifer* (*G. ruber* and *N. dutertrei* were added where sample was not adequate) of size range 250-

355µm. The foraminiferal samples were pre-treated with 1% HCl and washed with Milli-Q water of pH 6 prior to analyses. Dates obtained were converted to calendar age by using Calib 7.1 programme (Stuiver *et al.,* 2017). The chronology of core AAS-9/21 core was adopted from Govil and Naidu, (2010) except for three additional dates which were obtained to improve the chronology, from University of Cologne, Germany. Radiocarbon analyses were performed on 13 mg of sample consisting of mixed foraminiferal species of *G. sacculifer* and *G. ruber* using the same method as mentioned above. The age model for core SK-129/CR-02 was taken from Piotrowski *et al.,* 2009.

2.3.3 Identification of benthic species and calculation of Benthic Foraminiferal Number.

A representative sample of coarse fraction (> 63 µm) was split with the help of a splitter to pick minimum 300 specimens of benthic foraminifera. The sample was than weighed to calculate the Benthic Foraminiferal Number (BFN). The representative sample was then put on the picking tray and only benthic foraminifera were picked using a stereozoom microscope (OLYMPUS SZX 16). Picked specimens were counted and mount on labeled rectangular 60 chambered micro paleontological assemblage slides. Identification of the benthic foraminifera till generic level was done with the help of the Atlas of Benthic Foraminifera and online images obtained from website of World Register of Marine Species (WORMS). Benthic Foraminiferal Number was calculated by using the formula given below: -

Benthic Foraminiferal Number (BFN) = [(Number of benthic foraminifera in picking fraction/weight of picking fraction) * (Weight of coarse fraction/Weight of dry sediment)]

2.3.4 Identification of Cibicidoides wuellerstorfi (Schwager), 1866

Cibicidoides wuellerstorfi is an epifaunal benthic foraminiferal species and widely used in stable isotopic analysis for paleoclimate determination. The Scanning Electron Microscope (SEM) image of *C. wuellerstorffi* is given in Figure 2.5. It is an oval shaped and consist of alow trochospiral and planoconvex test having 8-12 chambers in the final whorl. The test shows the presence of sutures which are strongly curved and has an interiomarginal aperture. Identification of the *C. wuellerstorffi* specieswas done with the help of foraminifera taxonomy plates reported in various research papers (Rae *et al.*, 2011; Gottschalk *et al.*, 2016), additionally, the Atlas of Benthic Foraminifera and online images obtained from website of World Register of Marine Species (WORMS) were also used for identification.
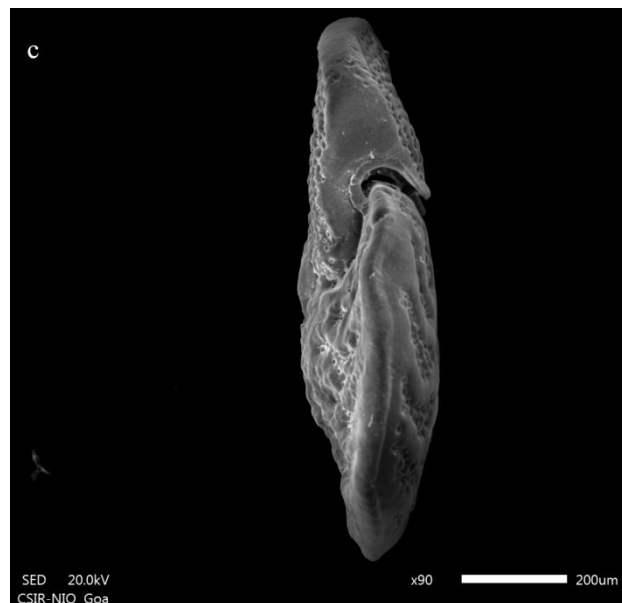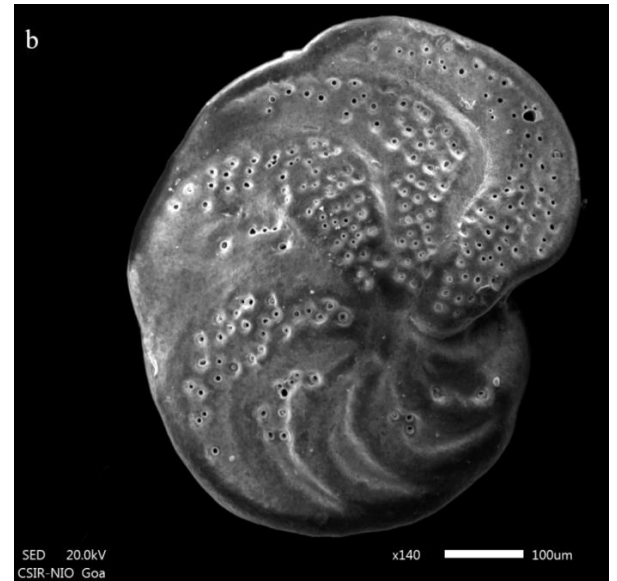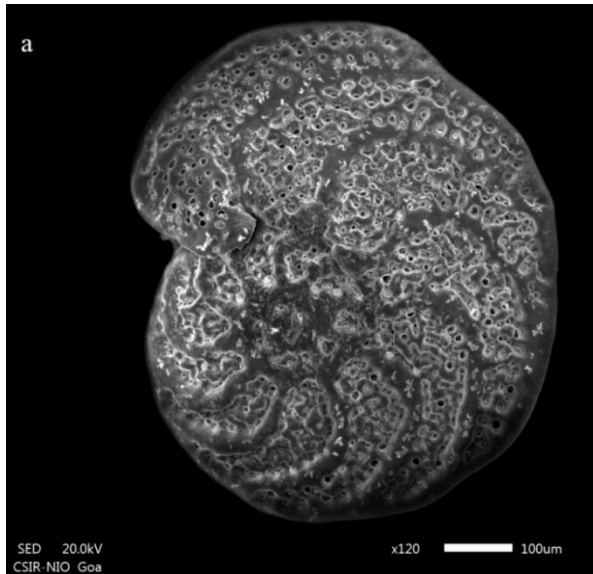
Figure 2.5: Scanning Electron Microscope images of epifaunal benthic foraminifera *Cibicidoides wuellerstorfi,* (a) spiral view, (b) umbilicalview and (c) lateral view.

2.3.5 Oxygen and carbon isotopes

For oxygen and carbon isotope analysis of benthic foraminifera, minimum of 2 shells of *C. wuellerstorfi* of the size range 250-500 µm were picked and analysed on a KIEL IV device coupled to a Delta V Isotope Ratio Mass Spectrometer (IRMS) at the CSIR-National Institute of Oceanography, Goa, India. The KIEL IV carbonate device (Figure 2.6) uses the principle of individual acid baths. Wherein the storage, transfer and chemical reaction of

phosphoric acid occurs at 70 °C and is operated under full temperature control. Carbon dioxide is evolved in septum-free vials and is transferred into a cryogenic trapping system. The trapping system consists of two LN_2 traps, two pneumatic valves, an expansion volume and a vacuum gauge. The first trap quantitatively cleans the CO_2 by removing non-condensable gases (e.g. O_2, N_2), H_2O produced during the carbonate-phosphoric acid reaction, and traces of water present in the nominally anhydrous phosphoric acid (104% of H_3PO_4 = 0.25 mol H_2O/L H_3PO_4). During the acid reaction, all CO_2 gas is introduced into the first trap at -190°C. Carbon dioxide is then transferred into the second trap (microvolume) where it is trapped at -190°C, leaving all of the water in the first trap. The microvolume is connected to the IRMS by a capillary and focuses the evolved CO_2 sample gas for $\delta^{13}C$ and $\delta^{18}O$ measurement. The overall precision for samples $\geq$ 20 µg is $\pm$ 0.04 ‰ for $\delta^{13}C$ and $\pm$ 0.08 ‰ for $\delta^{18}O$ (1σ). Calibration to the VPDB standard was performed by repeated measurements of international reference standards NBS-19 and Carrara marble.
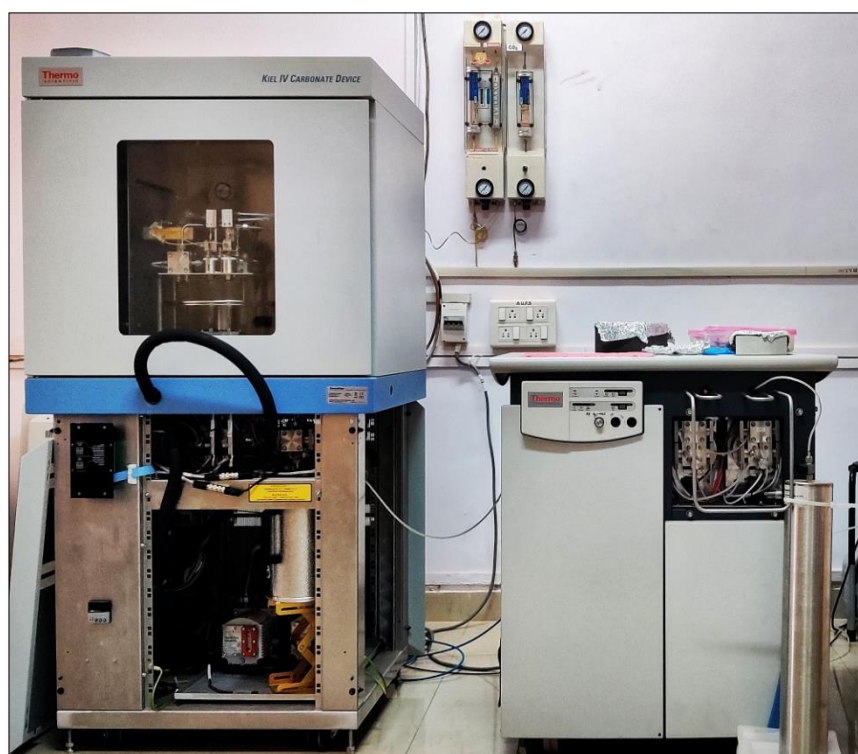
Figure 2.6: Photograph of KIEL IV carbonate device coupled to a Delta V Isotope Ratio Mass Spectrometer (IRMS) at CSIR-National Institute of Oceanography, Goa, India. The instrument was utilised for carbon and oxygen isotope analysis of benthic foraminiferal shells.

2.3.6 Boron/calcium analysis

For boron/calcium analysis of benthic foraminifera, a minimum of 7 shells of *C. wuellerstorfi* in the size range of 250-500 μm were picked. These foraminiferal shells were than partially crushed using two glass slides and transferred to 0.5 ml vials. Clean glass slides and acid cleaned vials were used inorder to avoid contamination. The partialy crushed samples were cleaned by standard oxidative and reductive cleaning protocols and clay particles, organic matter, oxides and adsorbed contaminants were removed (Boyle and Keigwin, 1985, as outlined in Rosenthal *et al*., 1997). Crushed and cleaned foraminiferal samples were than dissolved in ultrapure 0.065 N HNO$_3$ and the analysis were carried out on Sector-field inductively coupled mass spectrometer (Thermo Scientific Element XR) at Rutgers University. Anhydrous ammonia gas was injected into a high purity quartz cyclonic spray chamber and the pH of injected sample was raised to > 9.14, NBS scale, inorder to improve the washout efficiency and reduce boron memory effect between samples. The injected anhydrous ammonia gas reactes with boric acid and converts it to soluble ammonium borate, and it is easily removed during washout (Al-Ammaret *et al.,* 2000). Typical B blank levels are 0.15 ppb (< 2 % of [B] of foraminifera samples) and remain stable (± 1 %) throughout an analytical run (Babila *et al.,* 2014).

Contamination was identified by measuring Al/Ca, Fe/Ca and Mn/Ca ratios and their covariance with B/Ca ratios was checked for all samples. The clay and silicate contamination was monitored by measuring the Al/Ca and contamination from Mn-Fe oxide coatings was checked by measuring Fe/Ca and Mn/Ca. The values of Al/Ca should be within 100 μmol/mol (Rae *et al.,* 2011). In this study Al/Ca ratios obtained for maximum (43) samples were below 100 μmol/mol and for rest of the (7) samples exceeded 100 μmol/mol but no covariance of Al/Ca with B/Ca ratios was seen (Figure 2.7a, 2.8a and 2.9a). The contamination from Mn-Fe oxide coatings was checked by measuring Fe/Ca and Mn/Ca ratios and their values should also not exceed 100 μmol/mol and 1000μmol/mol respectively (Barker *et al.,* 2003). The Fe/Ca ratios in my samples varied from 28-80 μmol/mol and did not exceed the 100 μmol/mol. The Fe/Ca ratios did not show any covariance with the B/Ca ratios hence concluding an effective cleaning of foraminiferal shells (Figure 2.9c). Mn/Ca ratios were well below 1000 μmol/mol and showed a negative covariance (Figure 2.7b, 2.8b and 2.9b) with the B/Ca ratios which again indicate efficient cleaning of shells.
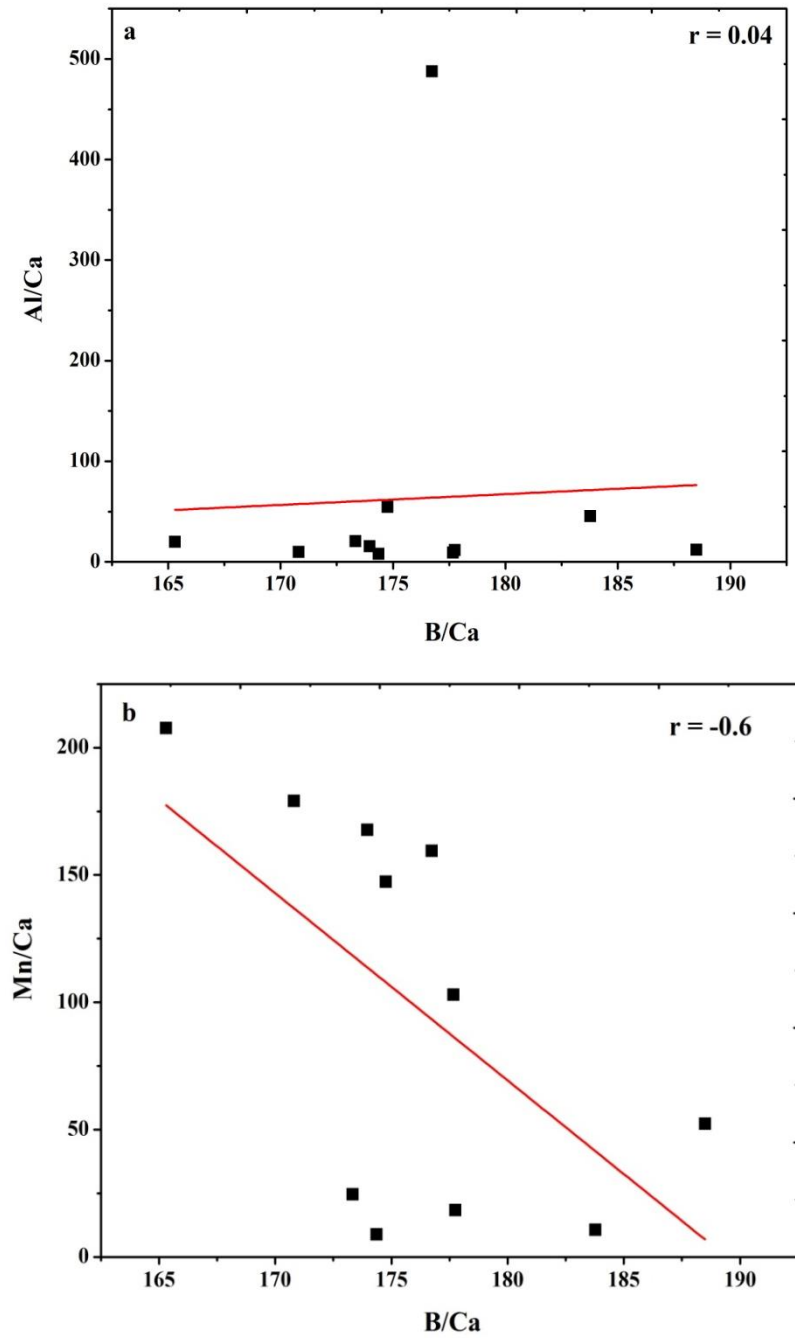
Figure 2.7: Graph showing the variance of a) Al/Ca v/s B/Ca and b) Mn/Ca v/s B/Ca obtained from analysis of benthic foraminifera shells in core SK-129/CR-02 on sector-field inductively coupled mass spectrometer (Thermo Scientific Element XR) at Rutgers University (See section 2.3.6) and the ratios are expressed in µmol/mol units.
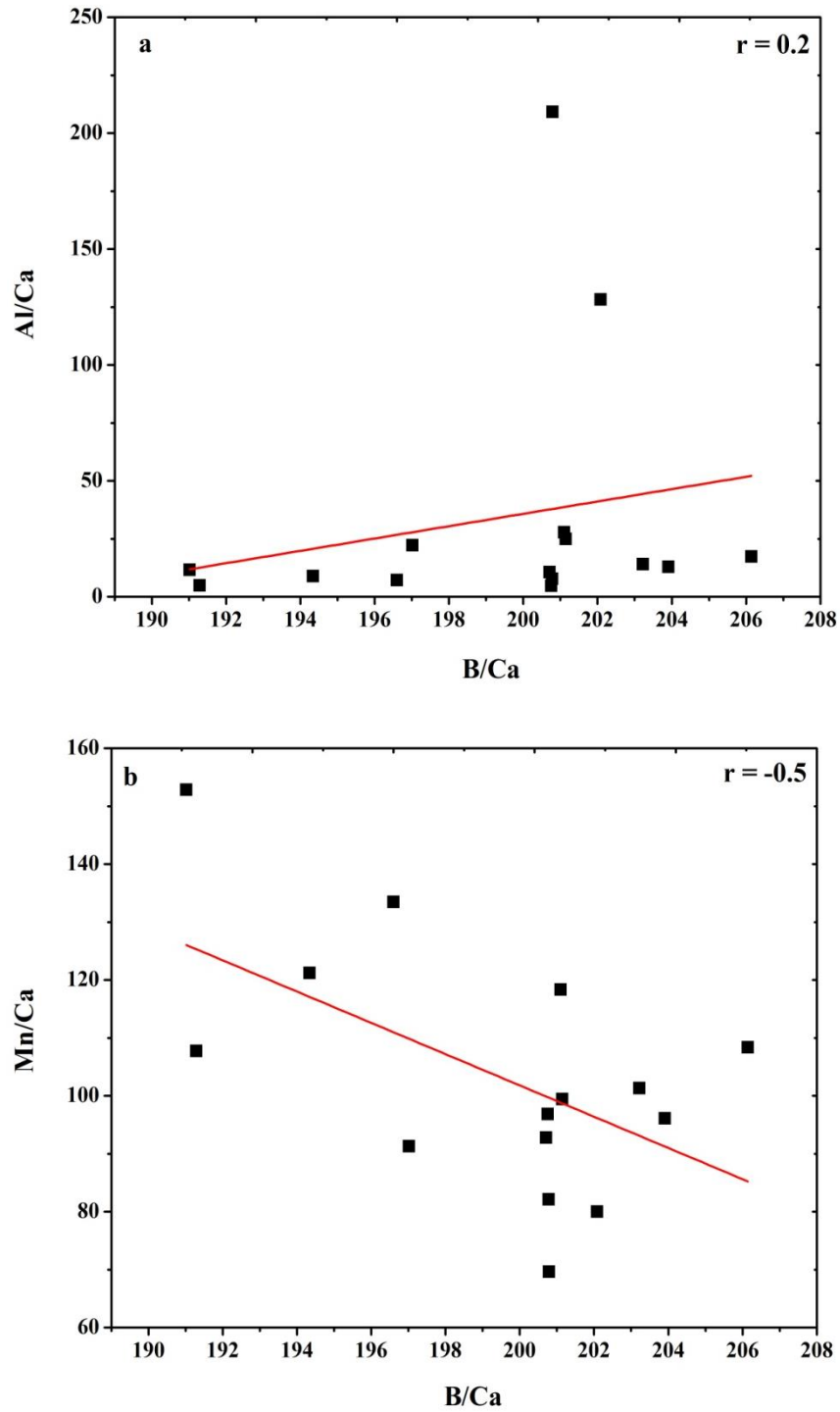
Figure 2.8: Graph showing the variance of a) Al/Ca v/s B/Ca and b) Mn/Ca v/s B/Ca obtained from analysis of benthic foraminifera shells in core SK-129/CR-05 on sector-field inductively coupled mass spectrometer (Thermo Scientific Element XR) at Rutgers University (See section 2.3.6) and the ratios are expressed in μmol/mol units.
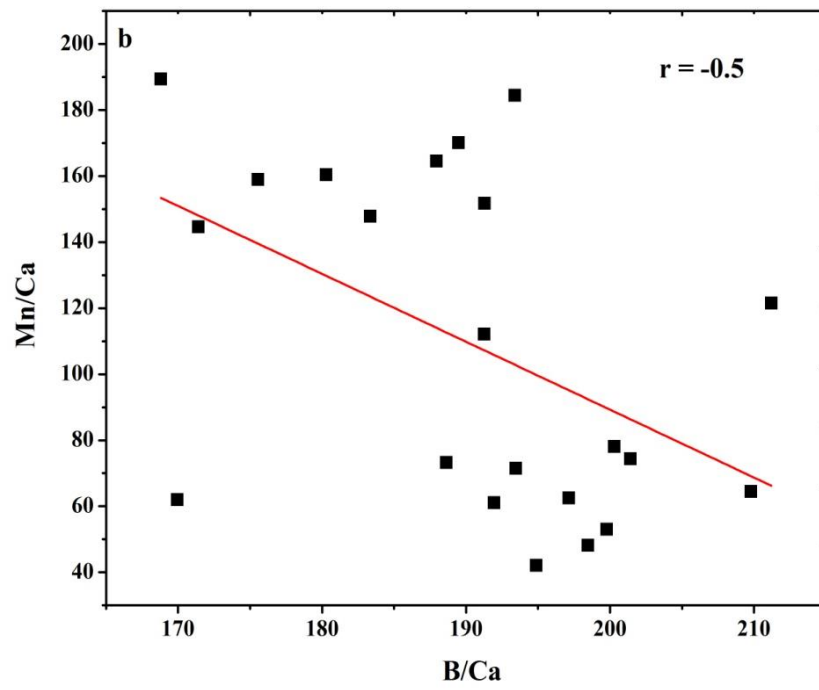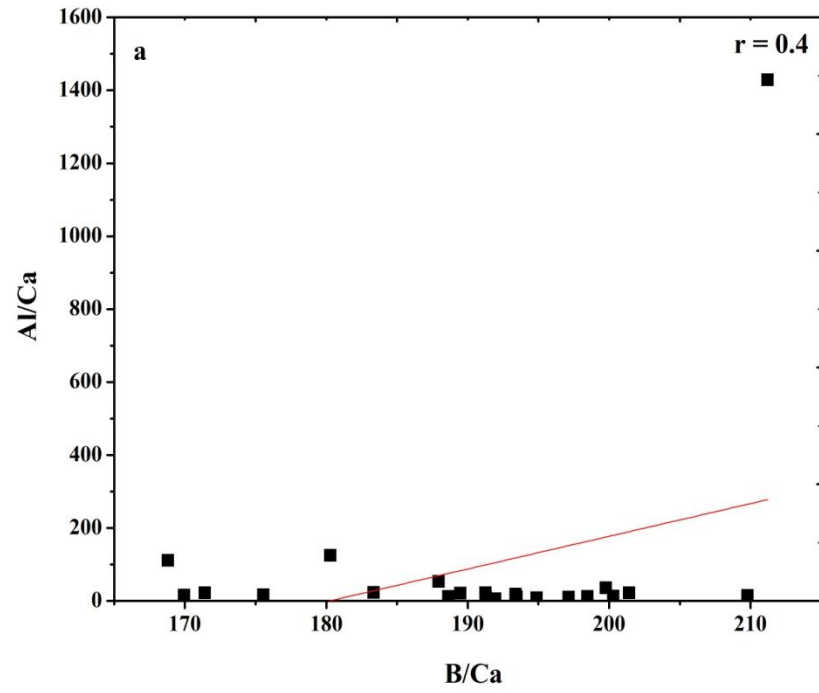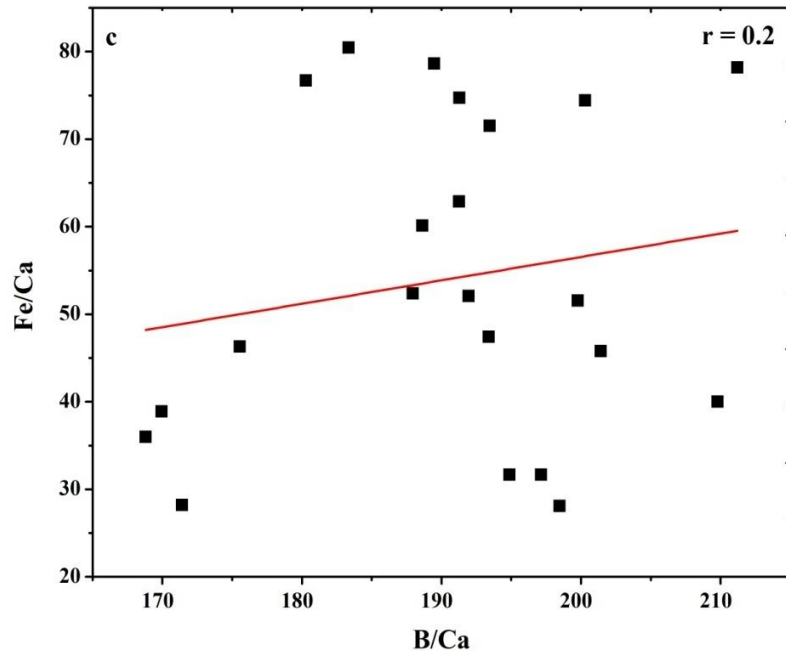
Figure 2.9: Graph showing the variance of a) Al/Ca v/s B/Ca, b) Mn/Ca v/s B/Ca and c) Fe/Ca v/s B/Ca obtained from analysis of benthic foraminifera shells in core AAS-9/21 on sector-field inductively coupled mass spectrometer (Thermo Scientific Element XR) at Rutgers University (See section 2.3.6) and the ratios are expressed in µmol/mol units.

2.3.7 Conversion of B/Ca ratios to $[CO_3^{2-}]$

The B/Ca ratios obtained from B/Ca analysis of *C. Wuellerstorffi* shells at Rutgers University were firstly converted to foraminiferal bottom water carbonate ion saturation (Δ $[CO_3^{2-}]$) by using the correlation equation given by Yu *et al.* (2013): -

$$Y = 1.14\ (X) + 176.6 \text{ ----------------------- (equation 1)}$$

Wherein,

Y is the B/Ca ratio obtained from B/Ca analysis

X is bottom water carbonate ion saturation ($\Delta[CO_3^{2-}]$)

Bottom water carbonate ion saturation ($\Delta[CO_3^{2-}]$) is the measure of the tendency for calcite to dissolve (Broecker and Peng, 1982). It is the difference between calcite saturation concentration ($[CO_3^{2-}]_{sat}$) and in-situ carbonate ion concentration ($[CO_3^{2-}]_{in\text{-}situ}$) of ambient water and is given by the formula: $\Delta[CO_3^{2-}] = [CO_3^{2-}]_{sat} - [CO_3^{2-}]_{in\text{-}situ}$.

The down core $[CO_3^{2-}]$ was calculated by using the equation: -

$$[CO_3^{2-}]_{in\ situ} = \Delta[CO_3^{2-}] + [CO_3^{2-}]_{sat} \text{----------------- (equation 2)}$$

Wherein,

$\Delta[CO_3^{2-}]$ was calculated from equation 1,

Calcite saturation concentration ($[CO_3^{2-}]_{sat}$) was calculated using the CO_2sys.xls (Ver. 12) programme wherein the required parameters such total alkalinity, total anthropogenic carbondioxide, nutrients, including phosphate (PO_4), silicate (SiO_3), Bottom Water Temperature (BWT) and salinity (S) of nearby station at the depth of core site was taken from the Global Ocean Data Analysis Project (GLODAP) (Key *et al*., 2004). The constants used in programme are K_1 and K_2–Millero (2010), KSO_4 – Dickson (1990), B & Chlorinity - Lee *et. al.* (2010) and pH in Total Scale. The down core in-situ carbonate ion concentrations ($[CO_3^{2-}]_{in\ situ}$) was obtained from the above equation 2 which was then plotted against age.

2.3.8 Planktic foraminifera shell weights

The coarse fraction of the processed sample was taken and sieved using a sieve size of 300-355 μm. After sieving the coarse fraction was taken and spread on metal trays and mounted on a Stereo Trinocular Microscope and around 50 *G. ruber* shells were identified and picked by using a fine brush. Any shells broken during the cleaning process were discarded and intact clean and clay-free shells were picked. The picked shells were then counted and transferred into 0.2 ml microcentrifuge vials and stored separately. This procedure was repeated for all the samples. The foraminiferal shells were then transferred to a thimble and weighed on a Sartorius microbalance (1σ Precision: $\pm 1\mu g$, n = 10) and this process was repeated for all the samples. The average foraminiferal shell weight for each sample was calculated.

2.3.9 Elemental analysis

Teflon beakers were soaked overnight in 2 N HCl and washed with distilled water and dried. Finely powdered 0.05 g of sediment was then transferred in Teflon beakers and 10 ml of 7:3:1 mixture of suprapure acids, HF: HNO_3: $HClO_4$ was added and digested at 130º C on a hot plate for one hour. Again, 5 ml of HF: HNO3: $HClO_4$ acid mixture was added and kept on hot plate till a solid lump was obtained. The solid lump was then dissolved in 4 ml of diluted 1:1 HNO_3 using Milli-Q water. The solution was then cooled and transferred to 100 ml volumetric flask, after filtering 1 ml of 1 ppm rhodium solution was added to it and finally it was diluted to 100 ml with ultrapure water and made up to the mark. The standard reference material MAG-1 and SGR-1were used to determine accuracy of the

analysis. The standard and the blank sample was also prepared along with the sediment sample by following a similar procedure. These samples were than analysed for trace elements on an Inductively Coupled Plasma-Mass Spectrometer (Thermo X Series 2) at CSIR- National Institute of Oceanography, Goa. The accuracy based on the standard reference material and the precession of data depending on duplicate analysis was better than ± 6 %.

3. RESULTS

3.1 Radiocarbon ages and Sedimentation Accumulation Rates

Radiocarbon ages for sediment cores SK-129/CR-05 and AAS-9/21 are provided in Table 3.1. Ages for the sediment intervals between the radiocarbon dated sections were calculated by linear interpolation wherein the sedimentation accumulation rate between two dated intervals is assumed to be constant. Calendar ages obtained from radiocarbon analysis of both the cores increases monotonically with depth of the core hence precluding the probability of sediment slumping and mixing. It is clear from the table that the core top of AAS-9/21 is preserved to a greater extent than that of SK-129/CR-05. Hence the Holocene period seems unscathed in core AAS-9/21. The recent sedimentation record of core SK-129/CR-05 upto˜2374 yr has been wiped out either due to loss of core-top during sampling or by natural abrasion of younger sediments by bottom water currents (Banakar *et al.*, 1991). However, since only upto˜2374 yr sediment is missing, the major portion of the Holocene period is intact, which is why the Last Glacial Maximum (LGM) and Holocene climatology can be compared well in this core.

Table 3.1: AMS Radiocarbon ages for core AAS-9/21

Sr. No.	AAS-9/21 sample interval (cm)	^{14}C age (yr BP)	Calibrated age (yr BP)	Species used	Sedimentation accumulation rate (cm/kyr)
1	0-3	850±25	512 ±9	*G. ruber*	5.4
2	53-56	9540±80	10343±326	*G. ruber*	13.4
3	*96-99	*12301±33	*13546±243	*G. ruber, G. sacculifer*	14.2
4	110-113	12770±80	14529±326	*G. ruber*	9.9
5	*116-119	*13326±36	*15133±286	*G. ruber, G. sacculifer*	8.6
6	*136-139	*14953±39	*17472±305	*G. ruber, G. sacculifer*	8
7	148-151	16070±115	18965±240	*G. ruber*	10.8
8	213-216	21290±180	24980±458	*G. ruber*	

(Radiocarbon dates for AAS-9/21 core are adopted from Govil and Naidu, 2010 except for * marked additional dates analysed for this study)

Table 3.2: AMS Radiocarbon ages for core SK-129/CR-05

Sr. No.	SK-129/CR-05 sample interval (cm)	^{14}C age (yr BP)	Calibrated age (yr BP)	Species used	Sedimentation accumulation rate (cm/kyr)
1	0-4	2743±25	2374±194	*G. sacculifer*	5.7
2	22-24	6240±29	6599±173	*G. sacculifer*	3.2
3	46-48	12598±39	14006±167	*G. sacculifer*	3.6
4	62-64	15654±49	18441±274	*G. sacculifer, G.ruber*	5.9
5	70-72	16910±62	19823±278	*G. sacculifer, G.ruber, N. dutertrei*	11.4
6	86-88	18042±59	21223±293	*G. sacculifer, G.ruber*	2.4
7	98-100	22434±66	26152±229	*G. sacculifer, G.ruber*	

The age versus depth graph and sedimentation accumulation rates for the studied cores AAS-9/21, SK-129/CR-05 and SK-129/CR-02 are shown in Figure 3.1a, b and c respectively. The average sedimentation accumulation rate of core AAS-9/21 during Holocene is 9.5 cm/kyr, during the deglaciation is 12.7 cm/kyr and during the LGM is 8.3 cm/kyr. Whereas, the average sedimentation accumulation rate obtained for core SK-129/CR-05 during Holocene is 4.5 cm/kyr, during the deglaciation is 3.6 cm/ky and during the LGM is 6.5 cm/kyr. Highest sedimentation accumulation rate of 14.2 cm/kyr was observed in core AAS-9/21 during deglaciation whereas SK-129/CR-05 exhibited highest sedimentation accumulation rate of 11.4 cm/kyr during the LGM.

Sedimentation accumulation rates for core SK-129/CR-02 were calculated from radiocarbon dates taken from Piotrowski *et al*., 2009. The sedimentation accumulation rate in this core varies between 1.2 to 6.6 cm/kyr, which is much lower as compared to the other two cores used in the study. The average sedimentation accumulation rate in this core during the Holocene is 2.5 cm/kyr, during the deglaciation is 3.3 cm/kyr and during the LGM is 1.9 cm/kyr. The average sedimentation accumulation rate during the Holocene and deglaciation is almost similar, but showed a decrease of 0.8 cm/kyr during the LGM. However, highest sedimentation accumulation rate in this core was seen to be 6.6 cm/kyr during the deglaciation. Overall, core AAS-9/21 showed higher sedimentation accumulation rates as compared to SK-129/CR-05 followed by SK-129/CR-02 for last 25 kyr.
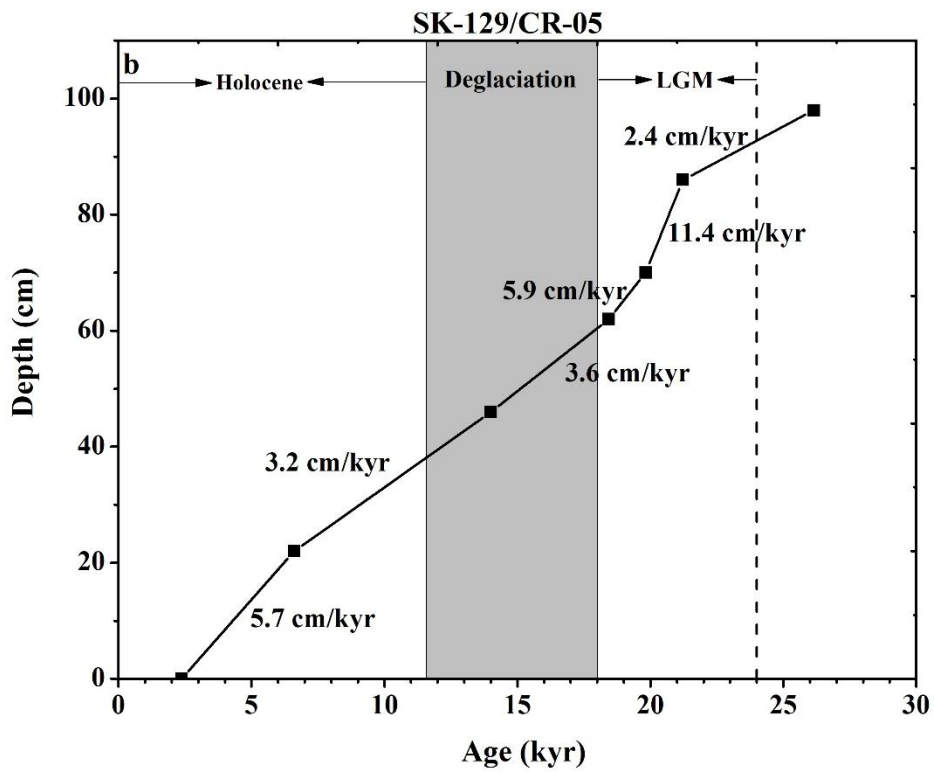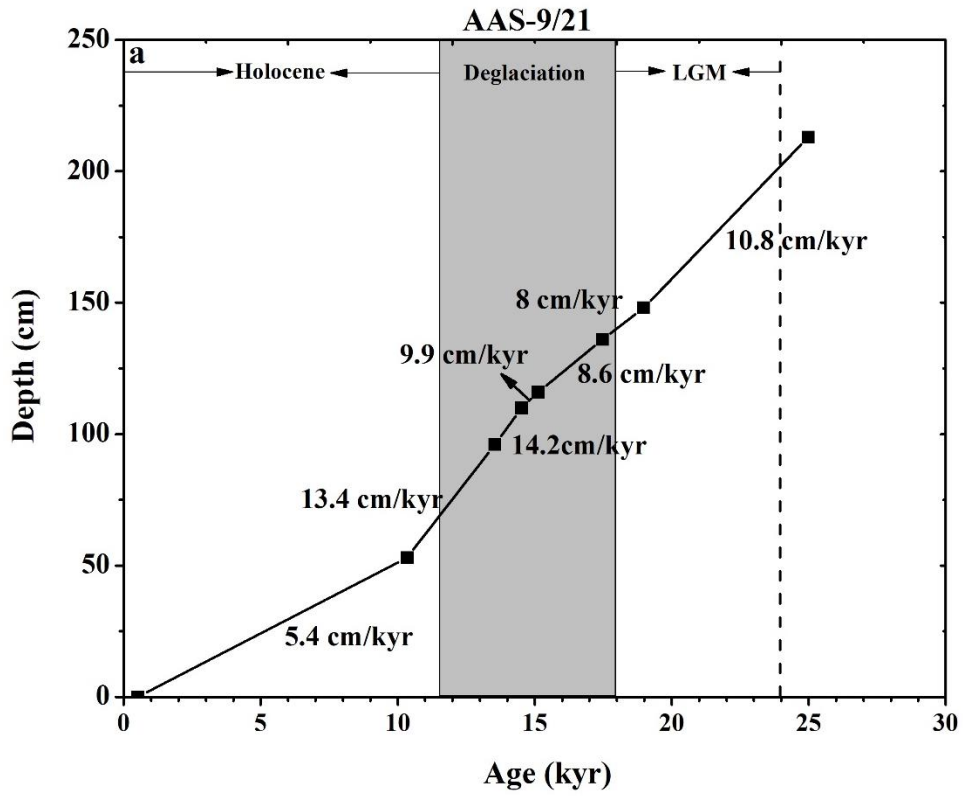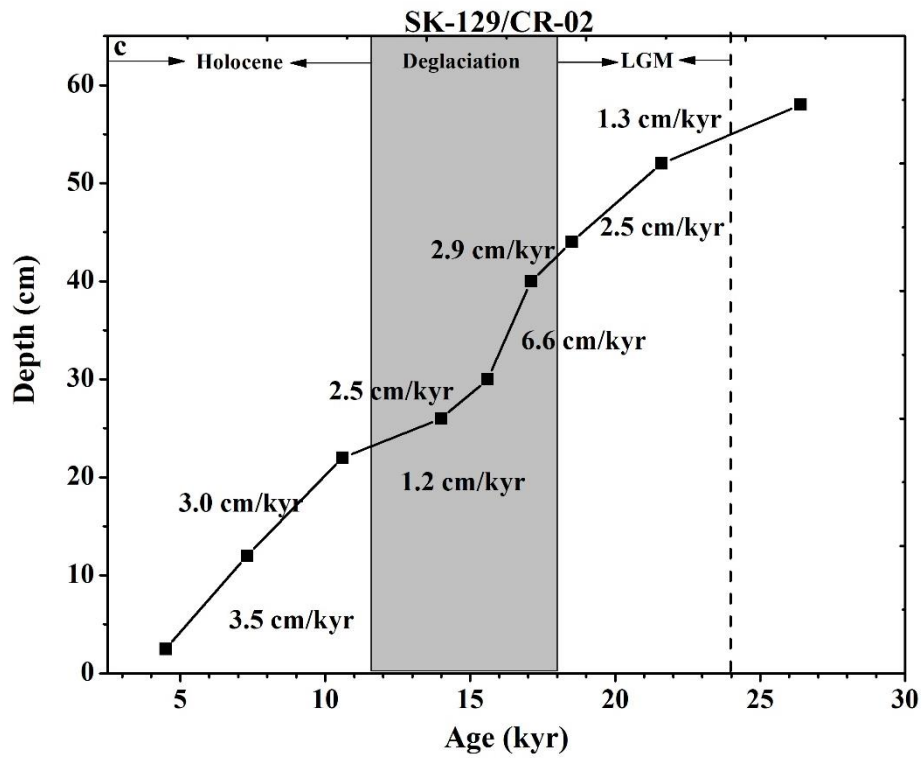
AAS-9/21

SK-129/CR-05

Figure 3.1: Age versus depth profile and sedimentation accumulation rates for cores a) AAS-9/21, b) SK-129/CR-05 and c) SK-129/CR-02. Grey band in the figure indicates the deglaciation period.

3.2 Physical properties of planktic and benthic foraminifera

3.2.1 Benthic Foraminifera Number (BFN) in Core SK-129/CR-05

Benthic foraminifera number (BFN) was counted only for one core, SK-129/CR-05, as it had sufficient number of benthic tests. The core SK-129/CR-02 lies below the Foraminiferal Lysocline and shows considerable amount of dissolution of foraminiferal shells. Moreover, the coarse fraction of both the cores, SK-129/CR-02 and AAS-9/21, was extensively used inprevious studies. Benthic foraminifera number varies from 9 - 324 per gm dry sediment weight (Figure 3.2). It is observed to be low at the initiation of LGM and remains low till~21.5 kyr after which a sudden increase is seen which reaches to maximum of 324 per gm dry sediment weight at~20 kyr. Sudden rise in BFN is immediately followed by a gradual decrease till 15 kyr. A gradual decrease in BFN is also noticed through the deglaciation showing a prominent lowering trend except for a slight increase at 14 kyr. Although minor variations can be seen in the Holocene, BFN remains stable and reaches to a minimum of 9 per gm dry sediment weight at~2 kyr.
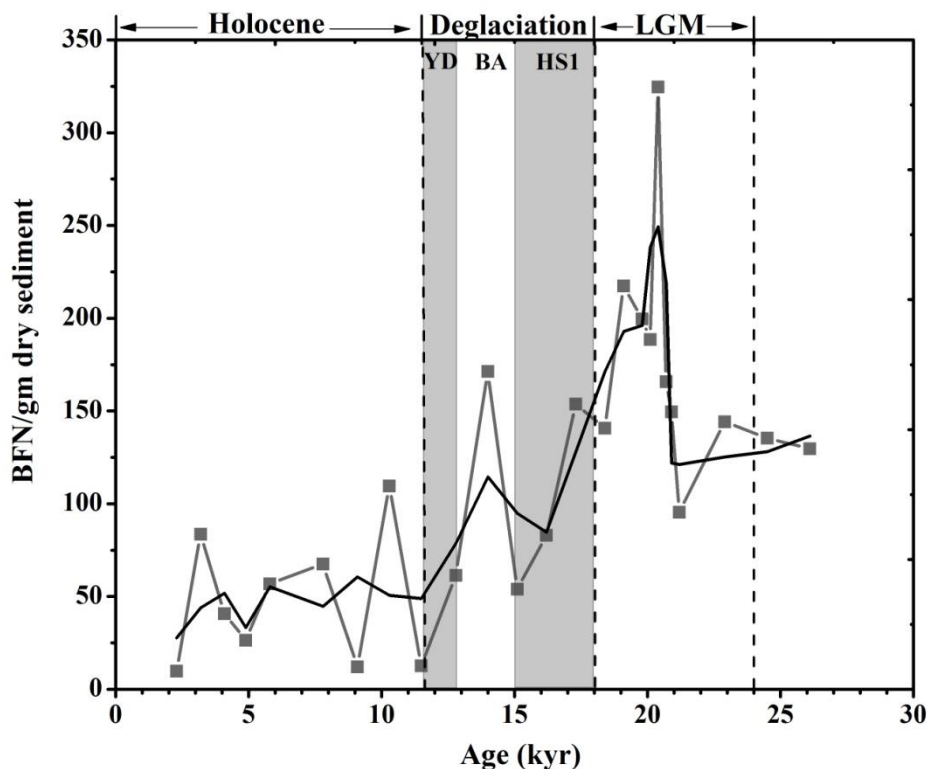
Figure 3.2: Variation in BFN per gm dry sediment weight (represented by grey line) in core SK-129/CR-05 for last 25 kyr. Black line indicates 3-point running average. Grey bands in the figure indicate Heinrich Stadial 1(HS1) and Younger Dryas (YD) and the white band indicates the Bølling-Ållerød (BA). The Last Glacial Maximum (LGM), deglaciation and Holocene are marked on the top axis.

3.2.2 Shell weights of planktic foraminifera in Core SK-129/CR-05

Shell weights of *G. ruber* in core SK-129/CR-05 varies from 14.1- 20.4 µg from the LGM to the Holocene (Figure 3.3). Low shell weights are observed during the LGM with average shell weight of 17.8 µg. From there on an increasing trend in shell weights is seen from LGM to deglaciation. Higher shell weights were recorded for entire period of deglaciation which depicts better shell preservation at that time. A prominent peak in shell weight is seen with a shell weight of 20.4 µg observed at ~16.2 kyr. Overall, the deglacial period shows an average shell weight of 19.4 µg and is ~2 µg higher than the LGM. The values further decrease during the Holocene and reach a minimum of 14.1 µg at ~4.9 kyr. The average shell weight during Holocene is 16.7 µg which is 3 µg lower as compared to the deglacial period.
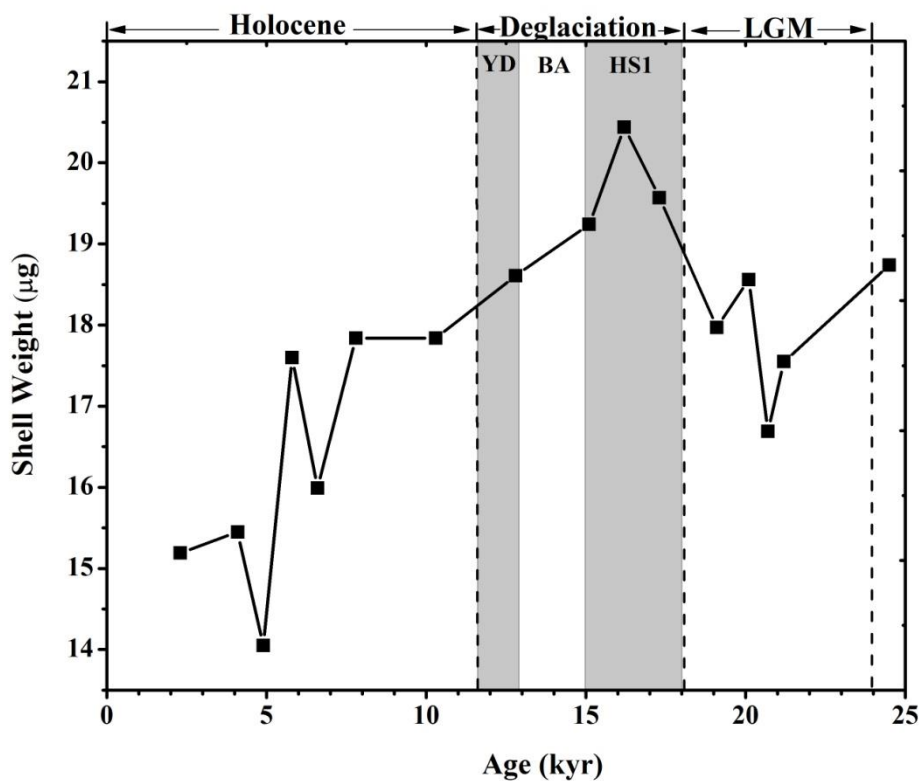
Figure 3.3: Variation in shell weight of *G. ruber* from core SK-129/CR-05 for last 25 kyr. Grey bands indicate Heinrich Stadial 1 (HS1) and Younger Dryas (YD) and the white band indicates the Bølling-Ållerød (BA). The Last Glacial Maximum (LGM), deglaciation and Holocene are marked on the top axis.

3.2.3 Shell weights of planktic foraminifera in Core SK-129/CR-02

Shell weights in core SK-129/CR-02 vary from 12.1 to 14.6 µg for last 25 kyr (Figure 3.4). Higher shell weights are observed in the LGM with an average of 14.2 µg. Shell weights increase from the onset of glaciation reaching to a highest value of 14.6 µg at ̃21 kyr and then decrease sharply till ̃18 kyr. Thereafter the shell weights slightly increase during the deglaciation and remain steady till ̃14 kyr. Shell weights again show a prominent low at 13.6 kyr followed by a sharp increase. An increase in shell weights is noticed at ̃12.5 kyr which remains steady till 10 kyr and they further decrease till 8 kyr through the Holocene. Overall, the deglaciation recorded an average shell weight of 13 µg and Holocene recorded an average shell weight of 12.8 µg.
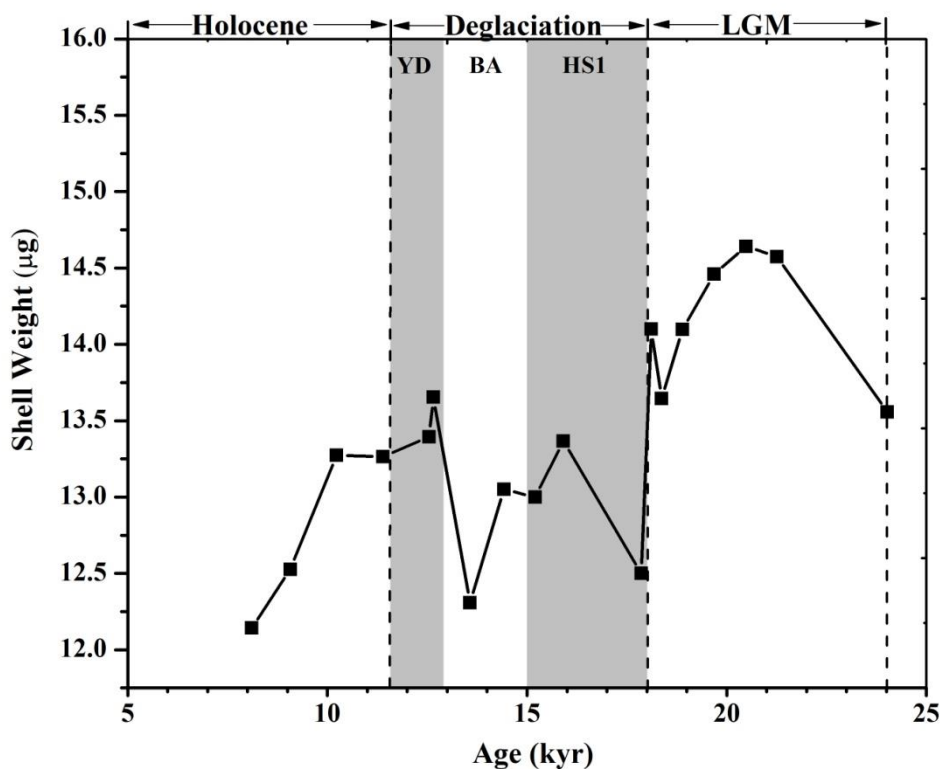
Figure 3.4: Variation in shell weight of *G. ruber* from core SK-129/CR-02 for last 25 kyr. Grey bands indicate Heinrich Stadial 1 (HS1) and Younger Dryas (YD) and the white band indicates the Bølling-Ållerød (BA). The Last Glacial Maximum (LGM), deglaciation and Holocene are marked on the top axis.

3.3 Geochemistry of sediments in Core AAS-9/21

The elemental analysis of sediment samples from this core were carried out to assess the bottom water oxygenation condition at the sediment water interface. In oxic conditions, Vanadium (V) exists as V^{+5} which is soluble in oxic waters and is reduced and precipitates out in sub-oxic waters. Elemental ratio of V/Ti (Figure 3.5) in sediment samples of this core shows rapid high and lows through the entire LGM but the values remain towards higher side indicating presence of sub-oxic water at core site. The ratio decreases at the onset of deglaciation followed by a slight increase at ˜14 kyr which is however lower than glacial values. Overall, notable lower values are observed during deglaciation indicating incursions of oxic waters at the site. Lowest V/Ti ratio of 106 is observed in the early Holocene. Later the values keep gradually increasing throughout the Holocene producing the highest value of 289 at ˜2 kyr in the Late Holocene. However, the gradual increase is interrupted by a brief drop at ~6 kyr in the mid-Holocene.
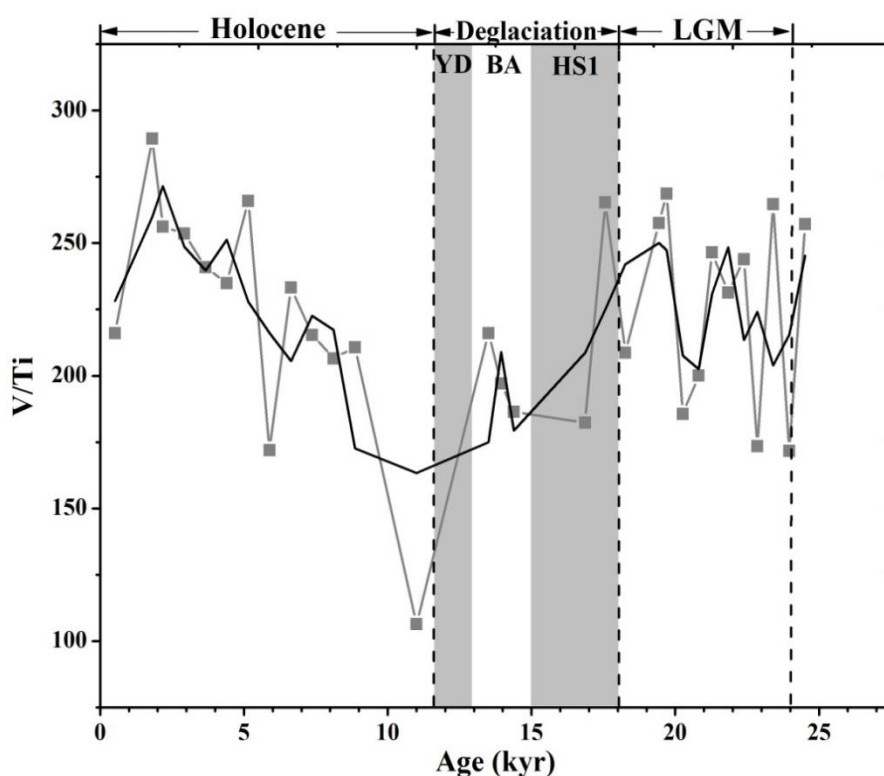
Figure 3.5: Graph showing the variation in V/Ti ratio (represented by grey line) in core AAS- 9/21 for last 25 kyr. Black line indicates 3 point average line. Grey bands in the figure indicate Heinrich Stadial 1(HS1) and Younger Dryas (YD). White band indicates the Bølling-Ållerød (BA). The Last Glacial Maximum (LGM), deglaciation and Holocene are marked on the top axis.

3.4 Chemical properties of benthic foraminifera shell

3.4.1 Carbon isotope ratios in Core AAS-9/21 and SK-129/CR-05

Carbon isotopic ratios (δ^{13}C) in core AAS-9/21 ranges from 0.28 to - 0.28 ‰ over last 25 kyr (Figure 3.6). Low values are recorded throughout the LGM which reach to a minimum of -0.28 ‰ at ~23 kyr. The onset of Heinrich Stadial 1 (HS1) is marked by a sudden increase in δ^{13}C reaching a maximum of 0.14 ‰ at ~16 kyr. Further a rapid decline is seen throughout the Bølling-Ållerød (BA). The Younger Dryas (YD) initially recorded low values of - 0.1 ‰ which then subsequently increase by the onset of the Holocene. The δ^{13}C values recorded during the Holocene vary from 0.04 to 0.28 ‰ with maximum of 0.28 ‰ observed at ~8.9 kyr. As can be seen in Figure 3.6, Holocene documented the highest δ^{13}C values for the entire time period studied, also it shows shift from negative values in the LGM and YD to positive values in the Holocene. Although minor variations are seen, the δ^{13}C values remain high throughout the Holocene.
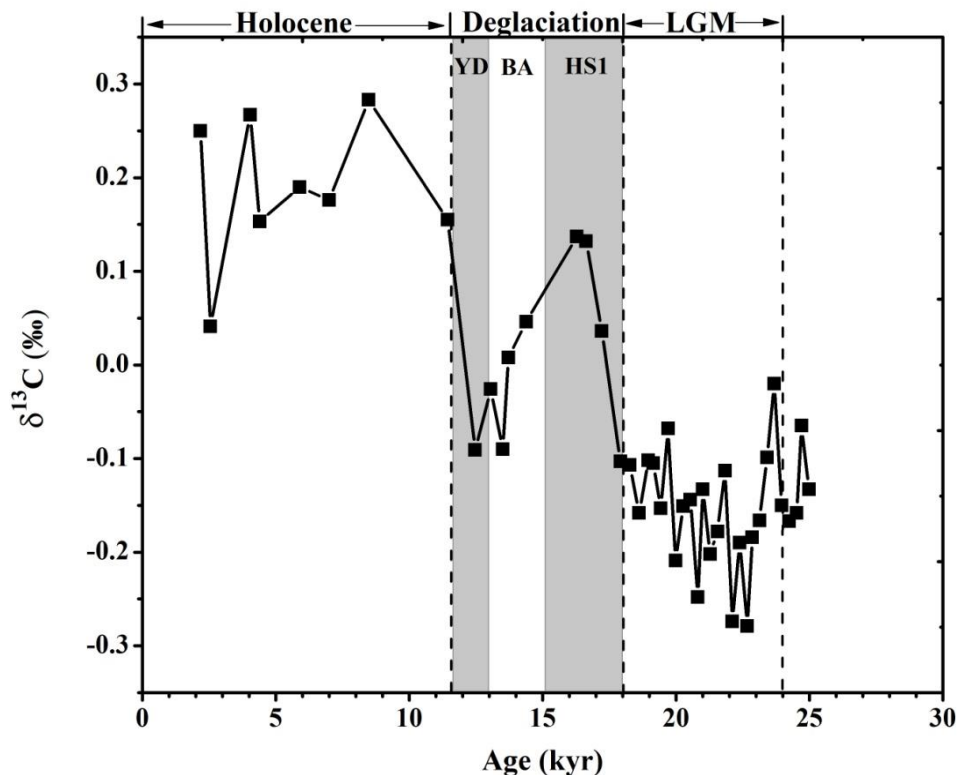
Figure 3.6: Graph representing variation of δ^{13}C (‰) in core AAS-9/21 for last 25 kyr. Grey bands in the figure indicate Heinrich Stadial 1(HS1) and Younger Dryas (YD). White band indicates the Bølling-Ållerød (BA). The Last Glacial Maximum (LGM), deglaciation and Holocene are marked on the top axis.

The $\delta^{13}C$ values in core SK-129/CR-05 ranges from - 0.33 to 0.52 ‰ for last 25 kyr (Figure 3.7). Lowest values were recorded in the LGM which range from - 0.33 to -0.14 ‰. At the onset of HS1, $\delta^{13}C$ values slightly increase which then quickly decline to a minimum of - 0.25 ‰ at ~14 kyr in the BA. Thus a prominent lowering in $\delta^{13}C$ values is observed during the BA. Thereafter a rapid rise in $\delta^{13}C$ values of 0.18 ‰ is seen at~13 kyr in the YD. The Holocene values vary from - 0.09 to 0.52 ‰ beginning with an increase from ~11 kyr to a high of 0.52 ‰ at ~5 kyr followed by a rapid decline till the Late Holocene. Overall the $\delta^{13}C$ values in this core show an increasing trend from LGM to Holocene with a distinguished low during BA.
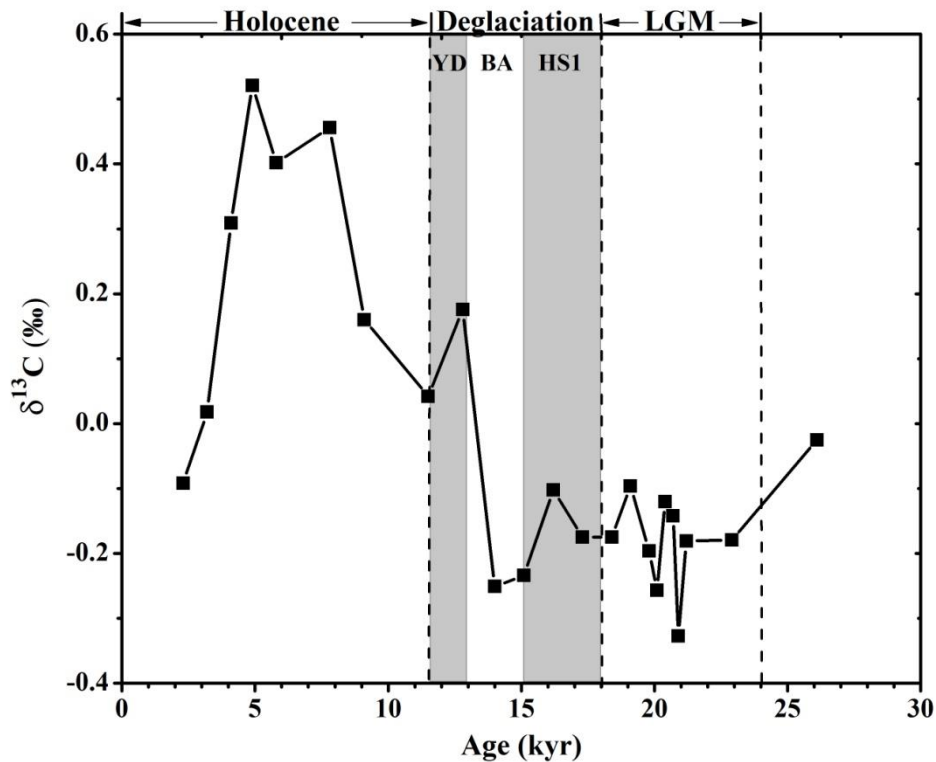
Figure 3.7: Graph representing variation of $\delta^{13}C$ (‰) in core SK-129/CR-05 for the last 25 kyr. Grey bands in the figure indicate Heinrich Stadial 1(HS1) and Younger Dryas (YD). White band indicates the Bølling-Ållerød (BA). The Last Glacial Maximum (LGM), deglaciation and Holocene are marked on the top axis.

3.4.2 Oxygen isotope ratios in Core AAS-9/21and SK-129/CR-05

Oxygen isotopic ratios ($\delta^{18}O$) in core AAS-9/21 vary from 2.1 to 3.7 ‰ for last 25 kyr (Figure 3.8). The Last Glacial Maximum recorded high values which vary from 3.4 to 3.7 ‰. The onset of HS1 is marked by decreasing $\delta^{18}O$ which reach to a minimum of 2.8 ‰ at~ 17 kyr and remain steady during late HS1 and early BA. A drop in values is again observed during BA which is then followed by a gradual increase during late BA. The Younger Dryas recorded a gradual fall in values from 3.4 to 2.8 ‰, which continue till the Late Holocene. The $\delta^{18}O$ values during Holocene range from 2.08 to 3.38 ‰ with the minimum $\delta^{18}O$ of 2.1‰ observed at 2.2 kyr. Overall a decreasing trend of $\delta^{18}O$ values is observed from LGM to Late Holocene
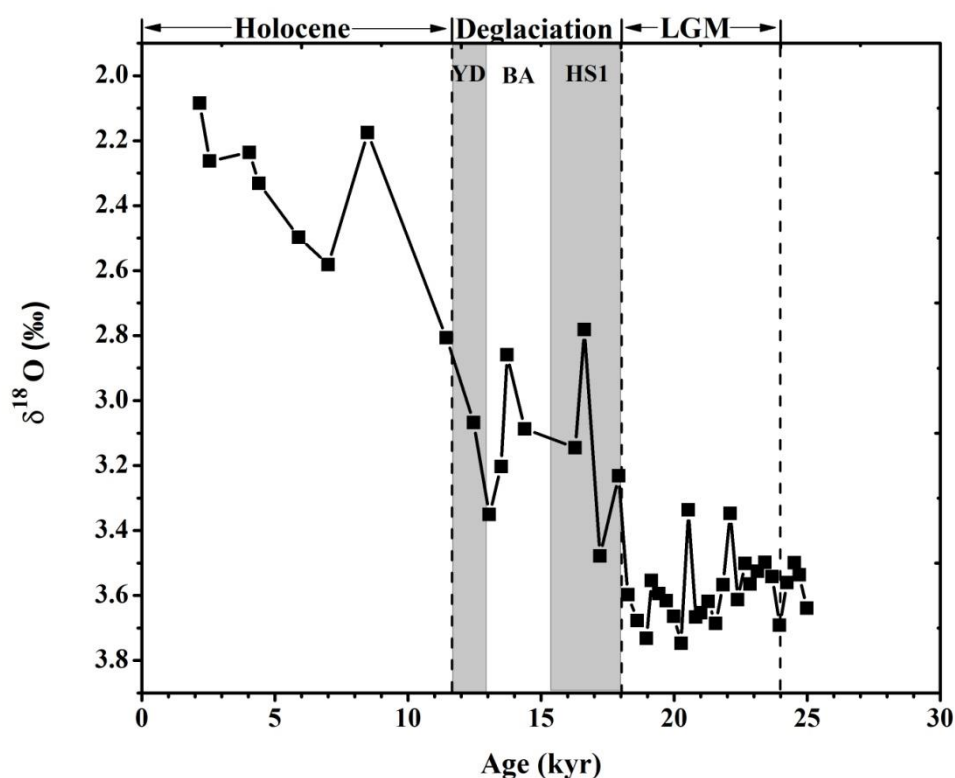
Figure 3.8: Graph representing variation of $\delta^{18}O$ (‰) in core AAS-9/21 for last 25 kyr. Grey bands in the figure indicate Heinrich Stadial 1(HS1) and Younger Dryas (YD). White band indicates the Bølling-Ållerød (BA). The Last Glacial Maximum (LGM), deglaciation and Holocene are marked on the top axis.

Oxygen isotope ratios ($\delta^{18}O$) in core SK-129/CR05 ranges from 1.79 to 4.14 ‰ over the last 25 kyr (Figure 3.9). The oxygen isotopic values during the LGM range from 3.87 to 4.08 ‰ and remain consistent till the termination of LGM. The $\delta^{18}O$ values gradually drop during HS1 followed by a slight rise of 3.76 ‰ at ~14 kyr in the BA. The YD shows lower $\delta^{18}O$ values. Overall, the deglacial $\delta^{18}O$ range from 3.16 to 4.14 ‰, with a decreasing trend and a minor rise during BA. The Holocene recorded the lowest $\delta^{18}O$ values which vary from 3.16 to 1.79 ‰. The $\delta^{18}O$ values during this time gradually decrease from early to mid-Holocene and increase at ~2 kyr in the Late Holocene. Overall, a decreasing trend in $\delta^{18}O$ values is seen from the LGM to Holocene.
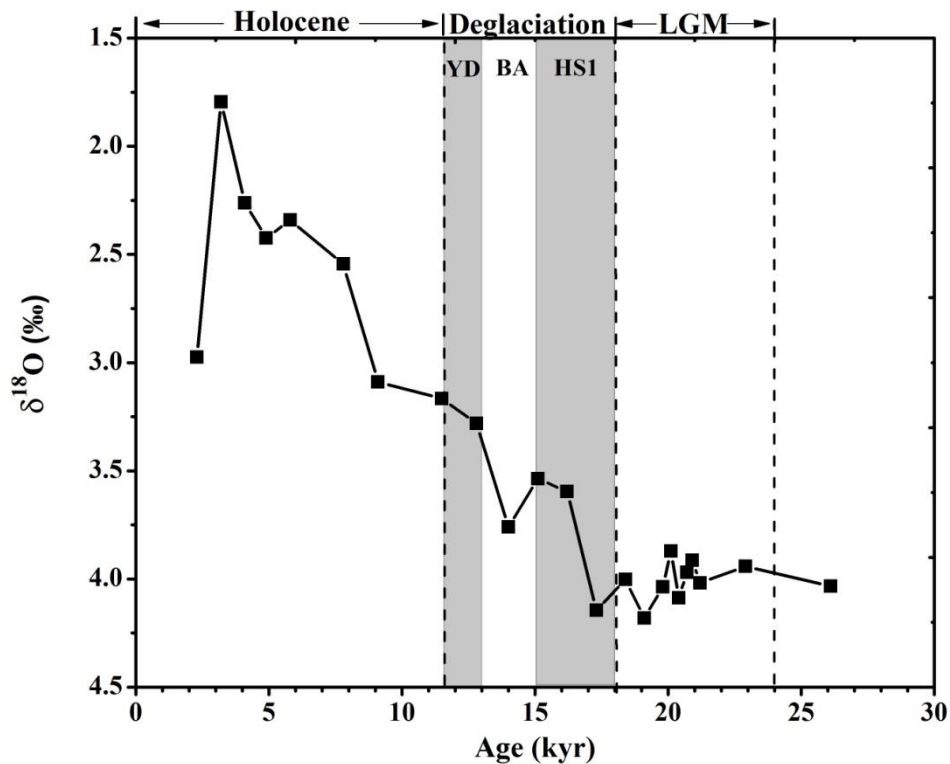
Figure 3.9: Graph representing variation of $\delta^{18}O$ (‰) in core SK-129/CR-05 for the last 25 kyr. Grey bands in the figure indicate Heinrich Stadial 1(HS1) and Younger Dryas (YD). White band indicates the Bølling-Ållerød (BA). The Last Glacial Maximum (LGM), deglaciation and Holocene are marked on the top axis.

3.4.3 [CO$_3^{2-}$] in Core AAS-9/21, Core SK-129/CR-05 and 02

The carbonate ion concentration [CO$_3^{2-}$] in core AAS-9/21 ranges from 53 to 91 µmol/kg for last 25 kyr (Figure 3.10). Lower [CO$_3^{2-}$] is seen during the LGM with an average of 76 µmol/kg and minimum value of 71 µmol/kg at ~18.3 kyr. This is followed by gradual increase throughout the HS1 reaching to a maximum of ~91 µmol/kg during the BA; except for a slight drop during 15 kyr. The carbonate ion concentration remained high during the entire HS1 and mid-BA which then sharply decreased during the late-BA. However, average [CO$_3^{2-}$] during the deglaciation was 81 µmol/kg, which was higher than the LGM. Overall, the deglaciation recorded a 5.3 µmol/kg rise in [CO$_3^{2-}$] over the LGM. Lower values are observed during the YD, which continued to decrease in the early and late Holocene. Lowest values are seen in the Holocene which vary from 52 to 75 µmol/kg and an overall decreasing trend is observed except for a prominent increase seen during the mid-Holocene which reaches a maximum of 75 µmol/kg at ~4.8 kyr. This translates to a [CO$_3^{2-}$] rise of 8.8 µmol/kg during mid-Holocene.
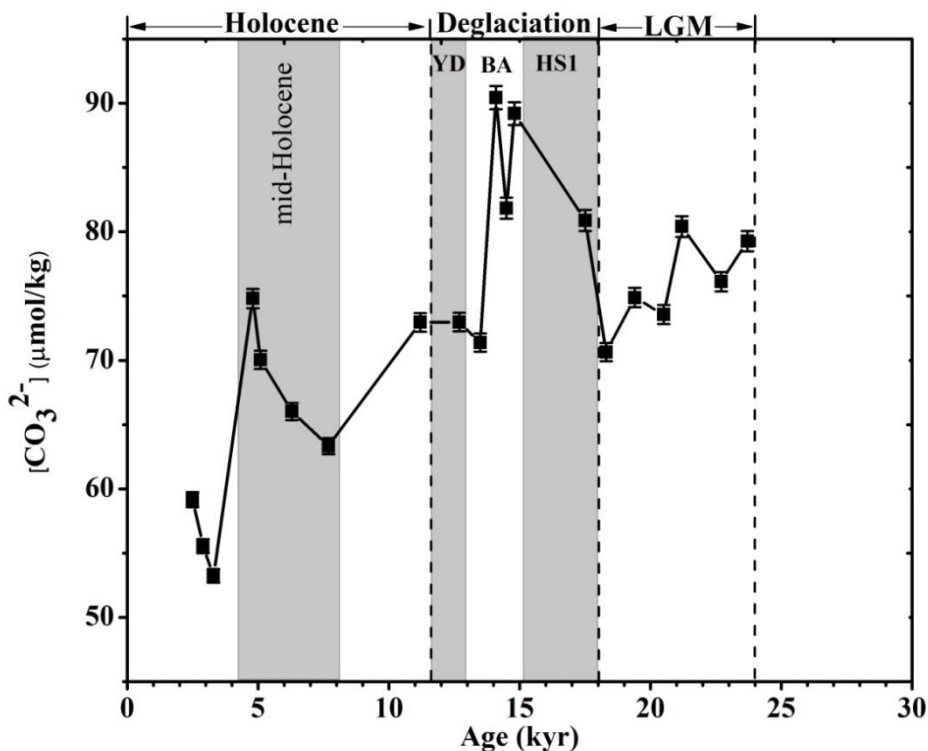
Figure 3.10: Graph showing variation in [CO$_3^{2-}$] (µmol/kg) in core AAS-9/21 for last 25 kyr along with measurement errors. Grey bands in the figure indicate Heinrich Stadial 1(HS1), Younger Dryas (YD) and mid-Holocene. White band indicates the Bølling-Ållerød (BA). The Last Glacial Maximum (LGM), deglaciation and Holocene are marked on the top axis.

.

Carbonate ion concentrations [CO_3^{2-}] in core SK-129/CR-05 ranges from 76 to 98 µmol/kg over the last 25 kyr (Figure 3.11). The [CO_3^{2-}] values are inconsistent during the LGM and vary between 88 to 94 µmol/kg with an average of 88 µmol/kg. Further, a very prominent hike of 98 µmol/kg is observed at~16 kyr during HS1. A considerable gap in [CO_3^{2-}] data exist between BA to early Holocene which is mainly due to lack of *C. wuellerstorfi* shells in sediment. However, a decreasing trend is observed from BA till 7 kyr. The carbonate ion concentration shows a slight increase during mid-Holocene after which it decreases to a minimum of 76.3 µmol/kg in the Late Holocene. Overall, low [CO_3^{2-}] values are seen during the LGM, followed by a rise during the deglaciation and a decreasing trend in the Holocene.
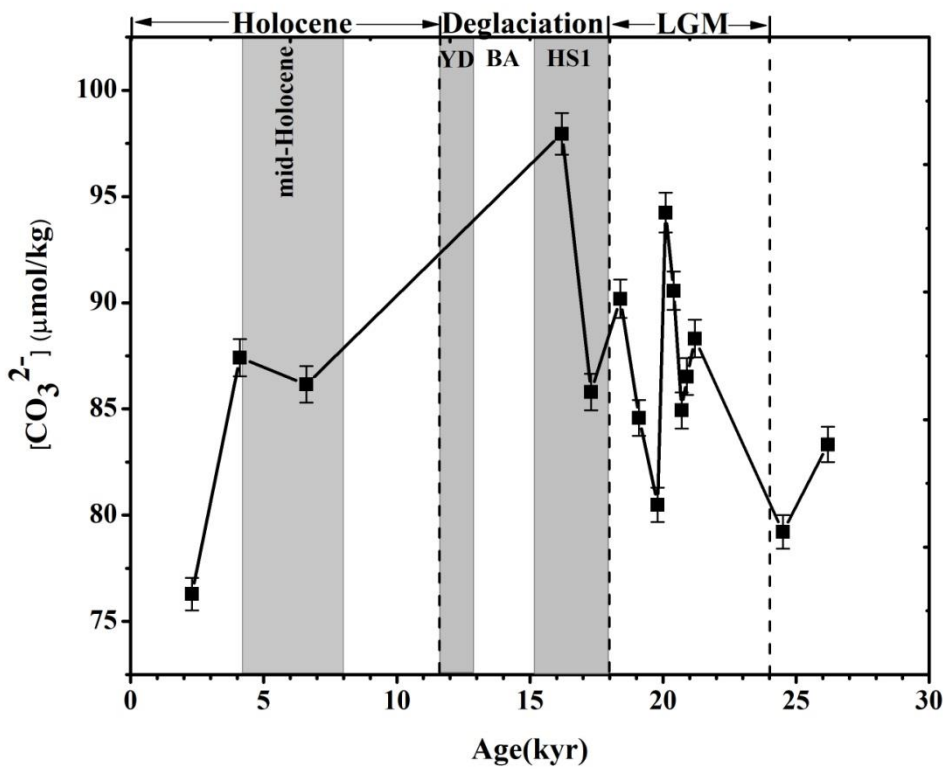
Figure 3.11: Graph showing the variation in [CO_3^{2-}] (µmol/kg) in core SK-129/CR-05 for last 30 kyr along with measurement errors. Grey bands in the figure indicate Heinrich Stadial 1(HS1), Younger Dryas (YD) and mid-Holocene. White band indicates the Bølling-Ållerød (BA). The Last Glacial Maximum (LGM), deglaciation and Holocene are marked on the top axis.

The reconstructed carbonate ion concentration in core SK-129/CR-02 varies from 80 to 100 μmol/kg over the last 25 kyr (Figure 3.12). The Last Glacial Maximum recorded a low carbonate ion concentration with average value of 90 μmol/kg. At the onset of HS1, $[CO_3^{2-}]$ shows a rapid increase leading to a peak of 100 μmol/kg at ~15 kyr. Thereafter the $[CO_3^{2-}]$ shows a gradual decrease throughout the BA and YD. Altogether the average $[CO_3^{2-}]$ during the deglaciation is 94 μmol/kg. The average $[CO_3^{2-}]$ for the Holocene is 90 μmol/kg with a decrease of $[CO_3^{2-}]$ during early Holocene and increase in the mid-Holocene to 96 μmol/kg at ~6 kyr. This $[CO_3^{2-}]$ rise accounts for 8.3 μmol/kg increase during the mid-Holocene. Overall, lower values of $[CO_3^{2-}]$ are seen in the Holocene as compared to the deglaciation with lowest value of 87 μmol/kg observed at ~10 kyr.
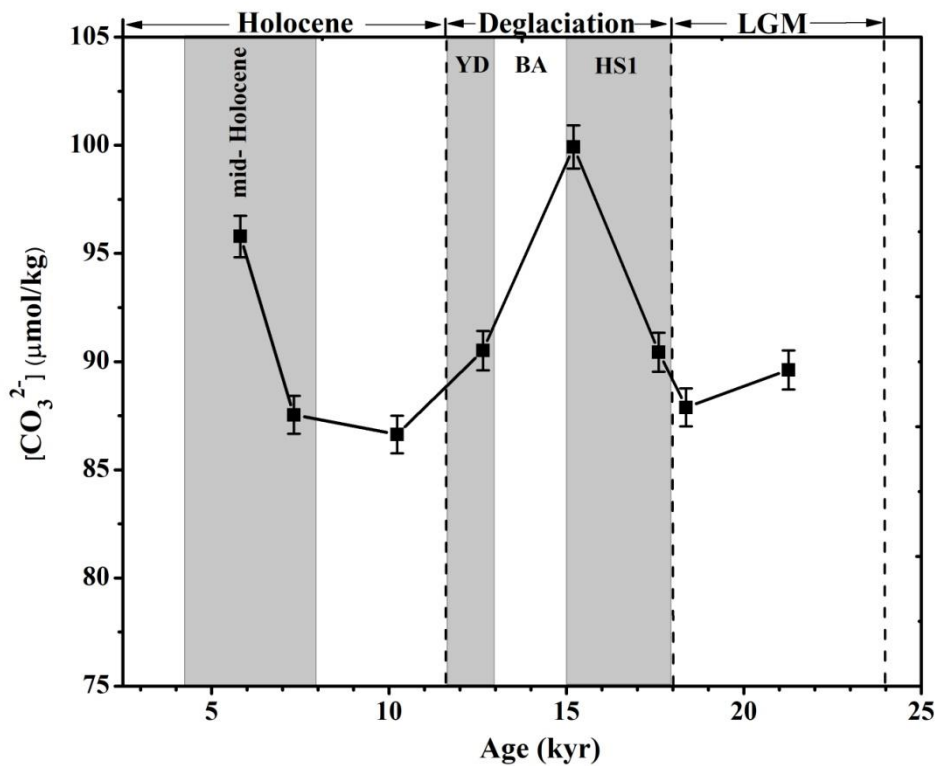
Figure 3.12: Graph showing the variation in $[CO_3^{2-}]$ (μmol/kg) in core SK-129/CR-02 for the last 25 kyr along with measurement errors. Grey bands in the figure indicate Heinrich Stadial 1(HS1), Younger Dryas (YD) and mid-Holocene. White band indicates the Bølling-Ållerød (BA). The Last Glacial Maximum (LGM), deglaciation and Holocene are marked on the top axis.

4. DISCUSSION

4.1 Modern day carbonate ion distribution in the Indian Ocean

The in-situ $[CO_3^{2-}]$ in the Eastern Arabian Sea (EAS) was calculated by using the salinity, temperature, pressure, total alkalinity and total CO_2 data from the Global Ocean Data Analysis Project (GLODAP) (Key *et al.,* 2004) using the CO2sys.xls (ver. 2.1) program (see section 2.3.7). The surface waters of the Indian Ocean show highest $[CO_3^{2-}]$ reaching upto ~225 µmol/kg, mostly because of the photosynthetic activity occurring in surface waters which increases dissolved oxygen, decreases CO_2 and increases the carbonate ion content (see section 1.1). Whereas, the Antarctic surface waters being iron limited, are less productive due to underutilisation of nutrients by phytoplankton and their $[CO_3^{2-}]$ decreases to 100 µmol/kg. The Antarctic Intermediate Waters (AAIW) having a carbonate ion content of 100 µmol/kg, similar to that of Antarctic surface waters, are seen to intrude into the Arabian Sea at intermediate depths, till 10° N (Figure 4.1). Below the surface waters, at ~200 m in the Arabian Sea, a low $[CO_3^{2-}]$ tongue is seen projecting at intermediate depths from north to south, with $[CO_3^{2-}]$ reaching to ~50 µmol/kg at its core. The thickness of this low carbonate ion layer in the Arabian Sea ranges from 200-2500 m water depth at 20°N and decreases towards the south. The Arabian Sea encompasses a perennial Oxygen Minimum Zone (OMZ) from a depth of 150-1200 m (Wyrtki, 1973; Naqvi, 1991) wherein the oxygen concentration reaches to values between 0-0.5 ml/l (Schulte *et al.,* 1999). Oxygen Minimum Zones are also termed as Carbon Maximum Zones (CMZ) (Paulimer, 2010) wherein due to excessive productivity in surface waters, organic matter sinks and undergoes decomposition, consuming oxygen and releasing CO_2 which further decrease the $[CO_3^{2-}]$ at mid-depths.

Below a depth of ~2000 m, better ventilated Circumpolar Deep Water (CDW) having $[CO_3^{2-}]$ of ~80 µmol/kg is seen to be intruding from the south (Figure 4.1). The $[CO_3^{2}]$ in deep Arabian Sea and Indian Ocean is affected by mixing of deep water masses which is seen in Figure 4.1. The Southern Ocean at a depth of 2000-3800 m clearly shows the presence of a deep watermass having high $[CO_3^{2-}]$ of ~100 µmol/kg which could be the North Atlantic Deep Water (NADW) reported to have the highest $[CO_3^{2-}]$ of ~125 µmol/kg (Broecker and Sutherland, 2000). The Antarctic Bottom Water (AABW) with a lower $[CO_3^{2}]$ of 75 µmol/kg is also seen to be intruding into the Indian Ocean. These two main deep and

bottom water masses along with the other water masses (see section 2.1.5) enter the Indian Ocean as 'CDW', which then upwells in the Arabian Sea and forms the High Salinity Deep Water (HSDW) with minor contribution from the Red Sea and Persian Gulf water masses (Shetye *et al.,* 1994; Kumar and Li, 1996) and occupies a depth of 1800 m in the Arabian Sea (see section 2.1.5).
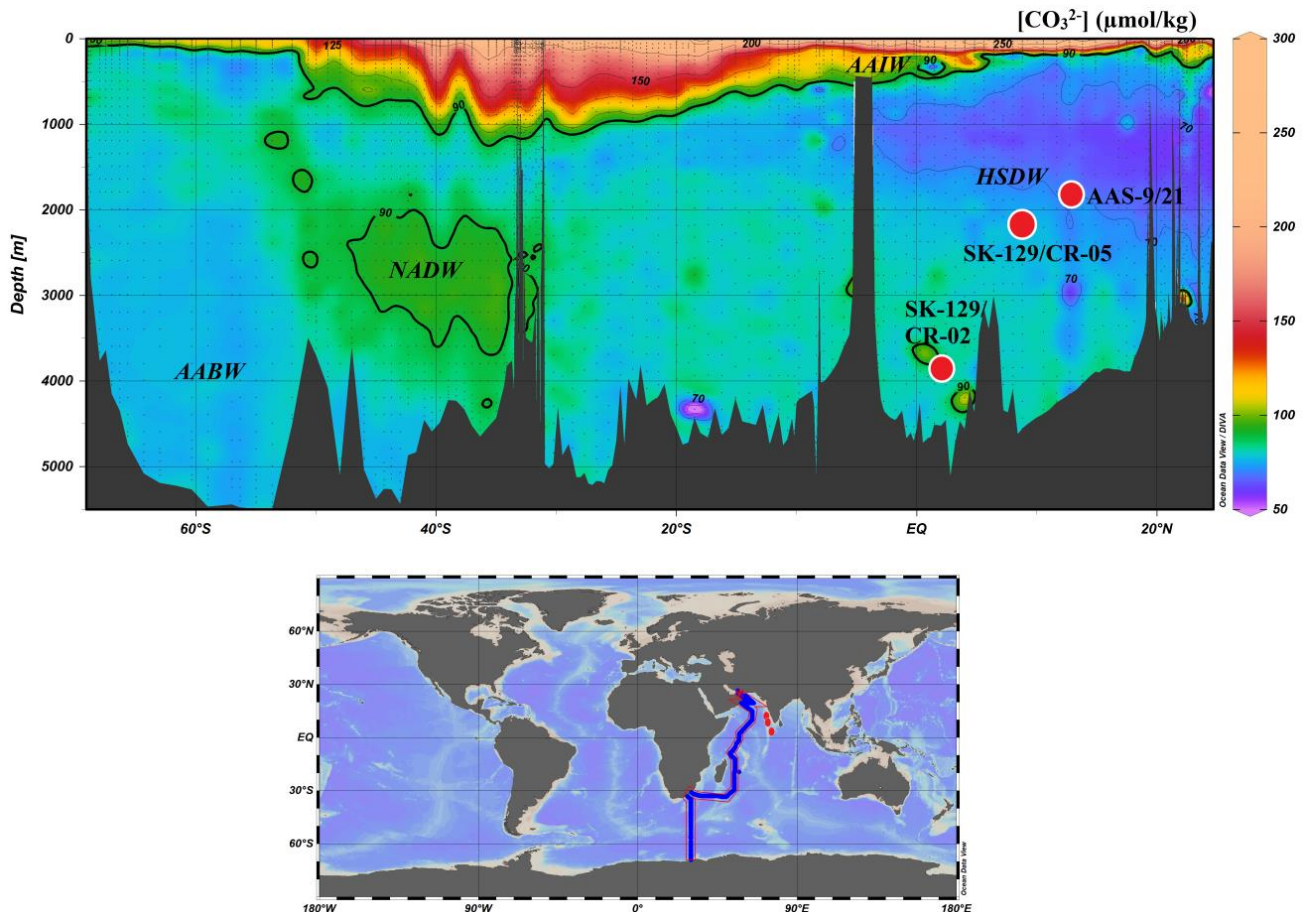
Figure 4.1: - Image showing $[CO_3^{2-}]$ distribution profile along a transect from the Arabian Sea to Antarctica based on GLODAP data (Key *et al.,* 2004). Red circles in profile indicate the three cores used for the study – AAS-9/21 (water depth = 1800 m), SK-129/CR-05 (water depth = 2300 m) and SK-129/CR-02 (water depth = 3800 m). Profile is generated using ODV (Schlitzer, 2006). CDW- Circumpolar Deep Water, HSDW- High Salinity Deep Water, NADW- North Atlantic Deep Water and AAIW –Antarctic Intermediate Water.

4.1.1 Carbonate ion variations in the EAS

The GLODAP stations selected in the EAS range from number 943– 956 and are distributed between 8.5 to 8.9° N and 70.5 to 75.6° E. Carbonate ion concentrations range from 67-290 µmol/kg (Figure 4.2) and show highest concentration in surface waters, decreasing with depth till~1000 m and further a slight increase till 4000 m. The higher $[CO_3^{2}]$ of surface waters are mainly due to the activity of the phytoplankton which fix dissolved

CO_2 into organic matter in the presence of sunlight through the process of photosynthesis. This activity consumes Dissolved Inorganic Carbon (DIC) and Alkalinity (ALK) in a ratio of 3.58:1 (Yu *et al.,* 2008) thus increasing the carbonate ion content of surface waters. The carbonate ion concentration in intermediate waters of the Arabian Sea at a depth of 800 m falls as low as 63 μmol/kg (Figure 4.2), which is due to the prevailing OMZ, wherein the excessive organic matter exported from increased surface productivity is decomposed, consuming oxygen and releasing CO_2 which lowers the $[CO_3^{2-}]$. At water depths >1500 m, $[CO_3^{2-}]$ shows a slight increase and remains constant thereafter which is due to influx of well-ventilated oxygen-rich deep waters. These deep waters originate from the polar regions and have a specific concentration of carbonate ion, which only changes due to oxidation of accumulated organic matter and mixing with other water masses.

In the Indian Ocean, Peterson and Prell, (1985) determined the foraminiferal lysocline to be at 3800 m by using dissolution proxies such as the percentage of whole planktic foraminifera, percentage of benthic foraminifera, weight percentage of carbonate and the percentage of coarse fraction in the sediments. Later Cullen and Prell, (1984) determined the foraminiferal lysocline to lie at a depth of 3800 m in the equatorial Indian Ocean, 3300 m in the Arabian Sea and 2600 m in the Bay of Bengal (BoB) by studying the changes in relative abundance of species. Initially, the CCD in the Arabian basin was determined to lie at 4800 m (Kolla *et al.,* 1976). But later Cullen and Prell, (1984) observed the absence of whole foraminiferal test below the depth of 4600 m in the eastern equatorial region, 5000 m in the western equatorial region and 3000 m in the BoB which is considered to be very similar to the foraminiferal compensation depth in the Indian Ocean. The red line in Figure 4.2 is the calcite saturation curve. In surface waters, calcite saturation is 41 μmol/kg but since the in-situ $[CO_3^{2-}]$ in surface water is very high and exceeds 280 μmol/kg, the surface is said to be oversaturated with carbonate ion, and calcium carbonate is usually precipitated in surface waters. As depth increases, carbonate saturation goes on increasing and intersects the in-situ $[CO_3^{2-}]$ curve at 3300 m, where the in-situ $[CO_3^{2-}]$ is equal to the carbonate ion saturation (in situ $[CO_3^{2-}]$ = $[CO_3^{2-}]$ saturation) and this depth is referred to as the 'calcite saturation horizon'. Above the calcite saturation horizon, calcium carbonate tends to remain preserved and below which it dissolves.
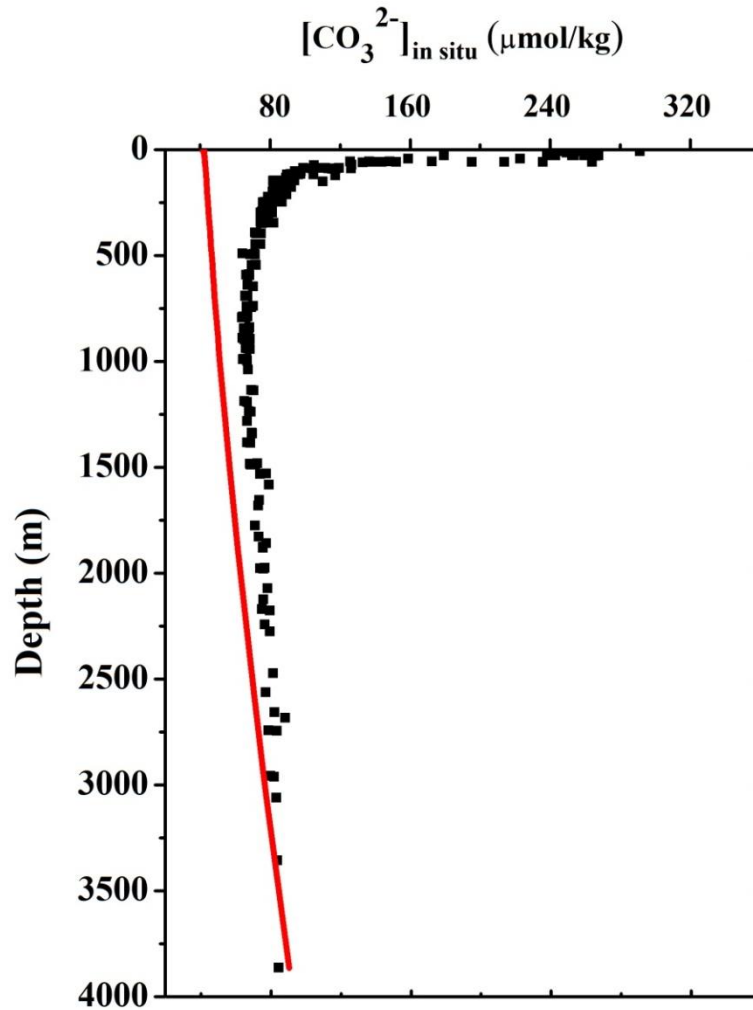
Figure 4.2:- Vertical distribution of $[CO_3^{2-}]$ in the EAS (GLODAP data; Key *et al.,* 2004) and red line shows the calcite saturation curve. The calcite saturation horizon is depth where, in situ $[CO_3^{2-}] = [CO_3^{2-}]$ saturation (is determined by pressure or water depth). Above the calcite saturation horizon, seawater is saturated with $CaCO_3$ causing preservation of $CaCO_3$ and below the calcite saturation horizon seawater is under saturated with $CaCO_3$ causing dissolution of $CaCO_3$.

4.2 Modern day dissolved oxygen distribution in the Indian Ocean

Dissolved oxygen concentration in the northern Indian Ocean varies between 0-300 µmol/kg (Figure 4.3). Oxygen concentration in surface waters is seen to be ̴ 200 µmol/kg in the Arabian Sea. High dissolved oxygen content is attributed to the photosynthetic activity of phytoplankton which captures carbon for synthesis of organic matter and release oxygen in the ambient water, thus increasing oxygen content of waters up to a depth of 150 m. Below this depth, from ̴ 200 m to 1500 m, an intense OMZ is observed where the oxygen levels go

down to <1 µmol/kg. An intense OMZ is observed towards the head of the Arabian Sea mainly due to the increased primary production and export of organic matter to intermediate waters, which utilises oxygen from the water column and undergoes degradation, releasing CO_2. The sluggish intermediate water ventilation also contributes to the intense OMZ of the Arabian Sea. The intensity of the Arabian Sea OMZ is seen to decreases towards the equator, however, comparatively low oxygenated waters can be seen upto 5° S. Further, oxygenated intermediate waters with oxygen concentration ranging from 100-150 µmol/kg are also seen to intrude into the Arabian Sea, however, this water is seen to penetrate only till 8° N.
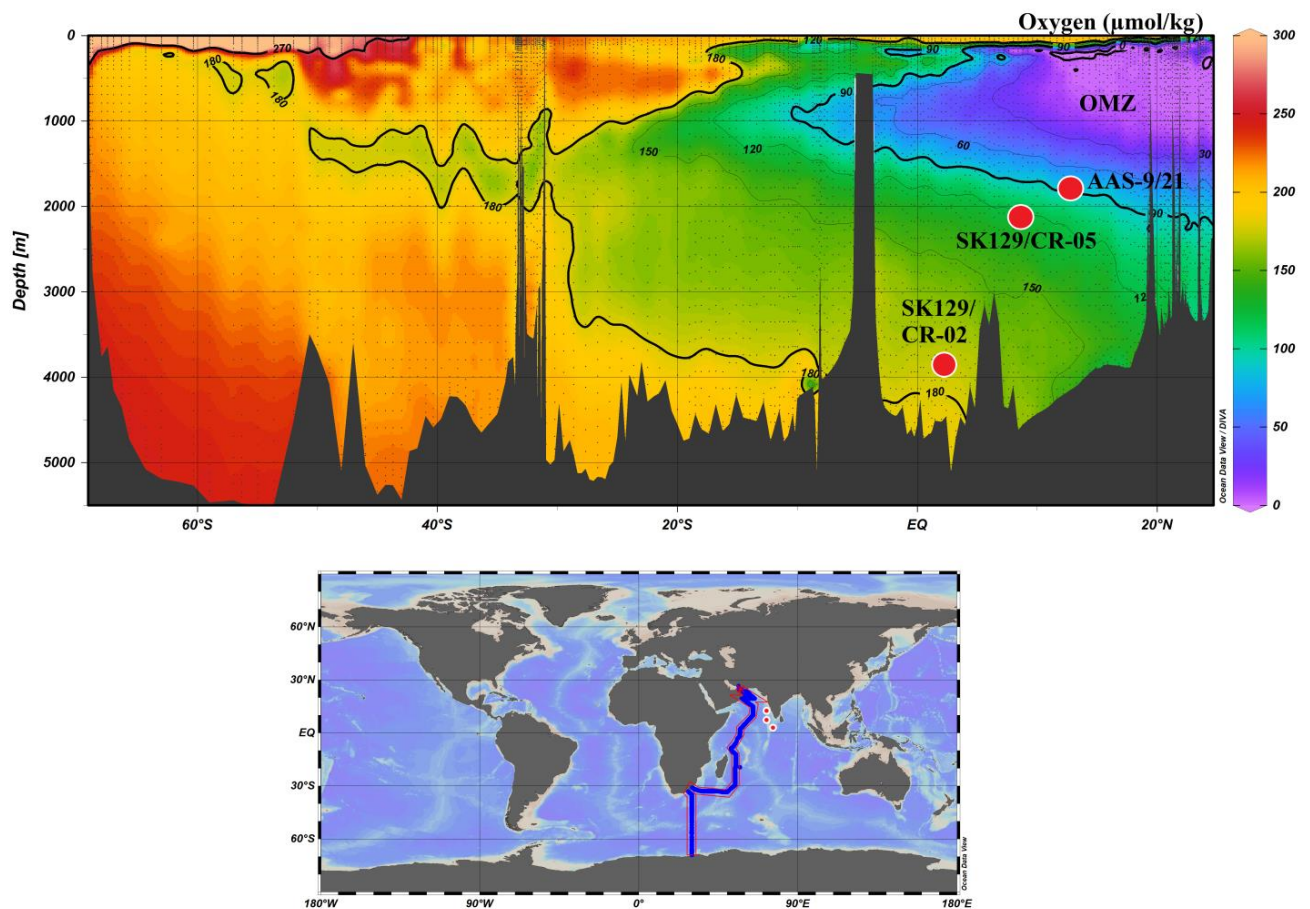
Figure 4.3:- Image showing dissolved oxygen distribution profile from the Arabian Sea to Antarctica based on GLODAP data (Key *et al.,* 2004). Red circles in profile indicate the three cores used for the study AAS-9/21 (water depth = 1800 m), SK-129/CR-05 (water depth = 2300 m) and SK-129/CR-02 (water depth = 3800 m). Profile is generated using ODV (Schlitzer, 2006). CDW- Circumpolar Deep Water, HSDW- High Salinity Deep Water, NADW- North Atlantic Deep Water and AAIW –Antarctic Intermediate Water.

Below the depth of 1500 m, well-ventilated waters can be seen with oxygen concentration ranging from 100-150 µmol/kg. These well-ventilated waters are the cold, high saline and oxygen rich, originating from the polar region, which are referred to as the

Upper Circumpolar Deep Water (UCDW) and mainly consist of NADW (see section 2.1.5). Below these waters lies the Lower Circumpolar Deep Water (LCDW) which are mainly formed from the mixture of extremely oxygenated water arising from the Antarctic region, the AABW which are the densest with oxygen concentration of these waters ranging from 200-250 µmol/kg. Both UCDW and the LCDW together enter the Arabian Sea as the deep western boundary current (see section 2.1.5).

4.2.1 *Dissolved oxygen concentration in the EAS*

The GLODAP stations selected for plotting the dissolved oxygen profile range from station number 943- 956 and are distributed between 8.5 to 8.9° N and 70.5 to 75.6° E (Key *et al.,* 2004), the same as those used for calculation of $[CO_3^{2-}]$. As can be seen in Figure 4.4, the dissolved oxygen concentrations of the surface waters are high and range from 50-250 µmol/kg. High dissolved oxygen concentration in surface waters mostly result from the photosynthetic activity of the phytoplankton which utilises CO_2 in the presence of sunlight and liberates oxygen. The Oxygen Minimum Zone is clearly seen from a depth of 200-1200 m wherein the oxygen concentrations drop to < 25 µmol/kg in the EAS. This is caused due to intensive oxidation of exported organic matter from increased surface productivity to intermediate depths, which consumes mid-depth oxygen. However, the west coast of India experiences an intense OMZ between 20º N to 14º N and its intensity keeps decreasing from north towards the south with oxygen concentration reaching to 5.4 µmol/kg at 18° N and 19.6 µmol/kg at 6.1° N (Goswami *et al*., 2012).

Below a depth of 1200 m, the oxygen concentration goes on increasing till a depth of 3500 m and further remains constant till a depth of 4000 m. However, the dissolved oxygen in deep-waters range from 100-150 µmol/kg which is due to the inflow of CDW with low temperature, high salinity and denser water having higher capacity to dissolve gasses thus giving rise to well oxygenated waters flowing in the Arabian Sea through the passage in Chagos-Laccadive Ridge (see section 2.1.5 and Figure 2.3).
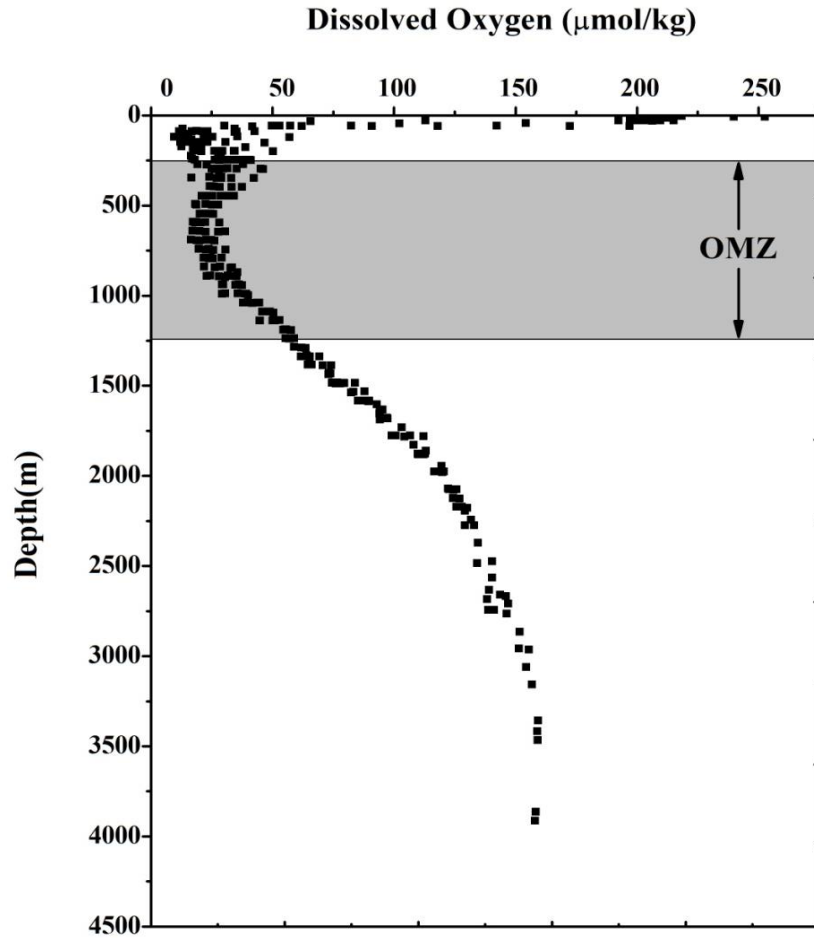
Figure 4.4:- Vertical distribution of dissolved oxygen in the EAS and grey box shows the Oxygen Minimum Zone (OMZ). Above graph is obtained using the GLODAP data (Key *et al.,* 2004).

4.2.2 Relationship between $[CO_3^{2-}]$ and dissolved oxygen

The carbonate ion content in deep waters are mainly controlled by dissolution/ precipitation of calcium carbonate in ambient waters, changes in alkalinity, mixing of deep waters and organic carbon remineralisation (see section 1.1). On the other hand, the dissolved oxygen content in deep waters is mostly controlled by temperature, as affinity of gases to dissolve in water increases with decreasing water temperature, ventilation of the deep water masses and export production from surface waters. Although carbonate ion and the oxygen content in water column are controlled by different parameters, the organic carbon remineralisation seems to be a common factor affecting both the parameters. The carbon dioxide gas evolved from organic matter degradation is seen to decrease the carbonate ion content in seawater. Thus a clear inverse relationship exists between CO_2 and

$[CO_3^{2-}]$ in seawater (Hoegh-Guldberg *et al.,* 2007). Such relationship between $[CO_3^{2-}]$ and oxygen has not been studied in deep waters. Thus I have investigated the relationship between $[CO_3^{2-}]$ and oxygen in deep waters (>1500 m) of the south eastern Arabian Sea. The profile obtained for $[CO_3^{2-}]$ (Figure 4.2) and dissolved oxygen concentration (Figure 4.3) shows similarities in surface and deep waters. In surface waters, the concentration of both parameters showed increase mainly due to the photosynthetic activity of phytoplankton which increased oxygen in surface layers and consumed carbon dioxide thus increasing the $[CO_3^{2-}]$ in the surface waters.

At mid-depths (200-1200 m) the dissolved oxygen decreased to < 25 µmol/kg and the $[CO_3^{2-}]$ also decreases to a minimum value of 63 µmol/kg. The carbonate ion concentration decreases at intermediate depths till 500 m depth but remained constant at >500 m depth, whereas dissolved oxygen showed depletion till 1200 m depth. This is because of the organic carbon remineralisation at 200-1200 m depth which can result in shallowing of the Aragonite Compensation Depth (ACD) in the Arabian Sea, which promotes calcium carbonate dissolution. Several studies have observed the dissolution of calcium carbonate shells in the OMZ (Calvert *et al.,* 1995; Singh, 1998; Singh *et al.,* 2006; Sing *et al.,* 2007; Naidu *et al.,* 2014; Naik *et al.,* 2014). Dissolution of calcium carbonate shells releases carbonate ion back to ambient waters. Hence the carbonate ion concentration is not severely depleted in the OMZ.

Below the OMZ, oxygen concentration starts to increase and a slight $[CO_3^{2-}]$ increase is also seen. This can be attributed to the presence of deep water masses from polar regions. Thus the oxygen and $[CO_3^{2-}]$ of seawater at depths greater than 1500 m shows a positive correlation with each other (Figure 4.5).
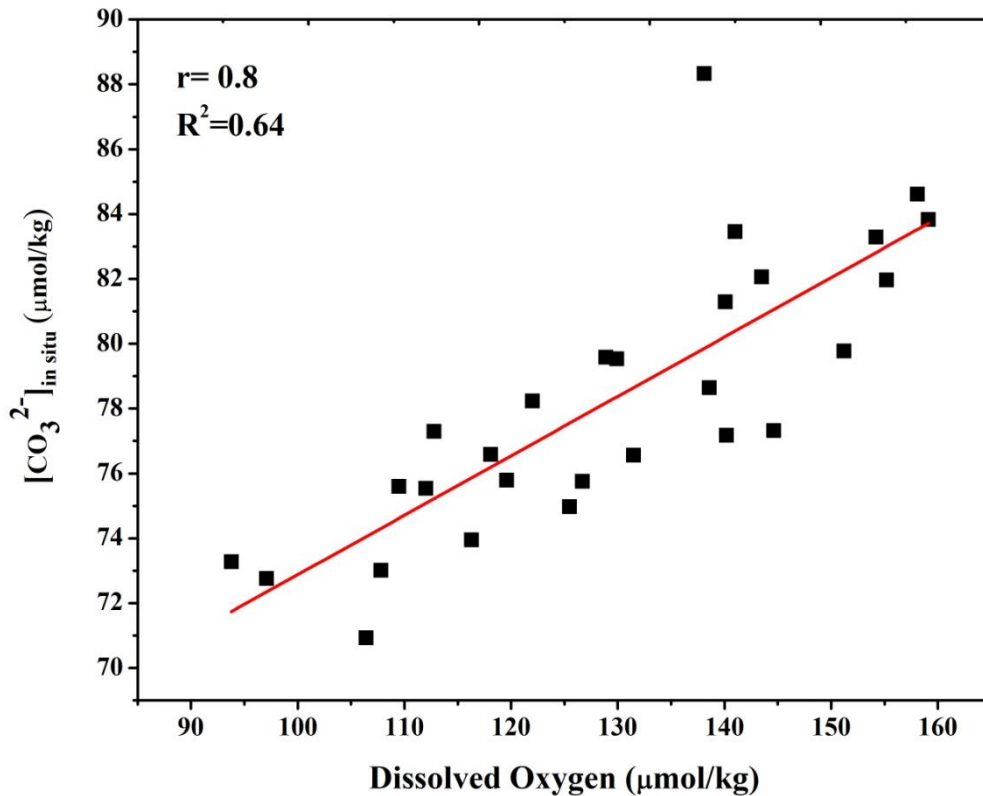
Figure 4.5:- Scatter plot showing a positive relationship between $[CO_3^{2-}]$ and dissolved oxygen in deep waters, >1500 m depth of the south eastern Arabian Sea using GLODAP data (Key *et al.,* 2004).

4.3 Sedimentation accumulation rates in sediment cores from the EAS

The sedimentation accumulation rate can be referred to as the amount of sediments getting deposited in an unit area in unit time and expressed in cm/kyr. Sedimentation accumulation rate is an important parameter as the sediments are the basic source of information which tell us about the depositional and post depositional changes occurring at the core location. The sedimentation is widely affected by a number of parameters such as climate i.e. monsoons, bottom topography, distance from the river mouth and water depth. Also the turbidity currents and dissolution in marine environment affects the sedimentation accumulation rates after deposition of sediments.

The sedimentation accumulation rates in all the three sediment cores (Figure 3.1 of results section) vary with water depth. The shallowest sediment core AAS-9/21 retrieved from a depth of 1800 m showed higher sedimentation accumulation rate (5.4-14.2 cm/kyr) than core SK-129/CR-05 retrieved from a depth of 2300 m (2.4-11.42 cm/kyr) and core SK-129/CR-02 retrieved from a depth of 3800 m (1.2-6.6 cm/kyr). The sedimentation accumulation rates in the three cores show significant changes from the LGM to the

Holocene. The average sedimentation accumulation rate in core AAS-9/21 during the LGM is similar to the Holocene, whereas average sedimentation accumulation rate in core SK-129/CR-05 was higher during the LGM than the Holocene. On contrary core SK-129/CR-02 recorded low average sedimentation accumulation rate during the LGM than the Holocene.

Core AAS-9/21 exhibited a similar average sedimentation accumulation rate during the Holocene and LGM. Such similarity in average sedimentation accumulation rate during the LGM and the Holocene is also observed by Singh *et al.,* (2017) by compiling sedimentation accumulation rates of 58 cores from the EAS. Such a sedimentation pattern is attributed to deepening of surface mixed layers due to a stronger winter monsoon leading to enhanced primary productivity, thus increasing the biogenic flux during the LGM (Singh *et al.,* 2017). Core SK-129/CR-05 showed higher average sedimentation accumulation rate during the LGM than the Holocene, probably due to higher Terrigenous Sediment Discharge (TSD) (Pattan *et al.,* 2005). Higher bulk Al concentrations (average $4.51 \pm 0.47\%$) and Marine Accumulation Rates (MAR) (average 0.105 g/cm^2/kyr) were observed in core SK-129/CR-05 during the glacial by Pattan *et al.* (2005). This was mainly attributed to the low sea level, erosion of exposed shelf and suspended load from the river directly getting discharged into the deep sea. This could have probably given rise to high sedimentation rate of 11.4 cm/kyr between the time interval 21.2-19.8 kyr. For the rest of the time, the sedimentation rate does not show significant changes and varies between 3-6 cm/kyr.

The sedimentation accumulation rate in core SK-129/CR-02 varied from 1.2 to 3.5 cm/kyr from the LGM to the Holocene with a considerable increase in sedimentation accumulation rate of 6.6 cm/kyr seen between 16-17 kyr during the deglaciation. Similarly, remarkably high sedimentation accumulation rate in core AAS-9/21 during the deglaciation is also very prominently observed all along the east coast of India (Singh *et al.*, 2017), which is attributed towards the rising sea level at that time. During the LGM the sea level was 120 m lower and the modern day shelf was exposed, the rivers flowing into the west coast of India would drain into the EAS, far to the west, draining the sediments in deeper regions as concluded from the incised valleys and paleo channels (Raju *et al.,* 1991). Later, as the sea level began to rise during the deglaciation, the rivers discharged sediments to shallower depths, thus increasing the sedimentation accumulation rates. However, the sedimentation accumulation rate during the deglaciation in core SK-129/CR-05 is seen to be lower, probably due to decreased TSD as observed by Pattan *et al.* (2005).

The sedimentation accumulation rate in core SK-129/CR-02 during the LGM is seen to be lower than the Holocene, which could have been due to the stronger southwest monsoon during the Holocene which increased runoff as well as productivity, thus leading to higher sedimentation accumulation rates in the Holocene (Shimmield, 1992; Reichart *et al.,* 1997; Schnetger *et al.,* 2000). Also the sedimentation accumulation rate in core SK-129/CR-05 slightly increased during the Late Holocene which is again due to the increased intensity of southwest monsoon and associated productivity hike observed by Pattan *et al.* (2003). Whereas, the sedimentation accumulation rate in the shallower core, AAS-9/21, is seen to be decreased during the Holocene in comparison to the deglaciation, which could have been due to the increased sea level and discharge of sediments brought by the rivers into the continental shelf.

4.4 Last Glacial Maximum to Holocene changes in deep-water circulation and temperature using carbon and oxygen isotope ratios

Carbon and oxygen isotope ratios of foraminiferal test are exclusively used for tracing past changes in ocean circulation, air-sea exchange, global carbon cycle and tracing water masses in the oceans. Every water mass has a unique $\delta^{13}C$ signature, which is acquired during its formation for eg. thermohaline circulation begins with the formation of NADW formed from warm surface waters brought by the Gulf Stream. These waters loose heat and moisture to the atmosphere, gain density and sink to greater depths, forming the NADW. The NADW has distinctive properties of low nutrients, highest $[CO_3^{2-}]$ ($\sim$ 125 µmol/kg) (Broecker and Sutherland, 2000) and highest $\delta^{13}C$ (1.1 ‰) (Raymo *et al.*, 2004), whereas, deep waters emerging from the Weddell Sea have a $\delta^{13}C$ of 0.2 to 0.4 ‰ and low nutrients (Mackensen *et al.*, 2001) and CDW has a $\delta^{13}C$ of 0.4 ‰ (Charles and Fairbanks, 1992; You, 2000). High $\delta^{13}C$ values in NADW is mainly due to the high productivity, wherein phytoplankton in the euphotic zone use sunlight, nutrients and aqueous CO_2 from seawater and fix lighter carbon (^{12}C) in organic matter (see section 1.4.5) which makes the surface water rich in heavier carbon (^{13}C). These waters after gaining appropriate density, sink to deeper depths forming the NADW with high $\delta^{13}C$ and low nutrients. The low $\delta^{13}C$ values in southern sourced water is the result of low productivity, evident from the high nutrient content, especially PO_4, which is the limiting nutrient and has high values of 1.95 µmol/kg (Broecker *et al.*, 1995) in surface waters due to underutilization of nutrients. In low productivity condition, the lighter carbon remains in the surface waters instead of getting fixed in organic carbon and dilutes the $\delta^{13}C$ of surface waters. These waters due to freezing

and brine rejections give rise to high density waters that sink to the bottom of the oceans with high underutilized nutrients and low $\delta^{13}C$ values. Thus the deeper water masses can be identified based on their temperature and salinity and can be traced using its $\delta^{13}C$ signature. At the deeper depths in the water column the organic carbon/ organic matter arriving from the euphotic zone undergoes microbial decomposition, which utilizes oxygen and releases CO_2 (rich in ^{12}C) and nutrients. The $\delta^{13}C$ values of deep water masses are affected more when the thermohaline circulation slows down, which endures enhanced carbon respiration. Hence $\delta^{13}C$ values do not only track the circulation but can also virtually determine the oxygen, CO_2 and nutrient contents of deep water masses. Along with the productivity and oxidation of organic carbon, the $\delta^{13}C$ of deep waters are also affected by mixing waters masses having different $\delta^{13}C$ values (can be seen in Figure 4.6). Also, different transport pathways of deep waters contribute to changes in $\delta^{13}C$ (Wilson *et al.,* 2015). The above properties make $\delta^{13}C$ a reliable tool to determine changes in circulation, ventilation of deeper oceans and changes in atmospheric CO_2 content on glacial to interglacial time scale. Numerous studies based on benthic foraminiferal carbon and oxygen isotopic variation in intermediate and deep waters on glacial to interglacial timescales have been carried out in the Indian Ocean. Most of these are located in the BoB (Kallel *et al.,* 1988; Naqvi *et al.,* 1994; Ahmad, 1995; Ahmad *et al.,* 2008; Raza and Ahmad 2013; Raza *et al.,* 2014; Ma *et al.,* 2019; Ma *et al.,* 2020), and in the south and equatorial Indian Ocean (Martison *et al.,* 1987; Boersma and Mikkelsen 1990; Waelbroeck *et al.,* 2006; Yu *et al.,* 2010; Romahn *et al.,* 2014) which suggest changes to the intermediate and deep water circulation in the Indian Ocean.

In comparison, similar studies in the Arabian Sea are few (Zahn and Pedersen, 1991; Hermelin and Schmiedl, 1995; Sirocko *et al.,* 2000; Schmiedl and Mackensen, 2006; Gupta *et al.,* 2008; Jung *et al.,* 2009; Gupta *et al.,* 2011; Ma *et al.,* 2020). Amongst these, some sediment cores have poor age constraints, and/or with coarse resolution and/or limited to the Holocene and/or involving the use of mixed benthic foraminifera other than *Cibicidoides Wullerstorfi* which is considered to produce isotopic values in equilibrium with seawater (Zhan *et al.,* 1986). Besides these difficulties, there are a few well dated/high resolution/longer records which focus on deep water oxygenation changes (Schmiedl and Mackensen, 2006) and monsoon intensity in combination with other proxies (Gupta *et al.,* 2008; Gupta *et al.,* 2011).
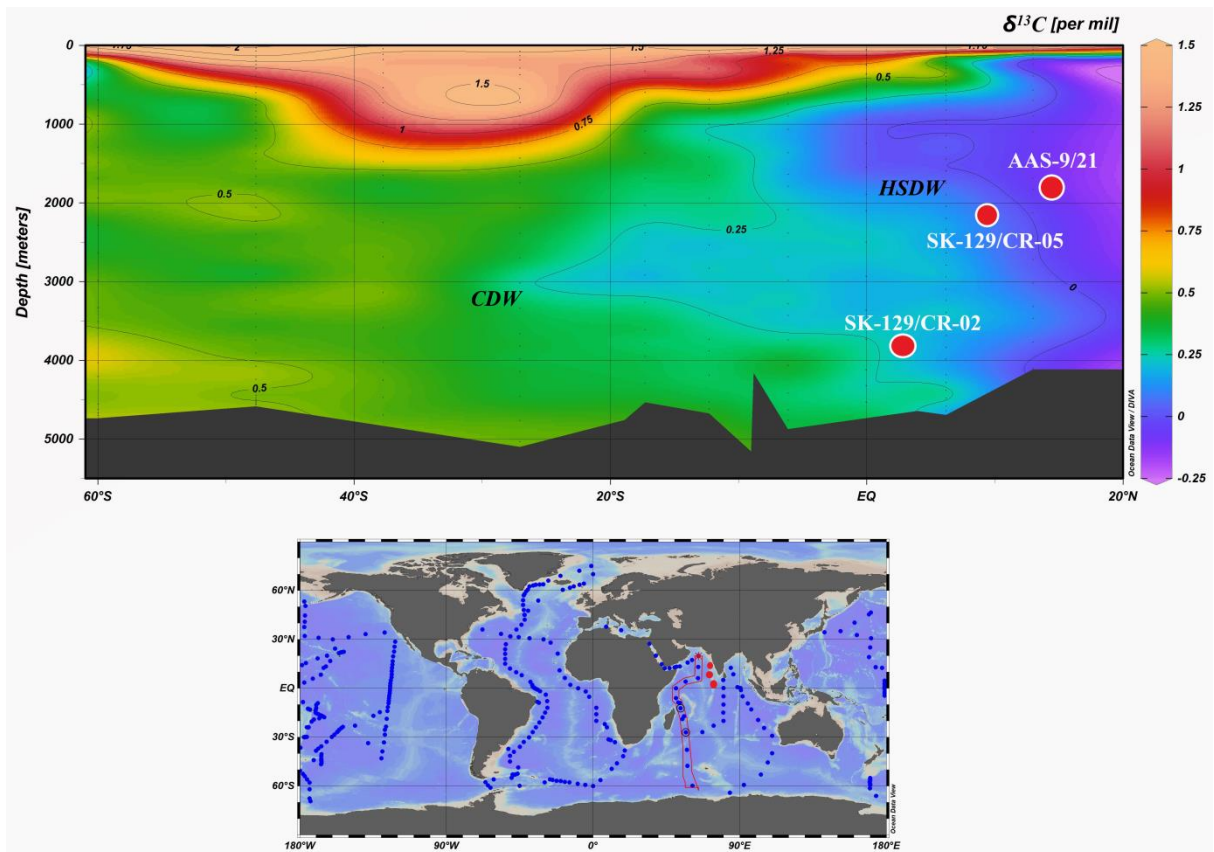
Figure 4.6:- Image showing $\delta^{13}C$ distribution profile along a transect from the Arabian Sea to Antarctica based on GEOSECS data (Key *et al.,* 2004). Red circles in profile indicate the three cores used for the study AAS-9/21 (water depth = 1800 m), SK-129/CR-05 (water depth = 2300 m) and SK-129/CR-02 (water depth = 3800 m). Profile is generated using ODV (Schlitzer, 2006). CDW- Circumpolar Deep Water and HSDW- High Salinity Deep Water.

The scarcity of $\delta^{13}C$ records in intermediate and deep waters of the Arabian Sea has led to diminished understanding of biogeochemical cycling of carbon and circulation changes on glacial to interglacial timescales.

Carbon isotope ratios ($\delta^{13}C$) from *C. wuellerstorfi* in cores AAS-9/21 and SK-129/CR-05 shows an increase over the last glacial-interglacial transition by~ 0.56 ‰ and 0.85 ‰ respectively (Figure 4.7). These values are slightly higher than the documented mean whole ocean glacial-interglacial $\delta^{13}C$ increase of ~0.46 ‰ (Curry *et al.,* 1988), but are very much similar to values obtained from a nearby core, SK-129/CR-02, showing a change of ~ 0.7 ‰ (Piotrowski *et al.,* 2009), a core from the southwest Indian Ocean showing a change of ~ 0.97 ‰ (Yu *et al.,* 2010) and BoB cores recording change of ~0.66 ‰, ~ 0.7 ‰,~ 0.9 ‰ and ~ 0.74 ‰ (Ahmad *et al.,* 2008; Raza and Ahmad, 2013; Raza *et al.,* 2014). Such values arise due to glacial $\delta^{13}C$ depletion with values reaching to -0.28 ‰ and -0.33 ‰ in

cores AAS-9/21 and SK-129/CR-05 respectively and point towards glacial to interglacial changes in circulation.

Glacial $\delta^{13}C$ values observed in both the cores are similar and at par with SK-129/CR-02 glacial values. Due to scarcity of benthic foraminiferal studies in intermediate waters of the southeastern Arabian Sea, glacial $\delta^{13}C$ values of both the cores are compared with the ODP Hole 117-724C retrieved from a depth of 603 m, from intermediate waters of the Western Arabian Sea. Glacial values of ODP Hole 117-724C (0.39‰) (Zhan and Pedersen, 1991) were found to be very high as compared to that of core AAS-9/21 and SK-129/CR-05. Such high values in intermediate waters and depletion in deep waters indicates the presence of stratified and isolated deep glacial water mass. Similar stratification between intermediate and deep waters was also reported by Kallel *et al.* (1988) and Naqvi *et al.* (1994) in the Arabian Sea and BoB respectively. Although there existed a strong $\delta^{13}C$ gradient between intermediate and deep waters, the similarity and tight coupling between $\delta^{13}C$ values of AAS-9/21 and SK-129/CR-02 at depths of ~ 1800 m and ~ 4000 m during the LGM, suggests poor ventilation below the depth of 1800 m. This could probably be due to the fact that during the LGM, the RSW and PGW sources were closed and so the only source was the southern sourced waters for all the three cores. Numerous studies have recorded weakened Atlantic Meridional Ocean Circulation (AMOC) during the LGM due to decreased production and shoaling of NADW (Elliot *et al.*, 2002, Marchitto and Broecker, 2006; Negre *et al.,* 2010; Menviel *et al.,* 2017). These changes in circulation were not only limited to the Atlantic Ocean but were also detected in the Pacific (Bostock *et al.,* 2004) and Indian Ocean (Piotrowski *et al.,* 2009; Ahmad *et al.,* 2008; Raza and Ahmad, 2013; Raza *et al.,* 2014; Naik *et al.,* 2019; Ma *et al.,* 2019).

The Last Glacial Maximum to Holocene variations in $\delta^{18}O$ suggests evolution of cooler to warmer bottom water temperatures in both the cores, AAS-9/21 and SK-129/CR-05. The SK-129/CR-05 $\delta^{18}O$ shift over the LGM to Holocene exceeds ice-volume effect by 0.4 ‰ and 0.7 ‰ respectively (Figure 4.8), indicating bottom water cooling of ˷ 2° C (Epstein *et al.,* 1963) during the LGM.
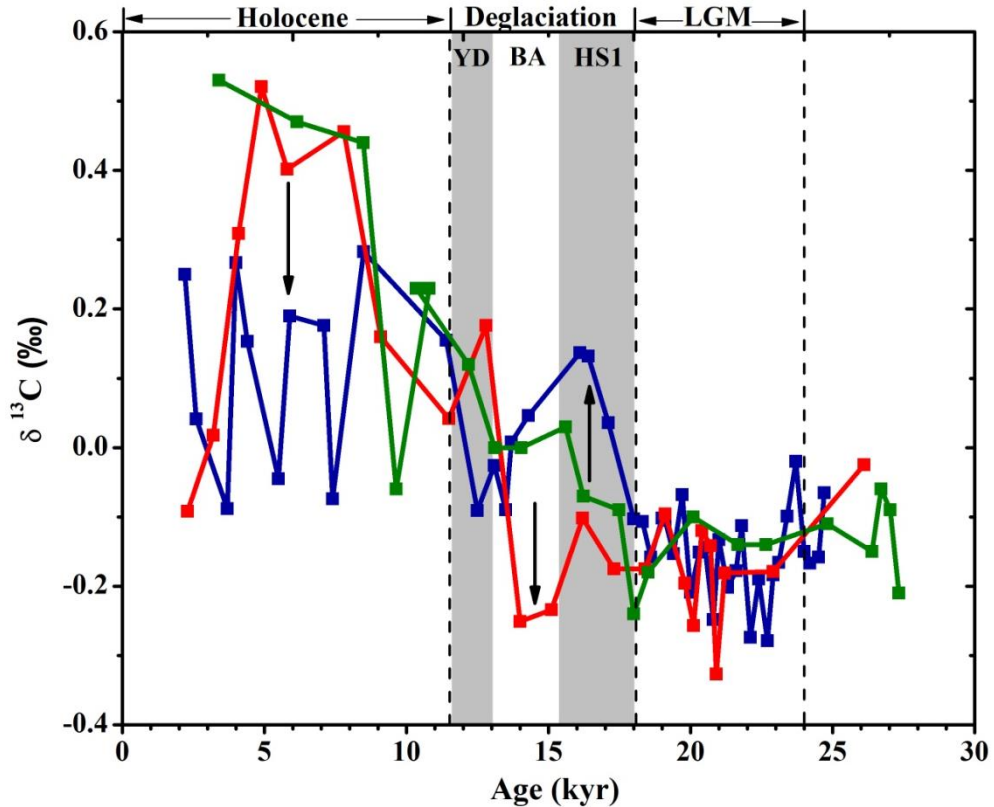
Figure 4.7:- Graph showing $\delta^{13}C$ variations in epifaunal benthic foraminifera *C. wuellerstorfi* from cores AAS-9/21 (water depth = 1800 m, blue line), SK-129/CR-05 (water depth = 2300 m, red line) and SK-129/CR-02 (Piotrowski *et al.,* 2009, water depth = 3800 m, green line). Grey bands in the figure indicate the Heinrich Stadial 1 (HS1) and Younger Dryas (YD). White band indicates the Bølling-Ållerød (BA). The Last Glacial Maximum (LGM), deglaciation and the Holocene are marked with arrows on the top axis. Vertical arrows indicate marked increase/decrease from normal values (see text for explanation).

Bottom-water cooling may have been caused due to circulation changes which occurred during the LGM. Further, cooling of bottom water can be expected due to shift in source of water reaching the core site from $\delta^{13}C$ enriched NADW to cooler and $\delta^{13}C$ depleted Southern Ocean Deep Waters (SODW), as the production of NADW reduced during the LGM (Elliot *et al.,* 2002; Marchitto and Broecker, 2006; Negre *et al.,* 2010). Pulses of aged and ^{14}C depleted waters (Bryan *et al.,* 2010) were reported in the western Arabian Sea during the deglaciation, which are thought to originate from less ventilated and stratified glacial deep waters. The Last Glacial Maximum also witnessed the sequestration of high amounts of organic carbon to the global deep ocean through enhanced biological pump via the Southern Ocean (Smetacek *et al.,* 2012; Muglia *et al.,* 2017). Furthermore, studies point to a stratified, less ventilated and ^{14}C aged deep water mass in global ocean during the LGM (Skinner *et al.,* 2010; Skinner *et al.,* 2014; Skinner *et al.,* 2017). These events when put together present a clear picture of organic carbon build up in deep waters and decreased NADW production

in the Atlantic Ocean which resulted in stratified and $\delta^{13}C$ depleted deep waters. The sluggish glacial circulation enhanced the degradation of organic carbon giving rise to depleted $\delta^{13}C$ values and nutrient enriched deep waters. Glacial $\delta^{13}C$ depleted values does not only suggest stratified and nutrient enriched waters but also indicate less oxygenated and pool of stored $^{12}CO_2$ in deep waters altering its carbonate chemistry.
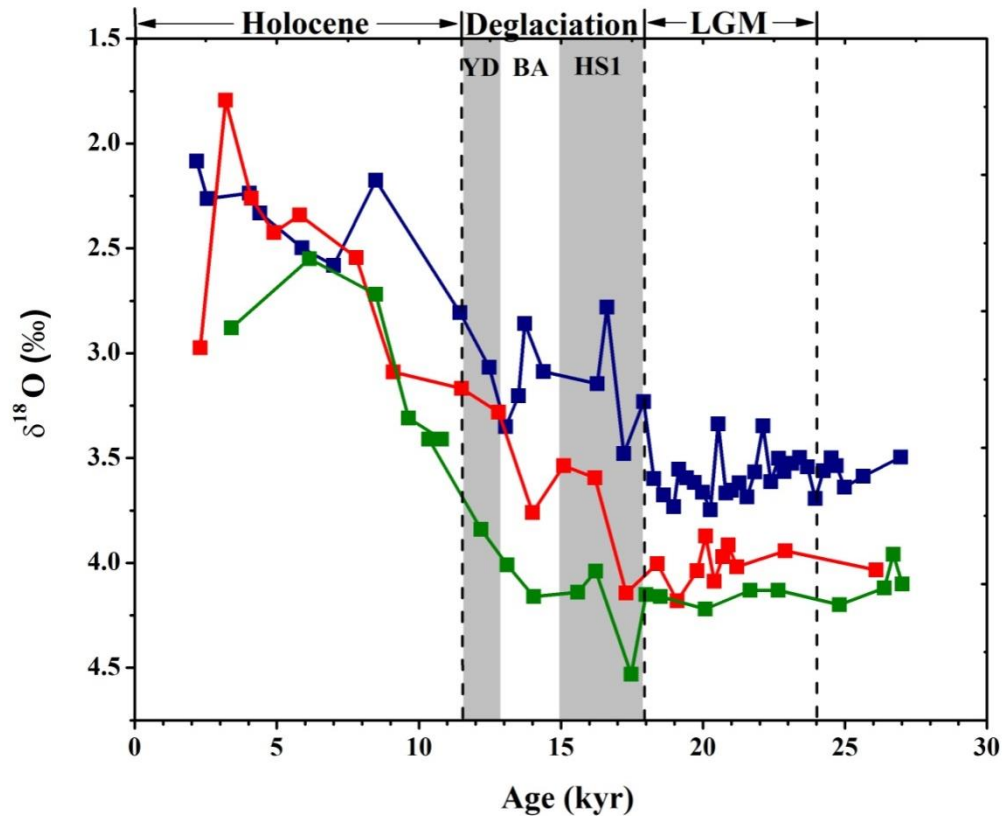
Figure 4.8 :- Graph showing $\delta^{18}O$ variations in epifaunal benthic foraminifera *C. wuellerstorfi* from core AAS-9/21 (water depth = 1800 m, blue line), core SK-129/ CR-05 (water depth = 2300 m, red line) and core SK-129/CR-02 (Piotrowski *et al.,* 2009, water depth = 3800 m, green line). Grey bands in the figure indicate Heinrich Stadial 1(HS1) and Younger Dryas (YD). White bands indicate Last Glacial Maximum (LGM), Bølling-Ållerød (BA) and Holocene respectively. White band indicates the Bølling-Ållerød (BA). The Last Glacial Maximum (LGM), deglaciation and Holocene are marked with arrows on the top axis.

The $\delta^{13}C$ signal in core AAS-9/21 is initially seen to increase during Heinrich Stadial 1 (HS1) and showed a decreasing trend from 16 kyr which continued throughout the Bølling-Ållerød (BA) and reached to a minimum of -0.09 ‰ at 12.5 kyr and then rose again in the Younger Dryas (YD) (Figure 4.9a). The elevated $\delta^{13}C$ signal during the HS1 involves an

increase in $\delta^{13}C$ from -0.103 ‰ at 18 kyr to 0.137 ‰ at 16 kyr. Similar increase in $\delta^{13}C$ was observed by Ma *et al.* (2020) in the southeastern Arabian Sea at a depth of 1254 m (Figure 4.9b). Also Yu *et al.* (2018) observed higher radiogenic Nd isotope (ϵ_{Nd}) values reaching to -6.8 during the HS1 and the YD (Figure 4.9c) in intermediate waters of the BOB and are comparable to ϵ_{Nd} values of AAIW observed during the last glaciation (-6.8 to -6.0) by Hu *et al.* (2016). This increase in $\delta^{13}C$ and ϵ_{Nd} values in the northern Indian Ocean during the HS1 is mainly attributed towards the intrusion of AAIW into the Indian Ocean during the deglaciation. Similar strong northward invasion of AAIW was also observed in the Atlantic (Cao *et al.,* 2005; Pahnke *et al.,* 2008; Mangini *et al.,* 2010) and Pacific oceans (Marchitto *et al.,* 2007; Stott *et al.,* 2009; Basak *et al.,* 2010). The enhanced invasion of AAIW in the northern hemisphere is ascribed to collapse of the extensive sea-ice formed during the LGM and increased formation of AAIW through strengthened deep water upwelling in the Southern Ocean (Basak *et al.,* 2010).

The $\delta^{13}C$ values in core SK-129/CR-05 (2300 m) did not show a prominent increase during HS1, instead severe depletion was seen during the BA. Similar depletion is also evident from BoB cores retrieved from deep waters; SK 157-14 (water depth = 3306 m) and SK 157-16 (water depth = 2920 m) (Ahmad *et al.,* 2008; Raza and Ahmad, *et al.,* 2013), except core SK 157-15 (water depth = 2855 m), which probably can be due to low resolution of the core. Organic carbon content in core SK-129/CR-05 ranges from 0.3-0.7% (Guptha *et al.,* 2005), which is very low and does not seem to affect the $\delta^{13}C$ of deeper waters. The $\delta^{13}C$ depletion timings (15-13 kyr) in the North Indian Ocean coincide well with the Melt Water Pulse1a (MWP-1a, 14.65–14.31 kyr; Deschamps *et al.,* 2012) and associated rise in sea level. The sea-level rise during this time could have influenced the discharge of terrigenous organic matter into the ocean and the input of lighter $\delta^{13}C$ terrigenous organic carbon may have contributed to the decrease in the benthic foraminifer $\delta^{13}C$ values in the North Indian Ocean (Ma *et al.,* 2019).

Gradual increase in $\delta^{13}C$ and $\delta^{18}O$ values are observed during the Holocene in cores SK-129/CR-05 and SK-129/CR-02 (Piotrowski *et al.,* 2009), which illustrate the evolution of cooler and nutrient enriched water-mass to warmer and nutrient depleted waters. Warmer water masses resulted in response to the shift in glacial to interglacial mode of climate. Enriched $\delta^{13}C$ in deep waters indicate well ventilated deep waters entering the Arabian Sea and point towards strengthening of AMOC and increased flow of NADW. Similar studies carried out in Indian Ocean showed increased proportion of NADW reaching the Indian Ocean during the Holocene (Piotrowski *et al.,* 2009; Ahmad *et al.,* 2008; Raza and Ahmad

2013; Raza *et al.,* 2014; Naik *et al.,* 2019; Ma *et al.,* 2019). Whereas, core AAS-9/21 exhibited δ^{13}C values which are very much lower than SK-129/CR-05 and SK-129/CR-02.
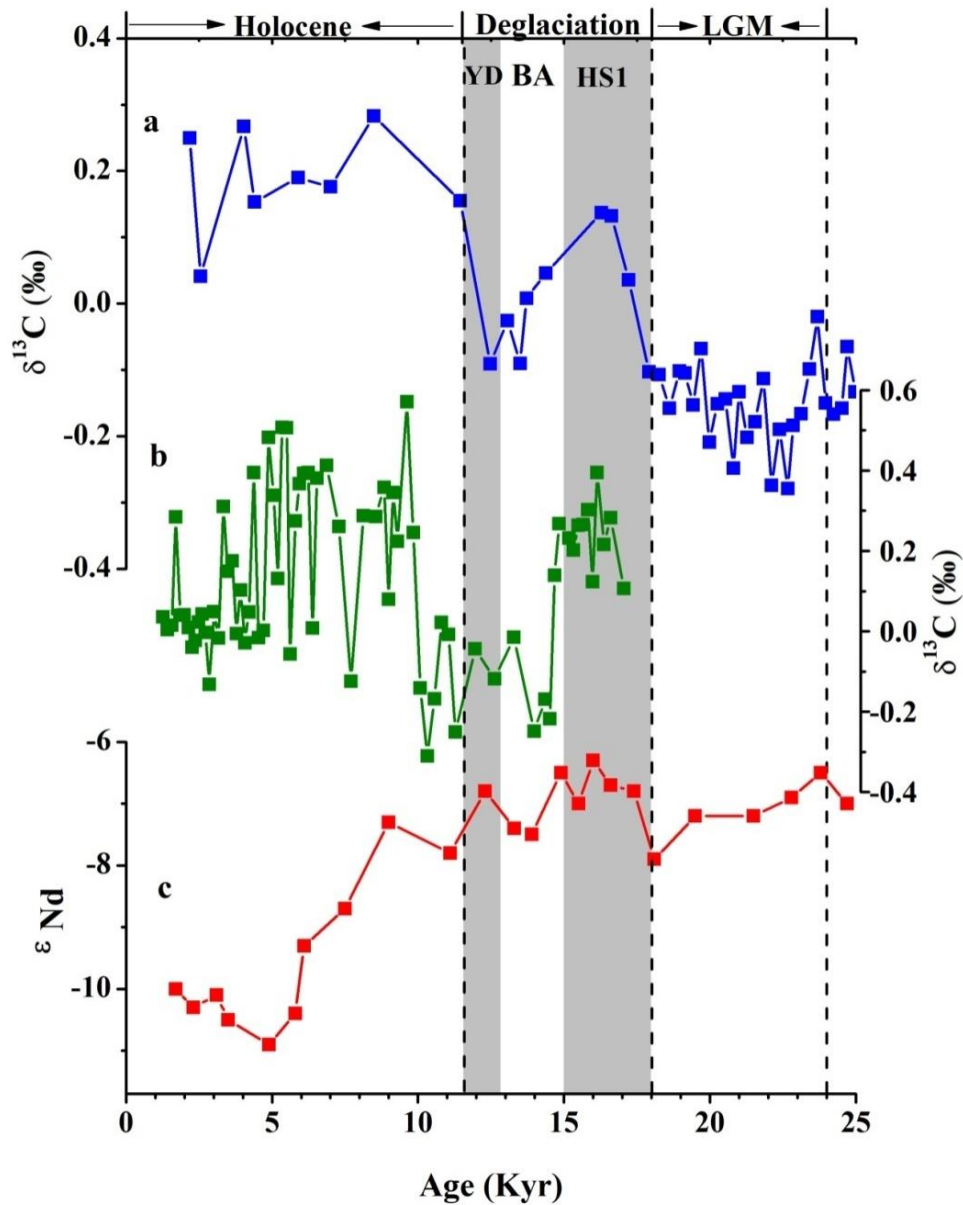
Figure 4.9 :- Graph showing, a) δ^{13}C variations in epifaunal benthic foraminifera *C. wuellerstorfi* from core AAS-9/21 (water depth = 1800 m), b) δ^{13}C variations in benthic foraminifera from core MD77-191 (Arabian Sea, water depth = 1254 m) (Ma *et al.,* 2020) and c) ε_{Nd} of mixed planktonic foraminifera from core MD77-176 (Bay of Bengal, water depth = 1375 m, Yu *et al.,* 2018). Grey bands in the figure indicate Heinrich Stadial 1(HS1) and Younger Dryas (YD). White band indicates theBølling-Ållerød (BA). The Last Glacial Maximum (LGM), deglaciation and Holocene are marked with arrows on the top axis.

4.5 Last Glacial Maximum to Holocene changes in $[CO_3^{2-}]$ of deep waters using the shell weight proxy

I have attempted to determine the calcium carbonate dissolution in core SK-129/CR-05 in order to understand the changes in carbonate ion content of deep waters from the LGM to the Holocene by using the shell weight proxy. The shell weight study in AAS-9/21 is carried out by Naik and Naidu, *et al.*, 2014 and thus is not discussed in this study. Also the *G. ruber* shells in core SK-129/CR-02 (Figure 3.4) showed a considerable amount of dissolution and are not suitable for determining the $[CO_3^{2-}]$ through shell weight proxy. As this core SK-129/CR-02 is retrieved from a depth of 3800 m which is placed below the Foraminiferal lysocline where the dissolution of foraminiferal shells begins in Arabian Sea. Oxygenated and high carbonate ion content of NADW favours preservation of $CaCO_3$ shells whereas low oxygen and low carbonate ion content of AABW causes it to be less ventilated and more corrosive, encouraging the dissolution of $CaCO_3$ shells. Shell weights in core SK-129/CR-05 were lighter during the LGM and the Holocene in comparison to the deglacial period (Figure 4.10a). This in turn reflects the preservation state in deeper waters wherein the LGM and the Holocene showed similar preservation reflecting similar carbonate chemistry and better preservation was noted in the deglaciation indicating considerable changes in carbonate ion content. The Atlantic Meridonial Ocean Circulation has experienced major changes and reorganisations from the LGM to the Holocene. The Last Glacial Maximum experienced a weaker AMOC as compared to the Holocene due to the reduced NADW production, which is the main driver of the AMOC (Elliot *et al.*, 2002; Marchitto and Broecker, 2006; Negre *et al.,* 2010; Menviel *et al.,* 2017) which was countervailed by incursions of high nutrient, less ventilated and low carbonate-ion southern-sourced waters in the North Atlantic (Curry and Oppo, 2005). These perturbations in AMOC are also very well recorded in the Pacific Ocean (Bostock *et al.,* 2004).

Neodymium isotopes (ε_{Nd}) have been used in the Indian Ocean by few studies (eg. Piotrowski *et al.,* 2009; Yu *et al.,* 2018; and Naik *et al.,* 2019) and together with $\delta^{13}C$ suggest changes in intermediate and deep-water circulation in the Indian Ocean such as decreased penetration of NADW in the Arabian Sea (Piotrowski *et al.,* 2009) and BoB (Yu *et al.,* 2018; and Naik *et al.,* 2019) during the LGM. Increased penetration of $\delta^{13}C$ depleted southern sourced deep waters in the BoB (Kallel *et al.,* 1988; Naqvi *et al.,* 1994; Ahmad, 1995; Ahmad *et al.,* 2008; Raza and Ahmad, 2013; Raza *et al.,* 2014; Ma *et al.,* 2019), Arabian Sea (Piotrowski *et al.,* 2009; Romahn *et al.,* 2014 and Ma *et al.,* 2020) and in the South and

equatorial Indian Ocean (Martison et $al.,$ 1987; Waelbroeck et $al.,$ 2006; Yu et $al.,$ 2010) was documented during the LGM. The southern sourced $\delta^{13}C$ depleted, less-ventilated and nutrient enriched deep waters originating from the Weddell and Ross Sea have low carbonate ion content and high CO_2 emerging from the decomposition of organic carbon, are highly corrosive and tend to dissolve $CaCO_3$ shells. The low shell weights in core SK-129/CR-05 during LGM could be the outcome of penetration of corrosive deep-waters of Southern Ocean origin which lowered the $[CO_3^{2-}]$ of ambient waters and enhanced dissolution at the core site.

The deglaciation recorded a maximum rise in shell weight of 20.4 µg observed at ~ 16 kyr and showed an average shell weight of 19.4 µg during the deglaciation which is 2 µg higher than the LGM. The increase in shell weight during the deglaciation goes well with the slight increase in the calcium carbonate percentage in the same core (SK-129/CR-05) (Figure 4.10b; Guptha et $al.$, 2005). This increase in calcium carbonate and shell weights could be due to an improved $[CO_3^{2-}]$ in deep waters during deglaciation thus enhancing preservation. Similar observation by Naik and Naidu, (2015) show a clear hike in shell weights from a period of 17.5 – 14.5 kyr in core SK-218 (water depth = 3307 m) and core SK-157 (water depth = 3171 m) from deep waters of the BoB and also in core AAS-9/21 (water depth =1800 m) and ODP Site 723 (water depth = 808 m) from the Arabian Sea (Naik and Naidu, 2016). Calcium carbonate preservation event in the deglaciation is recorded in the global oceans (Berger, 1977; Broecker, 2001; Broecker and Clark, 2003; Lalicata and Lea, 2011; Jaccard et $al.,$ 2009) which indicate changes in the carbonate chemistry of deep and the intermediate waters. Yu et $al.$ (2010) recorded a 10 µmol/kg rise in $[CO_3^{2-}]$ in the Indian and Pacific Ocean and a 20 µmol/kg in the Atlantic Ocean which favoured preservation of $CaCO_3$ in the deglaciation.

The deglacial calcium carbonate preservation spikes were attributed to the CO_2 degassing from the deeper waters through extensive upwelling in Southern Ocean (Anderson et $al.$, 2009) which resulted in an increase in $[CO_3^{2-}]$ of global ocean (Yu et $al.$, 2010). *Globigerinoides ruber* shell weights recorded in the Holocene were 3 µg lower than the deglacial shell weights, which suggest poor preservation in the Holocene. On contrary, the $CaCO_3$ percentage in Holocene ranges from 60-67% and shows an increasing trend from early to late Holocene (Pattan et $al.$, 2003; Guptha et $al.,$ 2005). This could be due to the surface processes occurring in the southeastern Arabian Sea which includes the intensification of southwest monsoon (Pattan et $al.$, 2003). Several studies in the

southeastern Arabian Sea indicate intensification of southwest monsoon during early to late Holocene (Thamban *et al*., 2007; Anand *et al*., 2008; Kessarkar *et al.,* 2013), which could have generated wind induced upwelling leading to higher productivity and greater supply of $CaCO_3$ to the sediments. The organic carbon content (<0.4 %) observed during the Holocene is also negligible to cause supralysoclinal dissolution of $CaCO_3$ at the core site and hence lower Holocene shell weights in core SK-129/CR-05 could be due to the dissolution of $CaCO_3$ shells due to $CaCO_3$ compensation during the Holocene. Preservation of $CaCO_3$ during the deglaciation resulted in removal of alkalinity from the deep ocean, and hence to compensate for alkalinity depletion, $CaCO_3$ shell dissolution began in the Holocene (Yu *et al.,* 2014).
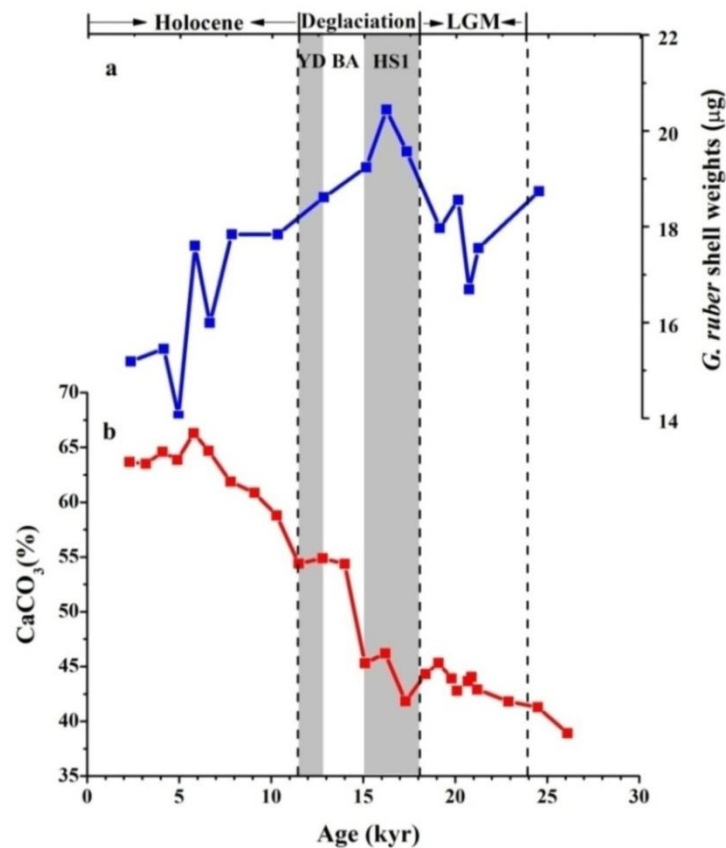
Figure 4.10:- Graph showing variations in a) shell weights of planktic foraminifera *G. ruber* in core SK-129/ CR-05 (water depth = 2300 m) and b) $CaCO_3$ in core SK-129/ CR-05 (Guptha *et al.,* 2005). Grey bands in the figure indicate Heinrich Stadial 1(HS1) and Younger Dryas (YD). White band indicates the Bølling-Ållerød (BA). The Last Glacial Maximum (LGM), deglaciation and Holocene are marked with arrows on the top axis.

4.6 Last Glacial Maximum to Holocene changes in [CO_3^{2-}] of deep waters using the B/Ca proxy

The selected sediment cores lie in the pathway of deep-water flow into the Arabian Sea. Benthic foraminiferal *Cibicidoides wullerstorfi* shells were picked and analysed for B/Ca. Values obtained were then converted to [CO_3^{2-}] (refer section 2.3.7) by using the equation given by Yu and Elderfield, (2007). The carbonate ion concentration varies from 53 to 91 µmol/kg in core AAS-9/21, 76 to 98 µmol/kg in core SK-129/CR-05 and 80 to 100 µmol/kg in core SK-129/CR-02, from the LGM to the Holocene. The carbonate ion concentration in these cores showed similar values to a nearby core, MD77-191, whose values ranged from 70 -110 µmol/kg (Ma *et al.,* 2020).

All the three cores bathing in different water masses showed a similar variation in [CO_3^{2-}] from the LGM to the Holocene (Figure 4.11a, 4.12a and 4.13a). This similarity in carbonate ion variation indicates similar processes controlling the CO_3^{2-} variations at these sites. Low carbonate ion concentration was recorded during the LGM in all the three cores, which is also supported by lower foraminiferal shell weights during the LGM in core AAS-9/21 and SK-129/CR-05 (Figure 4.11b and 4.12b). The Last Glacial Maximum is thought to have ˷60 µmol/kg higher [CO_3^{2-}] than preindustrial values, as the atmospheric CO_2 during this time was ˷90 ppmv lower than preindustrial times (Yu *et al*., 2010), but, the observed values are very much lower and similar to values seen in the Holocene. The lowering of [CO_3^{2-}] during the LGM is consistent with declined $\delta^{13}C$ values in all the three cores (Figure 4.11e, 4.12d, 4.13c). Depleted $\delta^{13}C$ values indicate lack of ventilation, higher nutrient concentration and isotopically light carbon emerging from decomposition/ carbon respiration of stored organic matter in deep-waters. Higher values of U/Th and V/Ti (Figure 4.11c and d respectively) in core AAS-9/21 observed during the LGM indicate sub-oxic conditions prevailing at the core site. Similar observations were made in core SK-129/CR-05 from the southeastern Arabian Sea retrieved from a water depth of 2300 m. It exhibited higher concentration of U/Th (Figure 4.12c) during the LGM, indicating sub-oxic conditions at core site (Pattan and Pearce, 2009).
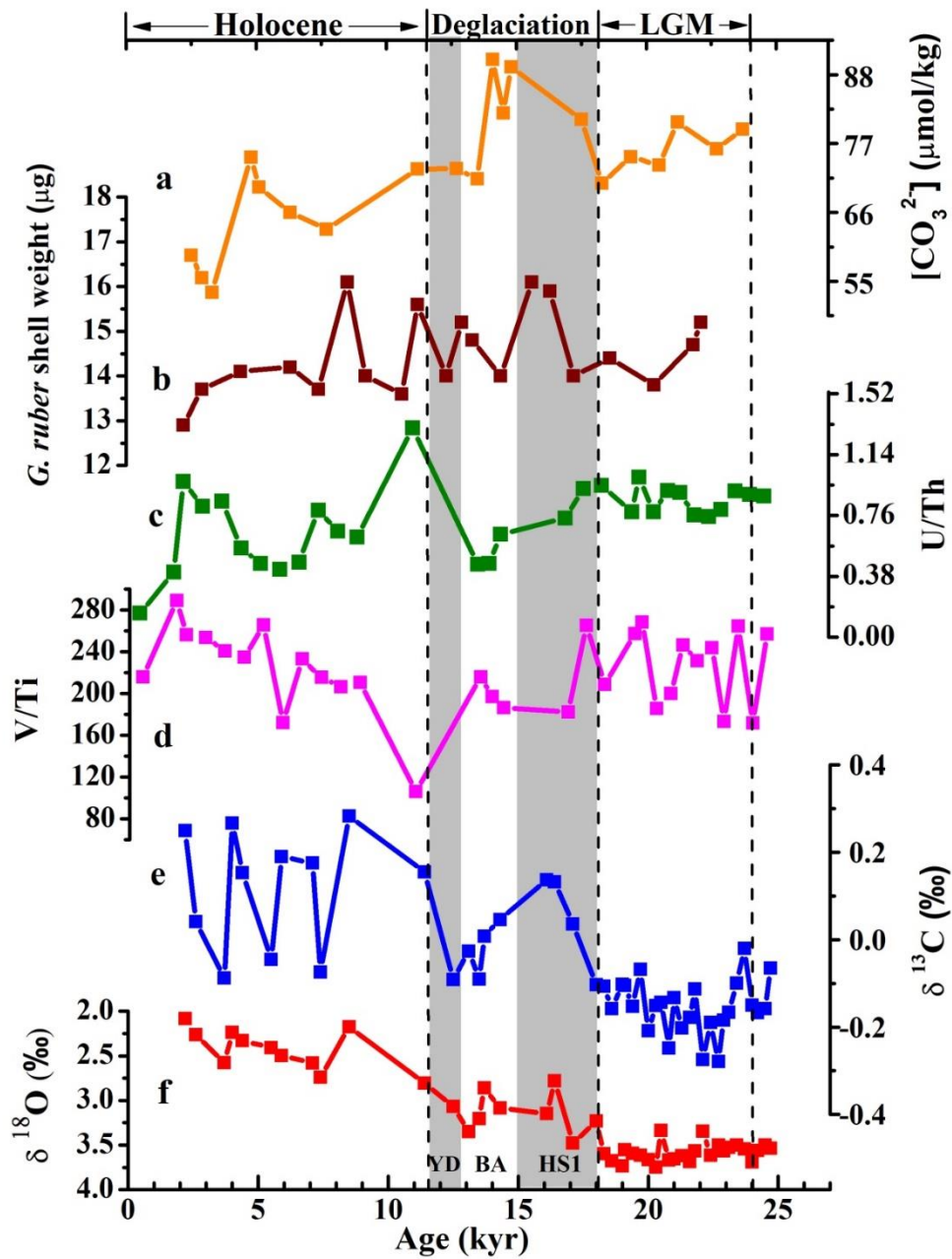
Figure 4.11: - Graph showing variations in a) [CO$_3^{2-}$], b) average *G. ruber* shell weight (µg), c) U/Th ratios (Godad *et al.,* 2017), d) V/Ti ratios, e and f) δ^{13}C and δ^{18}O of *C. wullerstorfi*, in core AAS-9/21. Grey bands in the figure indicate Heinrich Stadial 1(HS1) and Younger Dryas (YD). White band indicates the Bølling-Ållerød (BA). The Last Glacial Maximum (LGM), deglaciation and Holocene are marked with arrows on the top axis.

This time period coincides with lower [CO$_3^{2-}$] in cores AAS-9/21, SK-129/CR-02 as well as SK-129/CR-05 core. A number of studies have indicated sub-oxic conditions at deep water depths in the southeastern Arabian Sea (Sarkar *et al*., 1993; Pattan and Pearce, 2009)

and in the equatorial Indian Ocean (Chandana *et al.,* 2017). These conditions were attributed to changes in deep water circulation in the northern Indian Ocean. Due to the geographical setting of the northern Indian Ocean deep water masses are sourced only from the south i.e. the CDW (Mantyla and Reid, 1995), which plays an important role in the ventilation of the northern Indian Ocean. Neodymium isotope (ε_{Nd}) record of deep waters of the Arabian Sea (Piotrowski *et al.,* 2009) and BoB (Naik *et al.,* 2019; Ma *et al.,* 2019) also indicate decreased proportion of NADW reaching the core sites and resulting in decreased ventilation of glacial deep waters. The North Atlantic Deep Waters are well oxygenated, nutrient depleted and contain highest [CO_3^{2-}] of ~125 µmol/kg (Broecker and Sutherland, 2000). Studies carried out using $\delta^{13}C$ in the northern Indian Ocean showed $\delta^{13}C$ depleted and nutrient enriched water mass during LGM which could have resulted due to strong stratification/ poor ventilation of deep waters (Kallel *et al.*, 1988; Ahmad *et al.,* 2008; Piotrowski *et al.,* 2009). Numerous studies indicate the sequestration of organic carbon in deeper layers via the Southern Ocean by enhanced biological pump which transported high amounts of organic carbon to global deep ocean during the LGM (Smetacek *et al.,* 2012; Muglia *et al.,* 2017). This organic carbon dawdled in deep waters, accumulating respired CO_2 and the stratified deep waters further reduced its escape to mid-depths, yielding older and CO_2 rich deep waters (Skinner *et al.,* 2010; Skinner *et al,* 2014; Skinner *et al.*, 2017). Studies carried out in the Indian Ocean showed the presence of $\delta^{13}C$ depleted values (Kallel *et al.,* 1988; Piotrowski *et al.,* 2009; Yu *et al.,* 2010; Ma *et al.,* 2019) which point towards reduced ventilation and carbon respiration in LGM waters. Hence reduced transport of NADW and poor ventilation of deep waters in north Indian Ocean resulted in enhanced carbon respiration and depletion of $\delta^{13}C$ due to incoming as well as build-up of $^{12}CO_2$ in deep waters which all together resulted in lowering of oxygen and [CO_3^{2-}] of deep waters during LGM at our core sites.

During the deglaciation, an average rise of 4.3 µmol/kg and 4 µmol/kg in comparison to the LGM was seen in cores SK-129/CR-05 and SK-129/CR-02 respectively. A sudden hike in [CO_3^{2-}] of deep waters can result from change in circulation, or degassing of CO_2 from it. An increased proportion of deep waters rich in [CO_3^{2-}] could increase the carbonate ion content at the core sites. The North Atlantic Deep Water forms the major component of southern sourced UCDW and ventilates the northern Indian Ocean (Mantyla and Reid, 1995).
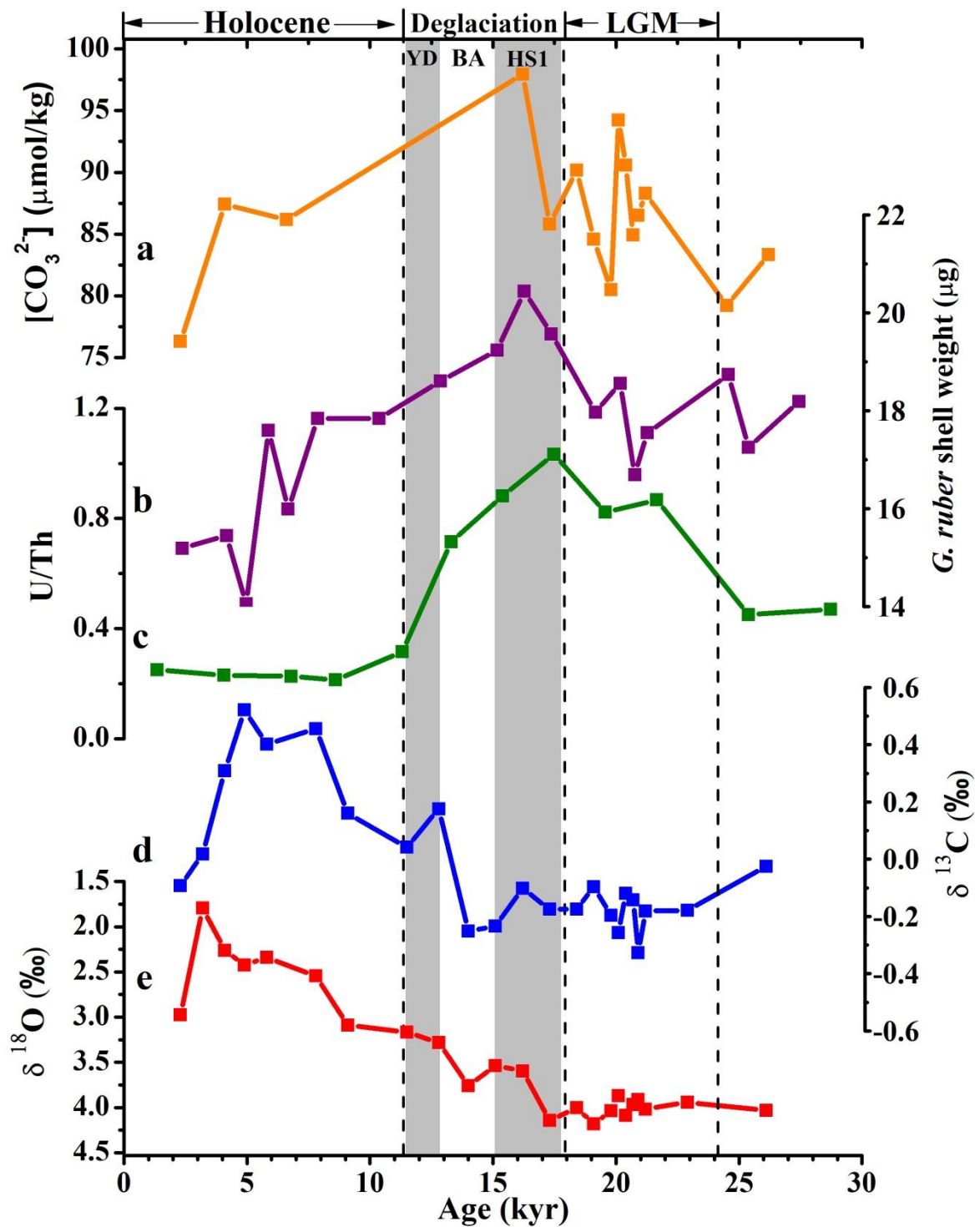
Figure 4.12:- Graph showing variations in a) [CO$_3^{2-}$], b) average *G. ruber* shell weight (µg), c) U/Th ratios (Pattan and Pearce, 2009), d and e) *C. wullerstorfi* δ^{13}C and δ^{18}O in core SK-129/ CR-05. Grey bands in the figure indicate Heinrich Stadial 1(HS1) and Younger Dryas (YD). White band indicates the Bølling-Ållerød (BA). The Last Glacial Maximum (LGM), deglaciation and Holocene are marked with arrows on the top axis.

The last deglacial circulation was interrupted during the HS1 wherein the NADW production was reduced, which lead to weakening of the AMOC (Vidal *et al*., 1996; McManus *et al.,* 2004). Studies from the Indian Ocean reveal an increased proportion of intermediate waters reaching the northern Indian Oceans during reduced NADW phases (Waelbroeck *et al.,* 2006; Jung *et al* 2009; Romahn *et al*., 2014; Ma *et al*., 2019). Better preservation of foraminiferal shells in the OMZ regions of the Arabian Sea was noted during stadials, which were associated with increased volume of southern sourced oxygenated waters encompassing the core sites as a result of diminished NADW (Klöcker *et al.,* 2006; Klöcker and Henrich, 2006; Böning and Bard, 2009; Naidu *et al*., 2014). These studies point towards lesser fraction of NADW ventilating the deglacial Indian Ocean. In such a scenario the increased $[CO_3^{2-}]$ in deglacial deep waters may not be because of incoming of carbonate ion rich waters /changed circulation but can be due to changes in CO_2 content of deep waters.

The elevated $[CO_3^{2-}]$ in deglacial deep waters consent well with depleted ^{14}C signal in intermediate waters of the western Arabian Sea (Bryan *et. al.,* 2010) along with increased *p*CO_2 in surface waters of the eastern Arabian Sea (Palmer *et al.,* 2010; Naik *et al.,* 2015). These observations suggest the evolution of CO_2 from deep waters thusly increasing its $[CO_3^{2-}]$, which are subsequently introduced into intermediate waters diluting its radiocarbon signal and finally enter surface waters giving a *p*CO_2 hike during deglaciation. The surface water CO_2 was eventually exhaled to the atmosphere and contributed to a deglacial rise of ~ 80 ppmv CO_2 in the atmosphere. The key to the detailed mechanism behind this process lies in the Southern Ocean. The Southern Ocean is said to play a significant role in sequestering as well expelling stored deep-water carbon back to the surface layers in the Southern Ocean. An increased Southern Ocean ventilation and rise of atmospheric CO_2 noticed during the deglacial reveals their relation (Skinner, 2010).

An average rise in $[CO_3^{2-}]$ of 5.3 μmol/kg is also noticed at ~ 14 kyr in core AAS-9/21 retrieved from a water depth of 1800 m. Currently this depth is occupied by the southward flowing NIDW (North Indian Deep Water) having high salinity and formed from upwelling of CDW entering the Arabian Basin and the BoB basin and is also referred to as the aged CDW (You, 2000). Shetye *et al.* (1994) refers to this water mass as the Modified North Atlantic Deep Water (MNADW) found below a water depth of 1500 m in the Arabian Sea.
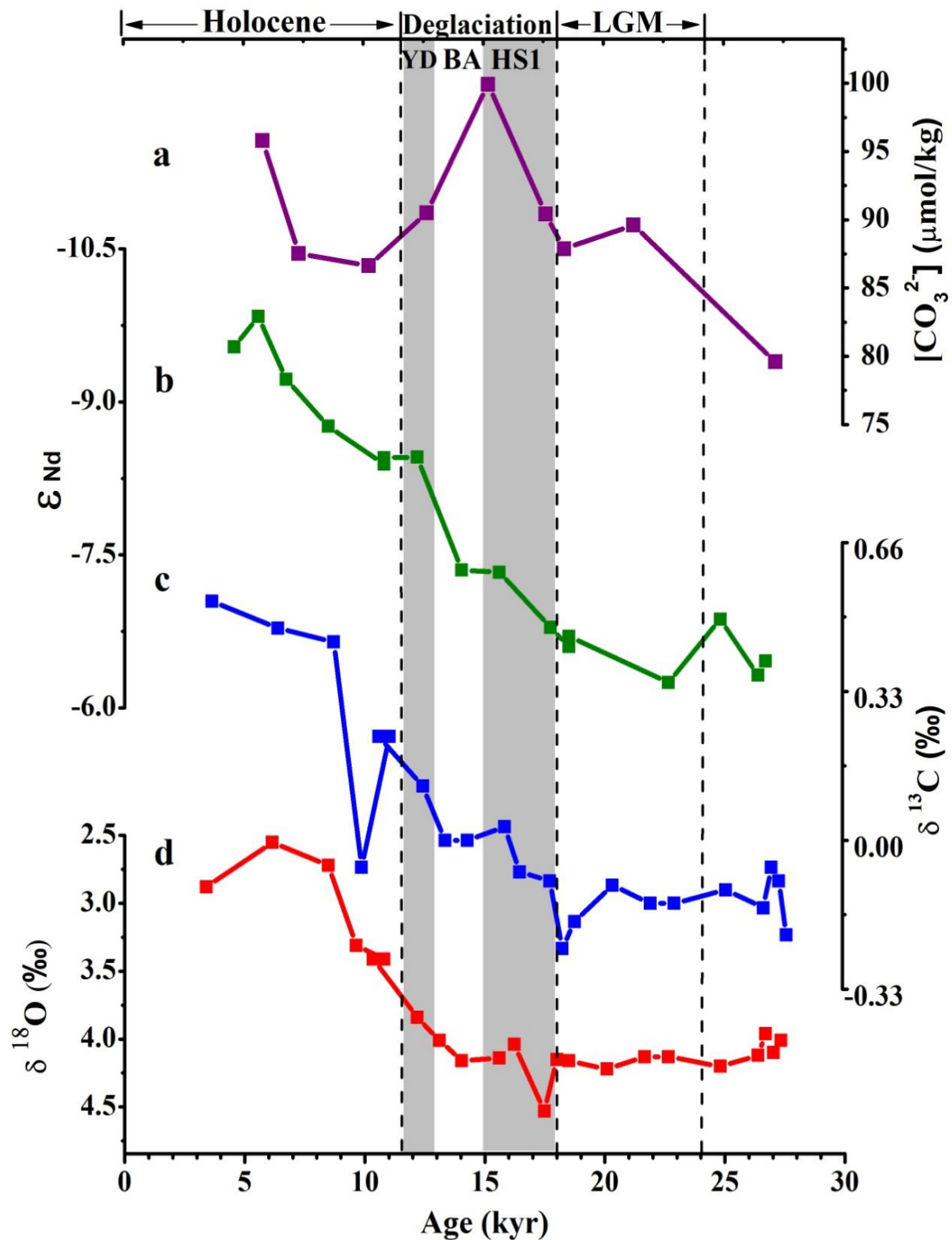
Figure 4.13:- Graph showing variations in a) [CO$_3$$^{2-}$], b) ε_{Nd} (Piotrowski *et al.,* 2009), c and d) *C. Wullerstorfi* δ^{13}C and δ^{18}O (Piotrowski *et al.,* 2009), in core SK-129/CR-02. Grey bands in the figure indicate Heinrich Stadial 1(HS1) and Younger Dryas (YD). White band indicates the Bølling-Ållerød (BA). The Last Glacial Maximum (LGM), deglaciation and Holocene are marked with arrows on the top axis.

The NIDW has major components of CDW and minor contributions from intermediate water masses such as PGW, RSW (Kumar and Li, 1996) and even the AAIW as it moves southwards. Kumar and Li (1996) also refer to this water mass as the High Salinity Deep Water (HSDW) observed in the Arabian Sea as well as in the BoB. It is evident from studies that during the last deglaciation, the NADW production was completely shut down during the HS1 and hence this water mass in the Indian Ocean was compensated by northward expansion of AAIW reaching the northern Indian Ocean (Duplessy *et al.,* 1984; Curry *et al.,* 1988; Naqvi *et al.,* 1994; Jung *et al.,* 2009; Yu *et al.,* 2018; Ma *et al.,* 2019). Several studies in the Indian Ocean have reported well preserved $CaCO_3$ shells in OMZ regions due to the increased proportion of well-ventilated and oxygenated southern sourced intermediate waters (Klöcker and Henrich, 2006; Boning and Bard, 2009; Naidu *et al.,* 2014). The carbon isotope record in core AAS-9/21 also reflects the increased proportion of AAIW entering the Arabian Sea as there is a sudden increase of $\delta^{13}C$ values from -0.103 at 18 kyr to 0.137 at 16 kyr, as compared to cores SK-129/CR-05 and SK-129/CR-02 (Figure 4.7). On contrary, the $\delta^{13}C$ values in core AAS-9/21 showed a tight coupling with the $\delta^{13}C$ signature in deeper cores SK-129/CR-05 and SK-129/CR-02 during the LGM (Figure 4.7). These $\delta^{13}C$ signature in core AAS-9/21 indicate circulation changes occurring at the core location wherein during the LGM $\delta^{13}C$ values reflect the presence of deep-waters at a depth of 1800 m, whereas during the deglaciation $\delta^{13}C$ values indicate the presence of AAIW at the same depth.

The core AAS-9/21 lies in the deep waters of the Arabian Sea, hence mixing of deep water masses can significantly contribute to the changes in $[CO_3^{2-}]$. Since every deep water-mass has a unique preformed $[CO_3^{2-}]$ and biological effects on the deep water masses are less significant, mixing plays an important role in affecting $[CO_3^{2-}]$ of deep waters (Yu *et al.,* 2008). North Indian Deep Water (NIDW) forms from the upwelling of UCDW and has greater proportion of NADW and minor contributions from RSW and PGW (Kumar and Li, 1996; You, 2000) (see section 2.1.5). Out of these water masses RSW and PGW has low oxygen content of 2.5-3 ml/l (Grasshoff 1969; Wyrtki, 1971) and are found in the Arabian Sea between a depth of 200–1000 m, where a severe and perennial OMZ is observed.
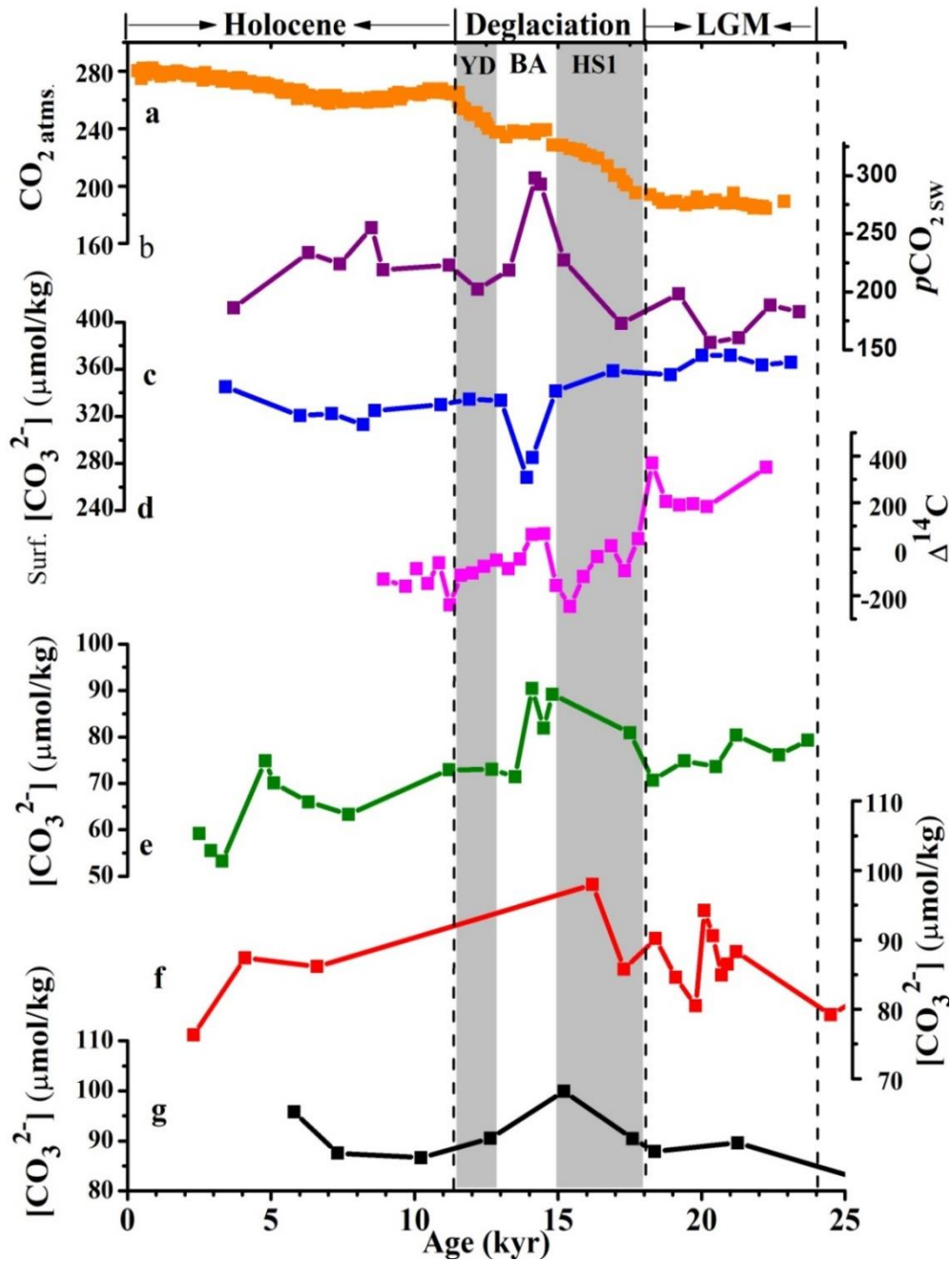
Figure 4.14:- Graph showing variations in a) atmospheric CO_2 from Dome C ice-core (Monnin *et al*., 2001; Lemieux-Dudon *et al*., 2010; Schmitt *et al*., 2012), b) surface water pCO_2 from core AAS-9/21 (Naik *et al*., 2015), c) surface water $[CO_3^{2-}]$ from core AAS-9/21 (Naik and Naik, 2018), d) $\Delta^{14}C$ of intermediate waters from core RC27-23 (Bryan *et al*., 2010), e) deep-water $[CO_3^{2-}]$ from core AAS-9/21 (water depth = 1800 m), f) deep-water $[CO_3^{2-}]$ from core SK-129/CR-05 (water depth = 2300 m), g) deep-water $[CO_3^{2-}]$ from core SK-129/CR-02 (water depth = 3800 m). Grey bands in the figure indicate Heinrich Stadial 1(HS1) and Younger Dryas (YD). White bands indicate the Bølling-Ållerød (BA). The Last Glacial Maximum (LGM), deglaciation and Holocene are marked with arrows on the top axis.

The waters of the OMZ are not only oxygen depleted but also have high concentration of DIC (Paulimer *et al.,* 2011) which signify low $[CO_3^{2-}]$ and is clearly seen in Figure 4.1. Hence, the minor proportions of water emerging from the OMZ also have low $[CO_3^{2-}]$ and thus do not contribute to a rise in $[CO_3^{2-}]$ during the deglaciation. However, the NADW present in the UCDW has the highest $[CO_3^{2-}]$ of ~120 µmol/kg and hence the mixing between NADW can subsequently increase the $[CO_3^{2-}]$ of deep waters as seen during the BA in core AAS-9/21.

Remineralisation of organic carbon can also play a significant role in the carbonate ion hike observed during the deglaciation in core AAS-9/21. Remineralisation of organic carbon includes the breaking down of dead organic matter which sinks down the water column and is broken down into simpler forms using dissolved oxygen, leading to a release of CO_2 and nutrients. The release of CO_2 increases DIC but decreases the alkalinity and hence decreases the $[CO_3^{2-}]$. The organic carbon content in core AAS-9/21 shows an increase during the deglaciation (Figure 4.15d) (Godad *et al.,* 2017), hence the remineralisation of this organic carbon should bring down the $[CO_3^{2-}]$ which is opposite to the observed carbonate ion signal. This could be due to the gradually increasing sedimentation rate (Figure 4.15e) in core AAS-9/21 from 8.6 -13.6 cm/kyr between 19 to 11 kyr, The increased sedimentation rate must have buried the organic carbon in sediments inhibiting the oxidation of organic carbon, which led to less utilisation of oxygen from the water column and low CO_2 liberation, which is also supported by lower V/Ti ratio (this study) and U/Th ratio (Godad *et al.,* 2017) (Figure 4.11d and c) which indicate oxygenated waters during deglaciation in core AAS-9/21.

The Holocene is marked by lowering of $[CO_3^{2-}]$ by 18 µmol/kg, 8.7 µmol/kg and 4.0 µmol/kg in cores AAS-9/21, SK-129/CR-05 and SK-129/CR-02 respectively. On the other hand, higher $\delta^{13}C$ values observed in same cores indicate well ventilated and nutrient depleted water mass like NADW reaching the core sites, which was further confirmed from ϵ_{Nd} studies from the northern Indian Ocean (Piotrowski *et al.,* 2009; Naik *et al.,* 2019). With increased proportion of NADW reaching core sites, an elevated $[CO_3^{2-}]$ is expected. But contrasting changes are observed in Indian and Pacific Ocean. These changes may be associated with reduction of oceanic alkalinity due to continued carbonate compensation and removal of alkalinity through coral reef build up (Opdyke and Walker, 1992; Yu *et al.,* 2014).
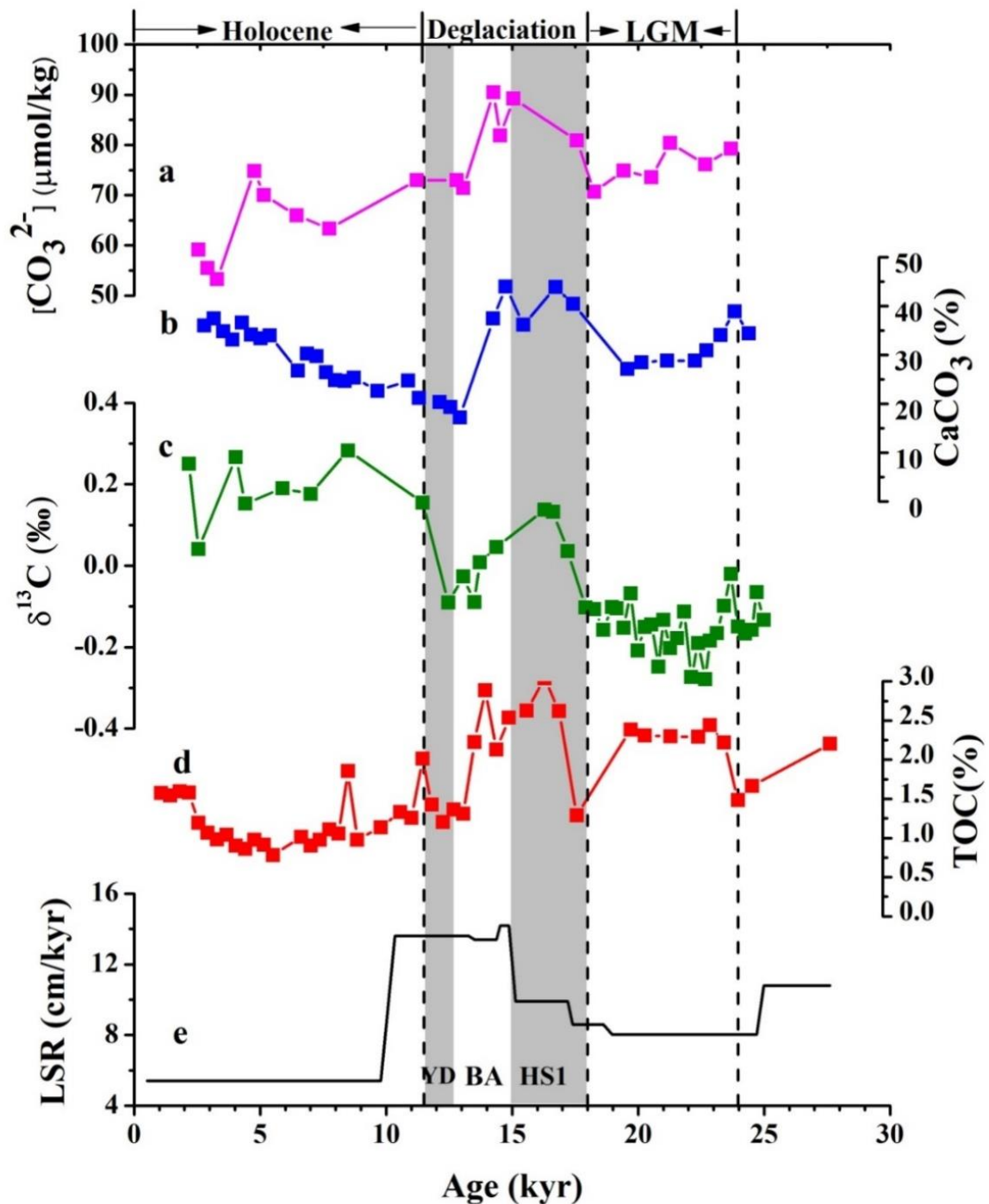
Figure 4.15 :- Graph showing variations in a) deep water [CO_3^{2-}], b) $CaCO_3$ (%) (Godad *et al.*, 2017), c) $\delta^{13}C$ from benthic foraminifera *C. Wullerstorfi*, d) Total Organic Carbon (TOC %) (Godad *et al.,* 2017), and e) Linear Sedimentation Rate (LSR), from core AAS-9/21 (water depth = 1800 m). Grey bands in the figure indicate Heinrich Stadial 1(HS1) and Younger Dryas (YD). White band indicates the Bølling-Ållerød (BA). The Last Glacial Maximum (LGM), deglaciation and Holocene are marked with arrows on the top axis.

4.6.1 Mechanism proposed for the observed [CO_3^{2-}] in deep waters

This study clearly indicates presence of deglacial hike in [CO_3^{2-}] in deep waters of the EAS (Figure 4.14). Similar increased deep water [CO_3^{2-}] is also observed in all the three major oceans of the world (Yu *et al*., 2010; Doss and Marchitto *et al.,* 2013; Yu *et al*., 2013; Allen *et al*., 2015). The observed [CO_3^{2-}] hike in the world oceans is best explained through the deep-ventilation hypothesis which begins from the shifting of Inter Tropical Convergence Zone (ITCZ) towards the south, which also shifted the westerlies to the South (Toggweiler, 2009). These westerlies converged with the polar front during the deglaciation, producing extensive wind driven upwelling of deep waters in the Southern Ocean as evident from opal burial rates (Anderson *et al*., 2009). The deep waters upwelled during the deglaciation contained excessive CO_2 emerging from the remineralisation of organic carbon sequestered during LGM through the enhanced biological pump (Smetacek *et al.,* 2012; Muglia *et al.,* 2017) and through increased efficiency of the North Atlantic carbon pump (Yu *et al.,* 2019). The upwelling of these deep waters caused substantial out gassing of CO_2 from the Southern Ocean, recorded in the South Atlantic Ocean (Martinez boti *et al.,* 2015; Shao *et al*., 2019; Shuttleworth *et al.,* 2021), South Pacific Ocean (Moy *et al*., 2019; Shuttleworth *et al.,* 2021) and South Indian Ocean (Gottschalk *et al.,* 2020; Ronge *et al.,* 2020; Narayana *et al.,* 2020) and contributed to an increase in atmospheric CO_2 of 80 ppmv during the deglaciation. Along with CO_2 outgassing sites in the Southern Ocean, CO_2 outgassing was also observed at equatorial regions of the the world oceans which includes the Equatorial Pacific (Palmer and Pearson, 2003; Martinez-Boti *et al.,* 2015; Gray *et al.,* 2018; Kubota *et al*., 2019), Atlantic (Foster and Sexton, 2014; Ezat *et al.,* 2017) and the eastern Arabian Sea (Naik *et al.,* 2015). This outgassing is been attributed to the excess CO_2 signal carried by the sub-Antarctic surface waters that are subducted in thesub-Antarctic Zone to form the AAIW which is then transported to and upwelled at the equatorial regions of the major oceans. The excessive formation of ^{14}C and carbonate ion depleted AAIW during the deglaciation in the Southern Ocean (Basak *et al.,* 2010) and its incursion in Arabian Sea (Bryan *et al.,* 2010; Ma *et al*., 2020) provides a major evidence for carrying the excess CO_2 to the Arabian Sea. Hence, the outgassing of CO_2 from deep waters resulted in increased [CO_3^{2-}] in deeper waters of the eastern Arabian Sea as seen in this study and promoted better preservation of foraminiferal shells and $CaCO_3$ during deglaciation.

4.7 Variations in bottom water oxygenation from the Last Glacial Maximum to the Holocene in accordance with [CO_3^{2-}] in deep waters of the EAS

The oceans have alternated between source and sinks of CO_2 in the past (Naik *et al.*, 2015; Martinez-Boti *et al.,* 2015). This has been inferred from paleo records showing changes in oceanic carbonate chemistry (Naik *et al.,* 2015; Martinez-Boti *et al.,* 2015) which include parameters like pCO_2, alkalinity and [CO_3^{2-}]. These three factors are intriguingly dependent on each other, pCO_2 is the partial pressure of CO_2 in water, if pCO_2 is higher in seawater than in the atmosphere, CO_2 gas escapes to atmosphere and vice versa, thus acting as source or sink respectively. pCO_2 is indeed controlled by the alkalinity of seawater, wherein increase in alkalinity results in formation of more CO_3^{2-} and decreases CO_2 in seawater, thus lowering pCO_2. Carbonate ion concentration in sea waters is again regulated by CO_2 as an inverse relation exists between both the parameters. At deep water-mass formation sites, photosynthesis consumes CO_2 and drives up oxygen content of surface waters. After sinking, the water mass gets isolated from the atmosphere and changes occurring within the water-mass are controlled by mixing as well as biological processes such as organic carbon respiration. During carbon respiration, oxygen is consumed and CO_2 is released, which then decreases the CO_3^{2-} content. Carbonate ion content of waters determine preservation or dissolution of calcium carbonate. Higher [CO_3^{2-}] favours preservation whereas lower enhances dissolution.

Several studies in the Arabian Sea have shown poor preservation or dissolution of $CaCO_3$ shells in OMZ regions (Calvert *et al.,* 1995; Singh, 1998; Singh *et al.,* 2006; Singh *et al.*, 2007; Naik *et al.,* 2014). On the other hand, better preservation of $CaCO_3$ shells is also observed in OMZ of the Arabian Sea due incursions of oxygenated waters during the stadials (Klöcker and Henrich, 2006; Boning and Bard, 2009; Naidu *et al.*, 2014). These studies figure out a close relationship between oxygen, CO_2 in seawater and $CaCO_3$ in sediment, wherein higher oxygen concentrations are associated with minimum CO_2 and better preservation of $CaCO_3$. The present study is aimed at finding the relationship between dissolved oxygen and [CO_3^{2-}] of seawater promoting preservation or dissolution of $CaCO_3$ in sediment from the LGM to the Holocene.
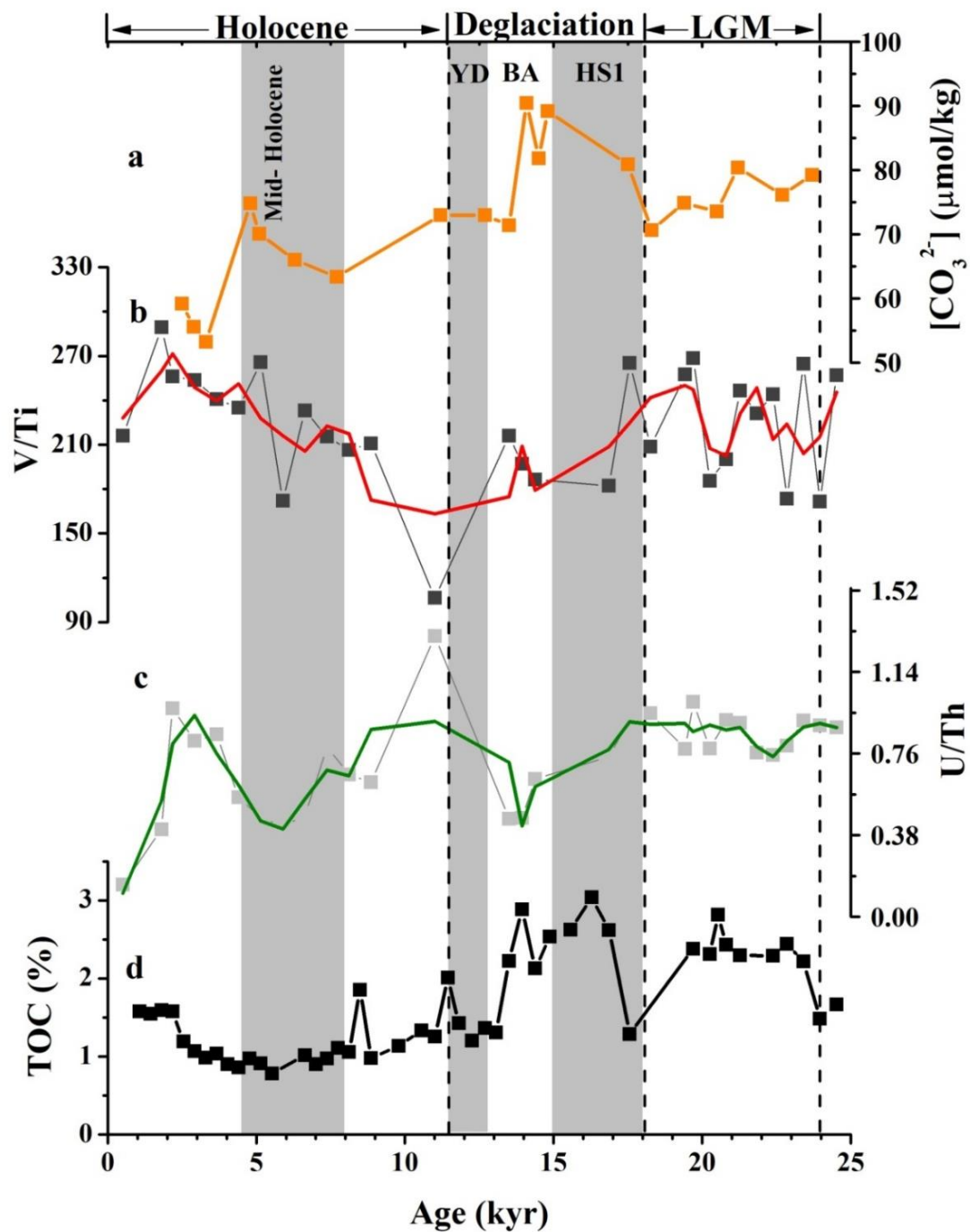
Figure 4.16: - Graph showing variations in a) $[CO_3^{2-}]$ in core AAS-9/21, b) Concentration of V/Ti ratios in core AAS-9/21 (This study), c) U/Th ratios in core AAS-9/21(Godad *et al.,* 2017), d) Total Organic Carbon (TOC %) in core AAS-9/21 (Godad *et al.,*2017). Grey bands in the figure indicate Heinrich Stadial 1(HS1) and Younger Dryas (YD). White band indicates the Bølling-Ållerød (BA). The Last Glacial Maximum (LGM), deglaciation and Holocene are marked with arrows on the top axis.

The objective was attained by first reconstructing the oxygenation condition in deep waters from the LGM to the Holocene using the V/Ti ratios and then comparing it with the $[CO_3^2]$ calculated from B/Ca ratios of *C. Wullerstorfi*.

Titanium (Ti) is a conservative element and is immensely resistant to weathering. It also remains unaffected due to changes in redox conditions at the sediment-waterinterface (Nesbitt and Markovics, 1997; Wei *et al.,* 2003). Hence it has been widely used to estimate the terrigenous input to sedimentary basins (Murray and Leinen, 1993, 1996; Schroeder *et al.,* 1997; Klump *et al.,* 2000). The V/Ti ratio in core AAS-9/21 showed higher values during the LGM and the Holocene and prominent lows were observed during the deglaciation and early Holocene (Figure 4.16b). The U/Th ratios also showed a similar pattern of variation for last 25 kyr (Figure 4.16c; Godad *et al.,* 2017). It exhibited higher values in the LGM, which declined during the deglaciation followed by a rise in early Holocene. In addition, the Benthic Foraminiferal Number (BFN) was also calculated to determine the organic carbon content in the sediments because BFN and their distribution is closely linked to the transport of organic carbon to the sea floor and organic carbon in the sediment (Caralp, 1984; Mackensen *et al.,* 1985; Caralp, 1989; Van der Zwaan *et al.,* 1990; Jorissen *et al.,* 1992; Gooday, 1993; Schmiedl *et al.,* 1997; De Stigter *et al.,* 1998; Altenbach *et al.,* 1999). Several studies have used benthic foraminifera as a proxy for indicating the organic carbon content in sediments (Smart, 1994; Wahyudi and Minagawa, 1997; Van der Zwaan *et al.,* 1999; Dulk *et al.*, 2000; Cappelli *et al.,* 2019). It is well understood that the organic carbon content in the sediments is closely related to the oxygen content. In sediments having higher organic carbon content, oxygen from the water column is utilised for the decomposition of organic matter which is very commonly observed in the OMZ of the Arabian Sea at the depth of 200-1500 m.

Higher values of V/Ti and U/Th in core AAS-9/21 observed during the LGM indicate sub-oxic conditions prevailed at the core site. Core SK-129/CR-05 from the southeastern Arabian Sea also showed higher V/Ti and U/Th ratios (Figure 4.17b and 4.17c respectively) during the LGM, indicating sub-oxic conditions at the core site (Pattan and Pearce, 2009). The Total Organic Carbon (TOC) content in core SK-129/CR-05 (Figure 4.17d, Pattan and Pearce, 2009) and in core AAS-9/21 (Figure 4.16d, Godad *et al.,* 2017), both show an increase during the LGM. The BFN in core SK-129/CR-05 also exhibited higher values during the LGM, indicating high organic carbon in sediments (Figure 4.16e). The sub-oxic

conditions at the core sites during the LGM could result from the oxidation of organic carbon wherein the dissolved oxygen was utilised for degradation of organic carbon in sediments. This time period also coincides with lower $[CO_3^{2-}]$ in core AAS-9/21 as well as core SK-129/CR-05 (Figure 4.16a and 4.17a). A number of studies have indicated sub-oxic conditions at deep water depths in the southeastern Arabian Sea (Sarkar *et al*., 1993; Pattan and Pearce, 2009) and in the equatorial Indian Ocean (Chandana *et al*., 2017). These conditions were attributed to changes in deep water circulation in the northern Indian Ocean. Strongly stratified and poorly ventilated deep waters not only existed in Indian Ocean but also resided in Atlantic and Pacific Ocean (Yu *et. al.,* 2007; Marchitto *et al*., 2007; Yu and Elderfield, 2008; Yu *et. al.,*2010; Freeman *et al*., 2015; and Fuente *et al.,* 2017).

The deglaciation recorded lower values of V/Ti and U/Th in core AAS 9/21. Similarly, SK-129/CR-05 also showed lower V and U/Th ratios during later part of the deglaciation. Whereas, increased $[CO_3^{2-}]$ was observed in both the cores during the deglaciation. These observations point out towards the presence of oxygenated and carbonate ion rich water mass as the organic carbon also decreased in both the cores during the deglaciation. The deglacial period is characterized by enhanced deep water upwelling in the Southern Ocean which broke the strong stratification formed during the LGM (Anderson *et. al.,* 2009). This extensive upwelling in the deglaciation brought deep waters to the surface, leading to escape of CO_2 stored during the LGM, thereby increasing the $[CO_3^{2-}]$ of deep-waters (Martinez-Boti, 2015). Oxygenated waters at this time must have resulted from decreased organic matter flux evident from changing iron supply in the Southern Ocean (Martinez-Garcia *et al.,* 2014).

Carbonate ion concentration in core AAS-9/21 and SK-129/CR-05 showed decreasing trend through the Holocene. Decrease in $[CO_3^{2-}]$ of the Indian Ocean can be attributed to decrease in global ocean alkalinity due to increase in coral reef build-up on shelves which led to removal of alkalinity from seawater and resulted in a decrease in whole ocean $[CO_3^{2-}]$ (Opdyke and Walker, 1992). Although a decrease in $[CO_3^{2-}]$ was observed thought the Holocene, a prominent rise initiated at 6.6 kyr and 6.3 kyr (Figure 4.16a and 4.17a) in core AAS-9/21and SK-129/CR-05 respectively, is seen. Rise in values continued and reached to a maximum at 4.1 kyr and 4.8 kyr in cores SK-129/CR-05 and AAS-9/21 respectively. The geochemical proxies suggest decreased oxygenation during early and late Holocene and better ventilated waters during mid-Holocene from 6.6 to 4.0
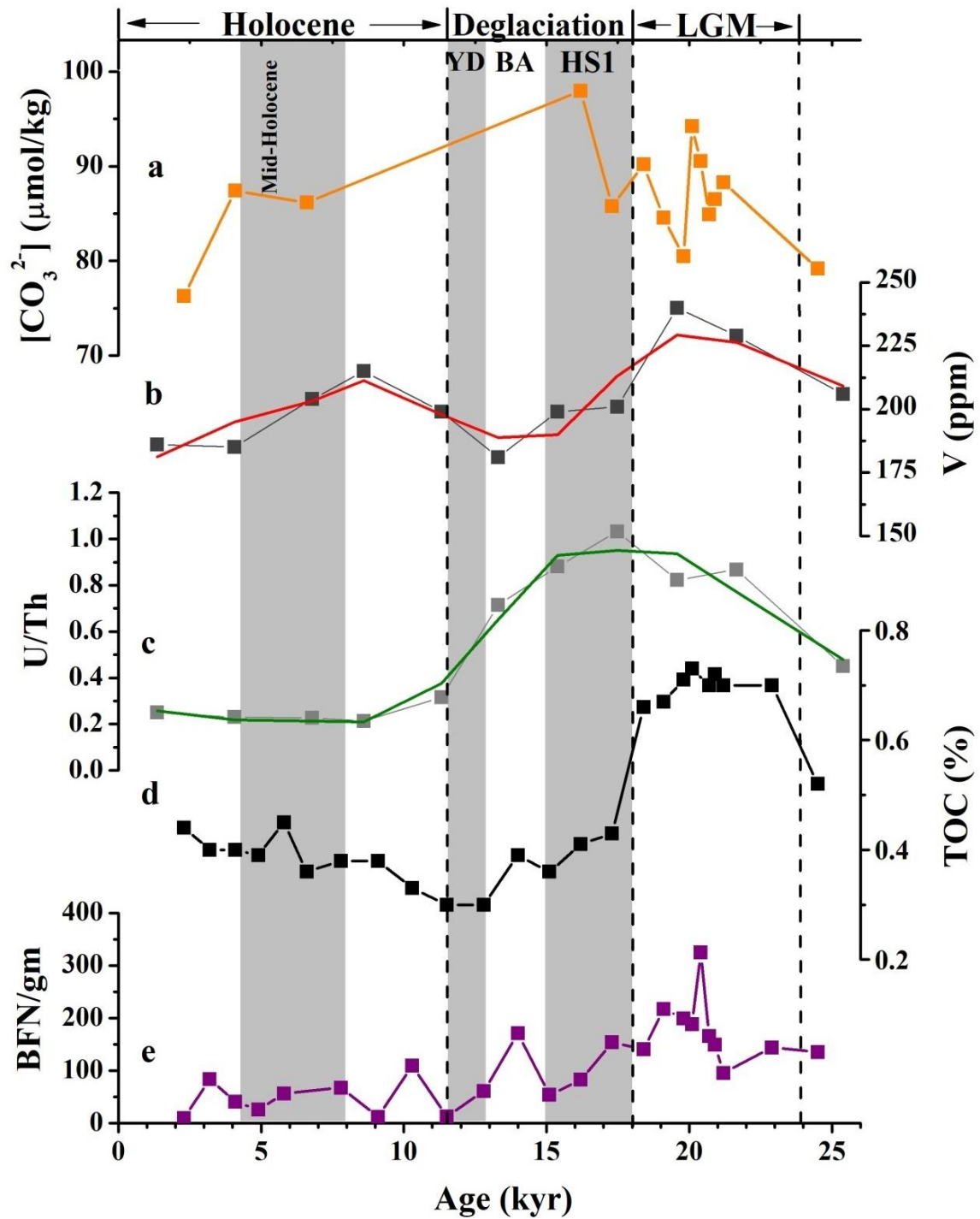
Figure 4.17:- Graph showing variations in a) [CO$_3^{2-}$] in core SK-129/CR-05, b) concentration of V (ppm) in core SK-129/CR-05 , c) U/Th ratios in core SK-129/CR-05 (Pattan and Pearce, 2009), d) Total Organic Carbon (TOC %) in core SK-129/CR-05 (Guptha *et al.,* 2005), e) Benthic Foraminiferal Number per gm dry weight of sediment (This study). Grey bands in the figure indicate Heinrich Stadial 1(HS1) and Younger Dryas (YD). White band indicates the Bølling-Ållerød (BA). The Last Glacial Maximum (LGM), deglaciation and Holocene are marked with arrows on the top axis.

kyr. The oxygenation proxies in core AAS-9/21 during the Holocene reflect the effect of Indian Summer Monsoon (ISM). Variability in ISM during the Holocene is reported in several studies which showed increased intensity of ISM from ~10 kyr and reaching to a maximum at~8 kyr (Thamban *et al*., 2007; Kessarkar *et al*., 2013).

Increased intensity of ISM must have intensified upwelling resulting in high primary productivity and increased carbon flux to deeper oceans, giving rise to decreased oxygenation due to carbon respiration. A decreased ISM intensity is observed from ~8 - ~5 kyr (Kessarkar *et al*., 2013) followed by a drier period from 5-4 kyr (Kessarkar *et al.,* 2013). The period of decreased ISM intensity (from~8 to 5 kyr) coincides with high oxygen and high $[CO_3^{2-}]$ at 1800 m depth. After 3 kyr, ISM intensity returned to stable conditions, productivity increased (Godad *et al.,* 2017) and resulted in decreased oxygenation. A clear relation and interdependence of the parameters, oxygen and $[CO_3^{2-}]$ was observed during the LGM, early and late Holocene wherein lowering in oxygen content coincided with decrease in $[CO_3^{2-}]$, whereas in the deglaciation and mid-Holocene $[CO_3^{2-}]$ increased simultaneously with increasing oxygen concentration in deep waters. The oxygenation and carbonate ion content of deep waters are mostly controlled by the deep water circulation from the LGM to the deglaciation and mid-Holocene, whereas during early and late Holocene it is controlled by the increased intensity of the ISM.

5. SUMMARY AND CONCLUSIONS

The fluctuations in atmospheric CO_2 are majorly said to be controlled by the oceans, as the oceans take up CO_2 and convert it to Dissolved Inorganic Carbon (DIC). Dissolved Inorganic Carbon comprises of aqueous CO_2, carbonic acid (H_2CO_3), bicarbonate (HCO_3^-) and carbonate ions (CO_3^{2-}). Aqueous CO_2 is taken by phytoplankton and is converted to organic carbon, which contributes to productivity, whereas, the rest of the components form the alkalinity, which controls the buffering system of the oceans. The carbonate ion concentration [CO_3^{2-}] is one important component of alkalinity which is responsible for formation/ dissolution of $CaCO_3$ shells in the oceans. Deep waters are formed from sinking of surface water at higher latitudes when they cool, become more saline and attain a specific [CO_3^{2-}], $\delta^{13}C$, nutrients and dissolved oxygen depending upon the photosynthesis occurring in it. Hence, the deep waters capture atmospheric CO_2 when at surface and take it to greater depths and store it, thus acting as a sink for atmospheric CO_2 on glacial to interglacial timescales. Thus the glacial to interglacial variation in atmospheric CO_2 can be reconstructed by studying the changes in [CO_3^{2-}], circulation and oxygenation condition of the deep waters.

As seen from the profile of modern day [CO_3^{2-}] in the eastern Arabian Sea, the carbonate ion saturation line crosses the in-situ [CO_3^{2-}] vertical profile at a depth of ~3500 m (saturation horizon). Out of the three sediment cores selected for this study, core AAS-9/21 and core SK-129/CR-05 lie well above the saturation horizon, which signifies that waters bathing these cores presently are saturated with respect to [CO_3^{2-}] and better preservation of the shells is expected. On the other hand, core SK-129/CR-02 lies below the carbonate saturation horizon and hence dissolution can be expected at this depth.

Deep-water circulation and temperature changes in the south eastern Arabian Sea (EAS) were reconstructed using $\delta^{13}C$ and $\delta^{18}O$ of epifaunal benthic foraminifera *Cibicidoides wuellestorfi*. The $\delta^{13}C$ reconstructions reveal significant circulation and ventilation changes occurring in deep and intermediate waters from the Last Glacial Maximum (LGM) to the Holocene. The $\delta^{13}C$ values in core AAS-9/21 and core SK-129/CR-05 were lower during the LGM, indicating a less-ventilated and nutrient-rich water mass. The increased efficiency of biological carbon pump during the LGM in the North Atlantic and the Southern Ocean led to incorporation of substantial amounts of organic carbon in

deep-waters. Through reduction in North Atlantic Deep Water (NADW) strength, the deep-waters became less ventilated, thus enhancing the decomposition of organic carbon, leading to depleted $\delta^{13}C$, stratified and nutrient rich deep-waters. The $\delta^{13}C$ signal in core AAS-9/21 were initially seen to increase during the Heinrich Stadial 1 (HS1) and showed a decreasing trend from 16 kyr, which continued throughout the Bølling-Ållerød (BA) and reached to a minimum of -0.09 ‰ at 12.5 kyr and then rose again in the Younger Dryas (YD). This increase in $\delta^{13}C$ values in core AAS-9/21 during HS1 is mainly attributed towards the intrusion of Antarctic Intermediate Water (AAIW) at 1800 m depth in the EAS. The $\delta^{13}C$ values in core SK-129/CR-05 (2300 m) did not show a prominent increase during the HS1, instead a severe depletion was seen during the BA (-0.25‰) which can be probably linked to Melt Water Pulse1a (14.65–14.31 kyr) and associated rise in sea-level. The sea-level rise during this time could have influenced the discharge of terrigenous organic matter enriched in $\delta^{13}C$ and contributed to the decrease in benthic foraminifera $\delta^{13}C$ values. The Holocene recorded an increased $\delta^{13}C$ values in both the cores, AAS-9/21 and SK-129/CR-05, which indicate better-ventilated and nutrient-depleted NADW entering the Indian Ocean as the production of NADW resumed during the Holocene.

Deep-water temperature changes at the two core sites (AAS-9/21 and SK-129/CR-05) from the LGM to the Holocene were estimated using oxygen isotopic ratios. The $\delta^{18}O$ shift exceeds ice-volume effect by 0.4 ‰ and 0.7 ‰ in cores AAS-9/21 and SK-129/CR-05 respectively, indicating bottom water cooling of~2º C during the LGM caused due to a shift in source of water reaching the core site, from $\delta^{13}C$ enriched NADW to cooler and $\delta^{13}C$ depleted Southern Ocean Deep Waters, as the production of NADW reduced during the LGM.

The changes in $[CO_3^{2-}]$ from the Last Glacial to the Holocene were studied using two proxies 1) B/Ca and 2) planktic foraminiferal shell weight. The planktic foraminiferal shell weight proxy determines the preservation/dissolution of shells thus determining CO_3^{2-} saturation/undersaturation in deep-waters, whereas the B/Ca proxy quantifies the $[CO_3^{2-}]$ of deep-waters. Shell weights from core SK-129/CR-05 were lighter during the LGM and the Holocene, indicating low $[CO_3^{2-}]$ in deep waters, whereas shell weights significantly increased during the deglaciation showing better preservation owing to increased $[CO_3^{2-}]$ of deep waters. Shell weights of core SK-129/CR-02 lying at a water depth of 3800 m did not show a peculiar trend, instead indicate prominent dissolution occurring at 3800 m depth as it is the depth where the foraminiferal lysocline is observed in the Arabian Sea.

Carbonate ion concentration was reconstructed from the eastern Arabian Sea for the very first time using B/Ca proxy in all three cores (AAS-9/21, SK-129/CR-05 and SK-129/CR-02) bathing in three different water masses, which showed similar pattern of variation in $[CO_3^{2-}]$ from the LGM to the Holocene. Lower $[CO_3^{2-}]$ was recorded during the LGM in all three cores, which is ascribed towards reduced ventilation and storage of CO_2 emerging from decomposition of organic carbon. Low $[CO_3^{2-}]$ in the LGM was followed by a prominent rise during deglaciation in all the three cores. This LGM to deglacial rise in $[CO_3^{2-}]$ was of 4.3 µmol/kg in core SK-129/CR-05, 4.8 µmol/kg in core SK-129/CR-02 and 5.3 µmol/kg in core AAS-9/21. Increased $[CO_3^{2-}]$ during deglaciation was linked to breakdown of stratification due to intense upwelling in the Southern Ocean which released significant amount of CO_2. The excess CO_2 was also incorporated in the AAIW during their formation in the Sub-Antarctic Zone. Thus the AAIW carried the Southern Ocean signal to the lower latitudes and then the excess CO_2 escaped to the atmosphere through surface waters resulting in a rise in atmospheric CO_2 during the deglaciation, thus confirming the hypothesis put forth in this study. A summary of salient variations in the proxies used in the study, and their interpretation with respect to time is given in Table 5.1 below.

Geochemistry of elements in cores AAS-9/21 and SK-129/CR-05 indicated sub-oxic conditions during the LGM and the Late Holocene, and oxic conditions during the deglaciation and the mid-Holocene. The oxygenated conditions complement well with increased $[CO_3^{2-}]$ and sub-oxic conditions agree with the lowered $[CO_3^{2-}]$ in both the cores, thus indicating a clear relation between dissolved oxygen and $[CO_3^{2-}]$ as also seen in the modern in-situ data.

Table 5.1: - Showing salient variations in proxies used in the study and their interpretation.

Parameter	Low/High	Core	Interval	Result/ Interpretation
$\delta^{13}C$	Low	AAS-9/21, SK-129/CR-05	LGM	Less ventilated, nutrient rich southern sourced deep water mass
	High	AAS-9/21	Heinrich Stadial 1 (HS1)	Enhanced flow of AAIW in EAS
	Low	SK-129/CR-05	Bølling-Ållerød	Meltwater pulse 1a
	High	AAS-9/21, SK-129/CR-05	Holocene	Well ventilated and nutrient depleted
$\delta^{18}O$	High	AAS-9/21, SK-129/CR-05	LGM	Presence of ~2° cooler southern sourced deep waters
	Low	AAS-9/21, SK-129/CR-05	Holocene	Presence of warmer NADW
Shell weight	Low	SK-129/CR-05	LGM	Low- shell preservation - Low $[CO_3^{2-}]$
	High	SK-129/CR-05	Deglaciation (HS1+B/A+YD)	Better shell preservation - High $[CO_3^{2-}]$
	Low	SK-129/CR-05	Holocene	Low shell preservation - Low $[CO_3^{2-}]$
B/Ca- $[CO_3^{2-}]$	Low	AAS-9/21, SK-129/CR-05, SK-129/CR-02	LGM	Presence of less ventilated, nutrient rich and CO_2 rich waters
	High	SK-129/CR-05, SK-129/CR-02	Deglaciation (HS1+B/A+YD)	Escape of stored CO_2 from deep waters (Deep ventilation hypothesis)
	High	AAS-9/21	Deglaciation (HS1+B/A+YD)	Reduced remineralisation of organic carbon at 1800 m depth
	Low	AAS-9/21, SK-129/CR-05, SK-129/CR-02	Holocene	Dissolution of $CaCO_3$ in order to compensate for deglacial preservation of $CaCO_3$

A two-step rise in atmospheric CO_2 during the deglaciation was attributed to the outgassing of CO_2 from the deep waters which led to an increase in deep water $[CO_3^{2-}]$. This rise in $[CO_3^{2-}]$ was observed in all the three major oceans of the world i.e. Atlantic, Pacific and Indian Ocean. Indian Ocean hosted only one study in the southwest Indian Ocean, whereas the rest of the Indian Ocean remained unexplored in terms of understanding deep water $[CO_3^{2-}]$. The Arabian Sea in the north western part of the Indian Ocean, hosts one of the largest OMZ, which also affects the $[CO_3^{2-}]$ of its waters. Hence, it is very necessary to understand the LGM to Holocene variation in deep water $[CO_3^{2-}]$ and to determine its role in deglacial venting of CO_2. This study has quantified the $[CO_3^{2-}]$ variation in deep-waters of the Arabian Sea and has also provided an evidence for evasion of CO_2 from deep waters of the Arabian Sea. This study has also determined the changes in deep water circulation and ventilation which occurred in the Indian Ocean from the LGM to the Holocene and their role in venting CO_2 during the deglaciation. However, the Indian Ocean still lacks studies in determining the carbonate chemistry of intermediate waters by using a reliable and well accepted proxy like B/Ca, which will confirm the transport of excess CO_2 from southern Indian Ocean to the Arabian Sea and the Bay of Bengal. Also there is a dearth of studies assessing the $[CO_3^{2-}]$ in deep waters of Indian Ocean over several glacial to interglacial periods.

References

Ahmad, S. M., Babu, G. A., Padmakumari, V. M., & Raza, W. (2008). Surface and deep water changes in the northeast Indian Ocean during the last 60 ka inferred from carbon and oxygen isotopes of planktonic and benthic foraminifera. *Palaeogeography, Palaeoclimatology, Palaeoecology*, *262*(3-4), 182-188. https://doi:10.1016/j.palaeo.2008.03.007.

Ahmad, S. M., & Labeyrie, L. D. (1994). Glacial to Holocene $\delta^{13}C$ variations in intermediate depth water masses of North Indian Ocean. *Geo-marine letters*, *14*(1), 36-40. https://doi.org/10.1007/BF01204469.

Al-Ammar, A., Reitznerová, E., & Barnes, R. (2000). Determination of boron in biological samples. *Journal of Radioanalytical and Nuclear Chemistry*, *244*(2), 267-272. https://doi.org/10.1023/A:1006730013295.

Allen, K. A., Hönisch, B., Eggins, S. M., & Rosenthal, Y. (2012). Environmental controls on B/Ca in calcite tests of the tropical planktic foraminifer species Globigerinoides ruber and Globigerinoides sacculifer. *Earth and Planetary Science Letters*, *(351-352)*, 270-280. https://doi.org/10.1016/j.epsl.2012.07.004.

Allen, K. A., Sikes, E. L., Hönisch, B., Elmore, A. C., Guilderson, T. P., Rosenthal, Y., &Anderson, R. F. (2015). Southwest Pacific deep water carbonate chemistry linked to high southern latitude climate and atmospheric CO2 during the Last Glacial Termination. *Quaternary Science Reviews*, *122*, 180-191. https://doi.org/10.1016/j.quascirev.2015.05.007.

Altenbach, A. V., Pflaumann, U., Schiebel, R., Thies, A., Timm, S., & Trauth, M. (1999). Scaling percentages and distributional patterns of benthic foraminifera with flux rates of organic carbon. *The Journal of Foraminiferal Research*, *29*(3), 173-185.

Anderson, R. F., Ali, S., Bradtmiller, L. I., Nielsen, S. H. H., Fleisher, M. Q., Anderson, B. E., & Burckle, L. H. (2009). Wind-driven upwelling in the Southern Ocean and the deglacial rise in atmospheric CO2. *Science*, *323*(5920), 1443-1448. https://doi.org/10.1126/science.1167441.

Archer, D. E. (1991). Equatorial Pacific calcite preservation cycles: Production or dissolution?. *Paleoceanography*, *6*(5), 561-571. https://doi.org/10.1029/91PA01630.

Archer, D., Winguth, A., Lea, D., & Mahowald, N. (2000). What caused the glacial/interglacial atmospheric pCO2 cycles?. *Reviews of Geophysics*, *38*(2), 159-189. https://doi.org/10.1029/1999RG000066.

Arrhenius, G. (1988). Rate of production, dissolution and accumulation of biogenic solids in the ocean. *Palaeogeography, Palaeoclimatology, Palaeoecology*, *67*(1-2), 119-146. https://doi.org/10.1016/0031-0182(88)90125-3.

Arrhenius, G. (1952). Sediment cores from tha east Pacific. *Rep. Swed. Deep Sea Exped. 1947-1948*, *5*, 1-228.

Babila, T. L. (2014). *Boron/calcium in planktonic foraminifera: Proxy development and application to the Paleocene-Eocene boundary*. Rutgers The State University of New Jersey-New Brunswick.

Babu, V. R., Varkey, M. J., Das, V. K., & Gouveia, A. D. (1980). Water masses and general hydrography along the west coast of India during early March.

Banerjee, B., Ahmad, S. M., Raza, W., & Raza, T. (2017). Paleoceanographic changes in the Northeast Indian Ocean during middle Miocene inferred from carbon and oxygen isotopes of foraminiferal fossil shells. *Palaeogeography, Palaeoclimatology, Palaeoecology*, *466*, 166-173. https://doi:10.1016/j.palaeo.2016.11.021.

Banse, K. (1959). On upwelling and bottom-trawling off the southwest coast of India. *Journal of the Marine Biological Association of India*, *1*(1), 33-49.

Banse, K. (1968). Hydrography of the Arabian Sea shelf of India and Pakistan and effects on demersal fishes. In *Deep sea research and oceanographic Abstracts*, 15, (1), 45-79.

Banse, K., & English, D. C. (1993). Revision of satellite-based phytoplankton pigment data from the Arabian Sea during the northeast monsoon. *Marine Research,2*, 83-103.

Barker, S., Greaves, M., & Elderfield, H. (2003). A study of cleaning procedures used for foraminiferal Mg/Ca paleothermometry. *Geochemistry, Geophysics, Geosystems*, *4* (9). https://doi.org/10.1029/2003GC000559.

Basak, C., Martin, E. E., Horikawa, K., & Marchitto, T. M. (2010). Southern Ocean source of ^{14}C -depleted carbon in the North Pacific Ocean during the last deglaciation. *Nature Geoscience*, *3*(11), 770-773. https://doi:10.1038/ngeo987

Bassinot, F. C., Beaufort, L., Vincent, E., Labeyrie, L. D., Rostek, F., Müller, P. J., Quidelleur, X., & Lancelot, Y. (1994). Coarse fraction fluctuations in pelagic carbonate sediments from the tropical Indian Ocean: A 1500-kyr record of carbonate dissolution. *Paleoceanography*, *9*(4), 579-600. https://doi.org/10.1029/94PA00860.

Beal, L. M., Ffield, A., & Gordon, A. L. (2000). Spreading of Red Sea overflow waters in the Indian Ocean. *Journal of Geophysical Research: Oceans*, *105*(C4), 8549-8564. https://doi.org/10.1029/1999JC900306.

Beaulieu S. E., (2002). Accumulation and fate of phytodetritus on the sea floor. *Oceanography and Marine Biology: an Annual Review*, *40*, 171-232. http://dx.doi.org/10.1201/9780203180594.ch4.

Beaulieu, S. E., & Smith Jr, K. L. (1998). Phytodetritus entering the benthic boundary layer and aggregated on the sea floor in the abyssal NE Pacific: macro-and microscopic composition. *Deep Sea Research Part II: Topical Studies in Oceanography*, *45*(4-5), 781-815. https://doi.org/10.1016/S0967-0645(98)00003-4.

Beer, C. J., Schiebel, R., & Wilson, P. A. (2010). Testing planktic foraminiferal shell weight as a surface water [CO32−] proxy using plankton net samples. *Geology*, *38*(2), 103-106. http://dx.doi.org/10.1130/G30150.1.

Behara, A., Vinayachandran, P. N., & Shankar, D. (2019). Influence of rainfall over eastern Arabian Sea on its salinity. *Journal of Geophysical Research: Oceans*, *124* (7), 5003-5020. https://doi.org/10.1029/2019JC014999.

Berger, W. H. (1970). Planktonic foraminifera: selective solution and the lysocline. *Marine Geology*, *8*(2), 111-138. https://doi.org/10.1016/0025-3227(70)90001-0.

Berger, W. H. (1973). Deep-sea carbonates; Pleistocene dissolution cycles. *The Journal of Foraminiferal Research*, *3*(4), 187-195. https://doi.org/10.2113/gsjfr.3.4.187.

Berger, W. H. (1978). Deep-sea carbonate: pteropod distribution and the aragonite compensation depth. *Deep Sea Research*, *25*(5), 447-452. https://doi.org/10.1016/0146-6291(78)90552-0.

Berger, W. H., Bonneau, M. C., and Parker, F. L. (1982). Foraminifera on the deep-sea floor-lysocline and dissolution rate. *Oceanologica Acta*, *5*(2), 249-258.

Bickert, T., & Mackensen, A. (2003). Last Glacial to Holocene changes in South Atlantic deep water circulation. In *The South Atlantic in the Late Quaternary* (pp. 671-693). Springer, Berlin, Heidelberg. https://doi.org/10.1007/978-3-642-18917-3_29.

Bijma, J., Spero, H. J., & Lea, D. W. (1999). Reassessing foraminiferal stable isotope geochemistry: Impact of the oceanic carbonate system (experimental results). In *Use of proxies in paleoceanography* 489-512. Springer, Berlin, Heidelberg. https://doi.org/10.1007/978-3-642-58646-0_20.

Boersma, A., & Mikkelsen, N. (1990). Miocene-age primary productivity episodes and oxygen minima in the central equatorial Indian Ocean. *Scientific Results, Proceedings of Ocean Drilling Program*, *115*. https://doi:10.2973/odp.proc.sr.115.162.1990

Böning, P., & Bard, E. (2009). Millennial/centennial-scale thermocline ventilation changes in the Indian Ocean as reflected by aragonite preservation and geochemical variations in Arabian Sea sediments. *Geochimica et Cosmochimica Acta*, *73*(22), 6771-6788. http://dx.doi.org/10.1016/j.gca.2009.08.028.

Bostock, H. C., Opdyke, B. N., Gagan, M. K., & Fifield, L. K. (2004). Carbon isotope evidence for changes in Antarctic Intermediate Water circulation and ocean ventilation in the southwest Pacific during the last deglaciation. *Paleoceanography*, *19* (4). https://doi:10.1029/2004PA001047

Borole, D. V., Sarin, M. M., & Somayajulu, B. L. K. (1982). Composition of Narmada and Tapti estuarine particles and adjacent Arabian Sea sediments.

Boyle, E. A. (1981). Cadmium, zinc, copper, and barium in foraminifera tests. *Earth and Planetary Science Letters*, *53*(1), 11-35. https://doi.org/10.1016/0012-821X(81)90022-4.

Boyle, E. A., & Keigwin, L. D. (1985). Comparison of Atlantic and Pacific paleochemical records for the last 215,000 years: Changes in deep ocean circulation and chemical inventories. *Earth and Planetary Science Letters*, *76*(1-2), 135-150. https://doi.org/10.1016/0012-821X(85)90154-2.

Boyle, E. A., & Keigwin, L. D. (1985). Comparison of Atlantic and Pacific paleochemical records for the last 215,000 years: Changes in deep ocean circulation and chemical inventories. *Earth and Planetary Science Letters*, *76*(1-2), 135-150. https://doi.org/10.1016/0012-821X(85)90154-2.

Broecker, W. S., (1971) Calcite accumulation rates and glacial to interglacial changes in oceanic mixing K.K. Turekian (Ed.), Late Cenozoic Glacial Ice Ages, Yale Univ. Press, New Haven, CN (1971), 239-265.

Broecker, W. S., & Clark, E. (1999). CaCO3 size distribution: A paleocarbonate ion proxy?. *Paleoceanography*, *14*(5), 596-604.

Broecker, W., & Clark, E. (2001a). An evaluation of Lohmann's foraminifera weight dissolution index. *Paleoceanography*, *16*(5), 531-534. https://doi.org/10.1029/2000PA000600.

Broecker, W. S., & Clark, E. (2001b). Glacial-to-Holocene redistribution of carbonate ion in the deep sea. *Science*, *294*(5549), 2152-2155. https://doi.org/10.1126/science.1064171.

Broecker, W., & Clark, E. (2001c). A dramatic Atlantic dissolution event at the onset of the last glaciation. *Geochemistry, Geophysics, Geosystems*, *2*(11). https://doi.org/10.1029/2001GC000185.

Broecker, W. S., & Clark, E. (2002a). Carbonate ion concentration in glacial-age deep waters of the Caribbean Sea. *Geochemistry, Geophysics, Geosystems*, *3*(3), 1-14. https://doi.org/10.1029/2001GC000231.

Broecker, W. S., & Clark, E. (2002b). A major dissolution event at the close of MIS 5e in the western equatorial Atlantic. *Geochemistry, Geophysics, Geosystems*, *3*(2), 1-5. https://doi.org/10.1029/2001GC000210.

Broecker, W. S., & Clark, E. (2003). Glacial-age deep sea carbonate ion concentrations. *Geochemistry, Geophysics, Geosystems*, *4*(6). https://doi.org/10.1029/2003GC000506.

Broecker, W. S., Peacock, S. L., Walker, S., Weiss, R., Fahrbach, E., Schroeder, M., Mikolajewicz, U., Heinze, C., Key, R., Peng, T. H., & Rubin, S. (1998). How much

Deepwater is formed in the Southern Ocean?. *Journal of Geophysical Research: Oceans*, *103*(C8), 15833-15843. https://doi.org/10.1029/98JC00248.

Broecker, W. S., & Peng, T. H. (1982). Tracers in the Sea. Eldigio Press *Lamont-Doherty Geological Observatory*.

Broecker, W. S., & Peng, T. H. (1992). Interhemispheric transport of carbon dioxide by ocean circulation. *Nature*, *356*(6370), 587-589. https://doi.org/10.1038/356587a0.

Broecker, W. S., & Sutherland, S. (2000). Distribution of carbonate ion in the deep ocean: Support for a post-Little Ice Age change in Southern Ocean ventilation?. *Geochemistry, Geophysics, Geosystems*, *1* (7). https://doi.org/10.1029/2000GC000039.

Bryan, S. P., Marchitto, T. M., & Lehman, S. J. (2010). The release of 14C-depleted carbon from the deep ocean during the last deglaciation: Evidence from the Arabian Sea. *Earth and Planetary Science Letters*, *298* (1-2), 244-254. https://doi.org/10.1016/j.epsl.2010.08.025.

Byrne, R. H., & Yao, W. (2008). Procedures for measurement of carbonate ion concentrations in seawater by direct spectrophotometric observations of Pb (II) complexation. *Marine Chemistry*, *112* (1-2), 128-135. https://dx.doi.org/10.1016/j.marchem.2008.07.009.

Bryan, S. P., & Marchitto, T. M. (2008). Mg/Ca–temperature proxy in benthic foraminifera: New calibrations from the Florida Straits and a hypothesis regarding Mg/Li. *Paleoceanography*, *23*(2). https://doi.org/10.1029/2007PA001553

Calvert, S. E., Pedersen, T. F., Naidu, P. D., & Von Stackelberg, U. (1995). On the organic carbon maximum on the continental slope of the eastern Arabian Sea. *Journal of Marine Research*, *53*(2), 269-296. https://doi.org/10.1357/0022240953213232.

Cao, L., Fairbanks, R. G., Mortlock, R. A., & Risk, M. J. (2007). Radiocarbon reservoir age of high latitude North Atlantic surface water during the last deglacial. *Quaternary Science Reviews*, *26*(5-6), 732-742. https://doi.org/10.1016/j.quascirev.2006.10.001

Cappelli Giudice, E. L., Clarke, J. L., Smeaton, C., Davidson, K., & Austin, W. E. N. (2019). Organic-carbon-rich sediments: benthic foraminifera as bio-indicators of depositional

environments. *Biogeosciences*, *16*(21), 4183-4199. https://doi.org/10.5194/bg-2019-125

Caralp, M. H. (1988). Late glacial to recent deep-sea benthic foraminifera from the Northeastern Atlantic (Cadiz Gulf) and Western Mediterranean (Alboran Sea): paleooceanographic results. *Marine Micropaleontology*, *13*(3), 265-289. https://doi.org/10.1016/0377-8398(88)90006-0

Carton, X., l'Hegaret, P., & Baraille, R. (2012). Mesoscale variability of water masses in the Arabian Sea as revealed by ARGO floats. *Ocean Science*, *8*(2), 227-248. https://doi.org/10.5194/os-8-227-2012.

Charles, C. D., & Fairbanks, R. G. (1992). Evidence from Southern Ocean sediments for the effect of North Atlantic deep-water flux on climate.*Nature* 355, 416–419. https://doi:10.1038/355416a0

Chandana, K. R., Bhushan, R., & Jull, A. J. T. (2017). Evidence of poor bottom water ventilation during LGM in the equatorial Indian Ocean. *Frontiers in Earth Science*, *5*, 84. https://doi.org/10.3389/feart.2017.00084

Chalk, T. B., Foster, G. L., & Wilson, P. A. (2019). Dynamic storage of glacial CO2 in the Atlantic Ocean revealed by boron [CO32−] and pH records. *Earth and Planetary Science Letters*, *510*, 1-11. https://doi.org/10.1016/j.epsl.2018.12.022.

Chandana, K. R., Bhushan, R., & Jull, A. J. T. (2017). Evidence of poor bottom water ventilation during LGM in the equatorial Indian Ocean. *Frontiers in Earth Science*, *5*, 84. https://doi.org/10.3389/feart.2017.00084.

Coxall, H. K., Wilson, P. A., Pälike, H., Lear, C. H., & Backman, J. (2005). Rapid stepwise onset of Antarctic glaciation and deeper calcite compensation in the Pacific Ocean. *Nature*, *433*(7021), 53-57. https://doi 10.1038/nature03135

Crowley, T. J. (1983). Calcium-carbonate preservation patterns in the central North Atlantic during the last 150,000 years. *Marine Geology*, *51*(1-2), 1-14. https://doi.org/10.1016/0025-3227(83)90085-3.

Cullen, J. L., & Prell, W. L. (1984). Planktonic foraminifera of the northern Indian Ocean: distribution and preservation in surface sediments. *Marine Micropaleontology*, *9*(1), 1-52. https://doi.org/10.1016/0377-8398(84)90022-7.

Curry, W. B., Duplessy, J. C., Labeyrie, L. D., & Shackleton, N. J. (1988). Changes in the distribution of δ13C of deep water ΣCO2 between the last glaciation and the Holocene. *Paleoceanography*, *3*(3),317-341. https://doi.org/10.1029/PA003i003p00317.

Darbyshire, M. (1967). The surface waters off the coast of Kerala, south-west India. In *Deep Sea Research and Oceanographic Abstracts* (Vol. 14, No. 3, pp. 295-320).

Dai, A., & Trenberth, K. E. (2002). Estimates of freshwater discharge from continents: Latitudinal and seasonal variations. *Journal of hydrometeorology*, *3*(6), 660-687. https://doi.org/10.1175/1525-7541(2002)003<0660:EOFDFC>2.0.CO;2.

Den Dulk, M., Reichart, G. J., Van Heyst, S., Zachariasse, W. J., & Van der Zwaan, G. J. (2000). Benthic foraminifera as proxies of organic matter flux and bottom water oxygenation? A case history from the northern Arabian Sea. *Palaeogeography, Palaeoclimatology, Palaeoecology*, *161*(3-4), 337-359. https://doi.org/10.1016/S0031-0182(00)00074-2

De Stigter, H. C., Jorissen, F. J., &Van der Zwaan, G. J. (1998). Bathymetric distribution and microhabitat partitioning of live (Rose Bengal stained) benthic foraminifera along a shelf to bathyal transect in the southern Adriatic Sea. *The Journal of Foraminiferal Research*, *28*(1), 40-65.

De Villiers, S. (2004). Optimum growth conditions as opposed to calcite saturation as a control on the calcification rate and shell-weight of marine foraminifera. *Marine Biology*, *144*(1), 45-49.

De Villiers, S. (2005). Foraminiferal shell-weight evidence for sedimentary calcite dissolution above the lysocline. *Deep Sea Research Part I: Oceanographic Research Papers*, *52*(5), 671-680. http://dx.doi.org/10.1016/j.dsr.2004.11.014.

Dickson, A. G. (1990). Thermodynamics of the dissociation of boric acid in synthetic seawater from 273.15 to 318.15 K. *Deep Sea Research Part A. Oceanographic Research Papers*, *37*(5), 755-766. https://doi.org/10.1016/0198-0149(90)90004-F.

Donohue, K. A., Hufford, G. E., & McCartney, M. S. (1999). Sources and transport of the deep western boundary current east of the Kerguelen Plateau. *Geophysical Research Letters*, *26*(7), 851-854. http://dx.doi.org/10.1029/1999GL900099.

Doss, W., & Marchitto, T. M. (2013). Glacial deep ocean sequestration of CO_2 driven by the eastern equatorial Pacific biologic pump. *Earth and Planetary Science Letters*, *377*, 43-54.https://doi:10.1016/j.epsl.2013.07.019

Doss, W., Marchitto, T. M., Eagle, R., Rashid, H., & Tripati, A. (2018). Deconvolving the saturation state and temperature controls on benthic foraminiferal Li/Ca, based on downcore paired B/Ca measurements and coretop compilation. *Geochimica et Cosmochimica Acta*, *236*, 297-314. https://doi.org/10.1016/j.gca.2018.02.029.

Dulk Den, M., Reichart, G. J., Van Heyst, S., Zachariasse, W. J., & Van der Zwaan, G. J. (2000). Benthic foraminifera as proxies of organic matter flux and bottom water oxygenation? A case history from the northern Arabian Sea. *Palaeogeography, Palaeoclimatology, Palaeoecology*, *161*(3-4), 337-359. https://doi.org/10.1016/S0031-0182(00)00074-2.

Duplessy, J. C., Shackleton, N. J., Matthews, R. K., Prell, W., Ruddiman, W. F., Caralp, M., & Hendy, C. H. (1984). 13C record of benthic foraminifera in the last interglacial ocean: implications for the carbon cycle and the global deep water circulation. *Quaternary Research*, *21*(2), 225-243. https://doi.org/10.1016/0033-5894(84)90099-1

Duplessy, J. C., Shackleton, N. J., Fairbanks, R. G., Labeyrie, L., Oppo, D., & Kallel, N. (1988). Deep water source variations during the last climatic cycle and their impact on the global deepwater circulation. *Paleoceanography*, *3*(3), 343-360. https://doi.org/10.1029/PA003i003p00343.

Durand, F., Shetye, S., Vialard, J., Shankar, D., Shenoi, S., Éthé, C., & Madec, G. (2004). Impact of temperature inversions on SST evolution in the south-eastern Arabian Sea during the pre-summer monsoon season. *Geophysical Research Letters*, 31, L01305. https://doi.org/10. 1029/2003GL018906.

Durand, F., Shankar, D., de Boyer Montégut, C., Shenoi, S. S. C., Blanke, B., & Madec, G. (2007). Modeling the barrier-layer formation in the southeastern Arabian Sea.*Journal of Climate*, 20 (10), 2109–2120. https://doi.org/10.1175/JCLI4112.1.

Elliot, M., Labeyrie, L., & Duplessy, J. C. (2002). Changes in North Atlantic deep-water formation associated with the Dansgaard–Oeschger temperature oscillations (60–10

ka). *Quaternary Science Reviews*, *21*(10), 1153-1165. https://doi.org/10.1016/S0277-3791(01)00137-8

Emerson, S.& Bender, M. (1981). Carbon fluxes at the sediment-water interface of the deep-sea: calcium carbonate preservation.

Emery, W. J., & Meincke, J. (1986). Global water masses-summary and review. *Oceanologica acta*, *9*(4), 383-391.

Emiliani, C., & Epstein, S. (1953). Temperature variations in the lower Pleistocene of southern California. *The Journal of Geology*, *61*(2), 171-181.

Emiliani, C. (1954). Depth habitats of some species of pelagic foraminifera as indicated by oxygen isotope ratios. *American Journal of Science*, *252*(3), 149-158.

Emiliani, C. (1955). Pleistocene temperatures. *The Journal of geology*, *63*(6), 538-578.

Epstein, S., Buchsbaum, R., Lowenstam, H. A., & Urey, H. C. (1953). Revised carbonate-water isotopic temperature scale. *Geological Society of America Bulletin*, *64*(11), 1315-1326. https://doi.org/10.1130/0016-7606(1953)64[1315:RCITS]2.0.CO;2

Ezat, M. M., Rasmussen, T. L., Hönisch, B., Groeneveld, J., & Demenocal, P. (2017). Episodic release of CO2 from the high-latitude North Atlantic Ocean during the last 135 kyr. *Nature communications*, *8*(1), 1-10. https://doi: 10.1038/ncomms14498 (2017).

Farrell, J. W., & Prell, W. L. (1989). Climatic change and $CaCO_3$ preservation: An 800,000 year bathymetric reconstruction from the central equatorial Pacific Ocean. *Paleoceanography*, *4*(4), 447-466. https://doi.org/10.1029/PA004i004p00447.

Fehrenbacher, J., & Martin, P. (2011). Western equatorial Pacific deep water carbonate chemistry during the Last Glacial Maximum and deglaciation: Using planktic foraminiferal Mg/Ca to reconstruct sea surface temperature and seafloor dissolution. *Paleoceanography*, *26*(2). https://doi.org/10.1029/2010PA002035.

Fehrenbacher, J. S., Martin, P., & Eshel, G. (2006). Pacific Deep Water Carbonate Chemistry during the Last Glacial Maximum: using foraminiferal Mg/Ca to reconstruct temperature and dissolution. In *AGU Fall Meeting Abstracts* (Vol. 2006, pp. PP13D-06).

Fieux, M., Schott, F., & Swallow, J. C. (1986). Deep boundary currents in the western Indian Ocean revisited. *Deep Sea Research Part A. Oceanographic Research Papers*, *33*(4), 415-426. https://doi.org/10.1016/0198-0149(86)90124-X.

Fisher, R. L., Sclater, J. G., & , McKenzie D. P. (1971). Evolution of the central Indian ridge, western Indian Ocean. *Geological Society of America Bulletin*, *82*(3), 553-562. https://doi.org/10.1130/0016-7606(1971)82[553:EOTCIR]2.0.CO;2.

Foster, G. L. (2008). Seawater pH, pCO2 and [CO^{2-}_3] variations in the Caribbean Sea over the last 130 kyr: A boron isotope and B/Ca study of planktic foraminifera. *Earth and Planetary Science Letters*, *271*(1-4), 254-266. https://doi.org/10.1016/j.epsl.2008.04.015.

Foster, G. L., Hönisch, B., Paris, G., Dwyer, G. S., Rae, J. W., Elliott, T., Gaillardet, J., Hemming, G. N., Louvat, P., & Vengosh, A. (2013). Interlaboratory comparison of boron isotope analyses of boric acid, seawater and marine CaCO3 by MC-ICPMS and NTIMS. *Chemical Geology*, *358*, (1). https://doi.org/10.1016/j.chemgeo.2013.08.027.

Foster, G. L., & Sexton, P. F. (2014). Enhanced carbon dioxide outgassing from the eastern equatorial Atlantic during the last glacial. *Geology*, *42*(11), 1003-1006. https://doi.org/10.1130/G35806.1

Gardner, J. V. (1975). Late Pleistocene carbonate dissolution cycles in the eastern equatorial Atlantic. *Cushman foundation for Foraminiferal Research, Special Publication U.S.A.,* 0013, P. 129 A 14.

George, M. D., Kumar, M. D., Naqvi, S. W. A., Banerjee, S., Narvekar, P. V., De Sousa, S. N., & Jayakumar, D. A. (1994). A study of the carbon dioxide system in the northern Indian Ocean during premonsoon. *Marine Chemistry*, *47*(3-4), 243-254. https://doi.org/10.1016/0304-4203(94)90023-X.

Godad, S. P., Naidu, P. D., & Malmgren, B. A. (2011). Sea surface temperature changes during May and August in the western Arabian Sea over the last 22 kyr: Implications as to shifting of the upwelling season. *Marine Micropaleontology*, *78*(1-2), 25-29.

Godad, S. P., Naik, S. S., & Naidu, P. D. (2017). 70 kyr record of denitrification and oxygenation changes in the eastern Arabian Sea. *Geochemical Journal*, *51*(4), 329-336. https://doi.org/10.2343/geochemj.2.0472

Gopalakrishna, V.V., Johnson, Z., Salgaonkar, G., Nisha, K., Rajan, C., & Rao, R. (2005). Observed variability of sea surface salinity and thermal inversions in the Lakshadweep Sea during contrast monsoons. *Geophysical Research Letters*, 32, L18605. https://doi.org/1029/ 2005GL023280.

Gooday, A. J. (1993). Deep-sea benthic foraminiferal species which exploit phytodetritus: characteristic features and controls on distribution. *Marine Micropaleontology*, *22*(3), 187-205.

Goswami, V., Singh, S. K., & Bhushan, R. (2012). Dissolved redox sensitive elements, Re, U and Mo in intense denitrification zone of the Arabian Sea. *Chemical Geology*, *291*, 256-268. https://dx.doi.org/10.1016/j.chemgeo.2011.10.021.

Goswami, V., Singh, S. K., & Bhushan, R. (2014). Impact of water mass mixing and dust deposition on Nd concentration and εNd of the Arabian Sea water column. *Geochimica et Cosmochimica Acta*, *145*, 30-49. https://doi.org/10.1016/j.chemgeo.2011.10.021

Gottschalk, J., Vázquez Riveiros, N., Waelbroeck, C., Skinner, L. C., Michel, E., Duplessy, J. C., & Mackensen, A. (2016). Carbon isotope offsets between benthic foraminifer species of the genus Cibicides (Cibicidoides) in the glacial sub-Antarctic Atlantic. *Paleoceanography*, *31*(12), 1583-1602. https://doi.org/10.1002/2016PA003029.

Gottschalk, J., Hodell, D. A., Skinner, L. C., Crowhurst, S. J., Jaccard, S. L., & Charles, C. (2018). Past carbonate preservation events in the deep Southeast Atlantic Ocean (Cape Basin) and their implications for Atlantic overturning dynamics and marine carbon cycling. *Paleoceanography and paleoclimatology*, *33*(6), 643-663. https://doi.org/10.1029/2018PA003353.

Gottschalk, J., Michel, E., Thöle, L. M., Studer, A. S., Hasenfratz, A. P., Schmid, N., Butzin, M., Mazaud A., Martinez-Gracia, A., & Jaccard, S. L. (2020). Glacial heterogeneity in Southern Ocean carbon storage abated by fast South Indian deglacial carbon

release. *Nature communications*, *11*(1), 1-14. https://doi 10.1038/s41467-020-20034-1

Govil, P., & Naidu, P. D. (2010). Evaporation-precipitation changes in the eastern Arabian Sea for the last 68 ka: Implications on monsoon variability. *Paleoceanography*, *25*, PA1210. https://doi.org/10.1029/2008PA001687.

Goyet, C., Millero, F. J., O'Sullivan, D. W., Eischeid, G., McCue, S. J., & Bellerby, R. G. J. (1998). Temporal variations of pCO2 in surface seawater of the Arabian Sea in 1995. *Deep Sea Research Part I: Oceanographic Research Papers*, *45*(4-5), 609-623. https://doi.org/10.1016/S0967-0637(97)00085-X.

Grasshoff, K., (1969). Chemical observations in the Red Sea and the inner Gulf of Aden during the International Indian Ocean Expedition 1964/65. *Pangea*, https://doi.org/10.1594/PANGAEA.603890

Gray, W. R., Rae, J. W., Wills, R. C., Shevenell, A. E., Taylor, B., Burke, A., Foster, G. L., & Lear, C. H. (2018). Deglacial upwelling, productivity and CO_2 outgassing in the North Pacific Ocean. *Nature Geoscience*, *11*(5), 340-344. https://doi10.1038/s41561-018-0108-6

Gupta, A. K., Das, M., Clemens, S. C., & Mukherjee, B. (2008). Benthic foraminiferal faunal and isotopic changes as recorded in Holocene sediments of the northwest Indian Ocean. *Paleoceanography*, *23*(2). https://doi:10.1029/2007PA001546

Guptha, M. V. S., Naidu, P. D., Haake, B. G., & Schiebel, R. (2005). Carbonate and carbon fluctuations in the Eastern Arabian Sea over 140 ka: Implications on productivity changes? *Deep Sea Research Part II: Topical Studies in Oceanography*, *52*(14-15), 1981-1993. https://doi:10.1016/j.dsr2.2005.05.003

Gupta, A. K., Mohan, K., Sarkar, S., Clemens, S. C., Ravindra, R., & Uttam, R. K. (2011). East–west similarities and differences in the surface and deep northern Arabian Sea records during the past 21 Kyr. *Palaeogeography, Palaeoclimatology, Palaeoecology*, *301*(1-4), 75-85. https://doi.org/10.1016/j.palaeo.2010.12.027

Hall, J. M., & Chan, L. H. (2004). Li/Ca in multiple species of benthic and planktonic foraminifera: Thermocline, latitudinal, and glacial-interglacial

variation. *Geochimica et Cosmochimica Acta*, *68*(3), 529-545. https://doi.org/10.1016/S0016-7037(03)00451-4.

Hemming, N. G., & Hanson, G. N. (1992). Boron isotopic composition and concentration in modern marine carbonates. *Geochimica et Cosmochimica Acta*, *56*(1), 537-543. https://doi.org/10.1016/0016-7037(92)90151-8.

Hemming, N. G., Reeder, R. J., & Hanson, G. N. (1995). Mineral-fluid partitioning and isotopic fractionation of boron in synthetic calcium carbonate. *Geochimica et Cosmochimica Acta*, *59* (2), 371-379. https://doi.org/10.1016/0016-7037(95)00288-B.

Henehan, M. J., Rae, J. W., Foster, G. L., Erez, J., Prentice, K. C., Kucera, M., Bostock H. C. Martinez-Boti, M. A., Milton J. A., Wilson P. A., Marshall, J., & Elliott, T. (2013). Calibration of the boron isotope proxy in the planktonic foraminifera Globigerinoides ruber for use in palaeo-CO2 reconstruction. *Earth and Planetary Science Letters*, *364*, 111-122. https://doi.org/10.1016/j.epsl.2012.12.029.

Hoegh-Guldberg, O., Mumby, P. J., Hooten, A. J., Steneck, R. S., Greenfield, P., Gomez, E., Harvell, C.D., Sale, P.F., Edwards, A. J., Caldeira, K., Knowlton, N., Eakin, C.M., Iglesias-Prieto, R., Muthiga, N., Bradbury, R. H., Dubi, A., & Hatziolos, M. E. (2007). Coral reefs under rapid climate change and ocean acidification. *science*, *318* (5857), 1737-1742. https://doi.org/10.1126/science.1152509.

Hönisch, B., & Hemming, N. G. (2005). Surface ocean pH response to variations in pCO2 through two full glacial cycles. *Earth and Planetary Science Letters*, *236* (1-2), 305-314. http://dx.doi.org/10.1016/j.epsl.2005.04.027.

Hoogakker, B., Elderfield, H., Schmiedl, G. H., McCave, I. N., & Rickaby, R. E. (2014). Glacial bottom water oxygen concentrations inferred from benthic foraminiferal interspecies carbon isotope gradients. In *AGU Fall Meeting Abstracts* (Vol. 2014, pp. PP11D-03).

Hoogakker, B. A., Elderfield, H., Schmiedl, G., McCave, I. N., & Rickaby, R. E. (2015). Glacial–interglacial changes in bottom-water oxygen content on the Portuguese margin. *Nature Geoscience*, *8*(1), 40-43.

Howard, W. R., & Prell, W. L. (1994). Late Quaternary CaCO3 production and preservation in the Southern Ocean: Implications for oceanic and atmospheric carbon cycling. *Paleoceanography*, *9*(3), 453-482. https://doi.org/10.1029/93PA03524.

Hufford, G. E., McCartney, M. S., & Donohue, K. A. (1997). Northern boundary currents and adjacent recirculations off southwestern Australia. *Geophysical Research Letters*, *24*(22), 2797-2800. https://doi.org/10.1029/97GL02278.

Jaccard, S. L., Galbraith, E. D., Sigman, D. M., Haug, G. H., Francois, R., Pedersen, T. F., Dulski, P., & Thierstein, H. R. (2009). Subarctic Pacific evidence for a glacial deepening of the oceanic respired carbon pool. *Earth and Planetary Science Letters*, *277*(1-2), 156-165. https://doi.org/10.1016/j.epsl.2008.10.017

Jensen, T. G. (2001). Arabian Sea and Bay of Bengal exchange of salt and tracers in an ocean model. *Geophysical Research Letters,* 28(20), 3967–3970. https://doi.org/10.1029/2001GL013422.

Jensen, T. G. (2003). Cross-equatorial pathways of salt and tracers from the Northern Indian Ocean: Modelling results. *Deep Sea Research Part II: Topical Studies in Oceanography,* 50(12), 2111–2127. https://doi.org/10.5670/oceanog.2016.42.

Jorissen, F. J., Barmawidjaja, D. M., Puskaric, S., & Van der Zwaan, G. J. (1992). Vertical distribution of benthic foraminifera in the northern Adriatic Sea: the relation with the organic flux. *Marine Micropaleontology*, *19* (1-2), 131-146. https://doi.org/10.1016/0377-8398 (92)90025-F

Johannessen, O. M., Subbaraju, G., & Blindheim, J. (1987). Seasonal variations of the oceanographic conditions off the southwest coast of India during 1971-1975.FiskDir; Skr. SeT. Hav Unders.18, 247-161.

Johnson, G. C., Musgrave, D. L., Warren, B. A., Ffield, A., & Olson, D. B. (1998). Flow of bottom and deep water in the Amirante Passage and Mascarene Basin. *Journal of Geophysical Research: Oceans*, *103*(C13), 30973-30984. https://doi.org/10.1029/1998JC900027.

Johnson, G. C., Warren, B. A., & Olson, D. B. (1991a). Flow of bottom water in the Somali Basin. *Deep Sea Research Part A. Oceanographic Research Papers*, *38*(6), 637-652. https://doi.org/10.1016/0198-0149(91)90003-X.

Johnson, G. C., Warren, B. A., & Olson, D. B. (1991b). A deep boundary current in the Arabian Basin. *Deep Sea Research Part A. Oceanographic Research Papers*, *38*(6), 653-661. https://doi.org/10.1016/0198-0149(91)90004-Y.

Jorissen, F. J., Barmawidjaja, D. M., Puskaric, S., & Van der Zwaan, G. J. (1992). Vertical distribution of benthic foraminifera in the northern Adriatic Sea: the relation with the organic flux. *Marine Micropaleontology*, *19*(1-2), 131-146. https://doi.org/10.1016/0377-8398(92)90025-F.

Jung, S. J., Kroon, D., Ganssen, G., Peeters, F., & Ganeshram, R. (2009). Enhanced Arabian Sea intermediate water flow during glacial North Atlantic cold phases. *Earth and Planetary Science Letters*, *280*(1-4), 220-228. https://doi.org/10.1016/j.epsl.2009.01.037

Kaiho, K. (1991). Global changes of Paleogene aerobic/anaerobic benthic foraminifera and deep-sea circulation. *Palaeogeography, Palaeoclimatology, Palaeoecology*, *83*(1-3), 65-85. https://doi.org/10.1016/0031-0182(91)90076-4.

Kakihana, H., & Kotaka, M. (1977). Equilibrium constants for boron isotope-exchange reactions. *Bulletin of the Research Laboratory for Nuclear Reactors (Tokyo Institute of Technology)*, *2*.

Kallel, N., Labeyrie, L. D., Juillet-Leclerc, A., & Duplessy, J. C. (1988). A deep hydrological front between intermediate and deep-wafpr, masses in the glacial Indian Ocean. *Nature*, *333*(6174), 651-655. https://doi.org/10.1038/333651a0.

Karlin, R., Lyle, M., &Zahn, R. (1992). Carbonate variations in the northeast Pacific during the late Quaternary. *Paleoceanography*, *7*(1), 43-61. https://doi.org/10.1029/91PA03077.

Kerr, J., Rickaby, R., Yu, J., Elderfield, H., & Sadekov, A. Y. (2017). The effect of ocean alkalinity and carbon transfer on deep-sea carbonate ion concentration during the past five glacial cycles. *Earth and Planetary Science Letters*, *471*, 42-53. https://doi.org/10.1016/j.epsl.2017.04.042.

Kessarkar, P. M., Purnachadra Rao, V., Naqvi, S. W. A., & Karapurkar, S. G. (2013). Variation in the Indian summer monsoon intensity during the Bølling-Ållerød and Holocene. *Paleoceanography*, *28*(3), 413-425. https://doi:10.1002/palo.20040

Key, R. M., Kozyr, A., Sabine, C. L., Lee, K., Wanninkhof, R., Bullister, J. L., Feely, R. A., Millero, F.J., Mordy, C., & Peng, T. H. (2004). A global ocean carbon climatology: Results from Global Data Analysis Project (GLODAP). *Global biogeochemical cycles*, *18*(4). https://doi.org/10.1029/2004GB002247.

Khare, N., Nigam, R., Mayenkar, D. N., & Saraswat, R. (2017). Cluster analysis of benthic foraminiferal morpho-groups from the western margin of India reflects its depth preference. *Continental Shelf Research*, *151*, 72-83. https://doi.org/10.1016/j.csr.2017.10.011.

Kolla, V., Bé, A. W.,& Biscaye, P. E. (1976). Calcium carbonate distribution in the surface sediments of the Indian Ocean. *Journal of Geophysical Research*, *81*(15), 2605-2616. https://doi.org/10.1029/JC081i015p02605.

Klöcker, R., Ganssen, G., Jung, S. J., Kroon, D., & Henrich, R. (2006). Late Quaternary millennial-scale variability in pelagic aragonite preservation off Somalia. *Marine Micropaleontology*, *59* (3-4), 171-183. https://doi.org/10.1016/j.marmicro.2006.02.004

Klöcker, R., & Henrich, R. (2006). Recent and Late Quaternary pteropod preservation on the Pakistan shelf and continental slope. *Marine Geology*, *231*(1-4), 103-111. https://doi.org/10.1016/j.margeo.2006.05.014.

Klump, J., Hebbeln, D., & Wefer, G. (2000). The impact of sediment provenance on barium-based productivity estimates. *Marine Geology*, *169*(3-4), 259-271. https://doi.org/10.1016/S0025-3227(00)00092-X

Kubota, K., Yokoyama, Y., Ishikawa, T., Sagawa, T., Ikehara, M., & Yamazaki, T. (2019). Equatorial Pacific seawater p CO 2 variability since the last glacial period. *Scientific reports*, *9*(1), 1-11. https://doi.org/10.1038/s41598-019-49739-0

Kumar, M. D., & Li, Y. H. (1996). Spreading of water masses and regeneration of silica and 226Ra in the Indian Ocean. *Deep Sea Research Part II: Topical Studies in Oceanography*, *43*(1), 83-110. https://doi.org/10.1016/0967-0645(95)00084-4

Lacerra, M., Lund, D., Yu, J., & Schmittner, A. (2017). Carbon storage in the mid-depth Atlantic during millennial-scale climate events. *Paleoceanography*, *32*, 780-795. https://doi.org/10.1002/2016PA003081.

Lacerra, M., Lund, D. C., Gebbie, G., Oppo, D. W., Yu, J., Schmittner, A., & Umling, N. E. (2019). Less remineralized carbon in the intermediate-depth South Atlantic during Heinrich Stadial 1. *Paleoceanography and Paleoclimatology*, *34*(7), 1218-1233. https://doi.org/10.1029/2018PA003537.

Lalicata, J. J., & Lea, D. W. (2011). Pleistocene carbonate dissolution fluctuations in the eastern equatorial Pacific on glacial timescales: Evidence from ODP Hole 1241. *Marine Micropaleontology*, *79*(1-2), 41-51. https://doi.org/10.1016/j.marmicro.2011.01.002

Lee, K., Kim, T. W., Byrne, R. H., Millero, F. J., Feely, R. A., & Liu, Y. M. (2010). The universal ratio of boron to chlorinity for the North Pacific and North Atlantic oceans. *Geochimica et Cosmochimica Acta*, *74*(6), 1801-1811. https://doi.org/10.1016/j.gca.2009.12.027.

Lemarchand, D., Gaillardet, J., Göpel, C., & Manhes, G. (2002). An optimized procedure for boron separation and mass spectrometry analysis for river samples. *Chemical Geology*, *182*(2-4), 323-334. http://dx.doi.org/10.1016/S0009-2541(01)00329-1.

Le Pichon, X. (1960). The deep water circulation in the southwest Indian Ocean. *Journal of Geophysical Research*, *65*(12), 4061-4074. https://doi.org/10.1029/JZ065i012p04061

LeKieffre, C., Spero, H. J., Fehrenbacher, J. S., Russell, A. D., Ren, H., Geslin, E., & Meibom, A. (2020). Ammonium is the preferred source of nitrogen for planktonic foraminifer and their dinoflagellate symbionts. *Proceedings of the Royal Society B*, *287*(1929), 20200620. https://doi.org/10.1098/rspb.2020.0620

Lindsay, C. M., Lehman, S. J., Marchitto, T. M., & Ortiz, J. D. (2015). The surface expression of radiocarbon anomalies near Baja California during deglaciation. *Earth and Planetary Science Letters*, *422*, 67-74. https://doi.org/10.1016/j.epsl.2015.04.012.

Lohmann, G. P. (1995). A model for variation in the chemistry of planktonic foraminifera due to secondary calcification and selective dissolution. *Paleoceanography*, *10*(3), 445-457. https://doi.org/10.1029/95PA00059.

Lüthi, D., Le Floch, M., Bereiter, B., Blunier, T., Barnola, J. M., Siegenthaler, U., Raynaud, D., Jouzel, J., Fischer, H., Kawamura, H., & Stocker, T. F. (2008). High-resolution carbon dioxide concentration record 650,000–800,000 years before present. *Nature*, *453*(7193), 379-382. https://doi.org/10.1038/nature06949.

Ma, R., Sepulcre, S., Bassinot, F., Haurine, F., Tisnérat-Laborde, N., & Colin, C. (2020). North Indian Ocean Circulation Since the Last Deglaciation as Inferred From New Elemental Ratio Records for Benthic Foraminifera Hoeglundina elegans. *Paleoceanography and Paleoclimatology*, *35*(6), e2019PA003801. https://doi.org/10.1029/2019PA003801.

Mackensen, A., Rudolph, M., & Kuhn, G., (2001). Late Pleistocene deep-water circulation in the subantarctic eastern Atlantic, *Global and Planetary Change*, 30, 197-229. https://doi.org/10.1016/S0921-8181(01)00102-3

Mackensen, A., Sejrup, H. P., & Jansen, E. (1985). The distribution of living benthic foraminifera on the continental slope and rise off southwest Norway. *Marine Micropaleontology*, *9*(4), 275-306. https://doi.org/10.1016/0377-8398(85)90001-5

McCreary Jr, J. P., Yu, Z., Hood, R. R., Vinaychandran, P. N., Furue, R., Ishida, A., & Richards, K. J. (2013). Dynamics of the Indian-Ocean oxygen minimum zones. *Progress in Oceanography*, *112*, 15-37. https://doi.org/10.1016/j.pocean.2013.03.002.

McManus, J. F., Francois, R., Gherardi, J. M., Keigwin, L. D., & Brown-Leger, S. (2004). Collapse and rapid resumption of Atlantic meridional circulation linked to deglacial climate changes. *Nature*, *428*(6985), 834-837. https://doi: 10.1038/nature02494

Madhupratap, M., Kumar, S. P., Bhattathiri, P. M. A., Kumar, M. D., Raghukumar, S., Nair, K. K. C., & Ramaiah, N. (1996). Mechanism of the biological response to winter cooling in the northeastern Arabian Sea. *Nature*, *384*(6609), 549-552. https://doi.org/10.1038/384549a0.

Mangini, A., Godoy, J. M., Godoy, M. L., Kowsmann, R., Santos, G. M., Ruckelshausen, M., Schroeder-Ritzrau, A., & Wacker, L. (2010). Deep sea corals off Brazil verify a poorly ventilated Southern Pacific Ocean during H2, H1 and the Younger Dryas. *Earth and Planetary Science Letters*, *293*(3-4), 269-276. https://doi.org/10.1016/j.epsl.2010.02.041

Manjunatha, B. R., & Shankar, R. (1992). A note on the factors controlling the sedimentation rate along the western continental shelf of India. *Marine Geology*, *104*(1-4), 219-224. https://doi.org/10.1016/0025-3227(92)90097-2.

Mantyla, A. W., & Reid, J. L. (1995). On the origins of deep and bottom waters of the Indian Ocean. *Journal of Geophysical Research: Oceans*, *100*(C2), 2417-2439. https://doi.org/10.1029/94JC02564.

Marchitto, T. M., Bryan, S. P., Doss, W., McCulloch, M. T., & Montagna, P. (2018). A simple biomineralization model to explain Li, Mg, and Sr incorporation into aragonitic foraminifera and corals. *Earth and Planetary Science Letters*, *481*, 20-29. https://doi.org/10.1016/j.epsl.2017.10.022

Marchitto Jr, T. M., Curry, W. B., & Oppo, D. W. (2000). Zinc concentrations in benthic foraminifera reflect seawater chemistry. *Paleoceanography*, *15*(3), 299-306. https://doi.org/10.1029/1999PA000420.

Marchitto Jr, T. M., Oppo, D. W., & Curry, W. B. (2002). Paired benthic foraminiferal Cd/Ca and Zn/Ca evidence for a greatly increased presence of Southern Ocean Water in the glacial North Atlantic. *Paleoceanography*, *17*(3), 10-1. https://doi.org/10.1029/2000PA000598.

Marchitto, T. M., & Broecker, W. S. (2006). Deep water mass geometry in the glacial Atlantic Ocean: A review of constraints from the paleonutrient proxy Cd/Ca. *Geochemistry, Geophysics, Geosystems*, *7*(12). https://doi.org/10.1029/2006GC001323

Marchitto, T. M., Lehman, S. J., Ortiz, J. D., Flückiger, J., & van Geen, A. (2007). Marine radiocarbon evidence for the mechanism of deglacial atmospheric CO_2 rise. *science*, *316*(5830), 1456-1459. https://doi: 10.1126/science.1138679

Martinson, D. G., Pisias, N. G., Hays, J. D., Imbrie, J., Moore Jr, T. C., & Shackleton, N. J. (1987). Age dating and the orbital theory of the ice ages: development of a high-resolution 0 to 300,000-year chronostratigraphy. *Quaternary research*, *27*(1), 1-29. https://doi.org/10.1016/0033-5894(87)90046-9

Martin, W., & Sayles, F. (1999). Benthic cycling of biogenic components of the particulate flux to the seafloor in the Southern Ocean in March and April, 1998. *EOS Transactions*, *80*(49), 241.

Martínez-Botí, M. A., Marino, G., Foster, G. L., Ziveri, P., Henehan, M. J., Rae, J. W., Mortyn P. G., & Vance, D. (2015). Boron isotope evidence for oceanic carbon dioxide leakage during the last deglaciation. *Nature*, *518*(7538), 219-222. https://doi.org/10.1038/nature14155.

Masson, S., Luo, J.-J., Madec, G., Vialard, J., Durand, F., Gualdi, S., Guilyardi, E., Behera, S., Delécluse, P., Navarra, A., & Yamagata, T. (2005). Impact of barrier layer on winter-spring variability of the southeastern Arabian Sea. *Geophysical Research Letters*, 32, L07703. https://doi.org/10.1029/2001JC000833.

McCave, I. N., Kiefer, T., Thornalley, D. J. R., & Elderfield, H. (2005). Deep flow in the Madagascar–Mascarene Basin over the last 150000 years. *Philosophical Transactions of the Royal Society A: Mathematical, Physical and Engineering Sciences*, *363*(1826), 81-99. https://doi.org/10.1098/rsta.2004.1480.

Menviel, L., Yu, J., Joos, F., Mouchet, A., Meissner, K. J., & England, M. H. (2017). Poorly ventilated deep ocean at the Last Glacial Maximum inferred from carbon isotopes: A data-model comparison study. *Paleoceanography*, *32*(1), 2-17. https://doi.org/10.1002/2016PA003024

Millero, F. J. (2010). Carbonate constants for estuarine waters. *Marine and Freshwater Research*, *61*(2), 139-142. https://doi.org/10.1071/MF09254.

Milliman, J. D., Quraishee, G. S., & Beg, M. A. A. (1984). Sediment discharge from the Indus River to the ocean: past, present and future. *Marine geology and oceanography of Arabian Sea and coastal Pakistan*, 65-70.

Minagawa, M., & Wahyudi (1997). Response of Benthic Foraminiferea to Organic Carbon Accumulation Rates in the Okinawa Trough. *Journal of Oceanography*, *53*(5), 411-420.

Monnin, E., Indermühle, A., Dällenbach, A., Flückiger, J., Stauffer, B., Stocker, T. F., Raynaud, D., & Barnola, J. M. (2001). Atmospheric CO2 concentrations over the

last glacial termination. *Science*, *291*(5501), 112-114. https://doi.org/10.1126/science.291.5501.112.

Moy, A. D., Palmer, M. R., Howard, W. R., Bijma, J., Cooper, M. J., Calvo, E., Pelejero, C., Gagan, M. K., & Chalk, T. B. (2019). Varied contribution of the Southern Ocean to deglacial atmospheric CO 2 rise. *Nature Geoscience*, *12*(12), 1006-1011. https://doi.org/10.1038/s41561-019-0473-9.

Muglia, J., Skinner, L. C., & Schmittner, A. (2018). Weak overturning circulation and high Southern Ocean nutrient utilization maximized glacial ocean carbon. *Earth and Planetary Science Letters*, *496*, 47-56. https://doi.org/10.1016/j.epsl.2018.05.038

Mungekar, T. V., Naik, S. S., Nath, B. N., & Pandey, D. K. (2020). Shell weights of foraminifera trace atmospheric CO 2 from the Miocene to Pleistocene in the central Equatorial Indian Ocean. *Journal of Earth System Science*, *129*(1), 1-9. https://doi.org/10.1007/s12040-020-1348-6.

Muraleedharan, P. M., & Prasannakumar, S. (1996). Arabian Sea upwelling-A comparison between coastal and open ocean regions.

Murgese, D. S., & De Deckker, P. (2007). The Late Quaternary evolution of water masses in the eastern Indian Ocean between Australia and Indonesia, based on benthic foraminifera faunal and carbon isotopes analyses. *Palaeogeography, Palaeoclimatology, Palaeoecology*, *247*(3-4), 382-401. https://doi.org/10.1016/j.palaeo.2006.11.002.

Murray, D. W., & Prell, W. L. (1992). Late Pliocene and Pleistocene climatic oscillations and monsoon upwelling recorded in sediments from the Owen Ridge, northwestern Arabian Sea. *Geological Society, London, Special Publications*, *64*(1), 301-321. https://doi.org/10.1144/GSL.SP.1992.064.01.20.

Murray, R. W., & Leinen, M. (1993). Chemical transport to the seafloor of the equatorial Pacific Ocean across a latitudinal transect at 135 W: tracking sedimentary major, trace, and rare earth element fluxes at the Equator and the Intertropical Convergence Zone. *Geochimica et Cosmochimica Acta*, *57*(17), 4141-4163. https://doi.org/10.1016/0016-7037(93)90312-K

Murray, R. W., & Leinen, M. (1996). Scavenged excess aluminum and its relationship to bulk titanium in biogenic sediment from the central equatorial Pacific Ocean. *Geochimica et Cosmochimica Acta*, *60*(20), 3869-3878. https://doi.org/10.1016/0016-7037 (96)00236-0

Naidu, P. D. (2007). Influence of monsoon upwelling on the planktonic foraminifera off Oman during Late Quaternary. *Indian Journal of Marine Sciences*, 36 (4), 322-331.

Naidu, P. D. (1991). Glacial to interglacial contrasts in the calcium carbonate content and influence of Indus discharge in two eastern Arabian Sea cores. *Palaeogeography, palaeoclimatology, palaeoecology*, *86*(3-4), 255-263. https://doi.org/10.1016/0031-0182%2891%2990084-5.

Naidu, P. D., Malmgren, B. A., & Bornmalm, L. (1993). Quaternary history of calcium carbonate fluctuations in the western equatorial Indian Ocean (Somali Basin). *Palaeogeography, palaeoclimatology, palaeoecology*, *103*(1-2), 21-30. https://doi.org/10.1016/0031-0182(93)90048-N.

Naidu, P. D., & Malmgren, B. A. (1996). A high-resolution record of late Quaternary upwelling along the Oman Margin, Arabian Sea based on planktonic foraminifera. *Paleoceanography*, *11*(1), 129-140. https://doi.org/10.1029/95PA03198.

Naidu, P. D., Singh, A. D., Ganeshram, R., & Bharti, S. K. (2014). Abrupt climate-induced changes in carbonate burial in the Arabian Sea: Causes and consequences. *Geochemistry, Geophysics, Geosystems*, *15*(4), 1398-1406. https://doi.org/10.1002/2013GC005065.

Naik, S. S., & Naidu, P. D. (2007). Calcite dissolution along a transect in the western tropical Indian Ocean: A multiproxy approach. *Geochemistry, Geophysics, Geosystems*, *8*(8). https://doi.org/10.1029/2007GC001615.

Naik, S. S., & Naidu, P. D. (2008). Possible factors that control calcite dissolution in the western tropical Indian Ocean. *Current Science*, 95, (1), 22-23.

Naik, S. S., & Naidu, P. D. (2010). Evaluation of the CaCO3 dissolution proxies in sediment cores from above the lysocline. *Quaternary International*, *213*(1-2), 69-73. https://doi.org/10.1016/j.quaint.2008.11.009.

Naik, S. S., Naidu, P. D., Govil, P., & Godad, S. (2010). Relationship between weights of planktonic foraminifer shell and surface water CO3= concentration during the Holocene and Last Glacial Period. *Marine Geology*, *275*(1-4), 278-282.https://doi.org/10.1016/j.margeo.2010.05.004.

Naik, S. S., Godad, S. P., & Naidu, P. D. (2011). Does carbonate ion control planktonic foraminifera shell calcification in upwelling regions? *Current Science*, 1370-1375.

Naik, S. S., Godad, S. P., Naidu, P. D., & Ramaswamy, V. (2013). A comparison of Globigerinoides ruber calcification between upwelling and non-upwelling regions in the Arabian Sea. *Journal of Earth System Science*, *122*(4), 1153-1159. https://doi.org/10.1007/s12040-013-0330-y.

Naik, S. S., & Naidu, P. D. (2014). Boron/calcium ratios in Globigerinoides ruber from the Arabian Sea: Implications for controls on boron incorporation. *Marine Micropaleontology*, *107*, 1-7. http://dx.doi.org/10.1016/j.marmicro.2014.01.004.

Naik, S. S., Naidu, P. D., Foster, G. L., & Martínez-Botí, M. A. (2015). Tracing the strength of the southwest monsoon using boron isotopes in the eastern Arabian Sea. *Geophysical Research Letters*, *42*(5), 1450-1458. https://doi.org/10.1002/2015GL063089.

Naik, S. S., & Naidu, P. D. (2016). Carbonate preservation during the 'mystery interval' in the northern Indian Ocean. *Geochemical Journal*, *50*(4), 357-362. https://doi.org/10.2343/geochemj.2.0420.

Naik, D. K., Saraswat, R., Lea, D. W., Kurtarkar, S. R., & Mackensen, A. (2017). Last glacial-interglacial productivity and associated changes in the eastern Arabian Sea. *Palaeogeography, Palaeoclimatology, Palaeoecology*, *483*, 147-156. https://doi.org/10.1016/j.palaeo.2016.07.014.

Naik, S. N., & Naik, S. S. (2018). Evidences of CO2 Leakage During the Last Deglaciation: The Need to Understand Deep-ocean Carbonate Chemistry of the Arabian Sea. *Journal of the Geological Society of India*, *92*(4), 404-406.

Naik, S. S., Basak, C., Goldstein, S. L., Naidu, P. D., & Naik, S. N. (2019). A 16-kyr record of ocean circulation and monsoon intensification from the Central Bay of

Bengal. *Geochemistry, Geophysics, Geosystems*, *20*(2), 872-882. https://doi.org/10.1029/2018GC007860

Naqvi, W. A., Charles, C. D., & Fairbanks, R. G. (1994). Carbon and oxygen isotopic records of benthic foraminifera from the Northeast Indian Ocean: implications on glacial-interglacial atmospheric CO2 changes. *Earth and Planetary Science Letters*, *121*(1-2), 99-110. https://doi.org/10.1016/0012-821X(94)90034-5.

Naqvi, W. A. (1991). Geographical extent of denitrification in the Arabian Sea in relation to some physical processes. *Oceanologica Acta*, *14*(3), 281-290. https://archimer.ifremer.fr/doc/00101/21257/.

Narayana, A. C., Naidu, P. D., Bhavani, P. G., & Ahmad, M. (2020). A coherent response of Southern Indian Ocean to the Antarctic climate: Implications to the lead, lags of atmospheric CO_2 during deglaciation. *Journal of Earth System Science*, *129*(1), 1-8. https://doi:10.1007/s12040-020-01484-z

Nath, B. N., Rao, V. P., & Becker, K. P. (1989). Geochemical evidence of terrigenous influence in deep-sea sediments up to 8 S in the Central Indian Basin. *Marine Geology*, *87*(2-4), 301-313. http://dx.doi.org/10.1016/0025-3227(89)90067-4.

Negre, C., Zahn, R., Thomas, A. L., Masqué, P., Henderson, G. M., Martínez-Méndez, G., Hall, I. R., & Mas, J. L. (2010). Reversed flow of Atlantic deep water during the Last Glacial Maximum. *Nature*, *468*(7320), 84-88. https://doi:10.1038/nature09508.

Nesbitt, H. W., & Markovics, G. (1997). Weathering of granodioritic crust, long-term storage of elements in weathering profiles, and petrogenesis of siliciclastic sediments. *Geochimica et Cosmochimica Acta*, *61*(8), 1653-1670. https://doi:10.1016/S0016-7037(97)00031-8

Ni, Y., Foster, G. L., Bailey, T., Elliott, T., Schmidt, D. N., Pearson, P., Haley, B., & Coath, C. (2007). A core top assessment of proxies for the ocean carbonate system in surface-dwelling foraminifers. *Paleoceanography*, *22*(3). https://doi.org/10.1029/2006PA001337.

Nigam, R., Khare, N., &Borole, D.V. (1992). Can benthic foraminiferal morpho groups be used as indicators of paleomonsoonal precipitation. *Esturine coastal and shelf science, 34, 533-542.*

Nyadjro, E. S., Subrahmanyam, B., Murty, V., & Shriver, J. F. (2012). The role of salinity on the dynamics of the Arabian Sea mini warm pool. *Journal of Geophysical Research,* 117, C09002. https://doi.org/10.1029/2012JC007978.

Oba, T. (1969). Biostratigraphy and isotopic paleotemperature of some deep-sea cores from the Indian Ocean Tohoku Univ. Sci. Rep., 2nd Ser (Geol.), 41 (2) (1969), p. 129.

Oi, T. (2000). Calculations of reduced partition function ratios of monomeric and dimeric boric acids and borates by the ab initio molecular orbital theory. *Journal of nuclear science and technology*, *37*(2), 166-172. https://doi.org/10.1080/18811248.2000.9714880.

Olausson, E. (1965). Climatological, geoeconomical and paleooceanographical aspects on carbonate deposition. *Progress in oceanography*, *4*, 245-265.

Oppo, D. W., Curry, W. B., & McManus, J. F. (2015). What do benthic δ13C and δ18O data tell us about Atlantic circulation during Heinrich Stadial 1?. *Paleoceanography*, *30*(4), 353-368. https://doi.org/10.1002/2014PA002667.

Opdyke, B. N., & Walker, J. C. (1992). Return of the coral reef hypothesis: Basin to shelf partitioning of $CaCO_3$ and its effect on atmospheric CO_2. *Geology*, *20*(8), 733-736.https://doi.org/10.1130/0091-7613(1992)020<0733:ROTCRH>2.3.CO;2

Pahnke, K., Goldstein, S. L., & Hemming, S. R. (2008). Abrupt changes in Antarctic Intermediate Water circulation over the past 25,000 years. *Nature Geoscience*, *1*(12), 870-874.https://doi:10.1038/ngeo360

Palmer, M. R., & Pearson, P. N. (2003). A 23,000-year record of surface water pH and *p*CO2 in the western equatorial Pacific Ocean. *Science*, *300*(5618), 480-482. https://doi.org/10.1126/science.1080796.

Palmer, M. R., Brummer, G. J., Cooper, M. J., Elderfield, H., Greaves, M. J., Reichart, G. J., Schouten, S.& Yu, J. M. (2010). Multi-proxy reconstruction of surface water pCO2 in the northern Arabian Sea since 29 ka. *Earth and Planetary Science Letters*, *295*(1-2), 49-57. https://doi.org/10.1016/j.epsl.2010.03.023

Pattan, J. N., Masuzawa, T., Naidu, P. D., Parthiban, G., & Yamamoto, M. (2003). Productivity fluctuations in the southeastern Arabian Sea during the last 140

ka. *Palaeogeography, Palaeoclimatology, Palaeoecology*, *193*(3-4), 575-590. https://doi.org/10.1016/S0031-0182(03)00267-0.

Pattan, J. N., Masuzawa, T., & Yamamoto, M. (2005). Variations in terrigenous sediment discharge in a sediment core from southeastern Arabian Sea during the last 140 ka. *Current Science*, 89(8),1421-1425.

Pattan, J. N., & Pearce, N. J. G. (2009). Bottom water oxygenation history in southeastern Arabian Sea during the past 140 ka: results from redox-sensitive elements. *Palaeogeography, Palaeoclimatology, Palaeoecology*, *280* (3-4), 396-405. https://doi.org/10.1016/j.palaeo.2009.06.027.

Pattan, J. N., Parthiban, G., Garg, A., & Moraes, N. C. (2017). Intense reducing conditions during the last deglaciation and Heinrich events (H1, H2, H3) in sediments from the oxygen minimum zone off Goa, eastern Arabian Sea. *Marine and Petroleum Geology*, *84*, 243-256. http://dx.doi.org/10.1016/j.marpetgeo.2017.03.034.

Pattan, J. N., Parthiban, G., & Amonkar, A. (2019). Productivity controls on the redox variation in the southeastern Arabian Sea sediments during the past 18 kyr. *Quaternary International*, *523*, 1-9. https://doi.org/10.1016/j.quaint.2019.05.034.

Paulmier, A., Ruiz-Pino, D., & Garçon, V. (2011). CO 2 maximum in the oxygen minimum zone (OMZ). *Biogeosciences*, *8*(2), 239-252. https://doi.org/10.5194/bg-8-239-2011.

Pearson, P. N., & Palmer, M. R. (1999). Middle Eocene seawater pH and atmospheric carbon dioxide concentrations. *Science*, *284*(5421), 1824-1826. https://doi.org/10.1126/science.284.5421.1824.

Peterson, L. C., & Prell, W. L. (1985). Carbonate dissolution in recent sediments of the eastern equatorial Indian Ocean: preservation patterns and carbonate loss above the lysocline. *Marine Geology*, *64*(3-4), 259-290. https://doi.org/10.1016/0025-3227(85)90108-2.

Petit, J. R., Jouzel, J., Raynaud, D., Barkov, N. I., Barnola, J. M., Basile, I., Bender, M., Chappellaz, J., Davis, M., Delaygue, G., Delmotte, M., Kotlyakov, V. M., Legrand, M., Lipenkov, V. Y., Loris, C., Pepin, L., Ritz, C., Saltzman, E., & Stievenard, M. (1999). Climate and atmospheric history of the past 420,000 years from the Vostok ice core, Antarctica. *Nature*, *399*(6735), 429-436. https://doi:10.1038/20859

Piotrowski, A. M., Banakar, V. K., Scrivner, A. E., Elderfield, H., Galy, A., & Dennis, A. (2009). Indian Ocean circulation and productivity during the last glacial cycle. *Earth and Planetary Science Letters*, *285*(1-2), 179-189. https://doi:10.1016/j.epsl.2009.06.007.

Prasad, T. G., Ikeda, M., & Kumar, S. P. (2001). Seasonal spreading of the Persian Gulf Water mass in the Arabian Sea. *Journal of Geophysical Research: Oceans*, *106*(C8), 17059-17071. https://doi.org/10.1029/2000JC000480.

Prasanna Kumar, S., Narvekar, J., Kumar, A., Shaji, C., Anand, P., Sabu, P., Rijomon, G., Josia, j., Jayaraj, K.A., Radhika, A., & Nair, K. K. C. (2004). Intrusion of the Bay of Bengal water into the Arabian Sea during winter monsoon and associated chemical and biological response. *Geophysical Research Letters*, *31*(15). https://doi.org/10.1029/2004GL020247.

Prasanna Kumar, S., & Prasad, T. G. (1999). Formation and spreading of Arabian Sea high-salinity water mass. *Journal of Geophysical Research: Oceans*, *104*(C1), 1455-1464. https://doi.org/10.1029/1998JC900022.

Prell, W. L. (1984). Variation of monsoonal upwelling: a response to changing solar radiation. *Climate processes and climate sensitivity*, *29*, 48-57.

Rae, J. W., Foster, G. L., Schmidt, D. N., & Elliott, T. (2011). Boron isotopes and B/Ca in benthic foraminifera: Proxies for the deep ocean carbonate system. *Earth and Planetary Science Letters*, *302*(3-4), 403-413. https://doi.org/10.1016/j.epsl.2010.12.034.

Raju, L. S., Krishna, K. S., & Chaubey, A. K. (1991). Buried late pleistocene fluvial channels on the inner continental shelf off Vengurla, West Coast of India. *Journal of Coastal Research*, 7(2),509-516.

Rao, R. R., & Sivakumar, R. (1999). On the possible mechanisms of the evolution of a mini-warm pool during the pre-summer monsoon season and the genesis of onset vortex in the South-Eastern Arabian Sea. *Quarterly Journal of the Royal Meteorological Society*, *125*(555), 787-809. https://doi.org/10.1002/qj.49712555503.

Ravelo, A. C., & Hillaire-Marcel, C. (2007). Chapter eighteen the use of oxygen and carbon isotopes of foraminifera in paleoceanography. *Developments in marine geology*, *1*, 735-764.

Raymo, M. E., Oppo, D. W., Flower, B. P., Hodell, D. A., McManus, J. F., Venz, K. A., Kleiven, K. F., & McIntyre, K. (2004). Stability of North Atlantic water masses in face of pronounced climate variability during the Pleistocene. *Paleoceanography*, *19*(2). https://doi:10.1029/2003PA000921

Raza, T., & Ahmad, S. M. (2013). Surface and deep water variations in the northeast Indian Ocean during 34–6 ka BP: evidence from carbon and oxygen isotopes of fossil foraminifera. *Quaternary International*, *298*, 37-44. https://doi.org/10.1016/j.quaint.2012.05.005.

Raza, T., Ahmad, S. M., Sahoo, M., Banerjee, B., Bal, I., Dash, S., Gorti, S., & Mukherjee, I. (2014). Hydrographic changes in the southern Bay of Bengal during the last∼ 65,000 y inferred from carbon and oxygen isotopes of foraminiferal fossil shells. *Quaternary International*, *333*, 77-85. https://doi.org/10.1016/j.quaint.2014.02.010.

Reichart, G. J., den Dulk, M., Visser, H. J., van der Weijden, C. H., & Zachariasse, W. J. (1997). A 225 kyr record of dust supply, paleoproductivity and the oxygen minimum zone from the Murray Ridge (northern Arabian Sea). *Palaeogeography, Palaeoclimatology, Palaeoecology*, *134*(1-4), 149-169. https://doi:10.1016/S0031-0182(97)00071-0

Reichart, G. J., Lourens, L. J., & Zachariasse, W. J. (1998). Temporal variability in the northern Arabian Sea oxygen minimum zone (OMZ) during the last 225,000 years. *Paleoceanography*, *13*(6), 607-621. https://doi.org/10.1029/98PA02203.

Rickaby, R. E., Elderfield, H., Roberts, N., Hillenbrand, C. D., & Mackensen, A. (2010). Evidence for elevated alkalinity in the glacial Southern Ocean. *Paleoceanography*, *25*(1).https://doi.org/10.1029/2009PA001762.

Romahn, S., Mackensen, A., Groeneveld, J., & Pätzold, J. (2014). Deglacial intermediate water reorganization: New evidence from the Indian Ocean. *Climate of the Past*, *10*(1), 293-303. https://doi:10.5194/cpd-9-4035-2013

Ronge, T. A., Prange, M., Mollenhauer, G., Ellinghausen, M., Kuhn, G., & Tiedemann, R. (2020). Radiocarbon evidence for the contribution of the Southern Indian Ocean to the evolution of atmospheric CO_2 over the last 32,000 years. *Paleoceanography and Paleoclimatology*, *35*(3), e2019PA003733. https://doi:10.1029/2019PA003733

Rosenthal, Y., Boyle, E. A., & Slowey, N. (1997). Temperature control on the incorporation of magnesium, strontium, fluorine, and cadmium into benthic foraminiferal shells from Little Bahama Bank: Prospects for thermocline paleoceanography. *Geochimica et Cosmochimica Acta*, *61*(17), 3633-3643. https://doi.org/10.1016/S0016-7037(97)00181-6.

Rosenthal, Y., Lear, C. H., Oppo, D. W., & Linsley, B. K. (2006). Temperature and carbonate ion effects on Mg/Ca and Sr/Ca ratios in benthic foraminifera: Aragonitic species Hoeglundina elegans. *Paleoceanography*, *21*(1). https://doi.org/10.1029/2005PA001158.

Ruddiman, W. F., & Heezen, B. C. (1967). Differential solution of planktonic foraminifera. In *Deep Sea Research and Oceanographic Abstracts* (Vol. 14, No. 6, pp. 801-808). Elsevier.

Russell, A. D., Hönisch, B., Spero, H. J., & Lea, D. W. (2004). Effects of seawater carbonate ion concentration and temperature on shell U, Mg, and Sr in cultured planktonic foraminifera. *Geochimica et Cosmochimica Acta*, *68*(21), 4347-4361. https://doi.org/10.1016/j.gca.2004.03.013.

Sadekov, A. Y., Bush, F., Kerr, J., Ganeshram, R., & Elderfield, H. (2014). Mg/Ca composition of benthic foraminifera Miliolacea as a new tool of paleoceanography. *Paleoceanography*, *29*(10), 990-1001. https://doi.org/10.1002/2014PA002654.

Sanyal, A., Bijma, J., Spero, H., & Lea, D. W. (2001). Empirical relationship between pH and the boron isotopic composition of Globigerinoides sacculifer: Implications for the boron isotope paleo-pH proxy. *Paleoceanography*, *16*(5), 515-519. https://doi.org/10.1029/2000PA000547.

Sanyal, A., Hemming, N. G., Broecker, W. S., Lea, D. W., Spero, H. J., & Hanson, G. N. (1996). Oceanic pH control on the boron isotopic composition of foraminifera:

evidence from culture experiments. *Paleoceanography*, *11*(5), 513-517. https://doi.org/10.1029/96PA01858.

Sanyal, A., Nugent, M., Reeder, R. J., & Bijma, J. (2000). Seawater pH control on the boron isotopic composition of calcite: evidence from inorganic calcite precipitation experiments. *Geochimica et Cosmochimica Acta*, *64*(9), 1551-1555. https://doi.org/10.1016/S0016-7037(99)00437-8.

Sarkar, A., Bhattacharya, S. K., & Sarin, M. M. (1993). Geochemical evidence for anoxic deep water in the Arabian Sea during the last glaciation. *Geochimica et Cosmochimica Acta*, *57*(5), 1009-1016. https://doi:10.1016/0016-7037(93)90036-V

Sarma, V. V. S. S. (2003). Monthly variability in surface pCO2 and net air-sea CO2 flux in the Arabian Sea. *Journal of Geophysical Research: Oceans*, *108*(C8). https://doi.org/10.1029/2001JC001062.

Sarma, V. V. S. S. (2004). Net plankton community production in the Arabian Sea based on O2 mass balance model. *Global biogeochemical cycles*, *18*, GB4001. https://doi.org/10.1029/2003GB002198.

Sarma, V. V. S. S., Kumar, M. D., & George, M. D. (1998). The central and eastern Arabian Sea as a perennial source of atmospheric carbon dioxide. *Tellus B: Chemical and Physical Meteorology*, *50*(2), 179-184. https://doi.org/10.1034/j.1600-0889.1998.t01-1-00005.x.

Schlitzer, R. (2015). Ocean data view.

Schmiedl, G., Mackensen, A., & Müller, P. J. (1997). Recent benthic foraminifera from the eastern South Atlantic Ocean: dependence on food supply and water masses. *Marine micropaleontology*, *32*(3-4), 249-287. https://doi.org/10.1016/S0377-8398(97)00023-6.

Schmiedl, G., & Mackensen, A. (2006). Multispecies stable isotopes of benthic foraminifers reveal past changes of organic matter decomposition and deepwater oxygenation in the Arabian Sea. *Paleoceanography*, *21*(4). https://doi.org/10.1029/2006PA001284.

Schmitz, B. (1987). Barium, equatorial high productivity, and the northward wandering of the Indian continent. *Paleoceanography*, *2*(1), 63-77. https://doi.org/10.1029/PA002i001p00063.

Schmiedl, G., & Mackensen, A. (2006). Multispecies stable isotopes of benthic foraminifers reveal past changes of organic matter decomposition and deepwater oxygenation in the Arabian Sea. *Paleoceanography*, *21*(4). https://doi:10.1029/2006PA001284

Schnetger, B., Brumsack, H. J., Schale, H., Hinrichs, J., & Dittert, L. (2000). Geochemical characteristics of deep-sea sediments from the Arabian Sea: a high-resolution study. *Deep Sea Research Part II: Topical Studies in Oceanography*, *47*(14), 2735-2768. https://doi:10.1016/S0967-0645(00)00047-3

Schott, F. A., & McCreary Jr, J. P. (2001). The monsoon circulation of the Indian Ocean. *Progress in Oceanography*, *51*(1), 1-123. https://doi.org/10.1016/S0079-6611(01)00083-0.

Schott, W. (1937). Die Foraminiferen in dem äquatorialen Teil des Atlantischen Ozeans. Wissenschaftliche Ergebnisse der Deutschen Atlantischen Expedition auf dem Forschungs- und *Vermessungsschiff Meteor* 1925–1927 3(3):43–134

Schulte, S., Rostek, F., Bard, E., Rullkötter, J., & Marchal, O. (1999). Variations of oxygen-minimum and primary productivity recorded in sediments of the Arabian Sea. *Earth and Planetary Science Letters*, *173*(3), 205-221. https://doi.org/10.1016/S0012-821X(99)00232-0.

Severin, K. P. (1983). Test morphology of benthic foraminifera as a discriminator of biofacies. *Marine Micropaleontology*, *8*(1), 65-76.

Shankar, D., Shenoi, S. S. C., Nayak, R. K., Vinayachandran, P. N., Nampoothiri, G., Almeida, A. M., Michael, G. S., Ramesh Kumar, M.R., Sundar, D., & Sreejith, O. P. (2005). Hydrography of the eastern Arabian Sea during summer monsoon 2002. *Journal of Earth System Science*, *114*(5), 459-474. https://doi.org/10.1007/BF02702023.

Shankar, D., & Shetye, S. R. (1999). Are interdecadal sea level changes along the Indian coast influenced by variability of monsoon rainfall? *Journal of Geophysical Research: Oceans*, *104*(C11), 26031-26042. https://doi.org/10.1029/1999JC900218.

Shao, J., Stott, L. D., Gray, W. R., Greenop, R., Pecher, I., Neil, H. L., Coffin, R. B., Davy, B., & Rae, J. W. (2019). Atmosphere-ocean CO2 exchange across the last deglaciation

from the Boron Isotope Proxy. *Paleoceanography and Paleoclimatology*, *34*(10), 1650-1670. https://doi.org/10.1029/2018PA003498.

Sharp, J. D., &Byrne, R. H. (2019). Carbonate ion concentrations in seawater: spectrophotometric determination at ambient temperatures and evaluation of propagated calculation uncertainties. *Marine Chemistry*, *209*, 70-80. https://doi.org/10.1016/j.marchem.2018.12.001.

Shackleton, N. (1967). Oxygen isotope analyses and Pleistocene temperatures re-assessed. *Nature*, *215*(5096), 15-17. https://doi.org/10.1038/215015a0.

Shackleton, N. J., & Opdyke, N. D. (1973). Oxygen isotope and palaeomagnetic stratigraphy of Equatorial Pacific core V28-238: Oxygen isotope temperatures and ice volumes on a 105 year and 106 year scale. *Quaternary research*, *3*(1), 39-55. https://doi.org/10.1016/0033-5894(73)90052-5.

Shenoi, S. S. C., Shankar, D., Michael, G. S., Kurian, J., Varma, K. K., Kumar, Ramesh Kumar, M.R., Almeida, A.M., Unnikrishnan, A.S., Fernandes, W., Barreto, N., Gnanaseelan, C., Mathews, R., Praju, K.V., & Mahale, V. (2005). Hydrography and water masses in the southeastern Arabian Sea during March–June 2003. *Journal of earth system science*, *114*(5), 475-491. https://doi.org/10.1007/BF02702024.

Shenoi, S. S. C., Shankar, D., & Shetye, S. R. (1999). On the sea surface temperature high in the Lakshadweep Sea before the onset of the southwest monsoon. *Journal of Geophysical Research: Oceans*, *104*(C7), 15703-15712. https://doi.org/10.1029/1998JC900080.

Shetye, S. R., Gouveia, A. D., Shenoi, S. S. C., Sundar, D., Michael, G. S., Almeida, A. M., & Santanam, K. (1990). Hydrography and circulation off the west coast of India during the southwest monsoon 1987. *Journal of Marine Research*, *48*(2), 359-378. https://doi.org/10.1357/002224090784988809.

Shetye, S. R., Gouveia, A. D., & Shenoi, S. S. C. (1994). Circulation and water masses of the Arabian Sea. *Proceedings of the Indian Academy of Sciences-Earth and Planetary Sciences*, *103*(2), 107-123. https://doi.org/10.1007/BF02839532.

Shimmield, G. B. (1992). Can sediment geochemistry record changes in coastal upwelling palaeoproductivity? Evidence from northwest Africa and the Arabian Sea. *Geological*

Society, London, Special Publications, *64*(1), 29-46. https://doi:10.1144/GSL.SP.1992.064.01.03

Shuttleworth, R., Bostock, H. C., Chalk, T. B., Calvo, E., Jaccard, S. L., Pelejero, C., Martinez- Gracia, & Foster, G. L. (2021). Early deglacial CO2 release from the Sub-Antarctic Atlantic and Pacific oceans. *Earth and planetary science letters*, *554*, 116649. https://doi.org/10.1016/j.epsl.2020.116649.

Siani, G., Michel, E., De Pol-Holz, R., DeVries, T., Lamy, F., Carel, M., Isguder, G., Dewilde, F., & Lourantou, A. (2013). Carbon isotope records reveal precise timing of enhanced Southern Ocean upwelling during the last deglaciation. *Nature Communications*, *4*(1), 1-9. https://doi.org/10.1038/ncomms3758.

Sigman, D. M., & Boyle, E. A. (2000). Glacial/interglacial variations in atmospheric carbon dioxide. *Nature*, *407*(6806), 859-869. https://doi.org/10.1038/35038000.

Singh, A. D. (1998). Late Quaternary oceanographic changes in the eastern Arabian Sea: Evidence from planktic foraminifera and pteropods. *Journal of Geological Society of India*, *52*, 203-212.

Singh, A. D., Kroon, D., & Ganeshram, R. S. (2006). Millennial scale variations in productivity and OMZ intensity in the eastern Arabian Sea. *Journal of Geological Society of India*, *68*(3), 369.

Singh, A. D. (2007). Episodic preservation of pteropods in the eastern Arabian Sea: Monsoonal change, oxygen minimum zone intensity and aragonite compensation depth. *Indian Journal of Marine Sciences*, 36 (4), 378-383.

Singh, D. P., Saraswat, R., & Naik, D. K. (2017). Does Glacial-Interglacial Transition Affect Sediment Accumulation in Monsoon-Dominated Regions? *Acta Geologica Sinica-English Edition*, *91*(3), 1079-1094. https://doi: 10.1111/1755-6724.13325

Skinner, L. C., Fallon, S., Waelbroeck, C., Michel, E., & Barker, S. (2010). Ventilation of the deep Southern Ocean and deglacial CO2 rise. *Science*, *328*(5982), 1147-1151. https://doi:10.1126/science.1183627

Skinner, L. C., Waelbroeck, C., Scrivner, A. E., & Fallon, S. J. (2014). Radiocarbon evidence for alternating northern and southern sources of ventilation of the deep

Atlantic carbon pool during the last deglaciation. *Proceedings of the National Academy of Sciences*, *111*(15), 5480-5484. https://doi:10.1073/pnas.1400668111

Skinner, L. C., Primeau, F., Freeman, E., de la Fuente, M., Goodwin, P. A., Gottschalk, J., Huang, E., McCave, I. N., Noble, T. L., & Scrivner, A. E. (2017). Radiocarbon constraints on the glacial ocean circulation and its impact on atmospheric CO_2. *Nature communications*, *8*(1), 1-10. https://doi:10.17863/CAM.12351

Smart, C. W., King, S. C., Gooday, A. J., Murray, J. W., & Thomas, E. (1994). A benthic foraminiferal proxy of pulsed organic matter paleofluxes. *Marine micropaleontology*, *23*(2), 89-99. https://doi.org/10.1016/0377-8398(94)90002-7.

Smetacek, V., Klaas, C. Strass, V. H., Assmy, P., Montresor, M., Cisewski, B., Savoye, N., Webb, A., d'Ovidio, F., Arrieta, J. M., Bathmann, U., Bellerby, R., Berg, G. M., Croot, P., Gonzalez, S., Henjes, J., Herndl, G. J., Hoffmann, L. J., Leach, H., Losch, M., Mills, M. M., Neill, C., Peeken, I., Ro¨ttgers, R., Sachs, O., Sauter, E., Schmidt, M. M., Schwarz, J. Terbruggen, A., & Wolf-Gladrow, D., (2012). Deep carbon export from a Southern Ocean iron-fertilized diatom bloom, *Nature*, 47, 313-319. https://doi:10.1038/nature11229

Stuiver, M., Reimer, P. J., & Reimer, R. W. (2017). CALIB 7.1. *WWW program] http://calib.org. Accessed Sept*.

Smith, C. R., Hoover, D. J., Doan, S. E., Pope, R. H., Demaster, D. J., Dobbs, F. C., & Altabet, M. A. (1996). Phytodetritus at the abyssal seafloor across 10 of latitude in the central equatorial Pacific. *Deep Sea Research Part II: Topical Studies in Oceanography*, *43*(4-6), 1309-1338. https://doi.org/10.1016/0967-0645(96)00015-X.

Smith, H. J., Spivack, A. J., Staudigel, H., & Hart, S. R. (1995). The boron isotopic composition of altered oceanic crust. *Chemical Geology*, *126*(2), 119-135.

Somasundar, K., Rajendran, A., Kumar, M. D., & Gupta, R. S. (1990). Carbon and nitrogen budgets of the Arabian Sea. *Marine Chemistry*, *30*, 363-377. https://doi.org/10.1016/0304-4203(90)90081-M.

Sosdian, S. M., Greenop, R., Hain, M. P., Foster, G. L., Pearson, P. N., & Lear, C. H. (2018). Constraining the evolution of Neogene ocean carbonate chemistry using the boron

isotope pH proxy. *Earth and Planetary Science Letters*, *498*, 362-376. https://doi.org/10.1016/j.epsl.2018.06.017.

Spero, H. J., Bijma, J., Lea, D. W., & Bemis, B. E. (1997). Effect of seawater carbonate concentration on foraminiferal carbon and oxygen isotopes. *Nature*, *390*(6659), 497-500.

Spivack, A. J., Palmer, M. R., & Edmond, J. M. (1987). The sedimentary cycle of the boron isotopes. *Geochimica et Cosmochimica Acta*, *51*(7), 1939-1949.

Sprintall, J., & Tomczak, M. (1993). On the formation of Central Water and thermocline ventilation in the southern hemisphere. *Deep Sea Research Part I: Oceanographic Research Papers*, *40*(4), 827-848. https://doi.org/10.1016/0967-0637(93)90074-D.

Stephens, M. P., & Kadko, D. C. (1997). Glacial-Holocene calcium carbonate dissolution at the central equatorial Pacific seafloor. *Paleoceanography*, *12*(6), 797-804.

Stott, L., Southon, J., Timmermann, A., & Koutavas, A. (2009). Radiocarbon age anomaly at intermediate water depth in the Pacific Ocean during the last deglaciation. *Paleoceanography*, *24*(2). https://doi.org/10.1029/2008PA001690

Stott, L. D., Shao, J., Yu, J., & Harazin, K. M. (2021). Evaluating the glacial-deglacial carbon respiration and ventilation change hypothesis as a mechanism for changing atmospheric CO2. *Geophysical Research Letters*, *48*(3), e2020GL091296. https://doi.org/10.1029/2020GL091296.

Suokhrie, T., Saalim, S. M., Saraswat, R., & Nigam, R. (2018). Indian monsoon variability in the last 2000 years as inferred from benthic foraminifera. *Quaternary International*, *479*, 128-140. https://doi.org/10.1016/j.quaint.2017.05.037.

Takahashi, T., Sutherland, S. C., Sweeney, C., Poisson, A., Metzl, N., Tilbrook, B., Bates, N., Wanninkhofe, R., Feely, R. A., Sabine, C., Olafssong, J., & Nojiri, Y. (2002). Global sea–air CO2 flux based on climatological surface ocean pCO2, and seasonal biological and temperature effects. *Deep Sea Research Part II: Topical Studies in Oceanography*, *49*(9-10), 1601-1622.

Takahashi, T., Sutherland, S. C., Wanninkhof, R., Sweeney, C., Feely, R. A., Chipman, D. W., Hales, B., Friederich, G., Chavez, F., Sabine, C., Watson, A., Bakker, D. C. E., Schuster, U., Metzl, N., Yoshikawa-Inoue, H., Ishii, M., Midorikawa, T., Nojiri, Y.,

& De Baar, H. J. (2009). Climatological mean and decadal change in surface ocean pCO2, and net sea–air CO2 flux over the global oceans. *Deep Sea Research Part II: Topical Studies in Oceanography*, *56*(8-10), 554-577. https://doi.org/10.1016/j.dsr2.2008.12.009.

Talley, L. D. (2013). Closure of the global overturning circulation through the Indian, Pacific, and Southern Oceans: Schematics and transports. *Oceanography*, *26*(1), 80-97. https://doi.org/10.5670/oceanog.2013.07.

Tappa, E., & Thunell, R. (1984). Late Pleistocene glacial/interglacial changes in planktonic foraminiferal biofacies and carbonate dissolution patterns in the Vema Channel. *Marine geology*, *58*(1-2), 101-122. https://doi.org/10.1016/0025-3227(84)90118-X.

Thadathil, P., & Gosh, A. K. (1992). Surface layer temperature inversion in the Arabian Sea during winter. *Journal of Oceanography*, *48*(3), 293-304. https://doi.org/10.1007/BF02233989.

Thadathil, P., Thoppil, P., Rao, R., Muraleedharan, P., Somayajulu, Y., Gopalakrishna, V.V., Murtugudde, R., Reddy, G.V., & Revichandran, C. (2008). Seasonal variability of the observed barrier layer in the Arabian Sea.*Oceanography*, *38*(3), 624-638. https://doi.org/10.1175/2007JPO3798.1.

Thamban, M., Kawahata, H., & Rao, V. P. (2007). Indian summer monsoon variability during the Holocene as recorded in sediments of the Arabian Sea: timing and implications. *Journal of oceanography*, *63*(6), 1009-1020. https://doi:10.1007/s10872-007-0084-8

Toggweiler, J. R. (2009). Shifting westerlies. *Science*, *323*(5920), 1434-1435. https://doi:10.1126/science.1169823

Tomczak, M., & Godfrey, J. S. (2003). *Regional oceanography: an introduction*. Daya books.

Tripati, A. K., Roberts, C. D., & Eagle, R. A. (2009). Coupling of CO2 and ice sheet stability over major climate transitions of the last 20 million years. *Science*, *326*(5958), 1394-1397. https://doi.org/10.1126/science.1178296.

Tripati, A. K., Roberts, C. D., Eagle, R. A., & Li, G. (2011). A 20 million year record of planktic foraminiferal B/Ca ratios: Systematics and uncertainties in pCO2 reconstructions. *Geochimica et Cosmochimica Acta*, *75*(10), 2582-2610. https://doi.org/10.1016/j.gca.2011.01.018.

Urey, H. C. (1948). Oxygen isotopes in nature and in the laboratory. *Science*, *108*(2810), 489-496.

Urey, H. C. (1947). The thermodynamic properties of isotopic substances. *Journal of the Chemical Society (Resumed)*, 562-581.

Urey, H. C., Lowenstam, H. A., Epstein, S., & McKinney, C. R. (1951). Measurement of paleotemperatures and temperatures of the Upper Cretaceous of England, Denmark, and the southeastern United States. *Geological Society of America Bulletin*, *62*(4), 399-416. https://doi.org/10.1130/0016-7606(1951)62[399:MOPATO]2.0.CO;2.

Van der Zwaan, G. J., Duijnstee, I. A. P., Den Dulk, M., Ernst, S. R., Jannink, N. T., & Kouwenhoven, T. J. (1999). Benthic foraminifers: proxies or problems?: a review of paleocological concepts. *Earth-Science Reviews*, *46*(1-4), 213-236. https://doi.org/10.1016/S0012-8252(99)00011-2

Van der Zwaan, G. J., Jorissen, F. J., & De Stigter, H. C. (1990). The depth dependency of planktonic/benthic foraminiferal ratios: constraints and applications. *Marine geology*, *95*(1), 1-16. https://doi.org/10.1016/0025-3227(90)90016-D.

Vidal, L., Labeyrie, L., Cortijo, E., Arnold, M., Duplessy, J. C., Michel, E., Becqué, S., & Van Weering, T. C. E. (1997). Evidence for changes in the North Atlantic Deep Water linked to meltwater surges during the Heinrich events. *Earth and Planetary Science Letters*, *146*(1-2), 13-27. https://doi.org/10.1016/S0012-821X(96)00192-6

Waelbroeck, C., Levi, C., Duplessy, J. C., Labeyrie, L., Michel, E., Cortijo, E., Bassinot, F., & Guichard, F. (2006). Distant origin of circulation changes in the Indian Ocean during the last deglaciation. *Earth and Planetary Science Letters*, *243*(1-2), 244-251. https://doi.org/10.1016/j.epsl.2005.12.031

Wahyudi & Minagawa, M. (1997). Response of Benthic Foraminiferea to Organic Carbon Accumulation Rates in the Okinawa Trough. *Journal of Oceanography*, *53*(5), 411-420.

Wan, S., Jian, Z., Gong, X., Dang, H., Wu, J., & Qiao, P. (2020). Deep water [CO_3^{2-}] and circulation in the South China Sea over the last glacial cycle. *Quaternary Science Reviews*, *243*, 106499. https://doi.org/10.1016/j.quascirev.2020.106499.

Warren, B. A. (1974). Deep flow in the Madagascar and Mascarene basins. In *Deep Sea Research and Oceanographic,* 21 (1),1-21. https://doi.org/10.1016/0011-7471(74)90015-1.

Warren, B. A. (1978). Bottom water transport through the Southwest Indian Ridge. *Deep Sea Research*, *25*(3), 315-321. https://doi.org/10.1016/0146-6291(78)90596-9.

Warren, B. A. (1981). Trans Indian hydrographic section at Lat. 18 S: Property distributions and circulation in the South Indian Ocean. *Deep Sea Research Part A. Oceanographic Research Papers*, *28*(8), 759-IN48. https://doi.org/10.1016/S0198-0149(81)80001-5.

Warren, B. A., & Johnson, G. C. (1992). Deep currents in the Arabian Sea in 1987. *Marine Geology*, *104,* (1-4), 279-288. https://doi.org/10.1016/0025-3227(92)90102-N.

Wei, G., Liu, Y., Li, X., Shao, L., & Liang, X. (2003). Climatic impact on Al, K, Sc and Ti in marine sediments: evidence from ODP Site 1144, South China Sea. *Geochemical Journal*, *37*(5), 593-602.https://doi.org/10.2343/geochemj.37.593

Wilson, D. J., Piotrowski, A. M., Galy, A., & Banakar, V. K. (2015). Interhemispheric controls on deep ocean circulation and carbon chemistry during the last two glacial cycles. *Paleoceanography*, *30*(6), 621-641.https://doi.org/10.1002/2014PA002707

Wu, G., Yasuda, M. K., & Berger, W. H. (1991). Late Pleistocene carbonate stratigraphy on Ontong-Java Plateau in the western equatorial Pacific. *Marine Geology*, *99*(1-2), 135-150. https://doi.org/10.1016/0025-3227(91)90087-K.

Wyrtki, K., Bennett, E. B., & Rochford, D. J. (1971). *Oceanographic atlas of the international Indian Ocean expedition* (Vol. 531). Washington, DC: National Science Foundation.

Wyrtki, K. (1973). An equatorial jet in the Indian Ocean. *Science*, *181*(4096), 262-264. https://doi.org/10.1126/science.181.4096.262.

Yentsch, C. S., & Phinney, D.A. (1992). The effect of wind direction and velocity on the distribution of phytoplankton chlorophyll in the western Arabian Sea. In:

Oceanography *of the Indian ocean.*, B.N. Desai, editor, Oxford & IBH, New Delhi, 57-66.

You, C. F., Spivack, A. J., Smith, J. H., & Gieskes, J. M. (1993). Mobilization of boron in convergent margins: implications for the boron geochemical cycle. *Geology*, *21*(3), 207-210. https://doi.org/10.1130/00917613(1993)021%3C0207:MOBICM%3E2.3.CO;2.

You, Y., & Tomczak, M. (1993). Thermocline circulation and ventilation in the Indian Ocean derived from water mass analysis. *Deep Sea Research Part I: Oceanographic Research Papers*, *40*(1), 13-56. https://doi.org/10.1016/0967-0637(93)90052-5.

You, Y. (1998). Intermediate water circulation and ventilation of the Indian Ocean derived from water-mass contributions. *Journal of Marine Research*, *56*(5), 1029-1067.

You, Y. (2000). Implications of the deep circulation and ventilation of the Indian Ocean on the renewal mechanism of North Atlantic Deep Water. *Journal of Geophysical Research: Oceans*, *105*(C10), 23895-23926. https://doi.org/10.1029/2000JC900105.

Yu, J., & Elderfield, H. (2007). Benthic foraminiferal B/Ca ratios reflect deep water carbonate saturation state. *Earth and Planetary Science Letters*, *258*(1-2), 73-86. https://doi.org/10.1016/j.epsl.2007.03.025.

Yu, J., Elderfield, H., & Hönisch, B. (2007). B/Ca in planktonic foraminifera as a proxy for surface seawater pH. *Paleoceanography*, *22* (2). https://doi.org/10.1029/2006PA001347.

Yu, J., Elderfield, H., & Piotrowski, A. M. (2008). Seawater carbonate ion-δ^{13}C systematics and application to glacial–interglacial North Atlantic Ocean circulation. *Earth and Planetary Science Letters*, *271*(1-4), 209-220. https://doi.org/10.1016/j.epsl.2008.04.010.

Yu, J. M. (2010). Multi-proxy reconstruction of surface water pCO_2 in the northern Arabian Sea since 29 ka. *Earth and Planetary Science Letters*, *295*(1-2), 49-57.https://doi.org/10.1016/j.epsl.2010.03.023.

Yu, J., Broecker, W. S., Elderfield, H., Jin, Z., McManus, J., & Zhang, F. (2010a). Loss of carbon from the deep sea since the Last Glacial Maximum. *Science*, *330*(6007), 1084-1087. https://doi.org/10.1126/science.1193221.

Yu, J., Foster, G. L., Elderfield, H., Broecker, W. S., & Clark, E. (2010b). An evaluation of benthic foraminiferal B/Ca and δ11B for deep ocean carbonate ion and pH reconstructions. *Earth and Planetary Science Letters*, *293* (1-2), 114-120. https://doi.org/10.1016/j.epsl.2010.02.029.

Yu, J., Anderson, R. F., Jin, Z., Rae, J. W., Opdyke, B. N., & Eggins, S. M. (2013). Responses of the deep ocean carbonate system to carbon reorganization during the Last Glacial–interglacial cycle. *Quaternary Science Reviews*, *76*, 39-52. https://doi.org/10.1016/j.quascirev.2013.06.020.

Yu, J., Anderson, R. F., & Rohling, E. J. (2014). Deep Ocean carbonate chemistry and glacial-interglacial atmospheric CO_2 changes. *Oceanography*, *27*(1), 16-25. https://doi.org/10.5670/oceanog.2014.04.

Yu, Z., Colin, C., Ma, R., Meynadier, L., Wan, S., Wu, Q., Kallel, N., Sepulcre, S., Dapoigny, A., & Bassinot, F. (2018). Antarctic Intermediate Water penetration into the Northern Indian Ocean during the last deglaciation. *Earth and Planetary Science Letters*, *500*, 67-75. https://doi.org/10.1016/j.epsl.2018.08.006.

Yu, J., Menviel, L., Jin, Z. D., Thornalley, D. J., Foster, G. L., Rohling, E. J., McCave, I. N., McManus, J. F., Dai Y., Ren, H., He , F., Zhang, F., Chen, P.J., & Roberts, A. P. (2019). More efficient North Atlantic carbon pump during the Last Glacial Maximum. *Nature communications*, *10* (1), 1-11.https://doi.org/10.1038/s41467-019-10028-z.

Zahn, R., Winn, K., & Sarnthein, M. (1986). Benthic foraminiferal $\delta^{13}C$ and accumulation rates of organic carbon: Uvigerina peregrina group and Cibicidoides wuellerstorfi. *Paleoceanography*, *1* (1), 27-42. https://doi.org/10.1029/PA001i001p00027.

Zahn, R., Pedersen, T. F., Bornhold, B. D., & Mix, A. C. (1991). Water mass conversion in the glacial subarctic Pacific (54 N, 148 W): Physical constraints and the benthic-planktonic stable isotope record. *Paleoceanography*, *6* (5), 543-560. https://doi.org/10.1029/91PA01327

Zahn, R; Pedersen, TF (1991): Late Pleistocene evolution of surface and mid-depth hydrography at the Oman margin: planktonic and benthic isotope records at Site 724. In: Prell, WL; Niitsuma, N; et al. (eds.), Proceedings of the Ocean Drilling Program,

Scientific Results, College Station, TX (Ocean Drilling Program), 117, 291-308. https://doi.org/10.2973/odp.proc.sr.117.162.1991

Zeebe, R. E., & Wolf-Gladrow, D. (2001). *CO$_2$ in seawater: equilibrium, kinetics, isotopes* (No. 65). Gulf Professional Publishing.

Papers Published

From thesis

1. **Smita N. Naik** and Sushant S. Naik, (2018) Evidences of CO_2 Leakage During the Last Deglaciation: The Need to Understand Deep-ocean Carbonate Chemistry of the Arabian Sea, *Journal of Geological Society of India*, 92, 404-406. **(IF - 1.459)**

2. **Smita N. Naik** and Sushant S. Naik, Glacial-interglacial contrast in deep-water $\delta^{13}C$ of the Arabian Sea, *Journal of Earth System Science.* (In Press). **(IF - 1.371)**

Conferences Participated

1. **Naik, S. N**., Naik, S. S., and Yair, R., (2018), *Carbonate ion variation in deep waters of the Eastern Arabian Sea from LGM to Holocene and its link to climate change.* at the 55th Annual Convention of Indian Geophysical Union on Changing Water Cycle and Water Resources held on 5-7 December 2018 at Rabindranath Tagore University, Bhopal. (Oral presentation)

2. **Naik, S. N**., and Naik, S. S., (2020), *A 25 kyr benthic foraminiferal carbon and oxygen isotope record from the southeast Arabian Sea,* at the International Conference on Paleoclimate Changes (ICPC-2020) held on July 9-10, 2020 on virtual platform, organised by Vellore *Institute of Technology,* Chennai. (Oral presentation)

3. **Naik S. N.,** and Naik, S. S., (2022), *Penetration of Antarctic Intermediate Water (AAIW) in to the Eastern Arabian Sea (EAS) during the last deglaciation,* at 1st Indian Quaternary Congress, International Virtual Conference from 19-21st January. (Poster presentation)